

University of Kentucky

UKnowledge

University of Kentucky Doctoral Dissertations

Graduate School

2007

POLYMORPHISM OF FOUR ENANTIOTROPIC CRYSTALLINE SYSTEMS CONTAINING Ni(II), H₂O, 15-Crown-5 AND NO₃⁻

Maxime Andre Siegler

University of Kentucky, maxime.siegler@uky.edu

[Right click to open a feedback form in a new tab to let us know how this document benefits you.](#)

Recommended Citation

Siegler, Maxime Andre, "POLYMORPHISM OF FOUR ENANTIOTROPIC CRYSTALLINE SYSTEMS CONTAINING Ni(II), H₂O, 15-Crown-5 AND NO₃⁻" (2007). *University of Kentucky Doctoral Dissertations*. 565.
https://uknowledge.uky.edu/gradschool_diss/565

This Dissertation is brought to you for free and open access by the Graduate School at UKnowledge. It has been accepted for inclusion in University of Kentucky Doctoral Dissertations by an authorized administrator of UKnowledge. For more information, please contact UKnowledge@lsv.uky.edu.

ABSTRACT OF DISSERTATION

Maxime André Siegler

The Graduate School

University of Kentucky

2007

POLYMORPHISM OF FOUR ENANTIOTROPIC CRYSTALLINE SYSTEMS
CONTAINING Ni(II), H₂O, 15-Crown-5 AND NO₃⁻

ABSTRACT OF DISSERTATION

A dissertation submitted in partial fulfillment of the
requirements for the degree of Doctor of Philosophy
in the College of Arts and Sciences
at the University of Kentucky

By
Maxime André Siegler

Lexington, Kentucky

Director: Dr. Carolyn P. Brock, Professor of Chemistry

Lexington, Kentucky

2007

Copyright © Maxime André Siegler 2007

ABSTRACT OF DISSERTATION

POLYMORPHISM OF FOUR ENANTIOTROPIC CRYSTALLINE SYSTEMS CONTAINING Ni(II), H₂O, 15-Crown-5 AND NO₃⁻

The series of compounds $[M(\text{H}_2\text{O})_2(15\text{-crown-5})](\text{NO}_3)_2$, $M = \text{Mg, Mn, Co, Cu and Zn}$, has been extended to include two new phases for $M = \text{Fe}$ and two new phases for $M = \text{Ni}$. The system $[M(\text{H}_2\text{O})_2(15\text{-crown-5})](\text{NO}_3)_2$ is remarkable for having many high- Z' phases ($Z' > 1$) with similar packing and for having solid-solid phase transitions through which there is no significant loss of crystallinity. The synthesis of the analogous Ni complex was carried out. Single-crystal X-ray diffraction showed that the coordination of the Ni²⁺ ion is different from that of the other six M^{2+} ions in the system $[M(\text{H}_2\text{O})_2(15\text{-crown-5})](\text{NO}_3)_2$.

High temperature phases with high Z' (8) were isolated for $M = \text{Mg, Fe and Zn}$. The refinements of such phases are challenging because of the lack of information in the diffraction patterns. Full details of the refinements for these three phases are discussed.

Six other Ni(II) complexes consisting of Ni²⁺, NO₃⁻, 15-crown-5 and different solvents were found when efforts were made to synthesize the compound $[\text{Ni}(\text{H}_2\text{O})_2(15\text{-crown-5})](\text{NO}_3)_2$. In these chemically different environments, the Ni²⁺ ions are not coordinated by the 15-crown-5 molecules; rather, one-dimensional H-bonded chains are formed from uncomplexed 15-crown-5 molecules and the Ni(II) complexes.

Among these six Ni(II) complexes, the compounds $[\text{Ni}(\text{H}_2\text{O})_6](\text{NO}_3)_2 \cdot (15\text{-crown-5}) \cdot \text{H}_2\text{O}$, $[\text{Ni}(\text{H}_2\text{O})_6](\text{NO}_3)_2 \cdot (15\text{-crown-5}) \cdot 2\text{H}_2\text{O}$ and $[\text{Ni}(\text{H}_2\text{O})_2(\text{MeCN})(\text{NO}_3)_2] \cdot (15\text{-crown-5}) \cdot \text{MeCN}$ were found to have reversible solid-solid phase transitions between structurally related phases. In all of these transitions, no significant crystal damage was detectable. The two latter systems are unusual because their phase sequences include three transitions and four phases between 90 and 295 K and because of the existence of high- Z' phases. These high- Z' phases are best depicted as being intermediate to low- and high-temperature phases. A method based on thermal analyses and X-ray diffraction has been developed for studying such sets of phase transitions.

KEYWORDS: Polymorphism, Phase Transitions, 15-crown-5, High-Z', Ni(II) complexes

Maxime Siegler

July 16, 2007

POLYMORPHISM OF FOUR ENANTIOTROPIC CRYSTALLINE SYSTEMS
CONTAINING Ni(II), H₂O, 15-Crown-5 AND NO₃⁻

By

Maxime André Siegler

Dr. Carolyn P. Brock
Director of Dissertation

Dr. Robert B. Grossman
Director of Graduate Studies

9/24/2007
Date

DISSERTATION

Maxime André Siegler

The Graduate School

University of Kentucky

2007

POLYMORPHISM OF FOUR ENANTIOTROPIC CRYSTALLINE SYSTEMS
CONTAINING Ni(II), H₂O, 15-Crown-5 AND NO₃⁻

DISSERTATION

A dissertation submitted in partial fulfillment of the
requirements for the degree of Doctor of Philosophy
in the College of Arts and Sciences
at the University of Kentucky

By
Maxime André Siegler

Lexington, Kentucky

Director: Dr. Carolyn P. Brock, Professor of Chemistry

Lexington, Kentucky

2007

Copyright © Maxime André Siegler 2007

ACKNOWLEDGMENTS

I would like to thank my advisor and Dissertation Chair, Dr. Carolyn Pratt Brock, who taught me the discipline of crystallography. Her rigorous attitude and her constant support for research in the field of solid-state chemistry allowed me to complete interesting projects. I am also grateful to Drs. Sean Parkin and Xiang Hao, who gave me precious advice on laboratory and data collection techniques in crystallography. Next, I wish to thank the other members of my Dissertation Committee, namely: Drs. Dennis J. Clouthier, Tonglei Li, Marcos A. Oliveira (former member) and John P. Selegue who provided expertise, comments and insights in my work throughout the period of my Ph.D program at the University of Kentucky. I also thank Dr. Mark D. Watson, who was willing to help me with the Differential Scanning Calorimetry measurements and Dr. Kwok-Wai Ng, who was willing to be the outside examiner of the final oral examination. I would like also to thank all persons (who remain anonymous) who believed in me and gave me moral support during the period of writing my dissertation.

Last of all, I give a special recognition to the Graduate School of the University of Kentucky, which awarded me the Kentucky Opportunity Fellowship during the period of June 2006 and June 2007.

TABLE OF CONTENTS

Acknowledgments.....	iii
List of Tables	viii
List of Figures.....	x
Chapter 1: Introduction	
Preamble	1
Problems	3
Aims of the Dissertation	5
Organization of the Dissertation	6
Some Important Ideas in Crystallography	8
<i>Z, Z'</i>	8
Disorder.....	8
Twinning.....	10
Polymorphism and Phase Transitions.....	13
Polymorphism.....	13
Phase Transitions	14
Investigation of Enantiotropic Polymorphic Systems.....	16
Differential Scanning Calorimetry.....	17
Optical Microscopy.....	18
Single Crystal X-ray Diffraction.....	19
Deduction of the Mechanism of Some First Order Enantiotropic Phase Transitions.....	21
Intermediate Phase	22
Modulated Structures	23
Chapter 2: Investigations of High Temperature Phases of $[M(H_2O)_2(15\text{-crown-5})](NO_3)_2$, $M = Mg, Zn$ and Fe	
Introduction.....	27
Experimental.....	29
Crystal Growth.....	29
<i>M = Mg, Zn</i>	29
<i>M = Fe</i>	29
Differential Scanning Calorimetry Measurements	30
<i>M = Mg, Zn</i>	30
<i>M = Fe</i>	30
X-ray Crystallography	33
Generalities	34
<i>M = Mg, Zn</i>	34
<i>M = Fe</i>	43
Results and Discussion	52
Cation Geometry.....	52
Analysis of the Packing	55

Enantiomeric Alternation.....	55
Phases Transitions.....	59
Conclusions.....	64
Chapter 3: Toward the Insertion of the Ni ²⁺ Ion Inside the 15-crown-5 Molecule	
Introduction.....	65
Experimental.....	67
Crystal Growth.....	67
Differential Scanning Calorimetry Measurements	70
Hot-Stage Microscopy	72
X-ray Crystallography	75
[Ni(H ₂ O) ₆](NO ₃) ₂ ·(15-crown-5)·H ₂ O (second polymorph)	76
[Ni(H ₂ O) ₆](NO ₃) ₂ · <i>trans</i> -[Ni(H ₂ O) ₄ (MeOH) ₂](NO ₃) ₂ ·2(15-crown-5)	78
<i>cis</i> -[Ni(H ₂ O) ₄ (NO ₃) ₂]· <i>trans</i> -[Ni(H ₂ O) ₄ (NO ₃) ₂]·2(15-crown-5)	85
[Ni(H ₂ O) ₂ (15-crown-5)](NO ₃) ₂ (phases I and II)	85
Phase II.....	89
Phase I.....	91
Crystallographic Data	91
Results and Discussion	99
[Ni(H ₂ O) ₆](NO ₃) ₂ ·(15-crown-5)·H ₂ O (second polymorph)	99
[Ni(H ₂ O) ₆](NO ₃) ₂ · <i>trans</i> -[Ni(H ₂ O) ₄ (MeOH) ₂](NO ₃) ₂ ·2(15-crown-5)	104
<i>cis</i> -[Ni(H ₂ O) ₄ (NO ₃) ₂]· <i>trans</i> -[Ni(H ₂ O) ₄ (NO ₃) ₂]·2(15-crown-5)	109
[Ni(H ₂ O) ₂ (15-crown-5)](NO ₃) ₂	116
Cation Geometry	116
Bond Lengths	116
Disorder of [Ni(H ₂ O) ₂ (15-crown-5)](NO ₃) ₂ , Why?	120
Synthesis of [Ni(H ₂ O) ₂ (15-crown-5)](NO ₃) ₂ , Why Is It Not Straightforward?	122
Analysis of the Packing in [Ni(H ₂ O) ₂ (15-crown-5)](NO ₃) ₂	123
Enantiomeric Alternation.....	123
Phase Transition.....	126
Conclusions.....	127
Chapter 4: The First Polymorph of [Ni(H ₂ O) ₆](NO ₃) ₂ ·(15-crown-5)·H ₂ O: a Dimorphic System	
Introduction.....	129
Experimental.....	131
Crystal Growth.....	131
Crystal Habit	131
Differential Scanning Calorimetry Measurements	133
X-ray Crystallography	133
Generalities	135
Phases I and II.....	136
Temperature Dependence of the Cell Dimensions	141
Results and Discussion	144
Analysis of the Packing	144

Disordered Lattice Water Molecule and the Hydrogen Bond Pattern	148
Conformation of the 15-crown-5 Molecule	150
Phase Transition II \rightarrow I	150
An Approach to the Mechanism of the Phase Transition II \rightarrow I	154
Comparisons of the first and second polymorphs of $[\text{Ni}(\text{H}_2\text{O})_6](\text{NO}_3)_2 \cdot (15\text{-crown-5}) \cdot \text{H}_2\text{O}$	158
Conclusions	162
Chapter 5: $[\text{Ni}(\text{H}_2\text{O})_6](\text{NO}_3)_2 \cdot (15\text{-crown-5}) \cdot 2\text{H}_2\text{O}$: an Uncommon Polymorphic System	
Introduction	163
Experimental	165
Crystal Growth	165
Crystal Habit	165
Differential Scanning Calorimetry Measurements	167
First Set of DSC Measurements (173-323K)	167
Second Set of DSC Measurements (298-373K)	169
X-ray Crystallography	173
Generalities	174
Phase I	176
Phase II	178
Phase III	183
Phase IV	189
Temperature Dependence of the Cell Dimensions	193
Results and Discussion	196
Analysis of the Packing	196
Are the Hydrogen Bond Interactions Different in the Four Phases?	203
Phase III: an Intermediate Phase	204
Enantiomeric Alternation	207
Phase Transitions	209
IV \rightarrow III and III \rightarrow II	209
II \rightarrow I	213
The Thermodynamics of the Phase Transitions	215
Conclusions	217
Chapter 6: $[\text{Ni}(\text{MeCN})(\text{H}_2\text{O})_2(\text{NO}_3)_2] \cdot (15\text{-crown-5}) \cdot \text{MeCN}$: An Analogous Polymorphic System to $[\text{Ni}(\text{H}_2\text{O})_6](\text{NO}_3)_2 \cdot (15\text{-crown-5}) \cdot 2\text{H}_2\text{O}$	
Introduction	219
Experimental	221
Crystal Growth	221
Differential Scanning Calorimetry Measurements	221
X-ray Crystallography	221
Generalities	223
Phase I	225
Phase II	228
Phase III	238
Phase IV	240

Temperature Dependence of the Cell Dimensions	244
Results and Discussion	247
Analysis of the Packing	247
Phase II: an Intermediate Phase	251
Enantiomeric Alternation.....	257
Phase Transitions	259
IV → III	259
III → II and II → I	261
Similarities and Differences Between the Two Polymorphic Systems	
[Ni(H ₂ O) ₆](NO ₃) ₂ ·(15-crown-5)·2H ₂ O and [Ni(MeCN)(H ₂ O) ₂ (NO ₃) ₂]·(15-	
crown-5)·MeCN.....	264
Similarities	264
Differences.....	266
Conclusions.....	269
 Chapter 7: General Conclusions	
Extension of [M(H ₂ O) ₂ (15-crown-5)](NO ₃) ₂	271
Attempts to Synthesize [Ni(H ₂ O) ₂ (15-crown-5)](NO ₃) ₂	271
Coordination Number of Ni ²⁺ in Seven Ni(II) Complexes	272
New Polymorphic Systems	273
Systematic Approach to Study Phase Transitions	274
The Ambiguous Nature of Intermediate Phase.....	275
Phase Predictions	277
New Polymorphic Systems in the Future.....	284
 Appendices	
Appendix A: Crystallographic Tables	285
Appendix B: Symbols	288
Appendix C: Glossary.....	290
 Bibliography	295
 Vita.....	302

LIST OF TABLES

Table 2.1 Crystallographic data of $[M(\text{H}_2\text{O})_2(15\text{-crown-5})](\text{NO}_3)_2$, $M = \text{Mg, Zn}$	41
Table 2.2 Crystallographic data of $[\text{Fe}(\text{H}_2\text{O})_2(15\text{-crown-5})](\text{NO}_3)_2$	50
Table 2.3 M -O distances (Å) averaged over the eight residues found in the high temperature phase ($B2_1$, $Z' = 8$) of $[M(\text{H}_2\text{O})_2(15\text{-crown-5})](\text{NO}_3)_2$, $M = \text{Mg, Zn}$ and Fe	54
Table 2.4 The five crystal structures and twelve phases of $[M(\text{H}_2\text{O})_2(15\text{-crown-5})](\text{NO}_3)_2$, $M = \text{Mg, Mn, Fe, Co, Cu}$ and Zn.....	61
Table 3.1 Bond distances (Å) between atoms for each component of the disorder of the crown ether in the compound $[\text{Ni}(\text{H}_2\text{O})_6](\text{NO}_3)_2 \cdot \text{trans-}[\text{Ni}(\text{H}_2\text{O})_4(\text{MeOH})_2](\text{NO}_3)_2 \cdot 2(15\text{-crown-5})$	83
Table 3.2 Crystallographic data for the second polymorph of $[\text{Ni}(\text{H}_2\text{O})_6](\text{NO}_3)_2 \cdot (15\text{-crown-5}) \cdot \text{H}_2\text{O}$	93
Table 3.3 Crystallographic data for $[\text{Ni}(\text{H}_2\text{O})_6](\text{NO}_3)_2 \cdot \text{trans-}[\text{Ni}(\text{H}_2\text{O})_4(\text{MeOH})_2](\text{NO}_3)_2 \cdot 2(15\text{-crown-5})$ [4] and <i>cis-}[\text{Ni}(\text{H}_2\text{O})_4(\text{NO}_3)_2] \cdot \text{trans-}[\text{Ni}(\text{H}_2\text{O})_4(\text{NO}_3)_2] \cdot 2(15\text{-crown-5}) [5]</i>	95
Table 3.4 Crystallographic data of the phases I and II of $[\text{Ni}(\text{H}_2\text{O})_2(15\text{-crown-5})](\text{NO}_3)_2$	97
Table 3.5 Hydrogen bond distances $\text{D} \cdots \text{A}$ (Donor \cdots Acceptor) for the second polymorph of $[\text{Ni}(\text{H}_2\text{O})_6](\text{NO}_3)_2 \cdot (15\text{-crown-5}) \cdot \text{H}_2\text{O}$ along the a direction (<i>i.e.</i> , the direction of the two types of 1-D H-bonded chains) and around the four independent $[\text{Ni}(\text{H}_2\text{O})_6]^{2+}$ cations in the 2-D planes of H-bonds	103
Table 3.6 Hydrogen bond distances $\text{D} \cdots \text{A}$ (Donor \cdots Acceptor) for the compound $[\text{Ni}(\text{H}_2\text{O})_6](\text{NO}_3)_2 \cdot \text{trans-}[\text{Ni}(\text{H}_2\text{O})_4(\text{MeOH})_2](\text{NO}_3)_2 \cdot 2(15\text{-crown-5})$ along the a direction (<i>i.e.</i> , the direction of the 1-D H-bonded chains) and the $[0\ 1\ 1]$, $[0\ 1\ -1]$ and $[1\ 0\ 2]$ directions	108
Table 3.7 Hydrogen bond distances $\text{D} \cdots \text{A}$ (Donor \cdots Acceptor) for <i>cis-}[\text{Ni}(\text{H}_2\text{O})_4(\text{NO}_3)_2] \cdot \text{trans-}[\text{Ni}(\text{H}_2\text{O})_4(\text{NO}_3)_2] \cdot 2(15\text{-crown-5}) along the a, b and c directions.....</i>	115
Table 3.8 Deviations (Å) of the Ni–O _{ether} (O1, O2, O3, O4, O5) and Ni–O _{water} (O6 and O7) distances from the average Ni–O _{ether} and Ni–O _{water} distances (Å) given for each residue in Ni I ($C\bar{1}$, $Z' = 2$) and Ni II ($P2_1/c$, $Z' = 3$) of $[\text{Ni}(\text{H}_2\text{O})_2(15\text{-crown-5})](\text{NO}_3)_2$	118
Table 4.1 Crystallographic data for the two phases (I and II) of the first polymorph of $[\text{Ni}(\text{H}_2\text{O})_6](\text{NO}_3)_2 \cdot (15\text{-crown-5}) \cdot \text{H}_2\text{O}$	139
Table 4.2 Hydrogen bond distances $\text{D} \cdots \text{A}$ (Donor \cdots Acceptor) along the a direction (<i>i.e.</i> , the direction of the 1-D H-bonded chains) and along the b and c directions (<i>i.e.</i> , the directions found along the 2-D planes) for the phases I and II of the first polymorph of $[\text{Ni}(\text{H}_2\text{O})_6](\text{NO}_3)_2 \cdot (15\text{-crown-5}) \cdot \text{H}_2\text{O}$	147
Table 5.1 Crystallographic data for the phases I and II of $[\text{Ni}(\text{H}_2\text{O})_6](\text{NO}_3)_2 \cdot (15\text{-crown-5}) \cdot 2\text{H}_2\text{O}$	181

Table 5.2 Crystallographic data for the phases III and IV of $[\text{Ni}(\text{H}_2\text{O})_6](\text{NO}_3)_2 \cdot (15\text{-crown-5}) \cdot 2\text{H}_2\text{O}$	191
Table 5.3 Hydrogen bond distances $\text{D} \cdots \text{A}$ (Donor \cdots Acceptor) along the c direction (<i>i.e.</i> , the direction of the 1-D H-bonded chains) for the phases I, II, III and IV of the compound $[\text{Ni}(\text{H}_2\text{O})_6](\text{NO}_3)_2 \cdot (15\text{-crown-5}) \cdot 2\text{H}_2\text{O}$	198
Table 5.4 Hydrogen bond distances $\text{D} \cdots \text{A}$ (Donor \cdots Acceptor) found in the 2-D H-bonded planes for the phases I, II, III and IV of the compound $[\text{Ni}(\text{H}_2\text{O})_6](\text{NO}_3)_2 \cdot (15\text{-crown-5}) \cdot 2\text{H}_2\text{O}$	200
Table 5.5 $\text{Ni} \cdots \text{O}$ (O18 and O19) and $\text{Ni} \cdots \text{Ni}$ distances found in the ordered region of phase III and in phase IV of the compound $[\text{Ni}(\text{H}_2\text{O})_6](\text{NO}_3)_2 \cdot (15\text{-crown-5}) \cdot 2\text{H}_2\text{O}$	206
Table 6.1 Crystallographic data for the phases I and II of $[\text{Ni}(\text{MeCN})(\text{H}_2\text{O})_2(\text{NO}_3)_2] \cdot (15\text{-crown-5}) \cdot \text{MeCN}$	236
Table 6.2 Crystallographic data for the phases III and IV of $[\text{Ni}(\text{MeCN})(\text{H}_2\text{O})_2(\text{NO}_3)_2] \cdot (15\text{-crown-5}) \cdot \text{MeCN}$	242
Table 6.3 Hydrogen bond distances $\text{D} \cdots \text{A}$ (Donor \cdots Acceptor) along the c direction (<i>i.e.</i> , the direction of the 1-D H-bonded chains) for the phases I, II, III and IV of the compound $[\text{Ni}(\text{MeCN})(\text{H}_2\text{O})_2(\text{NO}_3)_2] \cdot (15\text{-crown-5}) \cdot \text{MeCN}$	249
Table 6.4 Comparisons of the cell dimensions of phases II, III, IV of $[\text{Ni}(\text{H}_2\text{O})_6](\text{NO}_3)_2 \cdot (15\text{-crown-5}) \cdot 2\text{H}_2\text{O}$ (1) with the cell dimensions of phases I, II, III and IV of $[\text{Ni}(\text{MeCN})(\text{H}_2\text{O})_2(\text{NO}_3)_2] \cdot (15\text{-crown-5}) \cdot \text{MeCN}$ (2) at 90, 150 and 250 K (243 K)	268

LIST OF FIGURES

Figure 1.1 Scheme showing blocks of a constituent (<i>i.e.</i> , an arrow) in a two-dimensional space.....	9
Figure 1.2 Schematic example of an inversion twin (<i>i.e.</i> , the twin components are related by inversion symmetry) showing blocks of a constituent (<i>i.e.</i> , an arrow) in a two-dimensional space.....	12
Figure 1.3 Schematic plots of the Gibbs free energy G vs T for enantiotropic and monotropic systems with two phases.....	15
Figure 1.4 Scheme showing a one-dimensional commensurately modulated superstructure.....	24
Figure 1.5 Arbitrary reciprocal lattice slice of a commensurately modulated superstructure.....	25
Figure 2.1 The chemical line drawing of $[M(\text{H}_2\text{O})_2(15\text{-crown-5})](\text{NO}_3)_2$, $M = \text{Mg, Mn, Fe, Co, Cu}$ and Zn	28
Figure 2.2 DSC trace of the $[\text{Fe}(\text{H}_2\text{O})_2(15\text{-crown-5})](\text{NO}_3)_2$ compound.....	31
Figure 2.3 Parts of the DSC traces of the $[\text{Fe}(\text{H}_2\text{O})_2(15\text{-crown-5})](\text{NO}_3)_2$ compound measured at 1, 5, 10 and 20 K/min.....	32
Figure 2.4 Asymmetric unit of the high temperature phase ($B2_1$, $Z' = 8$) looking down the a direction.....	35
Figure 2.5 The displacement ellipsoids (50% probability level) of one disordered 15-crown-5 molecule of the Mg compound at 311 K.....	37
Figure 2.6 Separate Wilson plots for the Mg compound at 311 K.....	38
Figure 2.7 Separate Wilson plots for the Zn compound at 313 K.....	39
Figure 2.8 Parts of reciprocal lattice slices $h1\ell$ digitally reconstructed directly from the measured frames for the Zn and Fe structures with $Z' = 8$	44
Figure 2.9 The displacement ellipsoids (50% probability level) of the independent ions (8 cations and 16 nitrates) in the asymmetric units of the Mg, Zn and Fe compounds at 311, 313 and 90 K.....	45
Figure 2.10 The displacement ellipsoids (50% probability level) of one independent formula unit (1 cation and 2 nitrates) in the asymmetric units of the Mg, Zn and Fe compounds at 311, 313 and 90 K.....	46
Figure 2.11 Separate Wilson plots for the Fe compound at 90 K (data using Cu $K\alpha$ radiation).....	47
Figure 2.12 Parts of the reciprocal lattice slice $h1\ell$ digitally reconstructed directly from the measured frames for the Fe structure ($B2_1$, $Z' = 8$).....	48
Figure 2.13 The two conformational enantiomers found in the system $[M(\text{H}_2\text{O})_2(15\text{-crown-5})](\text{NO}_3)_2$, $M = \text{Mg, Mn, Fe, Co, Cu}$ and Zn	53
Figure 2.14 The basic building block of the H-bonding found in the three isostructural high temperature phases of $[M(15\text{-crown-5})(\text{H}_2\text{O})_2](\text{NO}_3)_2$, $M = \text{Mg, Zn}$ and Fe	56
Figure 2.15 The packing of the high temperature phase of $[M(15\text{-crown-5})(\text{H}_2\text{O})_2](\text{NO}_3)_2$, $M = \text{Mg, Zn}$ and Fe looking down the c direction.....	57
Figure 2.16 The packing of the high temperature phase of $[M(15\text{-crown-5})(\text{H}_2\text{O})_2](\text{NO}_3)_2$, $M = \text{Mg, Zn}$ and Fe , in the plane (0 1 0).....	58

Figure 2.17 Drawing of layers of the four crystal structures of $[M(H_2O)_2(15\text{-crown-5})](NO_3)_2$, $M = Mg, Mn, Fe, Cu$ and Zn	63
Figure 3.1 The chosen crystal (plate) of <i>cis</i> - $[Ni(H_2O)_4(NO_3)_2]$ · <i>trans</i> - $[Ni(H_2O)_4(NO_3)_2]$ ·2(15-crown-5) was grown from an acetone solution and was indexed near 90 K.....	69
Figure 3.2 Parts of the DSC traces of $[Ni(H_2O)_2(15\text{-crown-5})](NO_3)_2$ measured at -10 (cooling) and 10 K/min (heating)	71
Figure 3.3 Magnified digital frames of one part of a single crystal of $[Ni(H_2O)_6](NO_3)_2 \cdot (15\text{-crown-5}) \cdot 2H_2O$ at 327.4 and 335.4 K.....	73
Figure 3.4 Digital frames (10x magnification) obtained from hot-stage microscopy experiments	74
Figure 3.5 The displacement ellipsoids (50% probability level) of the asymmetric unit of the second polymorph of $[Ni(H_2O)_6](NO_3)_2 \cdot (15\text{-crown-5}) \cdot H_2O$ at 90 K.....	77
Figure 3.6 The displacement ellipsoids (50% probability level) of the 15-crown-5 molecule in the compound $[Ni(H_2O)_6](NO_3)_2 \cdot \textit{trans}-[Ni(H_2O)_4(MeOH)_2](NO_3)_2 \cdot 2(15\text{-crown-5}) at 90 K.....$	79
Figure 3.7 (a) Drawing showing the geometry of the two conformational enantiomers of the 15-crown-5 molecule. (b) The displacement ellipsoids (50% probability level) of the 15-crown-5 molecule in the compound $[Ni(H_2O)_6](NO_3)_2 \cdot \textit{trans}-[Ni(H_2O)_4(MeOH)_2](NO_3)_2 \cdot 2(15\text{-crown-5}) at 90 K. (c) Overlay of the two conformational enantiomers of the 15-crown-5 molecule$	80
Figure 3.8 The displacement ellipsoids (50% probability level) of the disordered 15-crown-5 molecule in the compound $[Ni(H_2O)_6](NO_3)_2 \cdot \textit{trans}-[Ni(H_2O)_4(MeOH)_2](NO_3)_2 \cdot 2(15\text{-crown-5}) at 90 K.....$	82
Figure 3.9 The displacement ellipsoids (50% probability level) of the asymmetric unit of the compound $[Ni(H_2O)_6](NO_3)_2 \cdot \textit{trans}-[Ni(H_2O)_4(MeOH)_2](NO_3)_2 \cdot 2(15\text{-crown-5}) at 90 K.....$	84
Figure 3.10 The displacement ellipsoids (50% probability level) of the two independent formula units in the asymmetric unit of <i>cis</i> - $[Ni(H_2O)_4(NO_3)_2]$ · <i>trans</i> - $[Ni(H_2O)_4(NO_3)_2]$ ·2(15-crown-5) at 90 K.....	86
Figure 3.11 The displacement ellipsoids (50% probability level) of the two isomers of $[Ni(H_2O)_4(NO_3)_2]$ at 90K	87
Figure 3.12 The atom-numbering scheme of one $[Ni(H_2O)_2(15\text{-crown-5})]^{2+}$ ion in the two phases of $[Ni(H_2O)_2(15\text{-crown-5})](NO_3)_2$	88
Figure 3.13 The displacement ellipsoids (50% probability level) of the independent ions (three cations and six nitrates) in the asymmetric units of phase II of $[Ni(H_2O)_2(15\text{-crown-5})](NO_3)_2$ at 90 K before and after treatment of the metal-ion disorder.....	90
Figure 3.14 The displacement ellipsoids (50% probability level) of the independent ions (2 cations and 4 nitrate ions) in the asymmetric unit of phase I of $[Ni(H_2O)_2(15\text{-crown-5})](NO_3)_2$ at 308 K.....	92
Figure 3.15 The two types of 1-D chains found in the second polymorph of $[Ni(H_2O)_6](NO_3)_2 \cdot (15\text{-crown-5}) \cdot H_2O$ looking down the a direction.....	100
Figure 3.16 The set of hydrogen bonds found in the second polymorph of $[Ni(H_2O)_6](NO_3)_2 \cdot (15\text{-crown-5}) \cdot H_2O$ along the a direction (<i>i.e.</i> , the direction of the 1-D chains)	101

Figure 3.17 The set of hydrogen bonds observed around the four independent $[\text{Ni}(\text{H}_2\text{O})_6]^{2+}$ cations along the normal to the plane (2 1 -1)	102
Figure 3.18 The packing of $[\text{Ni}(\text{H}_2\text{O})_6](\text{NO}_3)_2 \cdot \text{trans}-[\text{Ni}(\text{H}_2\text{O})_4(\text{MeOH})_2](\text{NO}_3)_2 \cdot 2(15\text{-crown-5})$ looking down the a direction	105
Figure 3.19 The set of hydrogen bonds in the asymmetric unit of the compound $[\text{Ni}(\text{H}_2\text{O})_6](\text{NO}_3)_2 \cdot \text{trans}-[\text{Ni}(\text{H}_2\text{O})_4(\text{MeOH})_2](\text{NO}_3)_2 \cdot 2(15\text{-crown-5})$ along the a direction (<i>i.e.</i> , along the 1-D H-bonded chains)	106
Figure 3.20 The set of hydrogen bonds along the [0 1 1], [0 1 -1] and [1 0 2] directions for the compound $[\text{Ni}(\text{H}_2\text{O})_6](\text{NO}_3)_2 \cdot \text{trans}-[\text{Ni}(\text{H}_2\text{O})_4(\text{MeOH})_2](\text{NO}_3)_2 \cdot 2(15\text{-crown-5})$	107
Figure 3.21 The packing of one layer of $\text{cis}-[\text{Ni}(\text{H}_2\text{O})_4(\text{NO}_3)_2] \cdot \text{trans}-[\text{Ni}(\text{H}_2\text{O})_4(\text{NO}_3)_2] \cdot 2(15\text{-crown-5})$ looking down the a direction	110
Figure 3.22 The set of hydrogen bonds in the asymmetric unit of $\text{cis}-[\text{Ni}(\text{H}_2\text{O})_4(\text{NO}_3)_2] \cdot \text{trans}-[\text{Ni}(\text{H}_2\text{O})_4(\text{NO}_3)_2] \cdot 2(15\text{-crown-5})$ along the c direction	111
Figure 3.23 The H-bond interactions between the <i>cis</i> (H-bond donor) and the <i>trans</i> (H-bond acceptor) isomers of $[\text{Ni}(\text{H}_2\text{O})_4(\text{NO}_3)_2]$ found along the a direction ..	112
Figure 3.24 The packing of one layer of $\text{cis}-[\text{Ni}(\text{H}_2\text{O})_4(\text{NO}_3)_2] \cdot \text{trans}-[\text{Ni}(\text{H}_2\text{O})_4(\text{NO}_3)_2] \cdot 2(15\text{-crown-5})$ looking down the b direction	113
Figure 3.25 1-D ribbon of <i>cis</i> (black) and <i>trans</i> (light grey) isomers of $[\text{Ni}(\text{H}_2\text{O})_4(\text{NO}_3)_2]$ down the c direction	114
Figure 3.26 The displacement ellipsoids (50% probability level) of one disordered cation $[\text{Ni}(\text{H}_2\text{O})_2(15\text{-crown-5})]^{2+}$ of phase II at 90 K	117
Figure 3.27 Drawing showing the five possibilities (a \rightarrow e) for the Ni^{2+} ion to be coordinated by the O atoms of the crown ether in $[\text{Ni}(\text{H}_2\text{O})_2(15\text{-crown-5})](\text{NO}_3)_2$	121
Figure 3.28 The similar packing of phase I and phase II of $[\text{Ni}(\text{H}_2\text{O})_2(15\text{-crown-5})](\text{NO}_3)_2$ down the [1 0 2] and c directions	124
Figure 3.29 Drawing of a layer of the two phases of $[\text{Ni}(\text{H}_2\text{O})_2(15\text{-crown-5})](\text{NO}_3)_2$ down the a direction	125
Figure 4.1 (a) A photograph of crystals of the first polymorph of $[\text{Ni}(\text{H}_2\text{O})_6](\text{NO}_3)_2 \cdot (15\text{-crown-5}) \cdot \text{H}_2\text{O}$. (b) Drawing describing the crystal habit of the first polymorph of $[\text{Ni}(\text{H}_2\text{O})_6](\text{NO}_3)_2 \cdot (15\text{-crown-5}) \cdot \text{H}_2\text{O}$	132
Figure 4.2 DSC traces of the first polymorph of $[\text{Ni}(\text{H}_2\text{O})_6](\text{NO}_3)_2 \cdot (15\text{-crown-5}) \cdot \text{H}_2\text{O}$ collected between 173 and 298 K at 10 K/min and between 298 and 173 K at -10 K/min	134
Figure 4.3 Projections of the two phases of the first polymorph of $[\text{Ni}(\text{H}_2\text{O})_6](\text{NO}_3)_2 \cdot (15\text{-crown-5}) \cdot \text{H}_2\text{O}$ down the a direction	137
Figure 4.4 The displacement ellipsoids (50% probability level) of the asymmetric unit of the first polymorph of $[\text{Ni}(\text{H}_2\text{O})_6](\text{NO}_3)_2 \cdot (15\text{-crown-5}) \cdot 2\text{H}_2\text{O}$ in phase I at 295 K and in phase II at 90 K	138
Figure 4.5 Plots of the cell dimensions <i>a</i> , <i>b</i> and <i>c</i> (Å) of the first polymorph of $[\text{Ni}(\text{H}_2\text{O})_6](\text{NO}_3)_2 \cdot (15\text{-crown-5}) \cdot \text{H}_2\text{O}$ versus <i>T</i> (K).....	142
Figure 4.6 Plots of the cell dimensions β ($^\circ$) and <i>V</i> (Å ³) of the first polymorph of $[\text{Ni}(\text{H}_2\text{O})_6](\text{NO}_3)_2 \cdot (15\text{-crown-5}) \cdot \text{H}_2\text{O}$ versus <i>T</i> (K).....	143

Figure 4.7 (a) The set of hydrogen bond interactions in the first polymorph of $[\text{Ni}(\text{H}_2\text{O})_6](\text{NO}_3)_2 \cdot (15\text{-crown-5}) \cdot \text{H}_2\text{O}$ along the a direction (<i>i.e.</i> , along the 1-D H-bonded chains). (b) The set of hydrogen bond interactions in the compound $[\text{Ni}(\text{H}_2\text{O})_6](\text{NO}_3)_2 \cdot (15\text{-crown-5}) \cdot \text{H}_2\text{O}$ along the b and c directions (<i>i.e.</i> , along the 2-D H-bonded planes).....	145
Figure 4.8 The packing of one layer in phase I of the first polymorph of $[\text{Ni}(\text{H}_2\text{O})_6](\text{NO}_3)_2 \cdot (15\text{-crown-5}) \cdot \text{H}_2\text{O}$ looking down the c direction.....	146
Figure 4.9 The set of hydrogen bond interactions as viewed down the a direction in the region where the lattice water molecules are disordered in phase II of the first polymorph of $[\text{Ni}(\text{H}_2\text{O})_6](\text{NO}_3)_2 \cdot (15\text{-crown-5}) \cdot \text{H}_2\text{O}$	149
Figure 4.10 Parts of the reciprocal lattice slices $h0\ell$ digitally reconstructed directly from the measured frames given at 190 (phase II), 195 (phase II) and 200 K (phase I)	152
Figure 4.11 Temperature dependences of the integrated intensities of the 10 strongest $h0\ell$ reflections with $h + \ell = 2n$ monitored between 90 and 200 K	153
Figure 4.12 The displacement ellipsoids (50% probability level) of the two independent 15-crown-5 molecules in phase II of the first polymorph of $[\text{Ni}(\text{H}_2\text{O})_6](\text{NO}_3)_2 \cdot (15\text{-crown-5}) \cdot \text{H}_2\text{O}$ at 90, 110, 130, 150 and 170 K	156
Figure 4.13 The displacement ellipsoids (50% probability level) of the two independent 15-crown-5 molecules in phase II of the first polymorph of $[\text{Ni}(\text{H}_2\text{O})_6](\text{NO}_3)_2 \cdot (15\text{-crown-5}) \cdot \text{H}_2\text{O}$ at 170, 175, 180, 185 and 190 K	157
Figure 4.14 Plot of the fitted rotation angle ω ($^\circ$) versus T (K)	159
Figure 4.15 Projections of the two crystallographically independent 15-crown-5 molecules in phase II of the first polymorph of $[\text{Ni}(\text{H}_2\text{O})_6](\text{NO}_3)_2 \cdot (15\text{-crown-5}) \cdot \text{H}_2\text{O}$ at 90 and 190 K viewed down the a direction	160
Figure 4.16 Projections of the first (only phase I is shown) and second polymorphs of $[\text{Ni}(\text{H}_2\text{O})_6](\text{NO}_3)_2 \cdot (15\text{-crown-5}) \cdot \text{H}_2\text{O}$ down the a direction (the direction of the 1-D H-bonded chains)	161
Figure 5.1 (a) A photograph of single crystals of $[\text{Ni}(\text{H}_2\text{O})_6](\text{NO}_3)_2 \cdot (15\text{-crown-5}) \cdot 2\text{H}_2\text{O}$. (b) Drawings describing the crystal habit of $[\text{Ni}(\text{H}_2\text{O})_6](\text{NO}_3)_2 \cdot (15\text{-crown-5}) \cdot 2\text{H}_2\text{O}$	166
Figure 5.2 DSC traces of the compound $[\text{Ni}(\text{H}_2\text{O})_6](\text{NO}_3)_2 \cdot (15\text{-crown-5}) \cdot 2\text{H}_2\text{O}$ measured between 298 and 173 K at -5 K/min and between 173 and 323 K at 5 K/min	168
Figure 5.3 DSC traces of the compound $[\text{Ni}(\text{H}_2\text{O})_6](\text{NO}_3)_2 \cdot (15\text{-crown-5}) \cdot 2\text{H}_2\text{O}$ made from 298 to 373 K at 5 K/min (traces 1 and 3) and from 373 to 298 K at -5 K/min (trace 2).....	170
Figure 5.4 DSC traces of the compound $[\text{Ni}(\text{H}_2\text{O})_6](\text{NO}_3)_2 \cdot (15\text{-crown-5}) \cdot 2\text{H}_2\text{O}$ collected from 298 to 348 K at 5 K/min (trace 1), from 298 to 373 K at 5 K/min (traces 3 and 5), from 348 to 298 K at -5 K/min (trace 2) and from 373 and 298 K at -5 K/min (trace 4).....	172
Figure 5.5 Projections of the four phases of $[\text{Ni}(\text{H}_2\text{O})_6](\text{NO}_3)_2 \cdot (15\text{-crown-5}) \cdot 2\text{H}_2\text{O}$ down the c direction.....	175
Figure 5.6 (a) Drawing showing the disordered 15-crown-5 molecule in phase IV (space group $I2/m$). (b) Drawing showing the displacement parameters of one half 15-crown-5 molecule in the space group $I2/m$	177

Figure 5.7 (a) Projections of the 15-crown-5 molecules and the $[\text{Ni}(\text{H}_2\text{O})_6]^{2+}$ ions in the phases II and IV down the a direction. (b) The projection of part (a) has been rotated by 90° around the horizontal so that the view is down the c direction	179
Figure 5.8 The displacement ellipsoids (50% probability level) of the asymmetric unit of the compound $[\text{Ni}(\text{H}_2\text{O})_6](\text{NO}_3)_2 \cdot (15\text{-crown-5}) \cdot 2\text{H}_2\text{O}$ in phase I at 295 K and in phase II at 250 K without and with the inclusion of disorder of the $[\text{Ni}(\text{H}_2\text{O})_6]^{2+}$ ion.....	180
Figure 5.9 Parts of the reciprocal lattice slices $h1 \ell$ digitally reconstructed directly from the measured frames for phase III ($B2_1, Z' = 7$) at 90 and 213 K.....	184
Figure 5.10 Separate Wilson plots for phase III ($B2_1, Z' = 7$) at 90 K.....	187
Figure 5.11 Parts of the reciprocal lattice slice $h1 \ell$ (given at 90 K) digitally reconstructed directly from the measured frames for phase III ($B2_1, Z' = 7$).....	188
Figure 5.12 The displacement ellipsoids (50% probability level) of the asymmetric unit of the compound $[\text{Ni}(\text{H}_2\text{O})_6](\text{NO}_3)_2 \cdot (15\text{-crown-5}) \cdot 2\text{H}_2\text{O}$ in phase III and phase IV at 90 K.....	190
Figure 5.13 Plots of the modified cell dimensions a , b and c (\AA) of $[\text{Ni}(\text{H}_2\text{O})_6](\text{NO}_3)_2 \cdot (15\text{-crown-5}) \cdot 2\text{H}_2\text{O}$ versus T (K).....	194
Figure 5.14 Plots of the modified cell dimensions β ($^\circ$) and V (\AA^3) of $[\text{Ni}(\text{H}_2\text{O})_6](\text{NO}_3)_2 \cdot (15\text{-crown-5}) \cdot 2\text{H}_2\text{O}$ versus T (K).....	195
Figure 5.15 (a) The set of hydrogen bond interactions observed in phase IV of the compound $[\text{Ni}(\text{H}_2\text{O})_6](\text{NO}_3)_2 \cdot (15\text{-crown-5}) \cdot 2\text{H}_2\text{O}$ along the c direction (<i>i.e.</i> , along the 1-D H-bonded chains). (b) The set of hydrogen bond interactions given for phase IV of the compound $[\text{Ni}(\text{H}_2\text{O})_6](\text{NO}_3)_2 \cdot (15\text{-crown-5}) \cdot 2\text{H}_2\text{O}$ along the $[0\ 1\ 0]$ and $[1\ 0\ \frac{1}{2}]$ directions.....	197
Figure 5.16 Projections of the asymmetric units of phases II, III and IV down the normal to the plane (1 0 0).....	205
Figure 5.17 Projections of the crystallographically independent 15-crown-5 molecules down the a direction for phase III and down the normal to the plane (1 0 1) for phase IV	208
Figure 5.18 (a) Parts of the reciprocal lattice slices $h1 \ell$ digitally reconstructed directly from the measured frames given for 205 K (phase IV) and 210 K (phase III). (b) Parts of the reciprocal lattice slice $h1 \ell$ digitally reconstructed directly from the measured frames given at 242 (phase III) and 253 K (phase II)....	210
Figure 5.19 Projections of the unit cells down the a direction for phases II and IV and down the normal to the plane (1 0 0) for phase III.....	212
Figure 5.20 (a) Parts of the reciprocal lattice slices $h1 \ell$ digitally reconstructed directly from the measured frames given at 290 (phase II) and 295 K (phase I). (b) Temperature dependence of the integrated intensities of the 10 strongest $h0 \ell$ reflections with $h + k + \ell = 2n + 1$ monitored between 250 and 303 K.....	214
Figure 5.21 Schematic plots of the Gibbs free energy and enthalpy versus T in the polymorphic system $[\text{Ni}(\text{H}_2\text{O})_6](\text{NO}_3)_2 \cdot (15\text{-crown-5}) \cdot 2\text{H}_2\text{O}$	216

Figure 6.1 DSC traces of the compound $[\text{Ni}(\text{MeCN})(\text{H}_2\text{O})_2(\text{NO}_3)_2] \cdot (15\text{-crown-5}) \cdot \text{MeCN}$ made from 243 to 143 K at -5 K/min and from 143 to 243 K at 5 K/min (scheme 1).....	222
Figure 6.2 Projections of the four phases of $[\text{Ni}(\text{MeCN})(\text{H}_2\text{O})_2(\text{NO}_3)_2] \cdot (15\text{-crown-5}) \cdot \text{MeCN}$ down the c direction	224
Figure 6.3 (a) Drawing showing the full disorder of the 15-crown-5 molecule in phase I. The major and minor components of the disorder are related by a pseudoinversion center (i). (b) Drawing showing the disordered metal complex $[\text{Ni}(\text{MeCN})(\text{H}_2\text{O})_2(\text{NO}_3)_2]$ in phase I.....	227
Figure 6.4 Parts of the reciprocal lattice slices $h1\ell$ digitally reconstructed directly from the measured frames for phase II ($B2_1, Z' = 5$) at 90 and 233 K	229
Figure 6.5 Separate Wilson plots for phase II ($B2_1, Z' = 5$) at 90 K.....	233
Figure 6.6 Part of the reciprocal lattice slice $h1\ell$ digitally reconstructed directly from the measured frames for phase II ($B2_1, Z' = 5$).....	234
Figure 6.7 The displacement ellipsoids (50% probability level) of the asymmetric unit and one formula unit of the compound $[\text{Ni}(\text{H}_2\text{O})_2(\text{MeCN})(\text{NO}_3)_2] \cdot (15\text{-crown-5}) \cdot \text{MeCN}$ respectively in phase I at 243 K and in phase II at 90 K.....	235
Figure 6.8 The displacement ellipsoids (50% probability level) of the $[\text{Ni}(\text{MeCN})(\text{H}_2\text{O})_2(\text{NO}_3)_2]$ metal complex in phase III at 150 K without and with the disorder of the monodentate nitrate ligand	239
Figure 6.9 The displacement ellipsoids (50 % probability level) of the asymmetric units of phase III (at 150 K) and phase IV (at 90 K) of the compound $[\text{Ni}(\text{MeCN})(\text{H}_2\text{O})_2(\text{NO}_3)_2] \cdot (15\text{-crown-5}) \cdot \text{MeCN}$	241
Figure 6.10 Plots of the modified cell dimensions a , b and c (Å) of the compound $[\text{Ni}(\text{MeCN})(\text{H}_2\text{O})_2(\text{NO}_3)_2] \cdot (15\text{-crown-5}) \cdot \text{MeCN}$ versus T (K).....	245
Figure 6.11 Plots of the modified cell dimensions β (°) and V (Å ³) of the compound $[\text{Ni}(\text{MeCN})(\text{H}_2\text{O})_2(\text{NO}_3)_2] \cdot (15\text{-crown-5}) \cdot \text{MeCN}$ versus T (K).....	246
Figure 6.12 The set of hydrogen bond interactions observed in phase IV of the compound $[\text{Ni}(\text{MeCN})(\text{H}_2\text{O})_2(\text{NO}_3)_2] \cdot (15\text{-crown-5}) \cdot \text{MeCN}$ along the c direction (<i>i.e.</i> , along the 1-D H-bonded chains)	248
Figure 6.13 Projections of the asymmetric units of phases I, II and III down the normal to the plane (1 0 0).....	254
Figure 6.14 Projections of five lattice acetonitrile molecules found in the phases I, II and III down the normal to the plane (1 0 0).....	256
Figure 6.15 Projections of the crystallographically independent 15-crown-5 molecules down the a direction for phase II and down the normal to the plane (-4 0 3) for the phases III and IV	258
Figure 6.16 (a) Part of the reciprocal lattice slices $h0\ell$ digitally reconstructed from the measured frames at 130, 140 and 150 K. (b) Temperature dependence of the integrated intensities of the 10 strongest $h0\ell$ reflections with $\ell = 2n + 1$ monitored between 90 and 150 K.....	260
Figure 6.17 (a) Parts of the reciprocal lattice $h1\ell$ digitally reconstructed directly from the measured frames given for 230 (phase III) and 233 K (phase II). (b) Parts of the reciprocal lattice $h3\ell$ digitally reconstructed directly from the measured frames given for 239 (phase II) and 243 K (phase I)	262

Figure 6.18 Projections of the units cells down the a direction for phases III and I and down the normal to the plane (1 0 0) for phase II	263
Figure 6.19 Projections down the c direction of phases IV of $[\text{Ni}(\text{H}_2\text{O})_6](\text{NO}_3)_2 \cdot (15\text{-crown-5}) \cdot 2\text{H}_2\text{O}$ and $[\text{Ni}(\text{MeCN})(\text{H}_2\text{O})_2(\text{NO}_3)_2] \cdot (15\text{-crown-5}) \cdot \text{MeCN}$	267
Figure 7.1 Projections of the asymmetric units of the $Z' = \frac{1}{4}, \frac{1}{2}$ and 1 phases of the system $[\text{Ni}(\text{H}_2\text{O})_6](\text{NO}_3)_2 \cdot (15\text{-crown-5}) \cdot 2\text{H}_2\text{O}$ down the direction of the 1-D H-bonded chains (<i>i.e.</i> , the c direction)	281
Figure 7.2 Projections of the asymmetric units of the $Z' = \frac{1}{2}, 1$ and 2 phases of the system $[\text{Ni}(\text{H}_2\text{O})_2(\text{MeCN})(\text{NO}_3)_2] \cdot (15\text{-crown-5}) \cdot \text{MeCN}$ down the direction of the 1-D H-bonded chains (<i>i.e.</i> , the c direction).....	283

LIST OF FILES

Tab01.pdf.....	120 KB
Tab02.pdf.....	120 KB
Tab03.pdf.....	117 KB
Tab04.pdf.....	121 KB
Tab05.pdf.....	51 KB
Tab06.pdf.....	35 KB
Tab07.pdf.....	38 KB
Tab08.pdf.....	42 KB
Tab09.pdf.....	71 KB
Tab10.pdf.....	31 KB
Tab11.pdf.....	41 KB
Tab12.pdf.....	26 KB
Tab13.pdf.....	50 KB
Tab14.pdf.....	110 KB
Tab15.pdf.....	31 KB
Tab16.pdf.....	61 KB
Tab17.pdf.....	98 KB
Tab18.pdf.....	33 KB
Tab19.pdf.....	41 KB

Chapter One

-

Introduction

Preamble

What is X-ray crystallography? X-ray crystallography provides a means of determining the crystal and molecular structure by analysis of the diffraction pattern resulting from the interaction of X-rays with crystals. Crystals are built of regularly repeating blocks of constituents (*i.e.*, atoms, ions, or molecules). In a single crystal, these blocks (or unit cells) have a characteristic orientation (*i.e.*, the crystal is essentially a stack of identical blocks). The unit cell itself is built of smaller, symmetry-independent units known as the asymmetric unit. However, not all crystals are single. In twinned crystals, there exist separate domains consisting of blocks that have two or more orientations with a distinct mathematical relationship (*e.g.*, a non-crystallographic 2-fold rotation). In addition, a crystalline sample could be an aggregate of two or more single crystals stuck together in some random arrangement or it could be a powder (*i.e.*, a mass of microscopic crystalline particles).

X-rays are electromagnetic radiation with wavelength in the range of 0.1 to 100 Å. When X-rays with a wavelength comparable to the atomic scale (*i.e.*, $\lambda \sim 1 \text{ \AA}$), pass through a crystal, the radiation interacts with the electrons of the atoms and is scattered. As a result of the periodic nature of the crystal, these scattered X-rays interfere, resulting in the phenomenon known as diffraction. It is the analysis of the diffraction pattern that allows determination of electron density within crystals, which in turn gives molecular structure, crystal packing, etc.

Why is X-ray structure determination important? In order to understand the properties of matter such as chemical reactivity, the shape and size of molecules must be known. To understand physical properties of solids, the arrangements of these molecules in the solid state must be known. Modern crystallography has benefitted greatly from advances in both instrumentation and software. As a result, the number of new crystal structures has grown rapidly for the last decade. In 1996, the Cambridge Structural Database¹ (hereafter, the CSD; Allen *et al.*, 1983; Allen *et al.*, 1987; Allen, 2002; Orpen *et al.*, 1989) contained about 160,000 small-molecules crystal structures. In 2006, the CSD listed more than 400,000 crystal structures².

Truly challenging crystallographic problems such as pseudosymmetry, modulated superstructures, twinning, disorder, supramolecular chemistry, which were difficult or impossible until recently can now be undertaken, provided sufficient care is taken. X-ray structure determination is of paramount importance because it provides the chemist, biologist and physicist an otherwise unattainable understanding of these areas. Advances in these areas have led to new and remarkable applications in solid state chemistry (Kitagawa *et al.*, 2004; Sato *et al.*, 2006). X-ray crystallography also plays a major role in structural biology (*i.e.*, the structural studies of macromolecules such as proteins and nucleic acids).

¹ The CSD includes only small-molecule organic and organometallic crystal structures.

² Most crystals in the CSD are simple (*i.e.*, crystals are ordered, not twinned and have one or two formula units in the asymmetric unit). If most crystals were not so simple, the CSD would not have grown so fast.

Problems

Given the very large number of known crystal structures (see the CSD) it is now possible to make rational predictions about certain aspects of crystal structures. For example, bond lengths and angles are predictable (Bruno *et al.*, 2004); conformations are often predictable (Bruno *et al.*, 2004); H-bonding is somewhat predictable. But, crystal packing is not predictable. For many compounds, several crystal structures are known to exist, *i.e.* these polymorphs (polymorphs of a given compound have same chemical composition but different crystal structures) are generally not predictable (but can be vitally important); phase transitions are not predictable³. Thus far, models for calculating the relative energies of packing arrangements (observed and hypothetical) are not especially successful in predicting the structures of even quite simple molecules.

Are crystal structures predictable? Eight years ago, a terse monosyllabic negative reply to this question was given by Gavezzotti⁴. Has anything important happened since then to change the answer? Experts in the field have tried their skills in two blind tests and discussed their methods, together with their successes and failures, at two meetings organized by the Cambridge Crystallographic Data Center in 1999 and 2001.^{5,6} Although some successes were reported, no method gave consistently reliable predictions (Dunitz, 2003).

³ This statement implies that the temperature at which a phase transition takes place cannot be predicted. However, the positive term $T\Delta S$ must offset the positive term ΔH when a system passes through a phase transition as T is raised.

⁴ Gavezzotti, 1994.

⁵ Lommerse *et al.*, 2000.

⁶ Motherwell *et al.*, 2002.

These models do not take into account subtle complications such as disorder and modulations, crystal defects and impurities. Moreover, they do not effectively include energetics and kinetics of crystal nucleation and growth. On occasion the thermodynamically most stable crystal form is not the first to nucleate, consequently, such systems cannot be modeled by the currently available theoretical models.

Crystal composition is not completely predictable because the same substance can crystallize with different amounts or types of solvent molecules, and this can depend upon experimental conditions of crystal growth. This variation has been called pseudopolymorphism. The use in the literature of this term has been debated recently and there is not yet any consensus⁷. In order to avoid confusion, the term pseudopolymorphism is not used in the dissertation.

Questions regarding crystal packing, polymorphism, phase transitions and phase relationships are of very great importance for pharmaceutical and chemical industries because polymorphs of a given compound may differ significantly in properties. More investigations of known⁸ and new systems having multiple related phases may help to elucidate new principles that can answer some of these questions.

⁷ Pseudopolymorphs are crystals formed by the same substance crystallized with different amounts or types of solvent molecules, *e.g.* hydrates or solvates (Nangia, 2006). In other words, pseudopolymorphs have different molecular compositions. Bernstein and Seddon emphasized that the term *pseudopolymorph* should be no longer used in the literature since its definition is flawed and argued in favor of the terms *solvates* and *hydrates* instead (Bernstein, 2005; Seddon, 2004). On the other hand, Desiraju claimed that the word *solvate* is too sterile and argued in favor of retaining the term *pseudopolymorph* (Desiraju, 2004; Nangia, 2006). The interpretation of the term pseudopolymorph may appear confusing since *pseudo* may stand for *close to* or *false* or even *artificial*. Pseudopolymorphs are not polymorphs since they do not have the same chemical composition.

⁸ The system $[M(\text{H}_2\text{O})_2(15\text{-crown-5})](\text{NO}_3)_2$, $M = \text{Mg, Mn, Fe, Co, Ni, Cu}$ and Zn , was found to be a good candidate. But the research should not be restricted to known systems.

Aims of the Dissertation

The dissertation is only concerned with small-molecule crystallography. The principal areas of interest explored are: polymorphism, phase transitions and modulated superstructures⁹. Both polymorphism and phase transitions have been subjected to intense investigation¹⁰. Nonetheless, they are not particularly well understood, primarily because of the lack of a suitable theory.

Most papers on phase transitions deal with the structures and properties of the individual phases and the differences between them in order to infer the driving force for the transformation. This is a combination of enthalpic (packing) and entropic (generally vibrational) factors. There are relatively few papers about the actual transition directly viewed by microscopic techniques in order to infer the mechanism, and not many about changes in crystal structure, including changes in cell dimensions, as the system passes through the transition... Lacunae in the literature are noted in the hope that this will encourage research to fill the gaps (Herbstein, 2006).

Previous investigations from this laboratory of systems that have solid-solid phase transitions during which there is no significant loss of crystallinity were extended. Additional systems were found with such transitions and these too were studied. These investigations were based in part on using a method to monitor changes in structure as the systems undergo a transition. The outcome should contribute to a better understanding of phase transitions (*i.e.*, location, mechanism, prediction).

⁹ The modulated superstructures have been investigated as they occur in a single system formed from a divalent metal ion, nitrate ions, 15-crown-5 molecule and water molecules.

¹⁰ Herbstein (2006) wrote ‘Solid-state phase transitions have been the subject of intense investigation for perhaps 200 years; their relevance to mineralogy, condensed matter physics, chemistry and crystallography is obvious. The literature is voluminous and confusing; in particular, many mechanisms have been proposed for such transitions and most systems are treated *sui generis*’.

Structures with $Z' > 1$ (*i.e.*, structures with at least two crystallographically independent formula units) are modulated when they are related by small fluctuations in position, orientation, occupation and/or thermal motion. Refinements of modulated structures can be challenging because of the lack of information in the diffraction pattern. The refinements of several modulated structures will be discussed in the dissertation.

Organization of the Dissertation

The dissertation is divided into seven chapters. A short overview of polymorphism, phase transitions, and modulated structures, as well as a few important ideas in crystallography, are discussed in the introductory chapter. References to some significant papers related to polymorphism and phase transitions are also given.

Chapters 2 and 3 follow up the investigation of the series of polymorphic systems $[M(\text{H}_2\text{O})_2(15\text{-crown-5})](\text{NO}_3)_2$, $M = \text{Mg, Mn, Fe, Co, Cu}$ and Zn (Hao *et al.*, 2005; Hao, Sieglar *et al.*, 2005). The synthesis of the analogous Ni complex, which took considerable effort to make, was eventually achieved (Sieglar, Hao *et al.*, unpublished results) and is discussed in Chapter 3. In the course of his research, Hao¹¹ discovered a large set of related phases with $Z' > 1$, but the refinement of one phase for $M = \text{Zn}$ with unusually high- Z' (8) remained unfinished. The analogous $Z' = 8$ phase was also found for $M = \text{Mg}$ and Fe (Hao, Sieglar *et al.*, 2005; Hao, Sieglar *et al.*, unpublished results). The refinements of these three modulated structures are discussed in Chapter 2. Chapter 3 is concerned with the study of the two phases of $[\text{Ni}(\text{H}_2\text{O})_2(15\text{-crown-5})](\text{NO}_3)_2$ and several Ni(II) complexes including Ni^{2+} , NO_3^- , 15-crown-5 and solvent (methanol, water) that were found during attempts to synthesize $[\text{Ni}(\text{H}_2\text{O})_2(15\text{-crown-5})](\text{NO}_3)_2$. This chapter emphasizes that $[\text{Ni}(\text{H}_2\text{O})_2(15\text{-crown-5})](\text{NO}_3)_2$ differs in several important ways from the series of compounds $[M(\text{H}_2\text{O})_2(15\text{-crown-5})](\text{NO}_3)_2$, $M = \text{Mg, Mn, Fe, Co, Cu}$ and Zn .

¹¹ Xiang Hao was a former graduate student of Dr. C. P. Brock. He received his PhD in chemistry from the University of Kentucky in 2005.

Attempts to synthesize the target compound $[\text{Ni}(\text{H}_2\text{O})_2(15\text{-crown-5})](\text{NO}_3)_2$ also led to three compounds: $[\text{Ni}(\text{H}_2\text{O})_6](\text{NO}_3)_2 \cdot (15\text{-crown-5}) \cdot n\text{H}_2\text{O}$, $n = 1$ and 2 , and to $[\text{Ni}(\text{H}_2\text{O})_2(\text{MeCN})(\text{NO}_3)_2] \cdot (15\text{-crown-5}) \cdot \text{MeCN}$, all of which are polymorphic systems. These three polymorphic systems are discussed separately in Chapters 4, 5 and 6. All phase transitions were found to be reversible with no significant loss of crystallinity throughout the phase sequences. The phase sequences of two of these polymorphic systems¹² were found to include three solid-solid phase transitions and four phases, which make them very unusual. Parts of these phase sequences are surprisingly similar. As the temperature is raised, both phase sequences go from a more ordered low- Z' phase ($Z' = 1$) through an intermediate modulated high- Z' phase ($Z' = 5, 7$) to a more disordered low- Z' phase ($Z' = \frac{1}{2}$). This result is very unusual. A method for studying such sets of phase transitions is described in these chapters. The results of these studies might help to resolve the apparent conflict between the views of Mnuykh and Ubbelohde about phase transitions in molecular crystals (Herbstein, 2006).

In all Ni(II) complexes presented in the dissertation (see Chapters 2 \rightarrow 6), the motif of alternating $[\text{Ni}(\text{H}_2\text{O})_2L_4]^{2+}$ ions ($L = \text{H}_2\text{O}, \text{MeOH}, \text{NO}_3^-$)¹³ or $[\text{Ni}(\text{H}_2\text{O})_2LL'_2]$ metal complexes ($L = \text{MeCN}; L' = \text{NO}_3^-$) and 15-crown-5 molecules always occurs along one dimension in the crystal structures.

The general conclusions of the dissertation are discussed in Chapter 7.

¹² $[\text{Ni}(\text{H}_2\text{O})_6](\text{NO}_3)_2 \cdot (15\text{-crown-5}) \cdot 2\text{H}_2\text{O}$ and $[\text{Ni}(\text{H}_2\text{O})_2(\text{MeCN})(\text{NO}_3)_2] \cdot (15\text{-crown-5}) \cdot \text{MeCN}$.

¹³ Depending on the compounds, there may be a combination of several types of ligands for the $[\text{Ni}(\text{H}_2\text{O})_2L_4]^{2+}$ ions.

Some Important Ideas in Crystallography

A short description of a few crystallographic ideas is given in the subsequent sections to ease the reading of the dissertation.

Z, Z'

Z and Z' are crystallographic quantities used to describe the crystal packing of a given compound. Z corresponds to the number of formula units (*i.e.*, the units of the chemical compound) in the unit cell. In the context of this thesis, the more useful quantity is Z' , which corresponds to the number of formula units in the asymmetric unit. The asymmetric unit is defined as the symmetry-independent part of the unit cell. The unit cell is built from the asymmetric unit and the associated units generated by the symmetry operations of the space group in question (*e.g.*, inversion center, twofold rotation axis, mirror plane, *etc.*).

Disorder

Ideally, crystals are built of atoms, ions or molecules regularly repeated in three-dimensional space and are ordered. In reality, defects occur in the crystal lattice and the long-range order may be imperfect, leading to disorder. This disorder can be dynamic or static. Dynamic disorder is the result of vibrations in the crystal lattice (Dunitz, 1979; Goetha & Howard; 2004) and is therefore temperature-dependent.

Static disorder occurs when a constituent (*i.e.*, an atom, an ion or a molecule) has more than one orientation in the crystal lattice and when transitions between them are very unlikely. Since the X-ray diffraction analysis leads to the determination of the average unit cell over time and space (Dunitz, 1979), the structure observed is an average. Static disorder requires that the different orientations have nearly the same space-filling properties (see Figure 1.1).

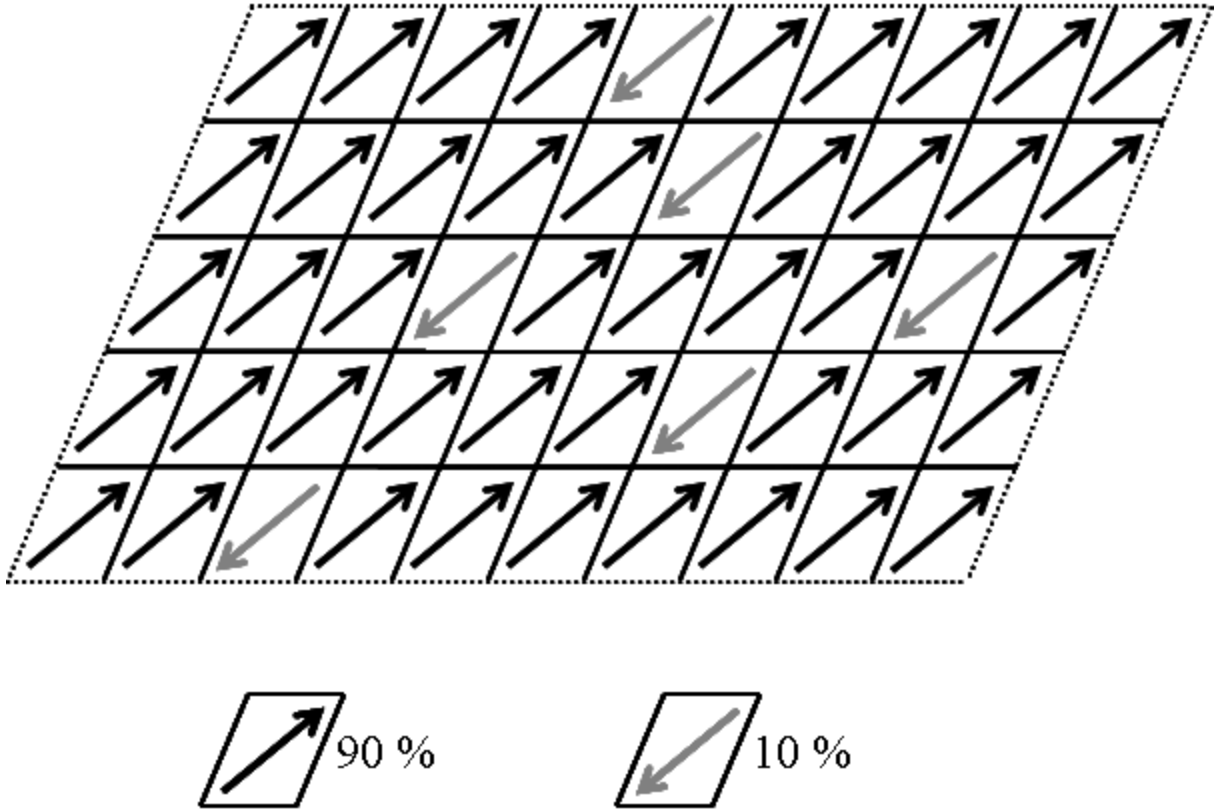


Figure 1.1. Scheme showing blocks of a constituent (*i.e.*, an arrow) in a two-dimensional space. Static disorder occurs because the unit structure has two different orientations randomly distributed in the lattice. The two different orientations are up (black arrows) and down (gray arrows). In this scheme, the unit structure has the up orientation most of the time (90 %) but has the down orientation some of the time (10%). In the case of disorder, the distribution of the two kinds of cells is random; the number of mistakes made during crystal growth is large.

Twinning

Twinning is the result of separate intergrowth of at least two separate single-crystal components joined together in some definite mutual orientation (Giacovazzo *et al.*, 1992). As a result, the components of a twinned crystal have the same crystal structure but have different orientations of the cell vectors. The components of a twinned crystal are related by a twin law (*i.e.*, a symmetry operation that is not part of the space group). For twinned crystals, the crystal is built of at least two domains for which the unit structure has different orientations (see Figure 1.2). Twinning can occur when the unit cell has higher symmetry than that of the space group of the crystal structure (*e.g.*, a triclinic unit cell can appear to be monoclinic when the α and γ angles are very close to 90°).

Inspection of the reconstructed reciprocal lattice slices (*i.e.*, the parts of the diffraction pattern) may or may not be helpful to confirm the existence of twinning. Three types of twinning can be distinguished:

- (i) non-merohedral twinning
- (ii) merohedral twinning
- (iii) pseudomerohedral twinning

In the case of non-merohedral twinning, the twin law does not belong to the crystal system (*e.g.*, the twin law may correspond to a twofold axis in the triclinic system). Non-merohedral twinning can be generally identified by inspection of the reconstructed reciprocal lattice slices. For a non-merohedrally twinned crystal with two different components, reflections of one twin component do not completely overlap with reflections of the other twin component.

In the case of merohedral twinning, reflections from each twin component are exactly superimposed so that the existence of twinning may not be directly identified by inspection of the reconstructed reciprocal lattice slices. Merohedral twinning can occur if the twin law is a symmetry operator of the crystal system but not of the Laue group (*i.e.*, diffraction symmetries) of the crystal system (*e.g.*, in the case of the tetragonal system, the twin law may correspond to two mirror planes so that the diffraction symmetry appears to be $4/mmm$ even though the true diffraction symmetry is $4/m$).

In the case of pseudomerohedral twinning, reflections from each twin components are nearly superimposed. In the latter case, the existence of twinning may or may not be found by inspection of reconstructed reciprocal lattice slices.

The determination of twinned crystal structures is possible nowadays because of the development of several programs, such as *GEMINI* (Sparks, 1999) or *PLATON-TwinRotMat* (Spek, 2005), that attempt to identify the twin law. Once the twin law has been identified and an appropriate way of partitioning the data is found, conventional means of solution and refinement can be used, albeit with some additional complexity.

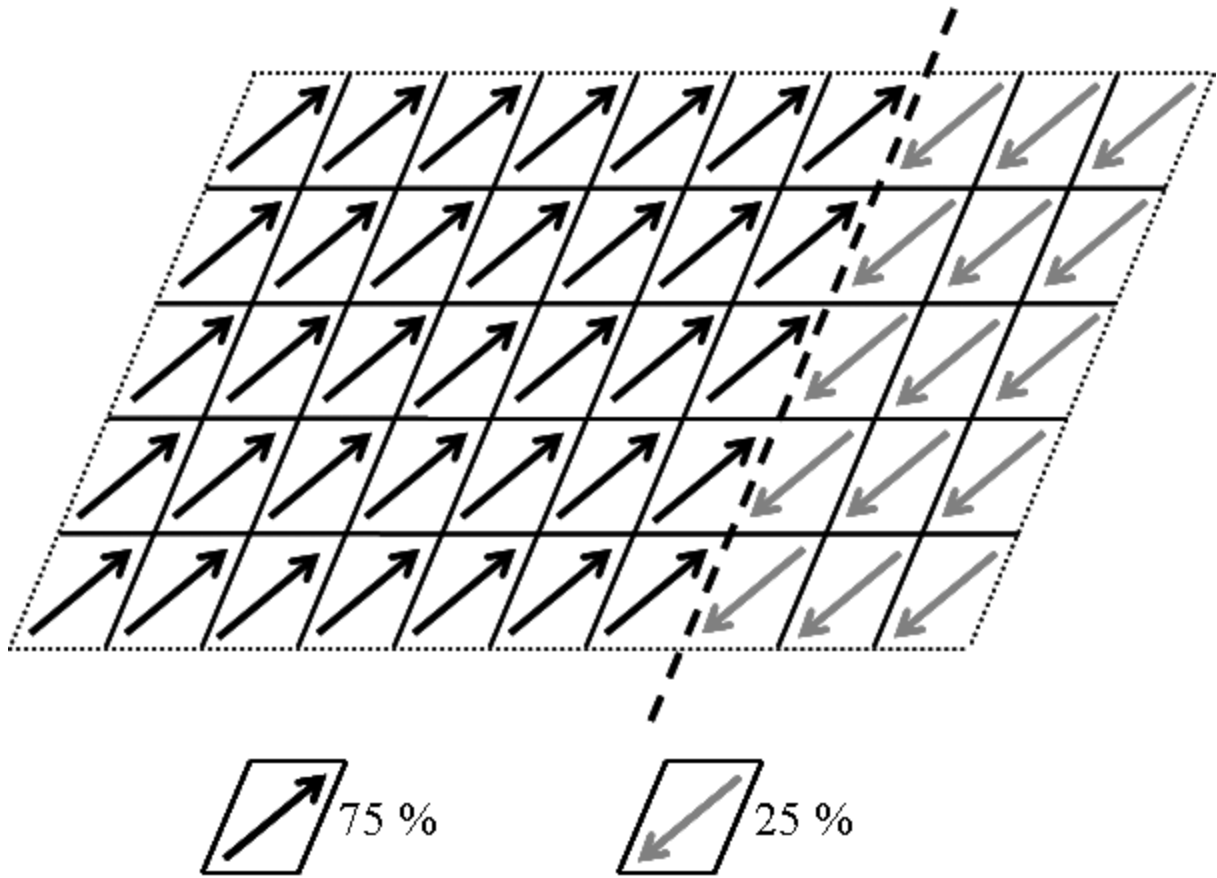


Figure 1.2. Schematic example of an inversion twin (*i.e.*, the twin components are related by inversion symmetry) showing blocks of a constituent (*i.e.*, an arrow) in a two-dimensional space. Twinning occurs because of the occurrence of at least two domains (only two domains are shown) for which the unit structure has different orientations. The different orientations are up (black arrows) or down (gray arrows). Domain 1 is built of blocks for which the unit structure has the up orientation and domain 2 is built of blocks for which the unit structure has the down orientation. In this scheme, the fractional contributions for domains 1 and 2 are 0.75 (or 75%) and 0.25 (or 25 %). The boundary between the two domains is showed by thick black dashed lines. In the case of twinning, the two kinds of unit cells are segregated; the number of mistakes made during crystal growth is relatively small.

Polymorphism and Phase Transitions

Polymorphism

What is polymorphism? The concept of polymorphism is complex¹⁴; even the definition of the term polymorphism is a matter of debate. McCrone defined polymorphism as follows:

A solid crystalline phase of a given compound resulting from the possibility of at least two different arrangements of the molecules of that compound in the solid state (McCrone, 1965).

The concept of having more than one crystalline form of a given compound (Bernstein, 2002) may be more suitable since there is no inference made about the magnitudes of the differences between the two structures. In other words, polymorphism is the existence of different crystal structures with the same chemical composition. In the case of single-crystal studies, two polymorphs must have different diffraction patterns. Therefore, single-crystal X-ray diffraction is a valuable technique to characterize polymorphism and solid-state phase transitions.

Polymorphic systems are defined as systems having at least two polymorphs. In the literature, polymorphs are also referred to as forms or phases. The numbering for polymorphs (Toledano *et al.*, 1998) is given by Roman numerals¹⁵ (I, II, III, *etc.*) or Greek letters (α , β , γ , *etc.*).

The study of polymorphism is especially relevant in the pharmaceutical industry because polymorphs of a drug may have dramatically different properties (*e.g.*, solubility, bioavailability, *etc.*). Other properties that are subject to change (but not necessarily) between different polymorphs are: crystal habit, melting point, chemical reactivity, dissolution rate, optical and electrical properties, *etc.*

¹⁴ The phenomenon of polymorphism cannot be predicted reliably.

¹⁵ In the dissertation, Roman numerals are chosen to refer to different phases of a given polymorphic system. The use of Greek letters may appear confusing because α , β , γ refer also to the unit-cell angles.

Phase Transitions¹⁶

Phase transitions can be classified in various ways. A first approach (Ehrenfest, 1933) is focused on the order of phase transitions. A phase transition is defined as n^{th} order when the n^{th} derivative of the Gibbs free energy with respect to temperature and pressure is discontinuous at the transition point¹⁷. First and second-order phase transitions are the most common in solid-state chemistry, although higher orders may exist. First-order phase transitions show a discontinuity in the first derivative of the Gibbs free energy with an intensive variable (generally the temperature T because the pressure P is maintained constant for most single-crystal X-ray experiments). As a result, discontinuities are also observed for extensive physical properties (such as volume, enthalpy and entropy) of the system (Herbstein, 2006). A change in enthalpy (latent heat) is associated with first-order phase transitions. Second-order phase transitions show a discontinuity in the second derivative of the Gibbs free energy with an intensive variable. There is no latent heat associated with second-order phase transitions.

In single-crystal X-ray experiments, the crystallographer is interested in studying phase transitions between two solid phases. These transitions are named solid-solid phase transitions (or solid-state phase transitions)

The relationship between pairs of phases in systems that have at least two phases can also be described as enantiotropic or monotropic (Westrum & McCullough, 1963). In an enantiotropic system the transition between two phases occurs below the melting temperatures of the two phases. At least one solid-solid phase transition can be observed for enantiotropic polymorphic systems. In a monotropic system, the transition between two phases would occur at a temperature above the melting points of the individual phases (see Figure 1.3). No solid-solid phase transition can be observed for monotropic polymorphic systems.

¹⁶ It is implied that the terminology ‘phase transitions’ denote ‘solid-solid phase transitions’ for all investigations presented in this dissertation.

¹⁷ The Gibbs free energies of the two phases are the same at the transition point.

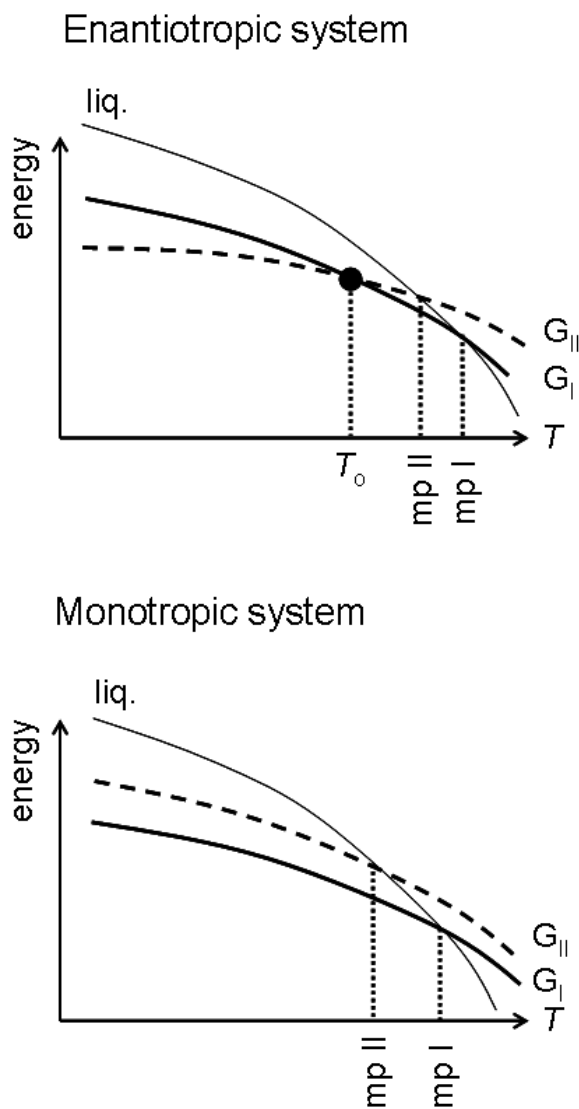


Figure 1.3. Schematic plots of the Gibbs free energy G vs T for enantiotropic and monotropic systems with two phases. For an enantiotropic system, the reversible solid-solid phase transition occurs below the melting points of polymorphs I and II (mp I and mp II). The intersection of the Gibbs free energy functions associated with polymorphs I and II corresponds to the transition point. Below the temperature of the transition point T_0 , polymorph II is stable because G_{II} is lower than G_I . Between T_0 and mp I, polymorph I is stable because G_I is lower than G_{II} . For a monotropic system, the phase transition must occur above mp I and mp II.

Investigation of Enantiotropic¹⁸ Polymorphic Systems

Investigations of enantiotropic polymorphic systems are based on determining the temperatures of solid-solid phase transitions. The temperature range (T -range) of stability for a given phase can be determined precisely, but the temperatures determined may depend on the method of experimentation used and the sizes of the crystals studied. There are several techniques that can be used to investigate enantiotropic polymorphic systems. The following techniques are often used to characterize polymorphic systems: differential scanning calorimetry (hereafter, DSC), optical microscopy and single-crystal X-ray diffraction. Other techniques (*e.g.*, NMR spectroscopy, atomic force microscopy) can sometimes be used, but these three techniques are used most often.

¹⁸ Enantiotropic polymorphic systems only are discussed in the dissertation. In order to limit the boundaries of the dissertation, there will be no further discussion about monotropic polymorphic systems.

Differential Scanning Calorimetry

DSC is a thermoanalytical technique that consists of recording the difference in the amount of heat absorbed or released between a sample, *i.e.* fine powder of single crystals¹⁹ contained in an aluminum pan, and a reference (aluminum pan) as a function of temperature. DSC measurements are recorded at constant pressure so that the heat flow corresponds to an enthalpy change ($\Delta H = q_p$). As the system passes through a phase transition, the enthalpy change is usually positive on heating (because the system may absorb heat) in which case it is negative on cooling (because the system may release heat). Subsequently, DSC traces show peaks on heating and cooling if the reversible solid-solid phase transitions are first-order. There should be no peak observed in the DSC traces for second-order phase transitions because no latent heat is associated with such transitions.

The onset temperature T_{onset} ²⁰ found for a peak is slightly different from the actual temperature of the phase transition. T_{onset} depends mainly on the nature of the sample (fine powder of single crystals or single crystals) and the heating (or cooling) rates. The behaviors of the sample on heating and cooling may not be the same because of the occurrence of hysteresis. When hysteresis occurs, the onset temperature on cooling is found to be lower than the onset temperature on heating.

It should be noted that the transition temperature given by DSC (differential scanning calorimetry) measurements is, in general, not equal to T_o . The onset temperatures (T_H , T_L for heating and cooling, respectively) often given are operational values dependent on sample quality and history, and heating (or cooling) rates). On heating, the transition from the low-temperature (L) phase to the high-temperature phase (H) begins at T_H , some degrees above T_o ; on cooling the H and L transitions begins at T_L , some degrees below T_o ...an approximation to T_o is sometimes obtained by averaging heating and cooling onset temperatures (Herbstein, 2006).

¹⁹ In DSC experiments, the sample preparation may matter. Samples can be either single crystals (of a size used for single crystal X-ray diffraction) or crystallites (*i.e.*, fine powder of single crystals). The latter type of sample is preferred because the thermal gradient is minimized when the sample is thinner and smaller. Using fine powder of single crystals improves thermal contact.

²⁰ The temperature at which the maximum of a peak is found.

One advantage of DSC over the other techniques is that the approximate temperature of a phase transition may be located relatively quickly. However, this technique is not able to locate second and higher-order phase transitions. DSC measurements are not always reproducible and may depend on the choice of heating rates (or cooling rates). Solid-solid phase transitions may be missed if a too-fast cooling rate is chosen. In cases for which the enthalpy change associated with a solid-solid phase transition is relatively low ($\sim 0.1 \text{ kJ.mol}^{-1}$ and lower), it has been sometimes observed that the solid-solid phase transition may be missed if the heating rate is too slow (see the section related to the DSC measurements in Chapter 2).

Optical Microscopy

Optical microscopy is a powerful technique that attempts to observe directly *via* a sophisticated microscope the behavior of crystals under controlled temperature conditions. Cold-stage microscopy is concerned with low-temperature phase transitions (typically below room temperature conditions) and hot-stage microscopy is concerned with high-temperature phase transitions (typically above room temperature conditions). Optical microscopy provides direct observations for structural changes as the system (*i.e.*, single crystal) is passing through a phase transition. Depending on the quality of the temperature controller and the heating (or cooling) rate, the temperature of a phase transition is generally well located. Expertise in this technique has led to some inferences about mechanism²¹ of solid-solid phase transitions (Mnyukh, 2001), even though the conclusions drawn from optical microscopy may be considered controversial (Ubbelohde, 1957).

Skilful use of the microscope can give useful supporting information about structural changes in transformation in solids, though the conclusions are necessarily more superficial (Ubbelohde, 1957).

²¹ In his book entitled 'Fundamentals of Solid-State Phase Transitions, Ferromagnetism and Ferroelectricity', Mnyukh claims that all first-order enantiotropic solid-solid phase transitions proceed by a nucleation-growth mechanism.

Single-Crystal X-Ray Diffraction

Single-crystal X-ray diffraction under controlled temperature conditions provides a large amount of information on the nature of solid-solid phase transitions. Given sufficient temperature control and good sample quality, data can be collected over the temperature range of interest and may therefore be analyzed as a function of temperature. Although this experiment can be lengthy, the information collected is generally very valuable. Unlike the two previous techniques, single-crystal X-ray diffraction provides information about the atomic arrangements in the crystal. In other words, if structural changes (occurring at the atomic scale through a solid-solid phase transition) can be monitored as a function of temperature, the conclusions drawn regarding the nature of solid-solid phase transitions may be very significant.

One way to locate a solid-solid phase transition is to look at the variations of the cell dimensions with temperature (*i.e.*, the temperature dependence of the cell dimensions). Provided that enough data were collected over a well defined T -range, plots of the cell dimensions (*i.e.*, a , b , c , α , β , γ and consequently V) or their ratios as a function of temperature may show some discontinuities or significant changes at a transition point (Bendeif *et al.*, 2005; Barnett *et al.*; 2006, David *et al.*, 2006).

Collecting full data sets, rather than limited data sets, is generally wise since more information can be obtained. Doing so allows reconstruction of the reciprocal lattice slices (*i.e.*, parts of the diffraction pattern) directly from the measured frames. Because two phases of a given compound have different diffraction patterns, it is straightforward to locate the solid-solid phase transition by examining the change in the diffraction patterns near the transition point.

For some phase transitions, some classes of reflections may appear or disappear at the transition point. In this case, the integrated intensities of some classes of reflections can be monitored as a function of temperature and the solid-solid phase transition can be located (Schranz *et al.*, 2005). The case of naphthazarin C provides a good example of that type of inspection (Herbstein *et al.*, 1985).

Solving and refining the structures for each phase of a polymorphic system at various temperatures²² is an additional way of studying phase transitions. The understanding of structural changes that may occur near the transition point might lead to a postulate of the mechanism of the phase transitions.

²² Nowadays, collecting full data sets at a large number of temperatures is feasible without any major effort because CCD diffractometers (introduced in the late 1990's) make data collections much faster than when serial diffractometers were used. For most structures, a few hours up to half-days are generally enough to collect full data sets using CCD diffractometers, whereas collections of full data sets can take days (and sometimes weeks for structures with very large unit cells) using serial diffractometers.

Deduction of the Mechanism of Some First-Order²³ Enantiotropic Phase Transitions

How does a first-order enantiotropic phase transition take place? The answer is certainly not trivial although some deductions to the mechanism of some first-order enantiotropic solid-solid phase transitions have been recently discussed (Herbstein, 2006). In his review paper, Herbstein distinguished two groups of first-order enantiotropic phase transitions.

In the first group, the structural differences between the low- and high-temperature phases are relatively large, whereas the structural differences are small in the second group. Multiple investigations *via* optical microscopy led to the inference that first-order enantiotropic phase transitions of the first group may proceed by a nucleation and growth mechanism (Mnyukh *et al.*, 1972; Mnyukh *et al.*, 1973; Mnyukh *et al.*, 1975; Mnyukh, 1983; Mnyukh, 2001).

Inferences about the mechanism of first-order enantiotropic phase transitions of the second group are found to be more ambiguous. Ubbelohde introduced the concept of 'hybrid' crystal, *i.e.* a single crystal on average that contains some domains of each of the two phases near the transition point (Ubbelohde, 1962; Ubbelohde, 1966). In the hybrid crystal, the long-range order remains and the domains for the two phases are large enough to produce their own diffraction patterns (as a result, there will be a superposition of the two diffractions patterns). One example²⁴ in the literature (Zuniga & Criado, 1995) might depict the concept of hybrid crystal. This concept was rejected by Mnyukh who claimed that a two-phase mixture takes place near the transition point. In Mnyukh's model, the long-range order within the crystal is lost; the domains are small and are randomly distributed. The diffraction pattern is then the result of the diffraction patterns produced by all individual domains.

²³ Second-order phase transitions are beyond the boundaries of the dissertation and are not discussed further.

²⁴ The compound is 4,4'-dichlorobenzophenone.

Intermediate Phase

The term ‘intermediate phase’ was mentioned in Herbststein’s review paper (Herbststein, 2006) and was referred as a phase that can be thermodynamically stable at intermediate regions (*i.e.*, at temperatures near the transition point) between two single-phase regions. It is however not clear whether this term may be in accordance with Ubbelohde’s concept, which suggests the existence of a *mélange* of the low- and high-temperature phases at temperatures near the transition. One compound²⁵ was found to have an intermediate phase that is not a *mélange* but rather an ordered phase related (but different) to the low- and high-temperature phases (Chernyshov *et al.*, 2003; Chernyshov *et al.*, 2004), even though limited studies have been done to understand the nature of such a phase.

In the dissertation, the term ‘intermediate phase’ will refer to a phase that has a distinctive diffraction pattern, which does not result from the superposition of the diffraction patterns of the low- and high-temperature phases. The intermediate phase may include separate regions of the low- and high-temperature phase that are found within a single unit cell.

Providing a sufficiently precise temperature control, more exhaustive single-crystal X-ray experiments of systems with an intermediate phase might give a better understanding on the nature of such a phase.

²⁵ The compound is $\text{Fe}(\text{2-picolylamine})\text{Cl}_2 \cdot \text{C}_2\text{H}_5\text{OH}$.

Modulated Structures

Modulated structures (or superstructures) are structures with at least two crystallographically independent formula units ($Z' > 1$), which are related by small fluctuations in position, orientation, occupation and/or thermal motion in the unit cell.

In a modulated structure, the period of the fluctuation T (*i.e.*, the period of the modulation) may or may not be an integer multiple of the period of the basic structure t (*i.e.*, the period based on the basic structure). If the ratio T/t is an integer n , the modulated structure is commensurate (commensurately modulated superstructure); if the ratio T/t is not a rational number, the modulated structure is incommensurate (incommensurately modulated superstructure). The cases of incommensurate modulated superstructures (Arackeeva & Chapuis, 2005; Arackeeva & Chapuis, 2006; Rodriguez *et al.*, 2006) are beyond the scope of the dissertation and are not discussed further. More about the latter case can be found in the paper ‘Incommensurate Crystal Structures’ (Van Smaalen, 1995). The unit cell of a modulated superstructure is called the supercell (or true cell). The supercell can be reduced to a smaller unit cell if the magnitudes of the fluctuations go to zero. The smaller unit cell is called a pseudocell (or subcell or basic cell), and is an approximation of the supercell. The fluctuations observed in the supercell are averaged in the pseudocell. The supercell and the pseudocell have respectively the periods T and t . Figure 1.4 summarizes the concept of commensurately modulated superstructures.

How can modulated superstructures be identified? Modulated superstructures have classes of systematically weak reflections. Reconstructed reciprocal lattices slices are very useful to identify classes of strong and weak reflections. The class of the strongest reflections corresponds to the primary (or main) reflections that are associated with the pseudocell. The other classes of reflections correspond to the superstructure (or satellite) reflections (see Figure 1.5). Quantitative examinations of systematic classes of strong and weak reflections can be made using separate Wilson plots (Xia *et al.*, 2001; Xia *et al.*, 2002). These plots are very useful to draw the intensity distribution of some specific classes of reflections.

commensurately modulated superstructure

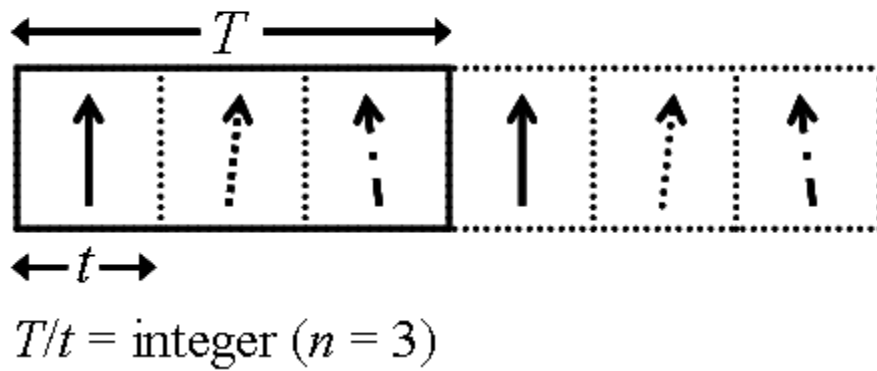


Figure 1.4. Scheme showing a one-dimensional commensurately modulated superstructure. The three crystallographically independent formula units (arrows) suffer from small fluctuations in orientation along one direction. The ratio of the period of modulation T over the period of the basic structure t is an integer n ($n = 3$). The supercell is shown as a black thick box and has the period T . The pseudocell is shown as a black dotted box and has the period t .

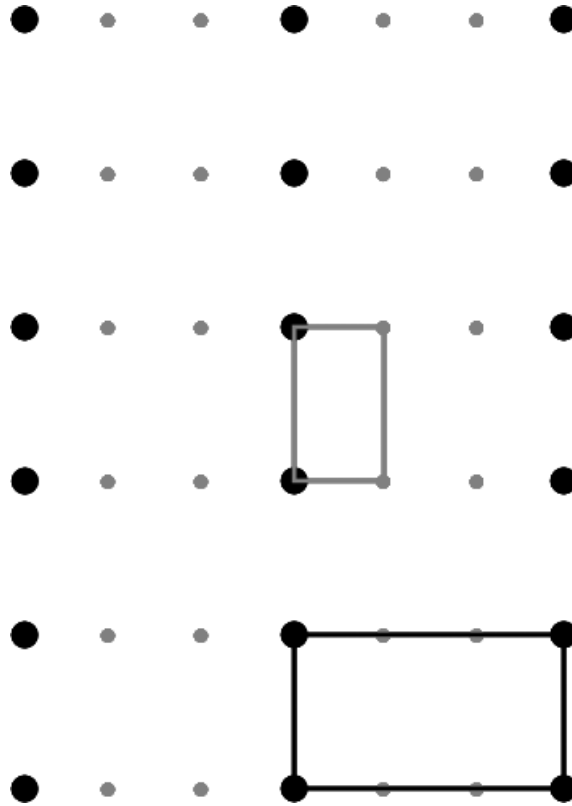


Figure 1.5. Arbitrary reciprocal lattice slice of a commensurately modulated superstructure. The inspection of the reciprocal lattice slice shows that there are two types of reflections. The more intense reflections are called primary (or main) reflections (black, bigger spots). The less intense reflections are called superstructure (or satellite) reflections (gray, smaller spots). The reciprocal pseudocell is defined when the primary reflections only are indexed (*i.e.*, the superstructure reflections are ignored). The reciprocal supercell is defined when the primary and superstructure reflections are both indexed. The reciprocal pseudocell is shown as an unfilled box with black thick lines. The reciprocal supercell is shown as an unfilled box with gray thick lines. In the reciprocal space, the reciprocal pseudocell is three times as big as the reciprocal supercell. In the direct space, the supercell is three times as big as the pseudocell.

The refinement of an n -fold modulated structure in the supercell is not always straightforward (Schmid & Wagner, 2005), although the full refinement gives the best crystallographic description of the structure. If a sufficient amount of information is available [*i.e.*, relatively large number of reflections having $I > 2\sigma(I)$], the independent refinement of atomic displacement parameters²⁶ (hereafter ADPs) of the independent formula units is generally problem-free. In the case of a weak modulation²⁷, many of the superstructures reflections are weak, but are still observable. As a result, there may be too little information available to allow independent refinement of ADPs of the n formula units without the use of constraints (same ADPs) and restraints (similar bond lengths and bond angles) in the refinement process.

The refinement of an n -fold modulated structure in the pseudocell (*i.e.*, only the primary reflections are used in the refinement) is generally more convenient if the modulation is very weak. Pseudocell refinements offer only an approximate description of the structure. One characteristic of pseudocell refinements is that the small fluctuations of the independent formula units are absorbed into the ADPs, which may provide useful information about the nature of the modulation. In the case for which there is insufficient information to refine the structure in the supercell, it may be wise to collect data using a more powerful X-ray source (*e.g.*, Cu $K\alpha$ or synchrotron radiations), *i.e.* to increase the number of reflections with $I > 2\sigma(I)$. Other attempts to refine modulated structures in supercells may be successful using the program suite *JANA2000* (Petricek & Dusek, 2000)²⁸. Calculations and accurate refinements for atomic positional parameters in a superstructure model may be facilitated using the program suite *JANA2000*.

Copyright © Maxime A. Sieglar 2007

²⁶ Anisotropic displacement parameters correspond to the measures of the mean-square amplitudes of the atomic oscillations. The anisotropic displacement parameters are defined by the six parameters U_{11} , U_{22} , U_{33} , U_{23} , U_{13} and U_{12} which describe the magnitudes and the orientations of the vibration ellipsoids.

²⁷ The weaker the modulation (the smaller the fluctuations), the weaker the intensities of the superstructure reflections.

²⁸ Using the program suite *JANA2000* in order to solve modulated superstructures requires to be familiar with the superspace approach [*i.e.*, the reciprocal lattice is defined in a (3 + d) D space], which is well beyond the boundaries of the dissertation. Applying the superspace approach was not necessary because all modulated superstructures discussed in the dissertation were successfully solved and refined using the conventional approach (*i.e.*, the reciprocal lattice is defined in a 3-D space).

Chapter Two

-

Investigations of High-Temperature Phases of $[M(\text{H}_2\text{O})_2(15\text{-crown-5})](\text{NO}_3)_2$, $M = \text{Mg, Zn and Fe}$

Introduction

Recently, Hao *et al.* have re-investigated the system $[M(\text{H}_2\text{O})_2(15\text{-crown-5})](\text{NO}_3)_2$, $M = \text{Mg, Co, Cu and Zn}$ (see Figure 2.1) because all structures reported in the literature were found to be incorrect in some significant way (overlooked inversion symmetry, missed weak reflections, misplaced origin). The discovery of a family of modulated superstructures for this system revealed a rich polymorphic system (Hao, Parkin & Brock, 2005). This study was later extended to the investigations of $[M(\text{H}_2\text{O})_2(15\text{-crown-5})](\text{NO}_3)_2$, $M = \text{Mn, Fe}$ (Hao, Siegler, Parkin & Brock, 2005). In the meantime, Hao *et al.* came across a series of isostructural high-temperature phases for $M = \text{Mg, Zn and Fe}$, which had never been reported before. The three high-temperature phases were found to be modulated superstructures, which all have $Z' = 8$, which is unusually high.

The process of refining superstructures is often problematic because some subsets of the data are often too weak to be measured accurately. Attempts to refine the modulated superstructures with $Z' = 8$ ($M = \text{Mg, Zn and Fe}$) using data measured with a standard CCD diffractometer were carried out with mixed success. A high degree of pseudosymmetry was partly responsible for generating convergence problems in the least-squares refinement. The convergence of the model was achieved using data collected with a more powerful X-ray source (Cu $K\alpha$ radiation) or when data were collected at low temperature (only for $M = \text{Fe}$).

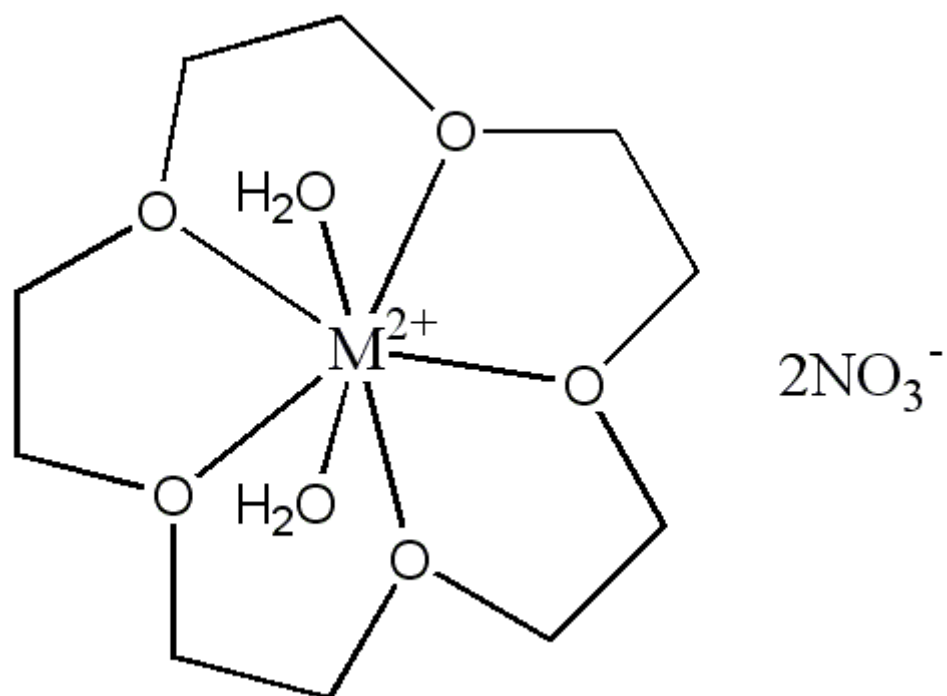


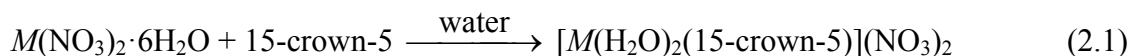
Figure 2.1. The chemical line drawing of $[M(H_2O)_2(15\text{-crown-}5)](NO_3)_2$, $M = Mg, Mn, Fe, Co, Cu$ and Zn . The H atoms of the 15-crown-5 molecule are omitted for clarity.

Experimental

Crystal Growth

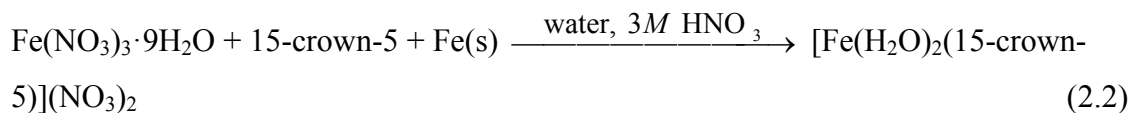
M = Mg, Zn

Colorless crystals of $[M(\text{H}_2\text{O})_2(15\text{-crown-5})](\text{NO}_3)_2$, $M = \text{Mg, Zn}$ were grown at room temperature by evaporation from a water solution equimolar in 15-crown-5²⁹ and $M(\text{NO}_3)_2 \cdot 6\text{H}_2\text{O}$ (see the chemical equation 2.1). Crystals are approximately colorless equidimensional blocks.



M = Fe

Colorless crystals of $[\text{Fe}(\text{H}_2\text{O})_2(15\text{-crown-5})](\text{NO}_3)_2$ were grown from a water solution approximately equimolar in 15-crown-5 and $\text{Fe}(\text{NO}_3)_3 \cdot 9\text{H}_2\text{O}$. Reducing the $\text{Fe}^{3+}(\text{aq})$ using iron powder and an acidic medium (a few drops of 3M HNO_3) was a preliminary but required step to synthesize the desired compound (see the chemical equation 2.2). The mixture was gently warmed to 333 – 343 K to remove some of the excess of water. Crystals, which are colorless thick rods, were grown by cooling the solution at room temperature.



²⁹ It is worth to point out that the structure of the 15-crown-5 molecule has been solved recently (Parsons, 2007).

Differential Scanning Calorimetry Measurements

***M* = Mg, Zn**

The compounds $[M(\text{H}_2\text{O})_2(15\text{-crown-5})](\text{NO}_3)_2$, $M = \text{Mg, Zn}$, were investigated using the 2920 Modulated DSC apparatus from TA instruments. Two solid-solid phase transitions³⁰ for the magnesium complex were identified: $T_{\text{onset}} = 308 \text{ K}$ and 349 K and $\Delta H_{\text{tr}} = 0.73$ and $1.19 \text{ kJ}\cdot\text{mol}^{-1}$ respectively (ΔH_{tr} is given for heating). Two other solid-solid phase transitions³¹ for the zinc compound were found: $T_{\text{onset}} = 304 \text{ K}$ and 365 K and $\Delta H_{\text{tr}} = 0.11$ and $0.51 \text{ kJ}\cdot\text{mol}^{-1}$ (Hao, 2005).

***M* = Fe**

The compound $[\text{Fe}(\text{H}_2\text{O})_2(15\text{-crown-5})](\text{NO}_3)_2$ was investigated using the DSC 822^e apparatus and the controlling software STAR^e (version 8.10) manufactured by *METTLER TOLEDO*. All DSC samples were prepared from fine powders. Heating rates of 1, 5, 10 and 20 K/min were used. The amount of the iron complex was fixed at 2.00(1) mg. Between 200 and 305 K, a single solid-solid phase transition was found at $T_{\text{onset}} = 278 \text{ K}$ (see Figures 2.2 and 2.3). The small peak heights in the DSC traces prevent a good estimation of ΔH_{tr} .

³⁰ The solid-solid phase transition that takes place near 349 K is not discussed further.

³¹ The solid-solid phase transition that takes place near 365 K is not discussed further.

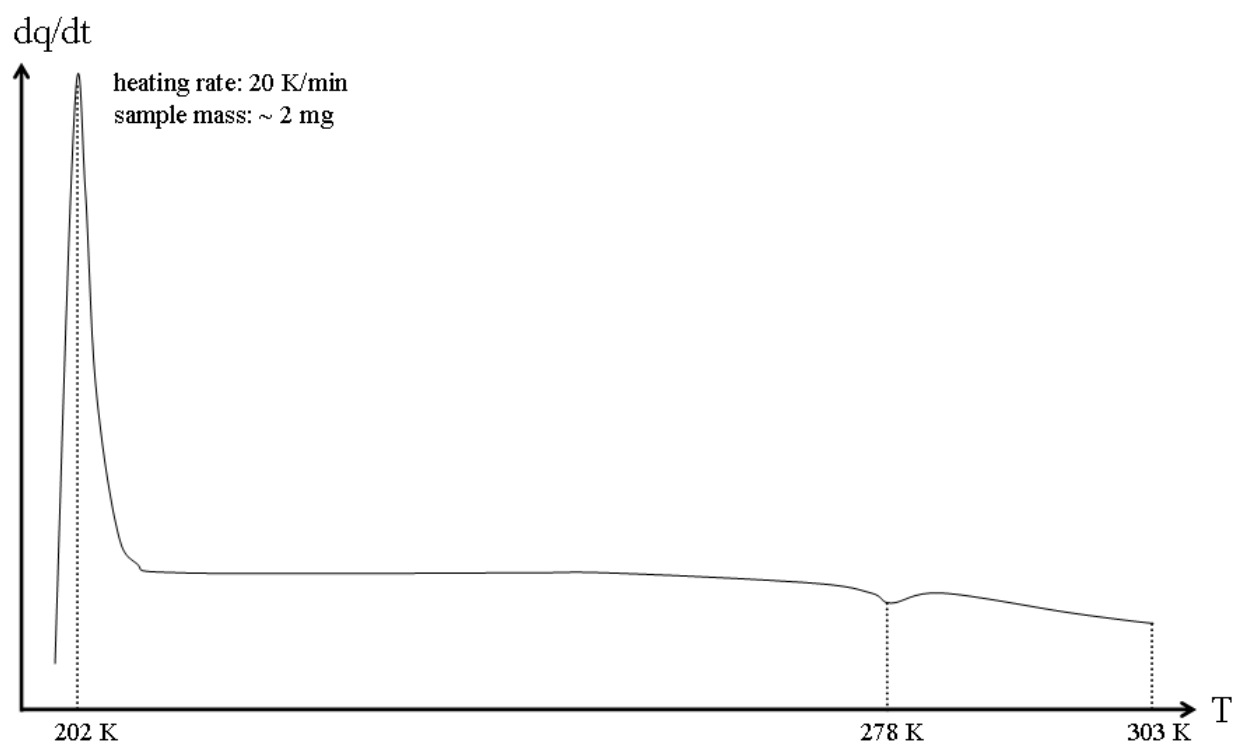


Figure 2.2. DSC trace of the $[\text{Fe}(\text{H}_2\text{O})_2(15\text{-crown-5})](\text{NO}_3)_2$ compound. The trace shows only one solid-solid phase transition near 278 K. DSC measurements were performed between 202 and 303 K at 20 K/min.

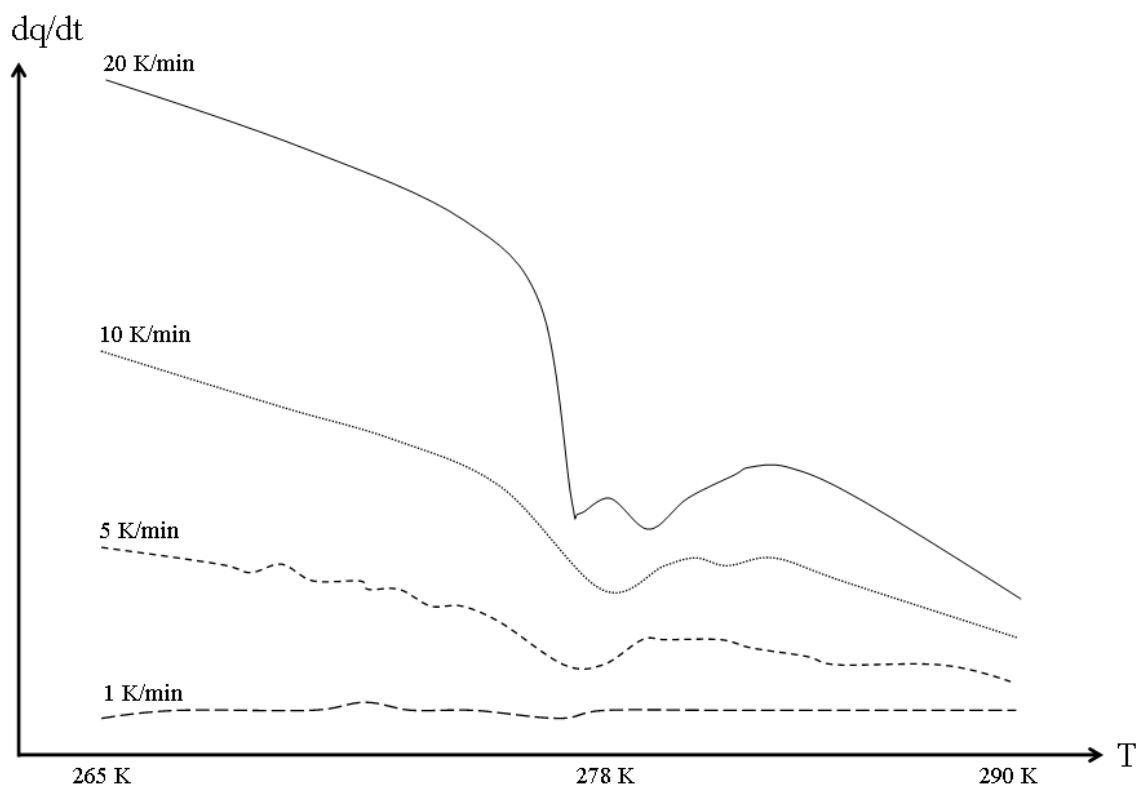


Figure 2.3. Parts of the DSC traces of the $[\text{Fe}(\text{H}_2\text{O})_2(15\text{-crown-5})](\text{NO}_3)_2$ compound measured at 1, 5, 10 and 20 K/min. At 1 K/min, the solid-solid phase transition near 278 K is no longer observable *via* DSC measurements.

X-Ray Crystallography

All reflection intensities were measured using either a Nonius KappaCCD diffractometer with graphite-monochromated Mo $K\alpha$ radiation ($\lambda = 0.71073 \text{ \AA}$) under the program *COLLECT* (Nonius, 1997) or a Bruker-Nonius X8 Proteum diffractometer equipped with graded multi-layer optics for Cu $K\alpha$ radiation ($\lambda = 1.54178 \text{ \AA}$) under the program *APEX2* (Bruker-Nonius, 2004). The program *DENZO-SMN* (Otwinowski & Minor, 1997) or *APEX2* were used to determine the cell dimensions. All structures were solved with the program *SIR92* (Altomare et al.) or with *SHELXS97* (Sheldrick, 1997a) and were refined on F^2 with *SHELXL97* (Sheldrick, 1997b). The temperature of data collection was controlled using the system *CRYOCOOL-LN2* (manufactured by *CRYO INDUSTRIES*). The H-atoms of the 15-crown-5 molecules were placed at calculated positions (*AFIX 23*) with isotropic displacement parameters having values 1.2 times U_{eq} of the attached C atom. The H-atoms of water ligands were located in difference Fourier maps and restrained such that the O-H distances and H-O-H angles had values within accepted ranges [bond length (O-H)_{90K} = 0.840 (1)Å, bond angle (H-O-H)_{90K} = 104.50 (2)°]. The H-atoms of water ligands have isotropic displacement parameters 1.5 times U_{eq} of the attached O atom. The atom-numbering scheme was made consistent for the three isostructural complexes and is consistent with related structures already published.

Previous studies (Hao, Parkin & Brock, 2005; Hao, Siegler, Parkin & Brock, 2005) showed that the system $[M(\text{H}_2\text{O})_2(15\text{-crown-5})](\text{NO}_3)_2$, $M = \text{Mg, Fe and Zn}$ has at least two phases for each metal: a low-temperature phase with $Z' = 3$ (LTP) and a high-temperature phase with $Z' = 8$ (HTP). The two phases are found to be commensurately modulated superstructures. The modulations along the c direction are threefold for the $Z' = 3$ structure and eightfold for the $Z' = 8$ structure. By convention, the two phases of $[M(\text{H}_2\text{O})_2(15\text{-crown-5})](\text{NO}_3)_2$ are numbered I and II, I for the high-temperature phase and II for the low-temperature phase. This chapter is only concerned with the former phase.

Generalities

The phase transition LTP \rightarrow HTP was found near $T_{\text{onset}} = 278, 304$ and 308 K for the iron, zinc and magnesium compounds. The high-temperature phase of $[M(\text{H}_2\text{O})_2(15\text{-crown-5})](\text{NO}_3)_2$, $M = \text{Mg, Fe and Zn}$, was originally solved in the noncentrosymmetric space group $P2_1$ with eight independent formula units ($Z' = 8$). The non-standard space group $B2_1$ was chosen so that the modulation would be along the same axis (**c**) as in the low-temperature phase; this makes comparisons of the two phases easier. This was done *via* the following transformation: $\mathbf{a}(B2_1) = (1\ 0\ 0 / 0\ -1\ 0 / -1\ 0\ -2)\ \mathbf{a}(P2_1)$.

The $Z' = 8$ phase is a racemic twin and the twinning was treated using the *TWIN* instruction with the default matrix $(-1\ 0\ 0 / 0\ -1\ 0 / 0\ 0\ -1)$.

The residue numbering scheme of the high-temperature phase (*RESI* instruction) is consistent with that for the $Z' = 3$ structure. The residues 1 \rightarrow 8 (residues 3 and 7 were found to be disordered and the minor parts are labeled as residues 9 and 10) are the cations $[M(\text{H}_2\text{O})_2(15\text{-crown-5})]^{2+}$, $M = \text{Mg, Fe and Zn}$, and the nitrates are assigned as residues 11 \rightarrow 26 (see Fig 2.4).

$M = \text{Mg, Zn}$

Data for the Mg and Zn compounds were collected near 311 K and 313 K using Cu $K\alpha$ radiation. Attempts to refine the modulated superstructure using data measured from a standard CCD diffractometer with Mo $K\alpha$ radiation ($\lambda = 0.71073$ Å) were not completely successful because the data were too weak. For the Zn structure, only 27.2% of the reflections have $I > 2\sigma(I)$. The cell constants at 311 K ($M = \text{Mg}$) of the standard primitive cell are: $a = 14.597$ (2)Å, $b = 14.135$ (2)Å, $c = 34.976$ (4)Å, $\beta = 95.00$ (2)°. The cell constants at 313 K ($M = \text{Zn}$) of the standard primitive cell are: $a = 14.737$ (2)Å, $b = 14.050$ (2)Å, $c = 34.847$ (4)Å, $\beta = 95.12$ (2)°.

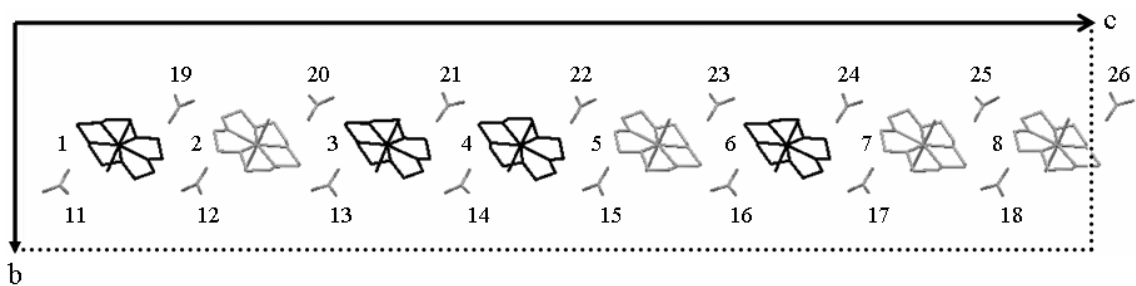


Figure 2.4. Asymmetric unit of the high-temperature phase ($B2_1$, $Z' = 8$) looking down the a direction. The cations $[M(\text{H}_2\text{O})_2(15\text{-crown-5})]^{2+}$, $M = \text{Mg, Zn and Fe}$, are numbered 1 to 8 and the nitrate anions are numbered 11 to 26. The black and grey cations correspond to conformational enantiomers R and S. The minor component of the disorder for residues 3 and 7 (residues 9 and 10) are omitted for clarity.

The refinement of the high-temperature phase was not straightforward, because of the weak diffraction and the high degree of pseudosymmetry (largest correlation matrix elements > 0.9) in the structure. The increase in thermal motion at high-temperature (311-313 K) makes all the reflections weaker and consequently lowers the number of reflections having $I > 2\sigma(I)$. Many of the superstructure reflections become too weak to measure. Near 311-313K, only 48% of the reflections have $I > 2\sigma(I)$ for the Mg and Zn compounds. The number of measured intensities over the number of variables ($N_{\text{obs}}/N_{\text{v}}$) was too low ($\sim 3-4$) to allow independent refinement of anisotropic displacement parameters for all independent non-H atoms. The anisotropic displacement parameters of all independent atoms related by pseudoinversion and pseudotranslation were therefore constrained to be identical using the *EADP* instruction. Doing so improved the ratio $N_{\text{obs}}/N_{\text{v}}$ to an acceptable value ($\sim 14-15$). Furthermore, the geometry of all cations and all nitrates anions related by pseudosymmetry were restrained to be similar (*SAME* instruction). The consistency of bond distances for all cations and anions (excluding hydrogen atoms) related by pseudosymmetry was acceptable; the estimated standard deviations for the sets of chemically equivalent distances of the Mg and Zn compounds averaged about 3.5 and 4.2 times the average uncertainty of an individual measurement.

Another problem was the disorder of two cations in the structures (residues 3 and 7). The major and minor components of the disorder are related by a pseudoinversion center located closed to the position of the metal (see Figure 2.5). The values of the occupancy factors given for the major components of the Mg and Zn compounds are 0.734(2) / 0.739(2) and 0.742(2) / 0.737(2). The minor components were treated as rigid groups to help the refinement of the low-occupancy atomic coordinates.

An examination of classes of reflections along the c^* direction was done using separate Wilson plots. The systematic classes of strong and weak reflections are the following: the $\ell = 8n$ reflections (primary reflections) are the strongest, the $\ell = 8n \pm 3$ reflections are strong, whereas the $\ell = 8n \pm 4$ reflections are the weakest; the $\ell = 8n \pm 1$ and $\ell = 8n \pm 2$ reflections are intermediate (see Figure 2.6 and 2.7).

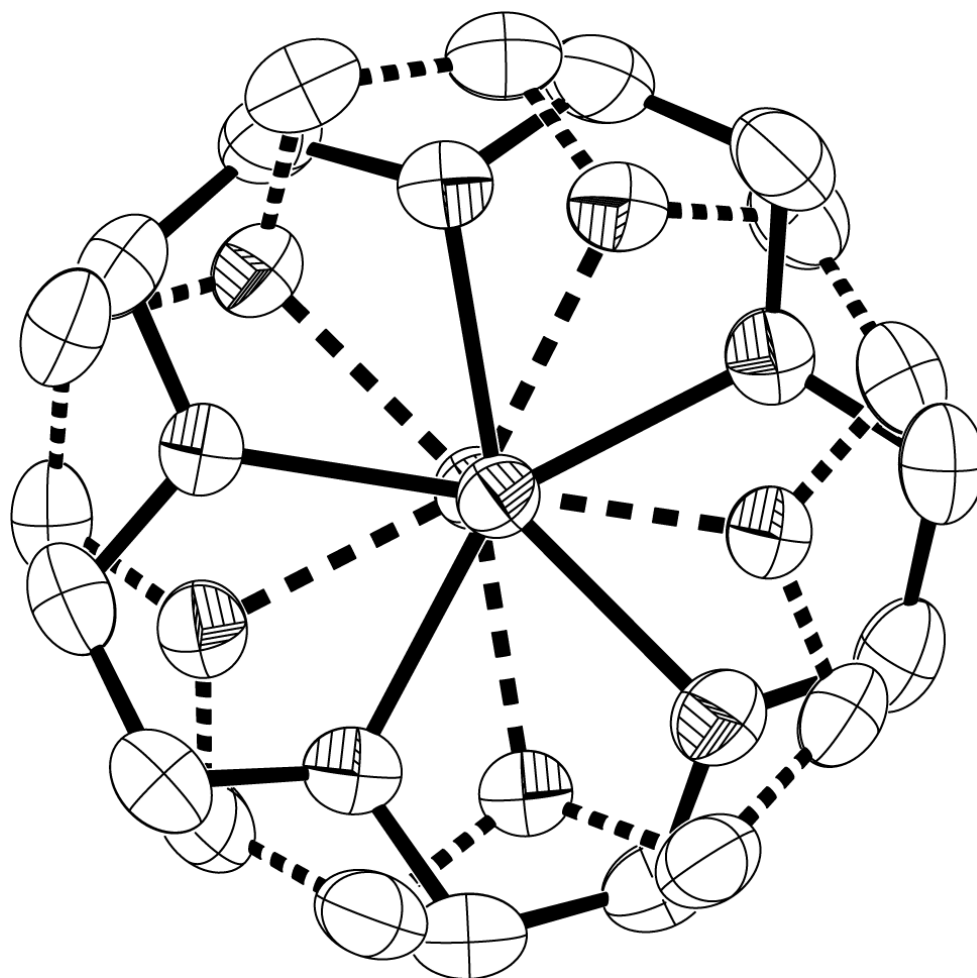


Figure 2.5. The displacement ellipsoids (50% probability level) of one disordered 15-crown-5 molecule of the Mg compound at 311 K. The major (solid) and minor (dashed) components of the disorder are related by a pseudoinversion center located nearly at the position of the metal. The two water molecules (ligands) and H atoms are omitted for clarity.

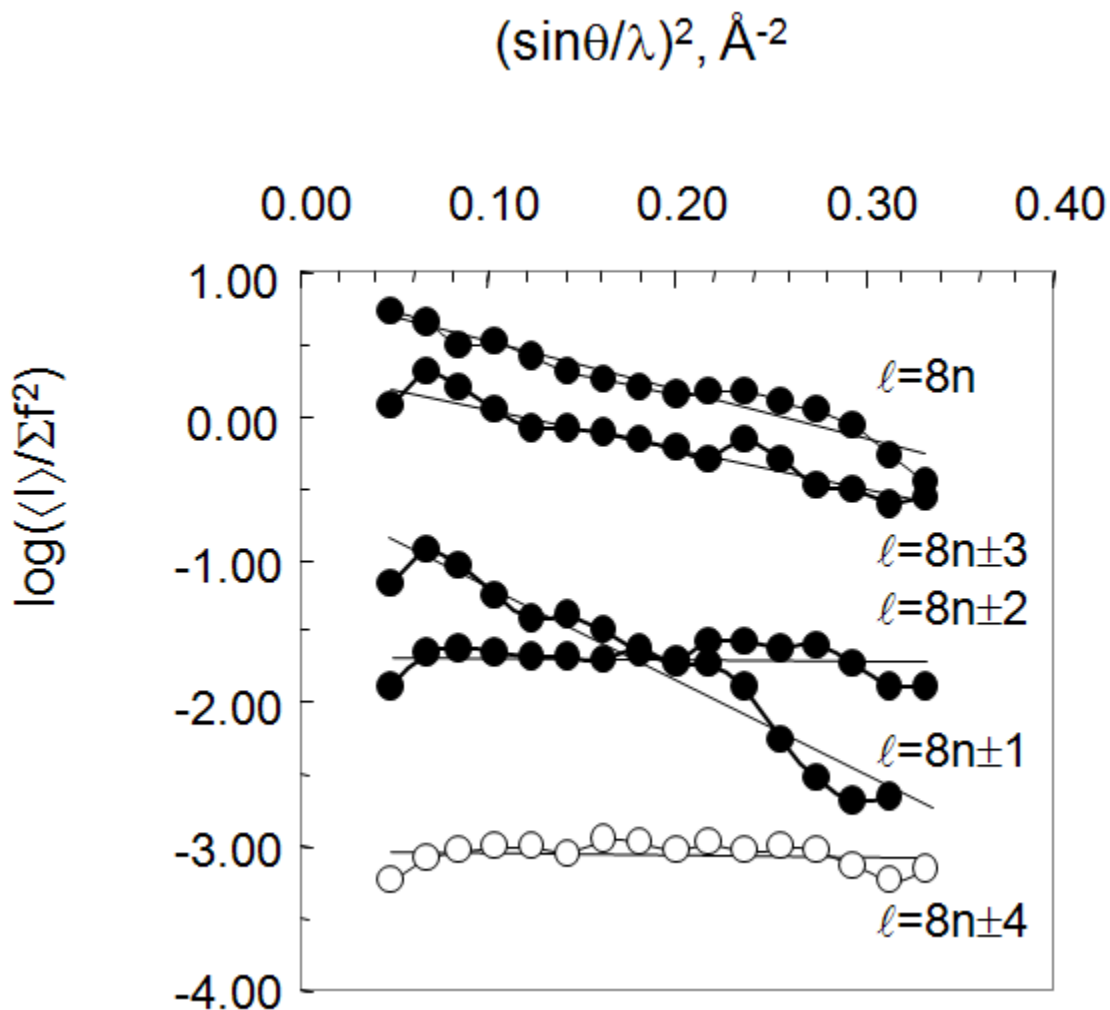


Figure 2.6. Separate Wilson plots for the Mg compound at 311 K. The reflections are divided into several classes with respect to the Miller index ℓ (*i.e.*, $\ell = 8n$, $8n \pm 1$, etc.). The intensities of the primary reflections ($\ell = 8n$) are systematically stronger than the intensities of the superstructure reflections ($\ell = 8n \pm 1$, $8n \pm 2$, $8n \pm 3$, $8n \pm 4$). The $\ell = 8n \pm 3$ and $\ell = 8n \pm 4$ reflections are systematically the strongest and weakest superstructure reflections. The $\ell = 8n \pm 1$ and $\ell = 8n \pm 2$ reflections are intermediate. The $\ell = 8n \pm 4$ reflections (open circles) are calculated rather than measured because their intensities are so low that the average value is often negative, which means its log is indeterminate.

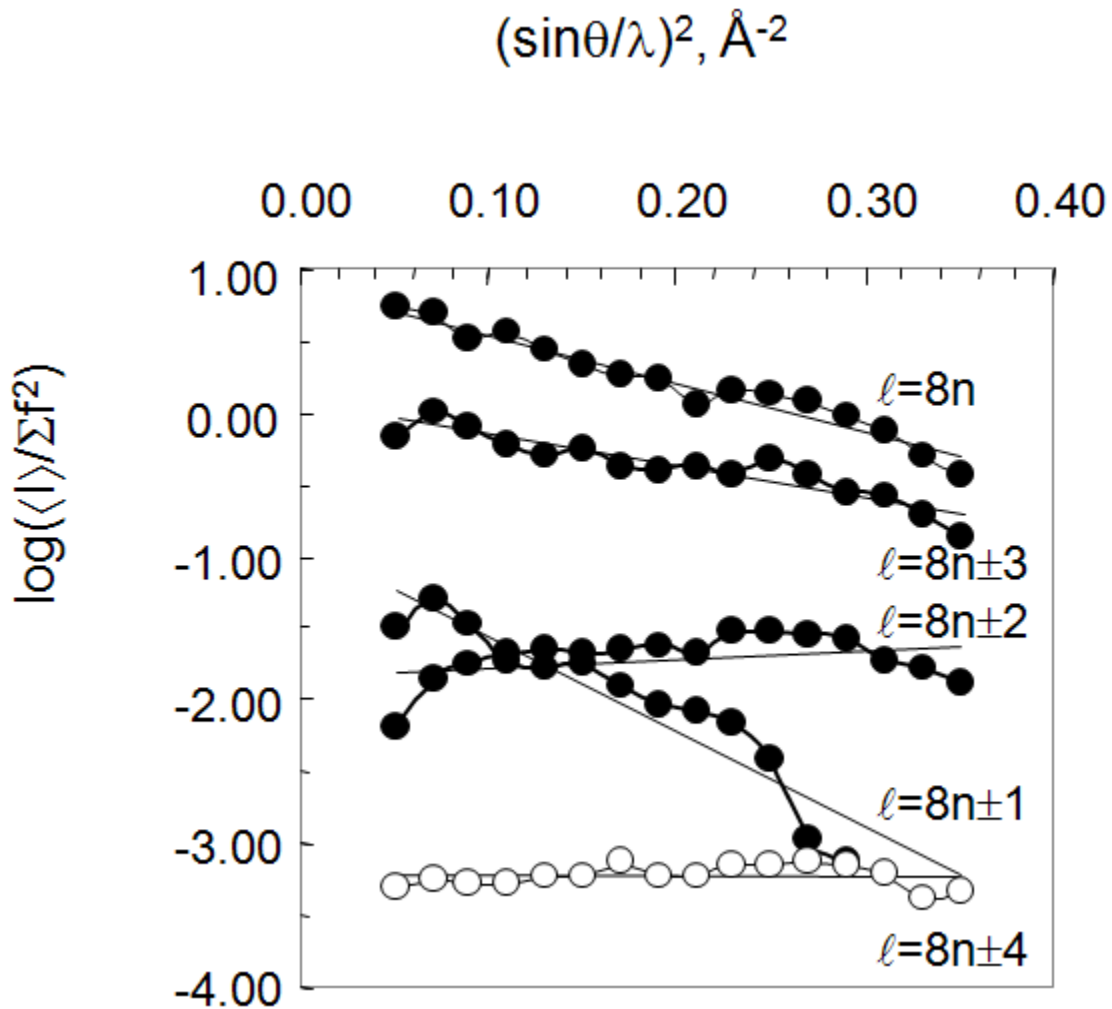


Figure 2.7. Separate Wilson plots for the Zn compound at 313 K. The reflections are divided into several classes with respect to the Miller index ℓ (i.e., $\ell = 8n$, $8n \pm 1$, etc.). The intensities of the primary reflections ($\ell = 8n$) are systematically stronger than the intensities of the superstructure reflections ($\ell = 8n \pm 1$, $8n \pm 2$, $8n \pm 3$, $8n \pm 4$). The $\ell = 8n \pm 3$ and $\ell = 8n \pm 4$ reflections are systematically the strongest and weakest superstructure reflections. The $\ell = 8n \pm 1$ and $\ell = 8n \pm 2$ reflections are intermediate. The $\ell = 8n \pm 4$ reflections (open circles) are calculated rather than measured because their intensities are so low that the average value is often negative, which means its log is indeterminate.

The refinement against F^2 was satisfactory (see Table 2.1) and convergence was reached. After applying the constraints and restraints, no correlation matrix elements were found to have absolute values larger than 0.70 or 0.68 for the Mg and Zn compounds. The final difference Fourier map showed no peak of residual electron density higher than 0.54 electron / \AA^3 for the two isostructural compounds.

The crystallographic data for the high-temperature phases of $[M(\text{H}_2\text{O})_2(15\text{-crown-5})](\text{NO}_3)_2$, $M = \text{Mg}, \text{Zn}$, are given in Table 2.1.

Table 2.1. Crystallographic data of $[M(\text{H}_2\text{O})_2(15\text{-crown-5})](\text{NO}_3)_2$, $M = \text{Mg}, \text{Zn}$.

	Mg I	Zn I
Crystal data		
Chemical formula	$\text{C}_{10}\text{H}_{24}\text{MgN}_2\text{O}_{13}$	$\text{C}_{10}\text{H}_{24}\text{ZnN}_2\text{O}_{13}$
M_r	404.62	445.68
Cell setting, space group	Monoclinic, $B2_1$	Monoclinic, $B2_1$
a, b, c (\AA) ³²	14.597 (1) 14.135 (1) 70.201 (5)	14.737 (1) 14.050 (1) 69.935 (5)
β ($^\circ$)	96.95 (1)	96.99 (1)
V (\AA^3)	14378 (3)	14373 (3)
$Z; Z'$	32; 8	32; 8
D_x (g cm^{-3})	1.495	1.648
Radiation type	Cu $K\alpha$	Cu $K\alpha$
No. of reflections for cell parameters	9743	8519
θ range ($^\circ$)	4.9–65.3	4.1–68.3
μ (mm^{-1})	1.52	2.56
Temperature (K)	311 (2)	313 (2)
Crystal form, colour	Block, colorless	Block, colorless
Crystal size (mm)	0.20 x 0.15 x 0.15	0.30 x 0.15 x 0.12
Data collection		
Diffractometer	Bruker-Nonius X8 Proteum	Bruker-Nonius X8 Proteum
Data collection method	ω and ϕ scans	ω and ϕ scans
Absorption correction	Multi-scan (based on symmetry-related measurements)	Multi-scan (based on symmetry-related measurements)

³² The estimated errors in the unit cell constants (a , b , c and β) were modified by multiplying the experimental estimated standard uncertainties (*i.e.*, su's) by at least a factor of ~ 5 for a , b , c and by a factor of ~ 16.5 for β . These factors were used in order to approximate the errors in the unit cell constants from one crystal to another (Herbstein, 2000).

Table 2.1. (continued)

T_{\min}	0.751	0.514
T_{\max}	0.804	0.749
No. of measured, independent and observed parameters	53583, 22712, 10777	91322, 25529, 12218
Criterion for observed reflections	$I > 2\sigma(I)$	$I > 2\sigma(I)$
R_{int}	0.030	0.046
θ_{\max} (°)	65.5	68.3
Range of h, k, ℓ	$-17 < h < 14$ $-16 < k < 16$ $-78 < \ell < 82$	$-16 < h < 17$ $-16 < k < 16$ $-83 < \ell < 83$
Refinement		
Refinement on	F^2	F^2
$R[F^2 > 2\sigma(F^2)], wR(F^2), S$	0.058, 0.151, 1.83	0.055, 0.156, 1.63
No. of reflections	22712 reflections	25529 reflections
No. of parameters	796	796
H-atom treatment	Constrained to parent site	Constrained to parent site
Weighting scheme	Calculated $w = 1/[\sigma^2(F_o^2) + (0.020P)^2]$ where $P = (F_o^2 + 2F_c^2)/3$	Calculated $w = 1/[\sigma^2(F_o^2) + (0.020P)^2]$ where $P = (F_o^2 + 2F_c^2)/3$
$(\Delta/\sigma)_{\max}$	0.002	0.002
$\Delta\rho_{\max}, \Delta\rho_{\min}$ (e Å ⁻³)	0.47, -0.36	0.73, -0.46
Extinction method	SHELXL	SHELXL
Extinction coefficient	0.000069(4)	0.000048(3)
Absolute Structure	Flack H D (1983), Acta Cryst. A39, 876-881	Flack H D (1983), Acta Cryst. A39, 876-881
Flack Parameter	-10 (10) - undetermined because racemic twin	-10 (10) - undetermined because racemic twin

Computer programs: *COLLECT* (Nonius, 1997); *DENZO-SMN* (Nonius, 1997); *SHELXS-97* (Sheldrick, 1990); *SHELXL-97* (Sheldrick, 1997); *XP in SHELXTL* (Bruker, 1995); *SHELX-97 and local procedures*.

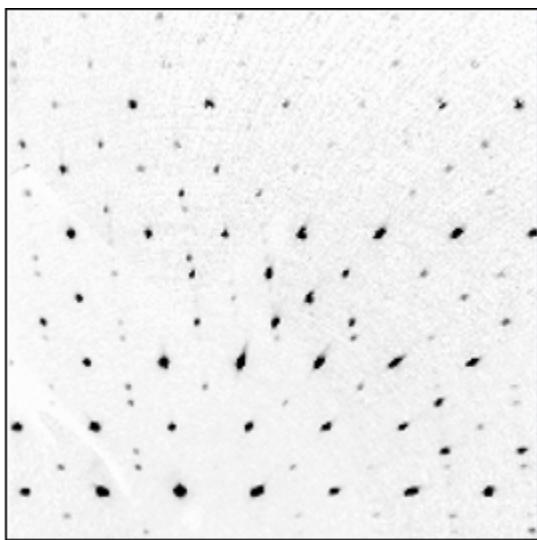
***M* = Fe**

Two sets of data for the Fe compound were collected at 90 K³³ using Cu *K*α and Mo *K*α radiations. The high-temperature phase was found to be metastable at 90 K if crystals had been flash-cooled. The cell constants at 90 K (radiation type: Cu *K*α) of the standard primitive cell are: *a* = 14.507 (1)Å, *b* = 14.226 (1)Å, *c* = 34.177 (2)Å, β = 95.95 (1)°. The cell constants at 90 K (radiation type: Mo *K*α radiation) of the standard primitive cell are: *a* = 14.521 (1)Å, *b* = 14.229 (1)Å, *c* = 34.200 (3)Å, β = 95.92 (1)°.

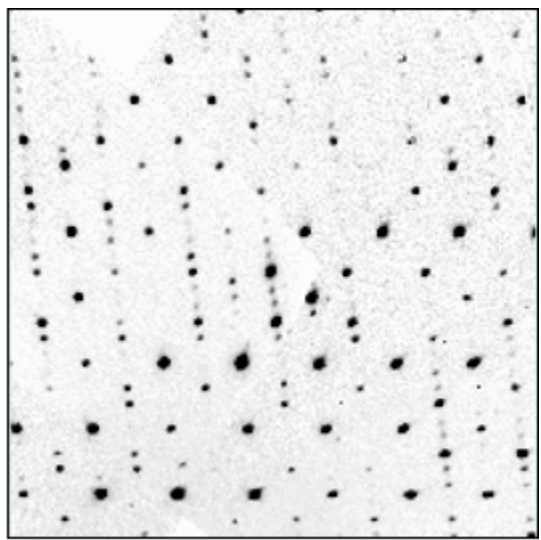
The method chosen for this refinement was very similar to the refinement used for the Mg and Zn compounds. The choice of constraints was identical but no restraints (*SAME* instruction) were needed to fix the geometries of the cations and anions related by pseudosymmetry. The decrease in thermal motion at low temperature improves the data: near 90 K, about 62.0% (Cu *K*α radiation) and 47.6% (Mo *K*α radiation) of the data have $I > 2\sigma(I)$ (see Figure 2.8). Figures 2.9 and 2.10 show the reduction of thermal motion for the $Z' = 8$ phase for the Fe compound (measured at 90 K) compared with the Mg and Zn compounds (measured at 311 and 313 K). The consistency of chemically equivalent bond distances for all cations and anions (excluding hydrogen atoms) related by pseudosymmetry was good; the estimated standard deviations for sets of chemically equivalent distances averaged about 1.8 times the average uncertainty of an individual measurement.

An examination of classes of reflections along the c^* direction was done using separate Wilson plots. The plots (see Figure 2.11) are similar to those for the Mg and Zn compounds. Qualitative observations obtained from a careful investigation of the reciprocal lattice slices are consistent with previous results (see Figure 2.12). The reconstructed reciprocal lattice slices were obtained using the program *PRECESSION* (Nonius, 1997). Phase purity was checked by looking at the reciprocal lattice slices. There was no indication of twinning or of the presence of another phase.

³³ 90 K is near the lower limit of stable temperature control when the cooling device is running with liquid nitrogen.



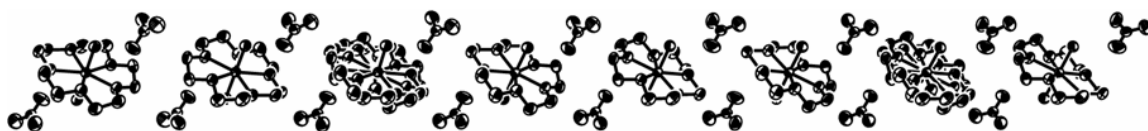
311 K, $M = \mathbf{Zn}$, $Z' = 8$ in $B2_1$



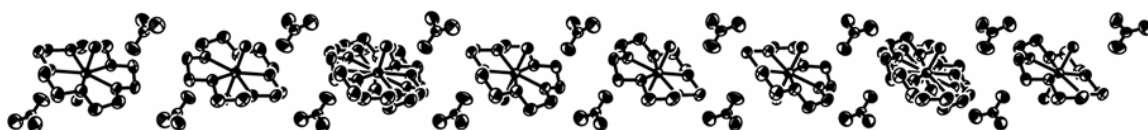
90 K, $M = \mathbf{Fe}$, $Z' = 8$ in $B2_1$

Figure 2.8. Parts of reciprocal lattice slices $h1\ell$ digitally reconstructed directly from the measured frames for the Zn and Fe structures with $Z' = 8$. The two sets of data were collected from a standard CCD diffractometer with Mo $K\alpha$ radiation ($\lambda = 0.71073 \text{ \AA}$) at 311 K for the Zn structure (left) and at 90 K for the Fe structure (right). At 311K, only 27.2% of the reflections have $I > 2\sigma(I)$. At 90 K, 47.6% of the reflections have $I > 2\sigma(I)$.

$M = \text{Mg}$, 311(2) K



$M = \text{Zn}$, 313(2) K

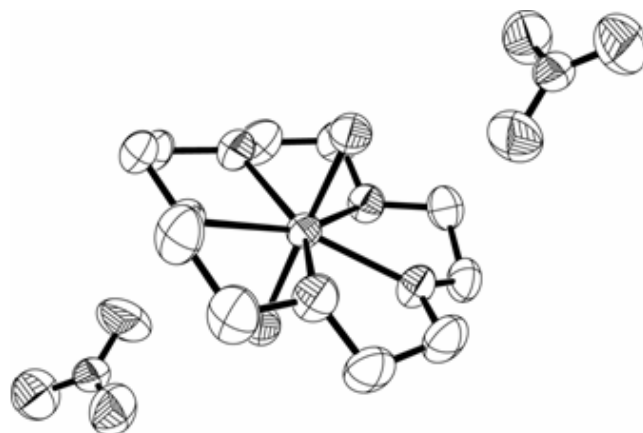


$M = \text{Fe}$, 90.0(2) K

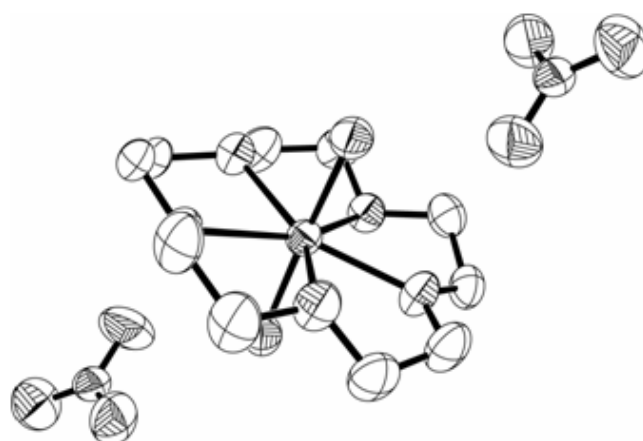


Figure 2.9. The displacement ellipsoids (50% probability level) of the independent ions (8 cations and 16 nitrates) in the asymmetric units of the Mg, Zn and Fe compounds at 311, 313 and 90 K. The reduction of thermal motion for the latter isostructural phase is obvious.

$M = \text{Mg}$, 311(2) K



$M = \text{Zn}$, 313(2) K



$M = \text{Fe}$, 90.0(2) K

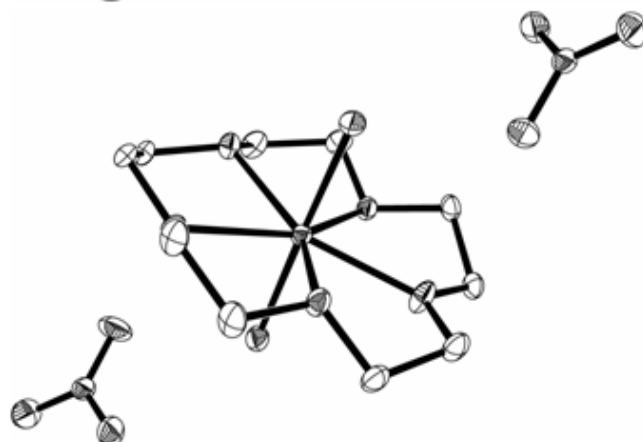


Figure 2.10. The displacement ellipsoids (50% probability level) of one independent formula unit (1 cation and 2 nitrates) in the asymmetric units of the Mg, Zn and Fe compounds at 311, 313 and 90 K. The reduction of thermal motion for the latter isostructural phase is obvious.

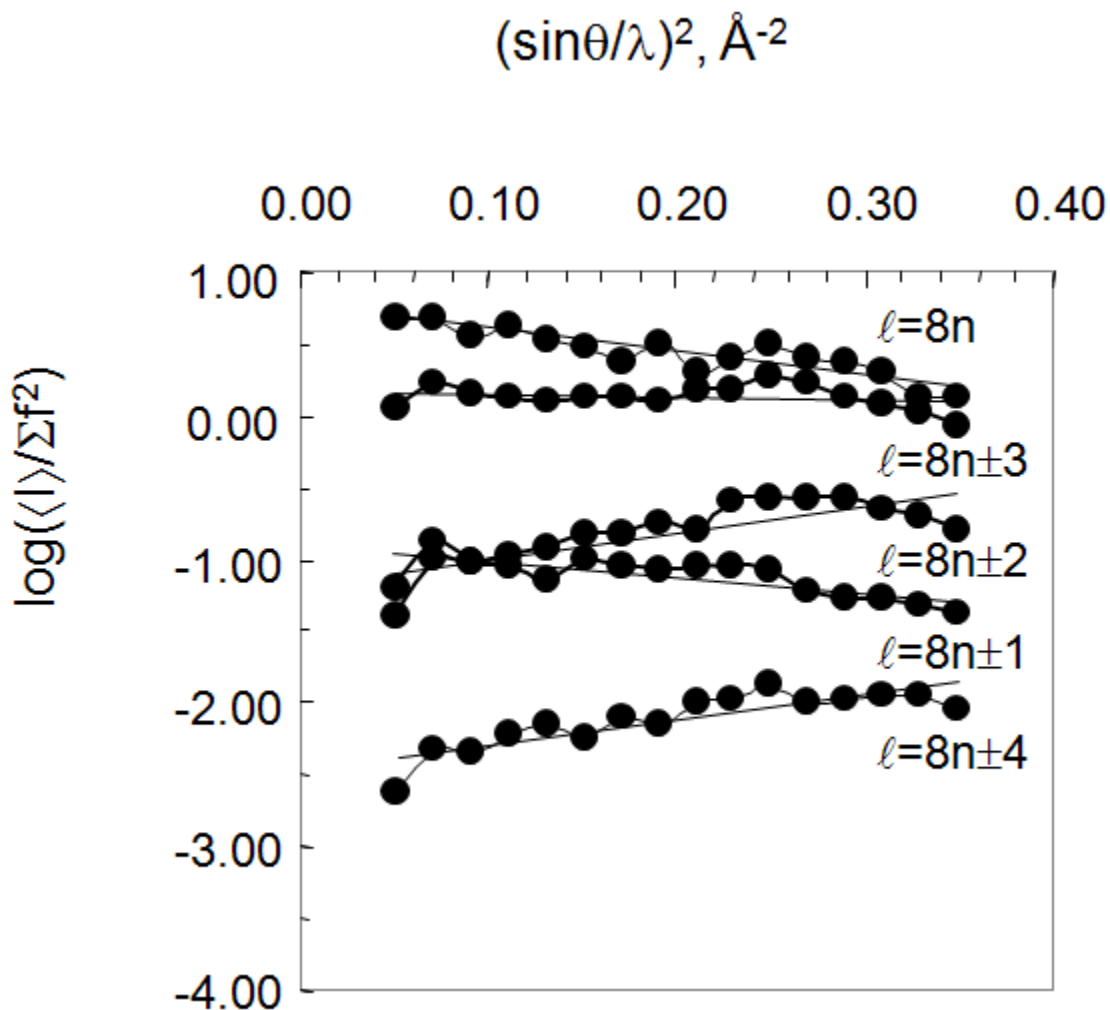


Figure 2.11. Separate Wilson plots for the Fe compound at 90 K (data using Cu $K\alpha$ radiation). The reflections are divided into several classes with respect to the Miller index ℓ (i.e. $\ell = 8n$, $8n \pm 1$, etc.). The intensities of the primary reflections ($\ell = 8n$) are systematically stronger than the intensities of the superstructure reflections ($\ell = 8n \pm 1$, $8n \pm 2$, $8n \pm 3$, $8n \pm 4$). The $\ell = 8n \pm 3$ and $\ell = 8n \pm 4$ reflections are systematically the strongest and weakest superstructure reflections. The $\ell = 8n \pm 1$ and $\ell = 8n \pm 2$ reflections are intermediate.

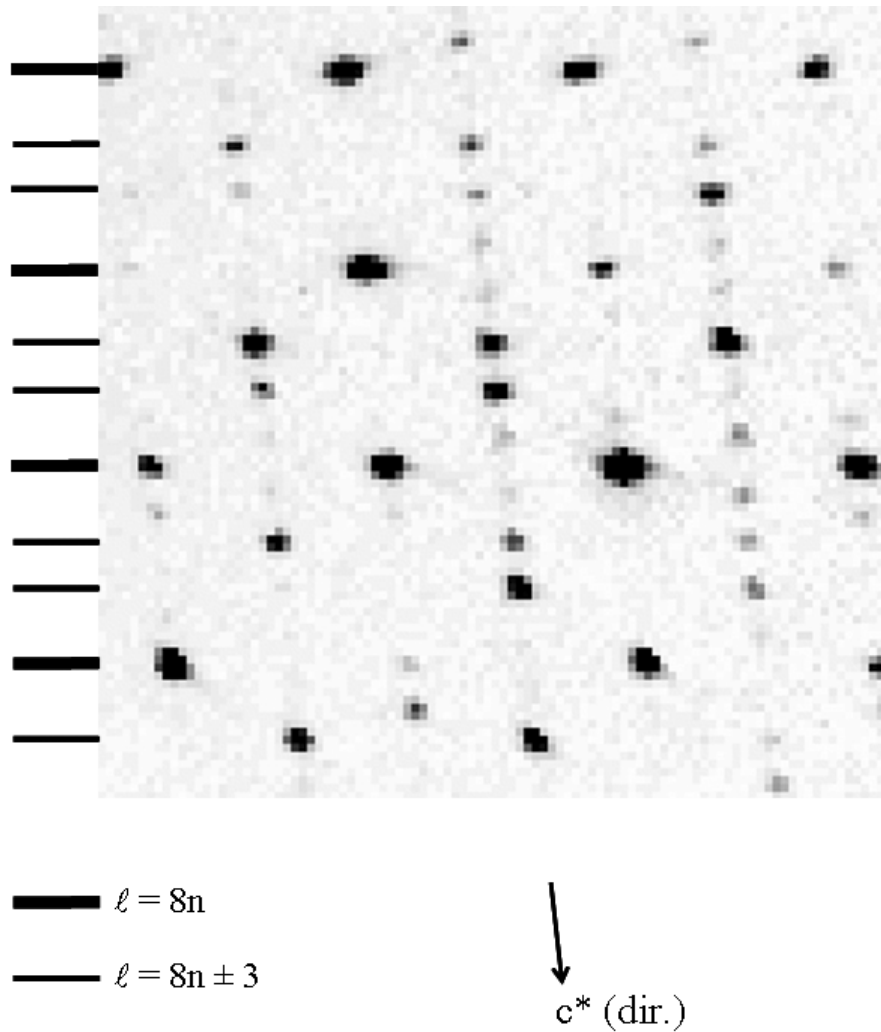


Figure 2.12. Parts of the reciprocal lattice slice $h1\ell$ digitally reconstructed directly from the measured frames for the Fe structure ($B2_1$, $Z' = 8$). Systematic classes of strong and weak reflections are observed. The $\ell = 8n$ reflections are the strongest, while the $\ell = 8n \pm 3$ reflections are generally strong. The $\ell = 8n \pm 4$ reflections are very weak. The $\ell = 8n \pm 1$ and $\ell = 8n \pm 2$ reflections are intermediate. The positions of the two strongest classes of reflections are indicated by thick black segments. The thickness of the segment depends on the intensity of the reflections. The positions of the three other classes of reflections are omitted for clarity.

The refinement on F^2 was good (see Table 2.2): the values of R factor [$(F^2 > 2\sigma(F^2))$] are lower than 0.05 for both sets of data. The convergence was smooth and no correlation matrix elements were found larger than 0.78. The enantiomeric disorder of some cations (residues 3 and 7) was treated as described previously and the occupancy factors given for major components were 0.900(2) / 0.878(2) [Cu $K\alpha$] and 0.866(2) / 0.860(2) [Mo $K\alpha$]. The final difference Fourier map suggested acceptable residual electron density with peaks no larger than 0.49 e \AA^{-3} . Higher peaks were located too close to some oxygen atoms of the nitrates to be considered meaningful. Data obtained from Cu $K\alpha$ radiation were corrected for both anisotropic absorption and for the resolution-dependent component of absorption using the program *SADABS* (Bruker-Nonius, 2004).

The crystallographic data for the high-temperature phase of $[\text{Fe}(\text{H}_2\text{O})_2(15\text{-crown-5})](\text{NO}_3)_2$ are given in Table 2.2.

Table 2.2. Crystallographic data of [Fe(H₂O)₂(15-crown-5)](NO₃)₂.

	Fe I	Fe I
Crystal data		
Chemical formula	C ₁₀ H ₂₄ FeN ₂ O ₁₃	C ₁₀ H ₂₄ FeN ₂ O ₁₃
<i>M_r</i>	436.16	436.16
Cell setting, space group	Monoclinic, <i>B</i> 2 ₁	Monoclinic, <i>B</i> 2 ₁
<i>a</i> , <i>b</i> , <i>c</i> (Å) ³⁴	14.507(1) 14.226 (1) 68.390 (5)	14.521 (1) 14.229 (1) 68.443 (5)
<i>β</i> (°)	96.23 (1)	96.26 (1)
<i>V</i> (Å ³)	14031 (3)	14057 (3)
<i>Z</i> ; <i>Z'</i>	32; 8	32; 8
<i>D_x</i> (g cm ⁻³)	1.652	1.649
Radiation type	Cu <i>Kα</i>	Mo <i>Kα</i>
No. of reflections for cell parameters	9152	16547
<i>θ</i> range (°)	4.2–68.0	1.0–27.5
<i>μ</i> (mm ⁻¹)	7.58	0.93
Temperature (K)	90.0 (2)	90.0 (2)
Crystal form, colour	Thick rod, colorless	Thick rod, colorless
Crystal size (mm)	0.30 x 0.15 x 0.11	0.40 x 0.15 x 0.11
Data collection		
Diffractometer	Bruker-Nonius X8 Proteum	Nonius KappaCCD
Data collection method	<i>ω</i> and <i>φ</i> scans	<i>ω</i> scans at fixed <i>χ</i> = 55°
Absorption correction	Multi-scan (based on symmetry-related measurements)	Multi-scan (based on symmetry-related measurements)

³⁴ The estimated errors in the unit cell constants (*a*, *b*, *c* and *β*) were modified by multiplying the experimental estimated standard uncertainties (*i.e.*, su's) by at least a factor of ~5 for *a*, *b*, *c* and by a factor of ~16.5 for *β*. These factors were used in order to approximate the errors in the unit cell constants from one crystal to another (Herbstein, 2000).

Table 2.2. (continued)

T_{\min}	0.210	0.708
T_{\max}	0.490	0.905
No. of measured, independent and observed parameters	89101, 25223, 15621	31488, 31488, 14989
Criterion for observed reflections	$I > 2\sigma(I)$	$I > 2\sigma(I)$
R_{int}	0.050	0.058
θ_{\max} (°)	68.2	27.4
Range of h, k, ℓ	$-17 < h < 17$ $-17 < k < 17$ $-74 < \ell < 82$	$-18 < h < 18$ $-18 < k < 18$ $-88 < \ell < 88$
Refinement		
Refinement on	F^2	F^2
$R[F^2 > 2\sigma(F^2)], wR(F^2), S$	0.043, 0.104, 1.33	0.046, 0.134, 1.02
No. of reflections	25223 reflections	31488 reflections
No. of parameters	796	795
H-atom treatment	Constrained to parent site	Constrained to parent site
Weighting scheme	Calculated $w = 1/[\sigma^2(F_o^2) + (0.020P)^2]$ where $P = (F_o^2 + 2F_c^2)/3$	Calculated $w = 1/[\sigma^2(F_o^2) + (0.0506P)^2]$ where $P = (F_o^2 + 2F_c^2)/3$
$(\Delta/\sigma)_{\max}$	0.002	0.003
$\Delta\rho_{\max}, \Delta\rho_{\min}$ (e Å ⁻³)	0.76, -0.39	0.70, -0.65
Extinction method	SHELXL	
Extinction coefficient	0.000054(2)	
Absolute Structure	Flack H D (1983), Acta Cryst. A39, 876-881	Flack H D (1983), Acta Cryst. A39, 876-881
Flack Parameter	10 (10) - undetermined because racemic twin	10 (10) - undetermined because racemic twin

Computer programs: *COLLECT* (Nonius, 1997); *DENZO-SMN* (Nonius, 1997); *SHELXS-97* (Sheldrick, 1990); *SHELXL-97* (Sheldrick, 1997); *XP in SHELXTL* (Bruker, 1995); *SHELX-97 and local procedures*.

Results and Discussion

Cation Geometry

The examination of the cation geometry in the system $[M(\text{H}_2\text{O})_2(15\text{-crown-5})](\text{NO}_3)_2$, $M = \text{Mg, Mn, Fe, Co, Cu}$ and Zn shows that all complexes adopt a seven-coordinate pentagonal bipyramidal geometry, in which the metal is coordinated by all five O_{ether} atoms of the crown ether and two water ligand molecules. Hao *et al.* showed that the cations $[M(\text{H}_2\text{O})_2(15\text{-crown-5})]^{2+}$, $M = \text{Mg, Mn, Fe, Co, Cu}$ and Zn , have nearly C_2 symmetry and have two conformational enantiomers (see Figure 2.13). Previous studies (Hao, Parkin & Brock, 2005; Hao, Siegler, Parkin & Brock, 2005) have shown that enantiomers can interconvert in the solid state when single crystals of $[M(\text{H}_2\text{O})_2(15\text{-crown-5})](\text{NO}_3)_2$, $M = \text{Mg, Mn, Fe, Co, Cu}$ and Zn undergo the reversible solid-solid phase transition $\text{LTP} \leftrightarrow \text{HTP}$ (see the section entitled ‘Relationship between LTP and HTP’ for further details).

The analysis of $M\text{-O}_{\text{ether}}$ (O1 to O5) distances for all three high-temperature phases of $[M(\text{H}_2\text{O})_2(15\text{-crown-5})](\text{NO}_3)_2$, $M = \text{Mg, Zn}$ and Fe , shows that the metal is unevenly coordinated by the five O atoms of the crown ligand. Consequently, the metal does not lie exactly at the center of the crown ligand. The $M\text{-O1}$ bond lengths are found to be the longest and the $M\text{-O5}$ bond lengths are found to be the shortest in all three HTPs (see Table 2.3). Hao *et al.* pointed out that the distortion around O5 and adjacent C atoms of the crown ligand makes the $M\text{-O5}$ bond length shorter than the average $M\text{-O}_{\text{ether}}$. The $M\text{-O}_{\text{water}}$ (O6, O7) bond lengths also vary between the three HTPs.

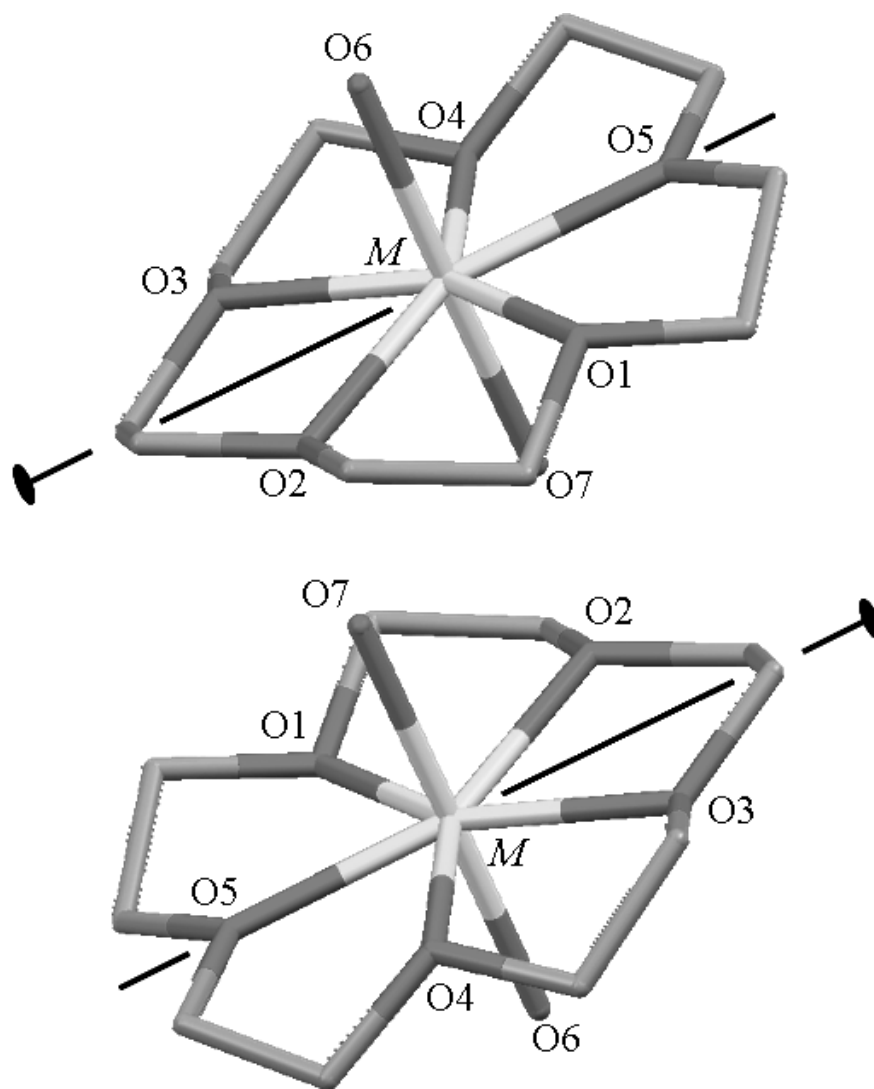


Figure 2.13. The two conformational enantiomers found in the system $[M(\text{H}_2\text{O})_2(15\text{-crown-5})](\text{NO}_3)_2$, $M = \text{Mg}, \text{Mn}, \text{Fe}, \text{Co}, \text{Cu}$ and Zn . The approximate twofold axis is found along the $M\text{-O5}$ axis.

Table 2.3. M -O distances (\AA) averaged over the eight residues found in the high-temperature phase ($B2_1$, $Z' = 8$) of $[M(\text{H}_2\text{O})_2(15\text{-crown-5})](\text{NO}_3)_2$, $M = \text{Mg}$, Zn and Fe .

	$M = \text{Mg}$	$M = \text{Zn}$	$M = \text{Fe}$
$M\text{-O1}$	2.228 (14)	2.226 (26)	2.247 (7)
$M\text{-O2}$	2.174 (6)	2.200 (17)	2.227 (17)
$M\text{-O3}$	2.193 (8)	2.220 (15)	2.240 (11)
$M\text{-O4}$	2.222 (14)	2.261 (15)	2.236 (8)
$M\text{-O5}$	2.115 (10)	2.139 (22)	2.184 (7)
$M\text{-O6}$	2.027 (42)	2.012 (47)	2.066 (9)
$M\text{-O7}$	2.005 (44)	1.997 (37)	2.063 (8)

Analysis of the Packing

In the three isostructural high-temperature phases of $[M(\text{H}_2\text{O})_2(15\text{-crown-5})](\text{NO}_3)_2$, $M = \text{Mg, Zn and Fe}$, the H-bonding network is two-dimensional (hereafter, 2-D) and is found along the **b** and **c** directions. The water ligands form hydrogen bonds to two distinct nitrate anions; whereas nitrate anions are H-bonded to two different cations (see Figure 2.14). The 2-D H-bonding network can be described as corrugated planes parallel to (1 0 0) (see Figure 2.15).

Enantiomeric Alternation

The crystal was found to be racemic; the two conformational enantiomers R and S of cations are present in a ratio 1:1. Enantiomers R/S form rows of cations in contact along the **a** and **c** directions. Rows of cations along the **a** and **c** directions differ in their enantiomeric alternation pattern (see Figure 2.16). Along, the **a** direction, enantiomers R/S are related only by pseudoinversion, and therefore, the alternation pattern is found to be perfect: one cation R is adjacent to two cations S (or one cation S is adjacent to two cations R). The perfect alternation pattern is given by: R S (or S R).

Along the other direction (**c**), enantiomers R/S are related by either pseudoinversion or pseudotranslation. Disorder is observed when two adjacent cations are the same enantiomers R R or S S (*i.e.*, when one alternation fault occurs). Enantiomers fail to alternate once every four contacts within a row of cations. The alternation pattern along the **c** direction is given by: R S R R S R S S or S R S S R S R R.

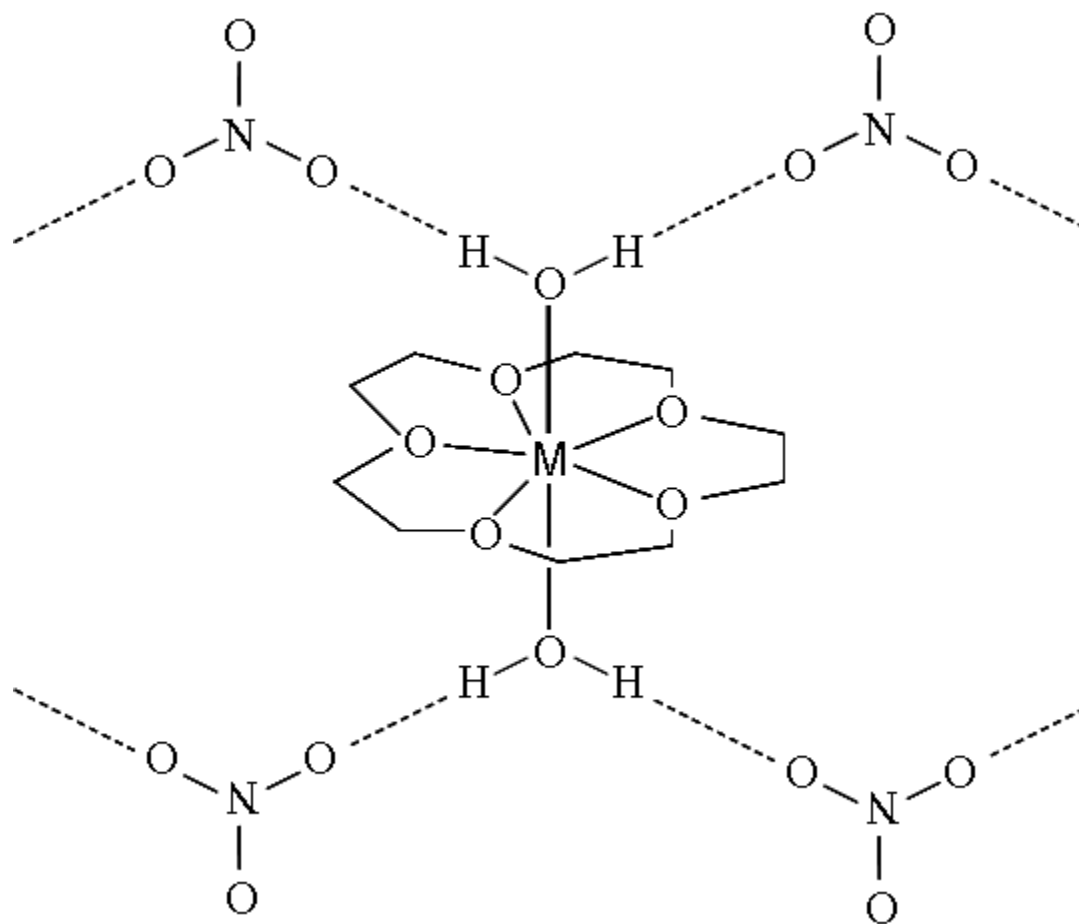


Figure 2.14. The basic building block of the H-bonding found in the three isostructural high-temperature phases of $[M(15\text{-crown-}5)(\text{H}_2\text{O})_2](\text{NO}_3)_2$, $M = \text{Mg}$, Zn and Fe . The H atoms of the 15-crown-5 molecule are omitted for clarity. The same basic pattern is found in the other phases that have 2-D H-bonding.

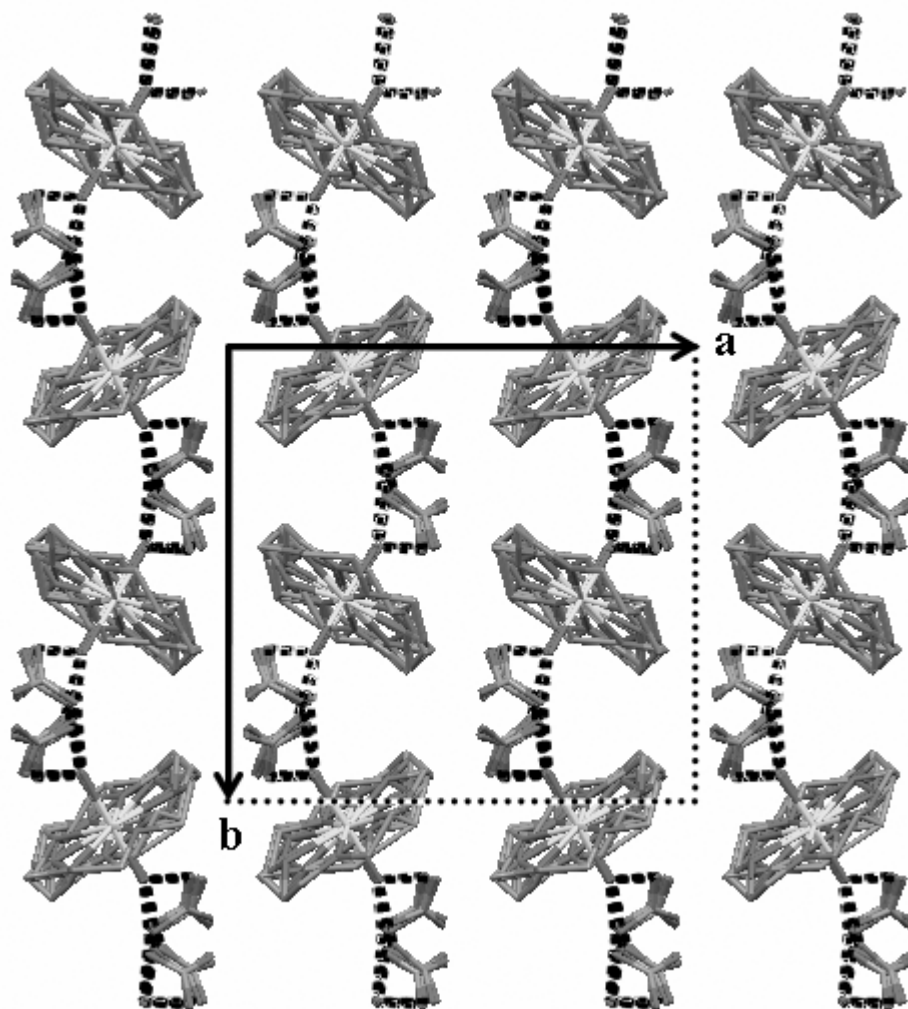


Figure 2.15. The packing of the high-temperature phase of $[M(15\text{-crown-}5)(\text{H}_2\text{O})_2](\text{NO}_3)_2$, $M = \text{Mg, Zn and Fe}$ looking down the c direction. The drawing illustrates the 2-D H-bonding pattern, which can be described as corrugated planes (layers) parallel to $(1\ 0\ 0)$. The a axis is not in the plane of the drawing. H atoms are omitted for clarity. H bonds are shown as black dotted lines. The same basic pattern is found in the other phases that have 2-D H-bonding.

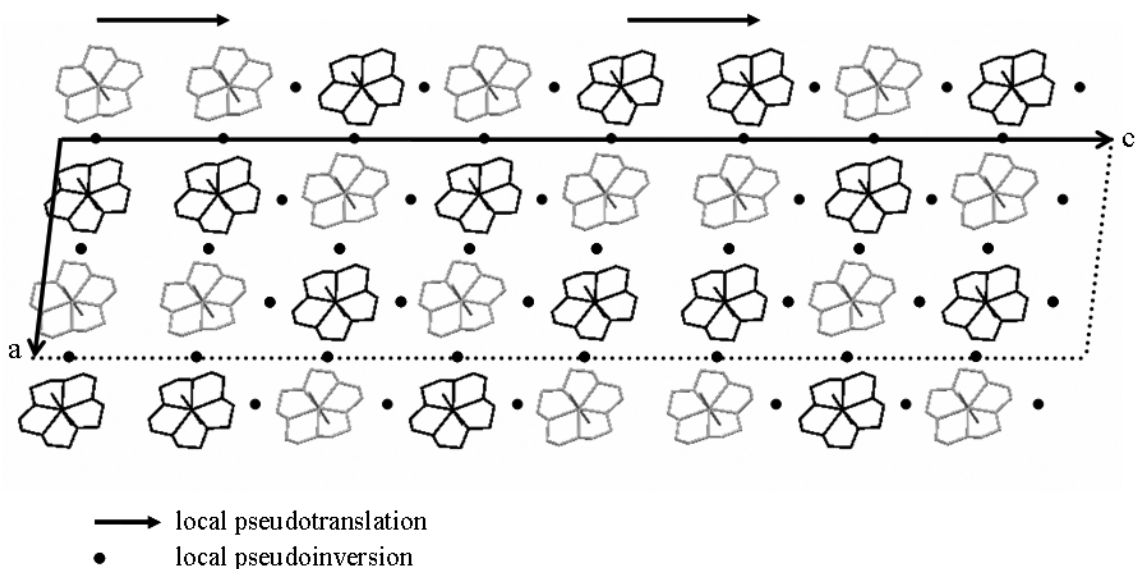


Figure 2.16. The packing of the high-temperature phase of $[M(15\text{-crown-}5)(\text{H}_2\text{O})_2](\text{NO}_3)_2$, $M = \text{Mg, Zn and Fe}$, in the plane $(0\ 1\ 0)$. The black and grey cations correspond to conformational enantiomers R/S. Along the **a** direction, adjacent cations are related only by local pseudoinversion (black dots) and the enantiomeric alternation pattern is perfect (R S or S R). Along the **c** direction, adjacent cations can be related by either local pseudoinversion or local pseudotranslation (black arrows). The latter pseudosymmetry is responsible for one non-alternation in every four contacts within a row of cations. The enantiomeric alternation pattern along *c* is given by R S R R S R S S (or S R S S R S R R). The minor disorder, H atoms and nitrate ions are omitted for clarity.

Phase Transitions

The previous and present studies show that the system $[M(\text{H}_2\text{O})_2(15\text{-crown-5})](\text{NO}_3)_2$, $M = \text{Mg, Mn, Fe, Co, Cu}$ and Zn can crystallize at least into five different crystal structures and has twelve phases (see Table 2.4). Hao *et al.* emphasized that the whole set of phases can be separated into two groups depending on the H-bonding network: one group consisting of a two-dimensional H-bonding network (2-D group), and another group consisting of a three-dimensional H-bonding network (3-D group). The subsequent discussion is only concerned with the 2-D group; the relationship between 2-D and 3-D structures is not explored in the dissertation.

The phase transitions for the compounds $[M(\text{H}_2\text{O})_2(15\text{-crown-5})](\text{NO}_3)_2$, $M = \text{Mg, Mn, Fe, Cu}$ and Zn , are found to be reversible solid-solid phase transitions with no detectable crystal damage. The temperatures of the phase transitions $\text{LTP} \rightarrow \text{HTP}$ (T_{tr}) are given in Table 2.4. The high-temperature phases for the Mn and Fe compounds were found to be metastable at 90 K when crystals had been flash-cooled from RT to 90 K. This indicates that the rate of conversion of HTP to LTP (over the cooling rate) is slow enough, so that the structure of HTP gets ‘frozen’ at temperatures lower than T_{tr} . It is worth noting that the temperatures of phase transitions of the Mn and Fe compounds are found to be below room-temperature conditions.

The four crystal structures ($C\bar{1}$, $Z' = 2$; $P2_1/c$, $Z' = 3$; $P2_1/n$, $Z' = 5$; $B2_1$, $Z' = 8$) have very similar packing and H-bonding patterns (see Figure 2.17). A comparison of the enantiomeric alternation patterns along $[1\ 0\ 2]$ for the triclinic structure and along the \mathbf{c} direction for the three monoclinic structures shows that all four patterns differ. In the triclinic structure, cations within a row parallel to $[1\ 0\ 2]$ are related by inversion centers and the enantiomeric alternation is perfect (R S or S R). In the monoclinic structures with $Z' = 3, 5$ and 8 , cations within a row parallel to the \mathbf{c} direction are related by either pseudoinversion or pseudotranslation. In the $Z' = 3$ structure, there is one non-alternation in every three contacts within a row of cations along the \mathbf{c} direction. The enantiomeric alternation pattern is R S S (or S R R). In the $Z' = 5$ structures, there is one non-

alternation in every five contacts within a row of cations along the **c** direction. The enantiomeric alternation pattern is R S R R S (or S R S S R). In the $Z' = 8$ structure, there is one non-alternation in every four contacts within a row of cations along the **c** direction. The enantiomeric alternation pattern is R S R R S R S S (or S R S S R S R R).

In all 2-D structures of $[M(\text{H}_2\text{O})_2(15\text{-crown-5})](\text{NO}_3)_2$, $M = \text{Mg, Mn, Fe, Cu}$ and Zn , the enantiomeric alternation pattern is found to become perfect ($M = \text{Mn, Cu}$) or more perfect ($M = \text{Mg, Fe, Zn}$) as single crystals undergo the solid-solid phase transition LTP \rightarrow HTP. Passing through the phase transition, enantiomers R/S can interconvert in the solid state because the change of handedness does not require much energy since enantiomers R/S are conformational isomers (Hao, Parkin & Brock, 2005; Hao, Siegler, Parkin & Brock, 2005). Furthermore, the atomic motions required for the transition are small.

Table 2.4. The five crystal structures and twelve phases of $[M(\text{H}_2\text{O})_2(15\text{-crown-5})](\text{NO}_3)_2$, $M = \text{Mg, Mn, Fe, Co, Cu}$ and Zn . The temperatures of the phase transitions $\text{LTP} \rightarrow \text{HTP}$ (T_{tr}) are given for the 2-D structures of the Mg, Mn, Fe, Cu and Zn compounds.

H-bonding	2-D network		T_{tr} (K)	3-D network
	LTP	HTP		
Mg ^{35,36}	$P2_1/c, Z' = 3$	$B2_1$ (or $P2_1$), $Z' = 8$	308 (2)	
Mn ³⁷	$P2_1/c, Z' = 3$	$C\bar{1}, Z' = 2$	285 (2)	$P4_1$ (or $P4_3$) $Z' = 2$
Fe ³⁷	$P2_1/c, Z' = 3$	$B2_1$ (or $P2_1$), $Z' = 8$	278 (2)	
Co ³⁵				$P4_1$ (or $P4_3$) $Z' = 2$
Cu ³⁵	$P2_1/n, Z' = 5$	$C\bar{1}, Z' = 2$	312 (2)	
Zn ^{35,36}	$P2_1/c, Z' = 3$	$B2_1$ (or $P2_1$), $Z' = 8$	304 (2)	

³⁵ Hao, Parkin & Brock. *Acta Cryst. B.* (2005).

³⁶ Hao, Siegler, Parkin & Brock. Unpublished Results.

³⁷ Hao, Siegler, Parkin & Brock. *Cryst. Growth & Des.* (2005)

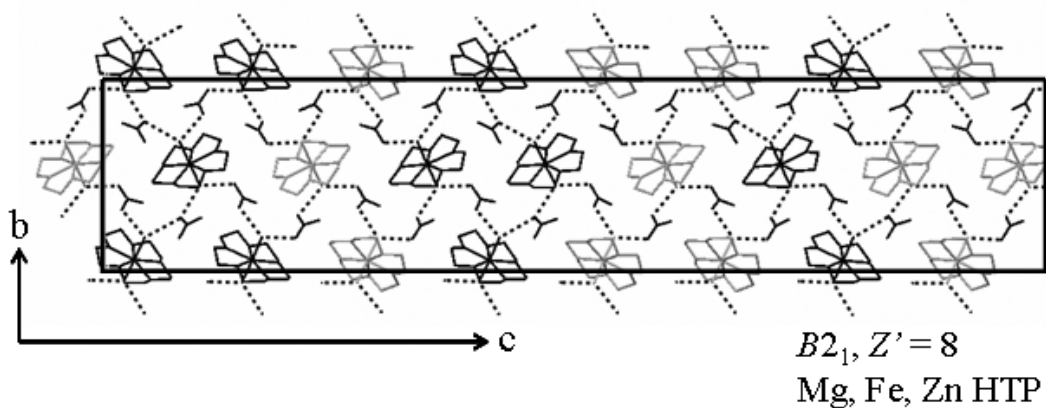
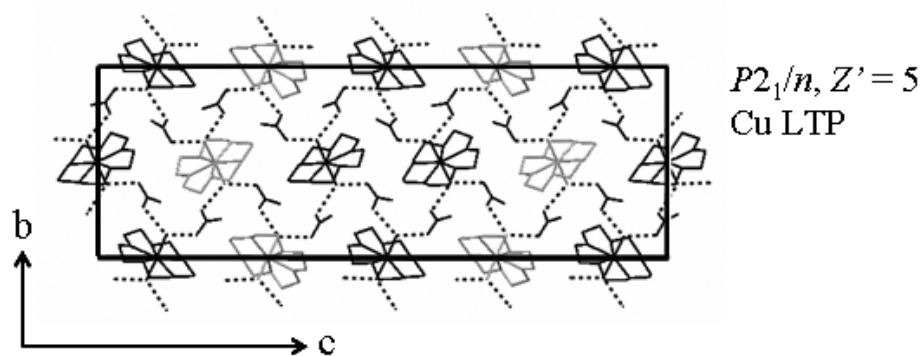
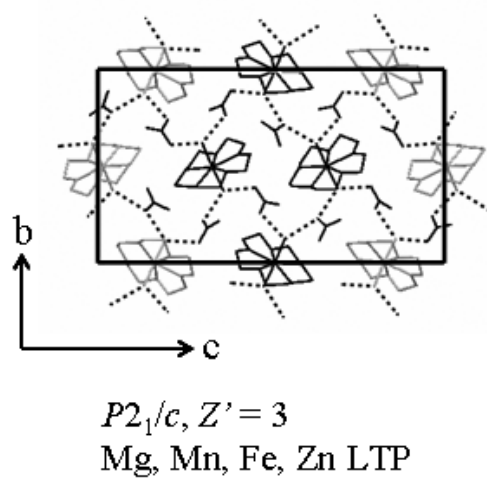
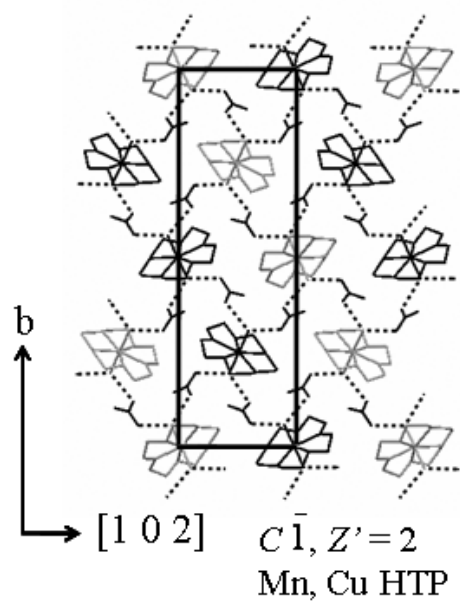


Figure 2.17. Drawing of layers of the four crystal structures of $[M(\text{H}_2\text{O})_2(15\text{-crown-5})](\text{NO}_3)_2$, $M = \text{Mg, Mn, Fe, Cu and Zn}$. In the triclinic structure ($C\bar{1}$, $Z' = 2$), cations within a row parallel to $[1\ 0\ 2]$ are related by inversion centers. In the three monoclinic structures ($P2_1/c$, $Z' = 3$; $P2_1/n$, $Z' = 5$; $B2_1$, $Z' = 8$), cations within a row parallel to the \mathbf{c} direction are related by either pseudoinversion or pseudotranslation. For the monoclinic structures, the c axis is not in the plane of the drawing. For the triclinic structures, neither the b axis, nor $[1\ 0\ 2]$ is in the plane of the drawing. The black and grey cations correspond to conformational enantiomers R/S. The minor disorder for the $Z' = 8$ and H atoms are omitted for clarity. H bonds are shown as black dotted lines.

Conclusions

The study of the high-temperature phases of $[M(\text{H}_2\text{O})_2(15\text{-crown-5})](\text{NO}_3)_2$, $M = \text{Mg}$, Fe and Zn is complementary to previous works of the system $[M(\text{H}_2\text{O})_2(15\text{-crown-5})](\text{NO}_3)_2$, $M = \text{Mg}$, Mn, Co, Cu and Zn. The system $[M(\text{H}_2\text{O})_2(15\text{-crown-5})](\text{NO}_3)_2$ turns out to be a rich polymorphic system in which all solid-solid phase transitions were investigated by DSC measurements and single-crystal X-ray experiments. The 2-D group has been extended to ten phases, which were solved and refined in four different space groups. All phases of the 2-D group have very similar packing and H-bonding patterns but are found to have different enantiomeric alternation patterns along one direction ($[1\ 0\ 2]$ for the triclinic phase and the c direction for the three monoclinic phases). The enantiomeric alternation pattern is found to become perfect ($M = \text{Mn}$, Cu) or more perfect ($M = \text{Mg}$, Fe, Zn) when single crystals of $[M(\text{H}_2\text{O})_2(15\text{-crown-5})](\text{NO}_3)_2$, $M = \text{Mg}$, Mn, Fe, Co, Cu and Zn, pass through the solid-solid phase transition LTP \rightarrow HTP. The study shows that there are at least two phases for each compound of the series (except for $M = \text{Co}$). All reversible solid-solid phase transitions are possible because enantiomers R/S can interconvert in the solid state without significant crystal damage.

The three isostructural high-temperature phases of the Mg, Fe and Zn compounds have never been reported in the literature. They are found to be commensurately modulated superstructures and have very unusual high- Z' values (8). The refinement of such a phase is not trivial. The high degree of pseudosymmetry and the lack of information [low percentage of reflections having $I > 2\sigma(I)$] were responsible for making the refinement unsatisfactory. Using a more powerful X-ray source (Bruker-Nonius X8 Proteum with Cu $K\alpha$ radiation) and using an appropriate set of constraints / restraints allowed acceptable refinements of the high-temperature phases of the Mg, Zn compounds. The high-temperature phase of the Fe compound was less problematic, because data could be collected at 90 K, which increased the ratio of reflections having $I > 2\sigma(I)$. This study may help to tackle the refinement process of other complicated commensurately modulated structures.

Chapter Three

-

Toward the Insertion of the Ni²⁺ Ion Inside the 15-crown-5 Molecule

Introduction

Several syntheses aimed at inserting an Ni²⁺ ion inside the 15-crown-5 molecule are presented in this chapter. The principal goal of this research was to synthesize the compound [Ni(H₂O)₂(15-crown-5)](NO₃)₂ in order to complete the series of compounds [M(H₂O)₂(15-crown-5)](NO₃)₂, M = Mg, Mn, Fe, Co, Cu and Zn (Hao, Parkin & Brock, 2005; Hao, Siegler, Parkin & Brock, 2005). Six Ni(II) complexes³⁸ that include Ni²⁺, NO₃⁻, 15-crown-5 and water, and sometimes acetonitrile or methanol were found in the course of this research. The single-crystal X-ray experiments showed that the Ni²⁺ ions is not coordinated by the 15-crown-5 molecules in any of these compounds. Three³⁹ of them turned out to be polymorphic systems for which the phase transitions were investigated methodically. The three polymorphic systems are discussed in the subsequent chapters (Chapters 4, 5 and 6). One part of this chapter is concerned with reporting the structures of the second polymorph of [Ni(H₂O)₆](NO₃)₂·(15-crown-5)·H₂O, [Ni(H₂O)₆](NO₃)₂·*trans*-[Ni(H₂O)₄(MeOH)₂](NO₃)₂·2(15-crown-5) and *cis*-[Ni(H₂O)₄(NO₃)₂]·*trans*-[Ni(H₂O)₄(NO₃)₂]·2(15-crown-5). The structure reports include details about the crystal growth, the refinement and the packing analysis of these three compounds.

³⁸ Six Ni(II) complexes containing uncoordinated 15-crown-5 molecules have been found. They are given in the subsequent list in order of increasing exclusion of water from the structure:

- i. [Ni(H₂O)₆](NO₃)₂·(15-crown-5)·2H₂O [Z' = 1 ↔ 7 ↔ 1/2 ↔ 1/4, (H₂O)/(Ni²⁺) = 8]
- ii. First polymorph of [Ni(H₂O)₆](NO₃)₂·(15-crown-5)·H₂O [Z' = 1 ↔ 2, (H₂O)/(Ni²⁺) = 7]
- iii. Second polymorph of [Ni(H₂O)₆](NO₃)₂·(15-crown-5)·H₂O [Z' = 3, (H₂O)/(Ni²⁺) = 7]
- iv. [Ni(H₂O)₆](NO₃)₂·*trans*-[Ni(H₂O)₄(MeOH)₂](NO₃)₂·2(15-crown-5) [Z' = 1/2, (H₂O)/(Ni²⁺) = 5]
- v. *cis*-[Ni(H₂O)₄(NO₃)₂]·*trans*-[Ni(H₂O)₄(NO₃)₂]·2(15-crown-5) [Z' = 2, (H₂O)/(Ni²⁺) = 4]
- vi. [Ni(H₂O)₂(MeCN)(NO₃)₂]·(15-crown-5)·MeCN [Z' = 2 ↔ 1 ↔ 5 ↔ 1/2, (H₂O)/(Ni²⁺) = 2]

³⁹ [Ni(H₂O)₆](NO₃)₂·(15-crown-5)·2H₂O, the first polymorph of [Ni(H₂O)₆](NO₃)₂·(15-crown-5)·H₂O and [Ni(H₂O)₂(MeCN)(NO₃)₂]·(15-crown-5)·MeCN

The synthesis of the target compound $[\text{Ni}(\text{H}_2\text{O})_2(15\text{-crown-5})](\text{NO}_3)_2$ was eventually achieved *via* a route that was designed to limit the amount of water available for inclusion in the structure. The series of compounds $[M(\text{H}_2\text{O})_2(15\text{-crown-5})](\text{NO}_3)_2$, $M = \text{Mg, Mn, Fe, Co, Cu}$ and Zn has then been extended to include two phases for $M = \text{Ni}$. Another part of this chapter is concerned with the crystallographic description of the relationship of the two phases of $[\text{Ni}(\text{H}_2\text{O})_2(15\text{-crown-5})](\text{NO}_3)_2$. The two phases (phases I and II) are modulated superstructures with $Z' = 2, 3$ (I, II) and the modulations are commensurate. The solid-solid phase transition was investigated *via* DSC measurements. This research also shows evidence that the coordination of the Ni^{2+} ion in $[\text{Ni}(\text{H}_2\text{O})_2(15\text{-crown-5})]^{2+}$ differs from that of the M^{2+} ion in $[M(\text{H}_2\text{O})_2(15\text{-crown-5})]^{2+}$, $M = \text{Mg, Mn, Fe, Co, Cu}$ and Zn .

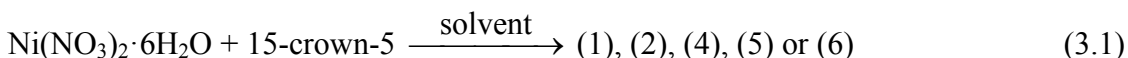
Experimental

Crystal Growth

The six Ni(II) complexes, for which the Ni²⁺ ions are not coordinated by the 15-crown-5 molecule, are given in the order of decreasing the ratio of water molecules to Ni²⁺ ions. Five of these complexes were obtained *via* the same route using different solvents. The second polymorph of [Ni(H₂O)₆](NO₃)₂·(15-crown-5)·H₂O was obtained *via* a different route. The six Ni(II) complexes are given in the following list:

- (1). [Ni(H₂O)₆](NO₃)₂·(15-crown-5)·2H₂O, (H₂O)/(Ni²⁺) = 8
- (2). The first polymorph of [Ni(H₂O)₆](NO₃)₂·(15-crown-5)·H₂O, (H₂O)/(Ni²⁺) = 7
- (3). The second polymorph of [Ni(H₂O)₆](NO₃)₂·(15-crown-5)·H₂O, (H₂O)/(Ni²⁺) = 7
- (4). [Ni(H₂O)₆](NO₃)₂·*trans*-[Ni(H₂O)₄(MeOH)₂](NO₃)₂·2(15-crown-5), (H₂O)/(Ni²⁺) = 5
- (5). *cis*-[Ni(H₂O)₄(NO₃)₂]·*trans*-[Ni(H₂O)₄(NO₃)₂]·2(15-crown-5), (H₂O)/(Ni²⁺) = 4
- (6). [Ni(H₂O)₂(MeCN)(NO₃)₂]·(15-crown-5)·MeCN, (H₂O)/(Ni²⁺) = 2

Pale green crystals of the compounds (1), (2), (4), (5) and (6) were grown at room temperature from a solvent solution of 15-crown-5 and Ni(NO₃)₂·6H₂O (see the chemical equation 3.1).



Crystals of (1) were obtained from a water solution and were found to be parallelepipeds. Details about the crystal habit of (1) are given in Chapter 5.

Crystals of (2) and (5) were obtained in the same vial from an acetone solution. The crystal growth of (5) took place first and was localized at the top of the vial. The crystal growth of (2) took place a few hours after the crystal growth of (5) and was localized at the bottom of the vial (with the mother liquor). Crystals of (2) and (5) were found to be respectively parallelepipeds and plates. Details about the crystal habit of (2) are given in

Chapter 4. The crystal growth of (5) seems to be favored along the **a** and **c** directions (see Figure 3.1). Crystals of (5) can be also obtained using 2-butanol or ethanol or THF as the solvent instead of acetone and were found to be blocks.

Crystals of (4) were obtained from a methanol solution and were found to be irregular blocks. Crystals of (6) were obtained from an acetonitrile solution and were found to be parallelepipeds. Crystal habit for this compound has not been investigated yet⁴⁰.

Pale green crystals of (3) and yellow crystals of $[\text{Ni}(\text{H}_2\text{O})_2(15\text{-crown-5})](\text{NO}_3)_2$ (target compound) were grown from several milligrams of pale green crystals of (1) *via* two different experiments by heating. In the first experiment, very few crystals of (3) were obtained after a small vial of single crystals of (1) inserted into a water bath had been heated from room temperature to nearly 348 K and had been subsequently cooled to room temperature (the cooling process took no more than 30 minutes). The procedure for the second experiment was very similar to that described above except that the crystal growth of the target compound was carried out near 373 K instead of 348 K. There are no available quantitative data⁴¹ (*i.e.*, amounts of starting materials, yield) for these two syntheses yet. Compound (1) was found to decompose completely near 339-341 K. The melting is thought to be incongruent because another unknown solid phase⁴² appeared just above 341 K. Evidence of extra phases (side products of the reaction) other than (3) and the target compound might have been carried out using X-ray powder diffraction. Crystals of the target compound started to appear near 350 K. The heating used in these two experiments aimed to limit the amount of water in the structure. The difference between the pale green color of crystals of (1) and the yellow color of crystals of the target compound is a clear indication that the coordination around the Ni^{2+} ion is different in the two compounds.

⁴⁰ The synthesis of the compound $[\text{Ni}(\text{H}_2\text{O})_2(\text{MeCN})(\text{NO}_3)_2] \cdot (15\text{-crown-5}) \cdot \text{MeCN}$ seems to be more difficult to reproduce. The compounds $[\text{Ni}(\text{H}_2\text{O})_6](\text{NO}_3)_2 \cdot (15\text{-crown-5}) \cdot \text{H}_2\text{O}$ (first polymorph) and *cis*- $[\text{Ni}(\text{H}_2\text{O})_4(\text{NO}_3)_2] \cdot \text{trans-}[\text{Ni}(\text{H}_2\text{O})_4(\text{NO}_3)_2] \cdot 2(15\text{-crown-5})$ were also found while several attempts were made to synthesize $[\text{Ni}(\text{H}_2\text{O})_2(\text{MeCN})(\text{NO}_3)_2] \cdot (15\text{-crown-5}) \cdot \text{MeCN}$. Temperature conditions during crystal growth might be taken into consideration for the lack of reproducibility for growing crystals of the acetonitrile compound.

⁴¹ Such information is relevant for the organic and inorganic chemists.

⁴² Maybe the second polymorph of $[\text{Ni}(\text{H}_2\text{O})_6](\text{NO}_3)_2 \cdot (15\text{-crown-5}) \cdot \text{H}_2\text{O}$.

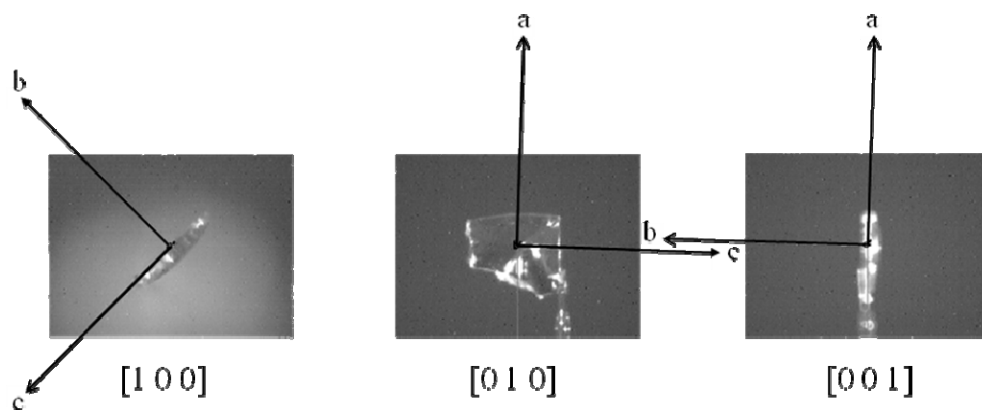


Figure 3.1. The chosen crystal (plate) of *cis*-[Ni(H₂O)₄(NO₃)₂]*·trans*-[Ni(H₂O)₄(NO₃)₂]*·2*(15-crown-5) was grown from an acetone solution and was indexed near 90 K. The crystal projections down [1 0 0], [0 1 0] and [0 0 1] were obtained using the program *COLLECT* (Nonius, 1997). The crystal growth appears to be more favored along the **a** and **c** directions and less favored along the **b** direction.

Differential Scanning Calorimetry Measurements

The compound $[\text{Ni}(\text{H}_2\text{O})_2(15\text{-crown-5})](\text{NO}_3)_2$ was investigated using the DSC 822^e apparatus and the controlling software STAR^e (version 8.10) manufactured by *METTLER TOLEDO*. The DSC sample was prepared from fine powders. The heating rate and cooling rates were set at 10 and -10 K/min in the range 173-298 K. The amount of the nickel complex was 2.10(1) mg. Only one solid-solid phase transition was found at $T_{\text{onset}} = 288$ K (given for heating). The phase transition is first-order because of the occurrence of hysteresis. The small peak heights in the DSC traces prevent a good estimation of ΔH_{tr} (see Figure 3.2).

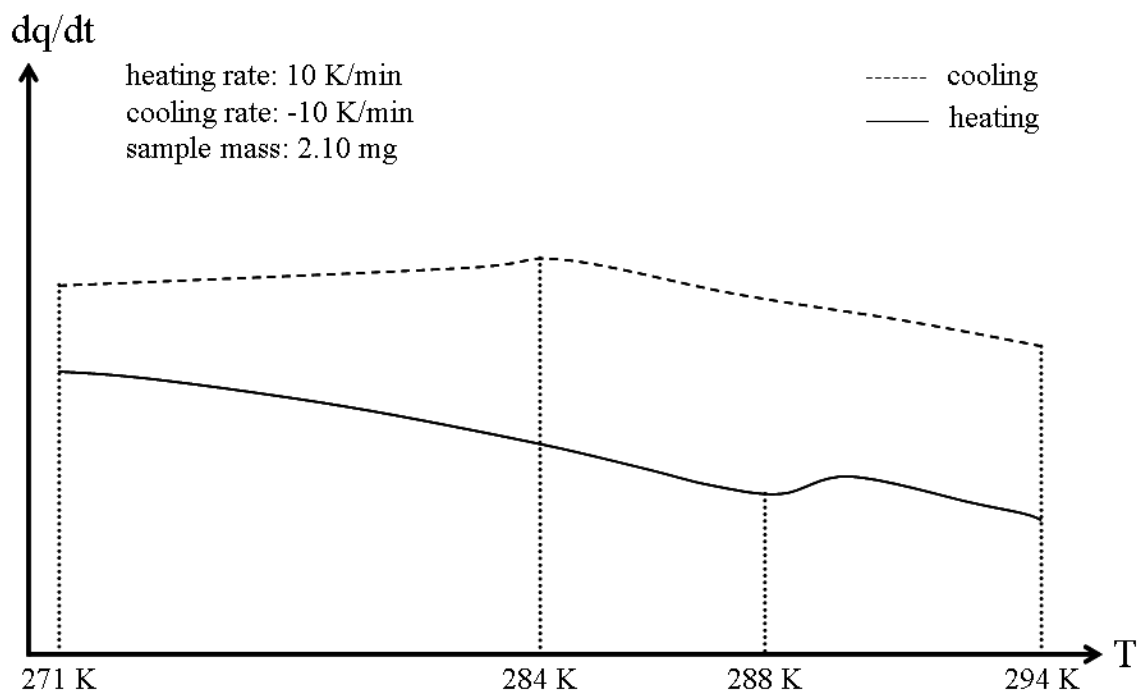


Figure 3.2. Parts of the DSC traces of $[\text{Ni}(\text{H}_2\text{O})_2(15\text{-crown-5})](\text{NO}_3)_2$ measured at -10 (cooling) and 10 K/min (heating). The two traces show only one solid-solid phase transition near 284 (cooling) and 288 K (heating).

Hot-Stage Microscopy

The crystal growth of the compound $[\text{Ni}(\text{H}_2\text{O})_2(15\text{-crown-5})](\text{NO}_3)_2$ was investigated *via* hot-stage microscopy experiments. The temperature was controlled using the *STC200* temperature controller and the *HCS302* hot-stage chamber (*INSTECH*). All digital frames were collected using the *Olympus BX51* research microscope and the *Insight Firewire 4 MegaSample Colour Mosaic* digital camera under the program *SPOT advanced 4.6* (*DIAGNOSTIC INSTRUMENTS INC.*). Single crystals of the starting material $[\text{Ni}(\text{H}_2\text{O})_6](\text{NO}_3)_2 \cdot (15\text{-crown-5}) \cdot 2\text{H}_2\text{O}$ as it underwent transformation to the target compound $[\text{Ni}(\text{H}_2\text{O})_2(15\text{-crown-5})](\text{NO}_3)_2$ were monitored from 298 to 373 K at 1 and 5 K/min. Hot-stage microscopy experiments were more informative when a slower heating rate (*i.e.*, 1 K/min) was chosen. Crystals of $[\text{Ni}(\text{H}_2\text{O})_6](\text{NO}_3)_2 \cdot (15\text{-crown-5}) \cdot 2\text{H}_2\text{O}$ were found to be stable between 298 and 317 K. Near 317 K, cracks appeared on the surface of the crystal and became larger as the temperature increased. These cracks most likely correspond to a solid-solid phase transition and parallel faces of many new crystallites appear. From 328 to 337 K, defects became more and more important and the crystal looked very fragmented (see Figure 3.3). Above 338 K, crystals of $[\text{Ni}(\text{H}_2\text{O})_6](\text{NO}_3)_2 \cdot (15\text{-crown-5}) \cdot 2\text{H}_2\text{O}$ melted; melting was complete at 341-342 K. Crystals of an undetermined compound grew beginning at 341 K but then began to disappear as yet another phase grew above 350 K. Further investigation will be required to identify the intermediate compound. Nucleation of crystals of $[\text{Ni}(\text{H}_2\text{O})_2(15\text{-crown-5})](\text{NO}_3)_2$ took place near 350 K and the crystal growth continued to 373K (see Figure 3.4).

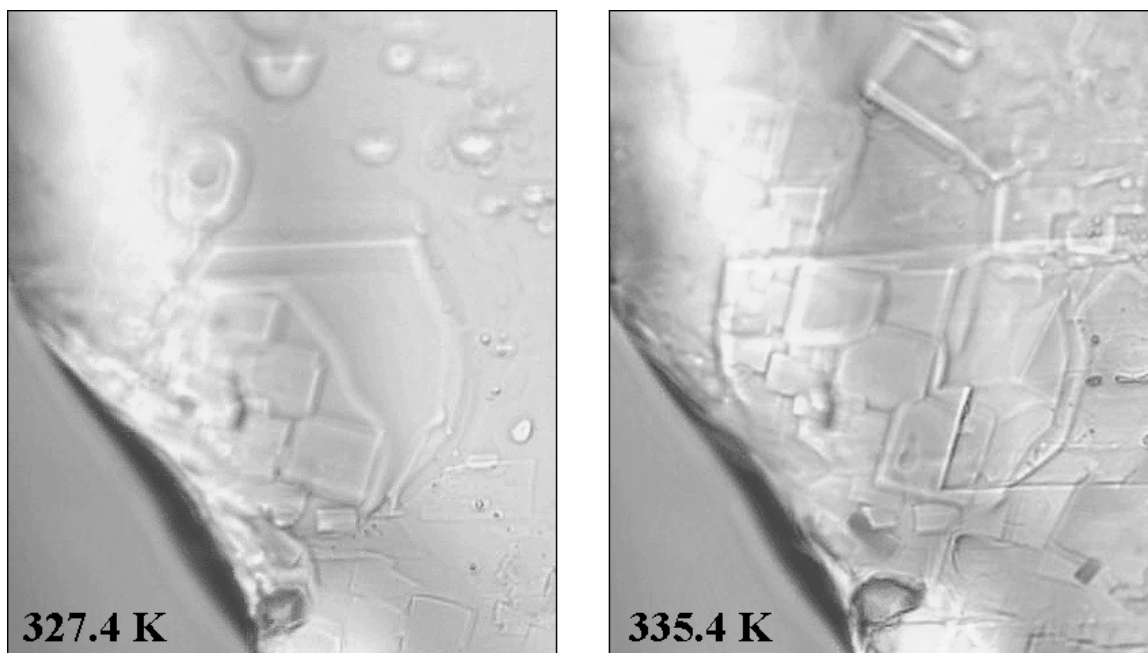


Figure 3.3. Magnified digital frames of one part of a single crystal of $[\text{Ni}(\text{H}_2\text{O})_6](\text{NO}_3)_2 \cdot (15\text{-crown-5}) \cdot 2\text{H}_2\text{O}$ at 327.4 and 335.4 K. Parallel faces of many new crystallites are observed at these temperatures.

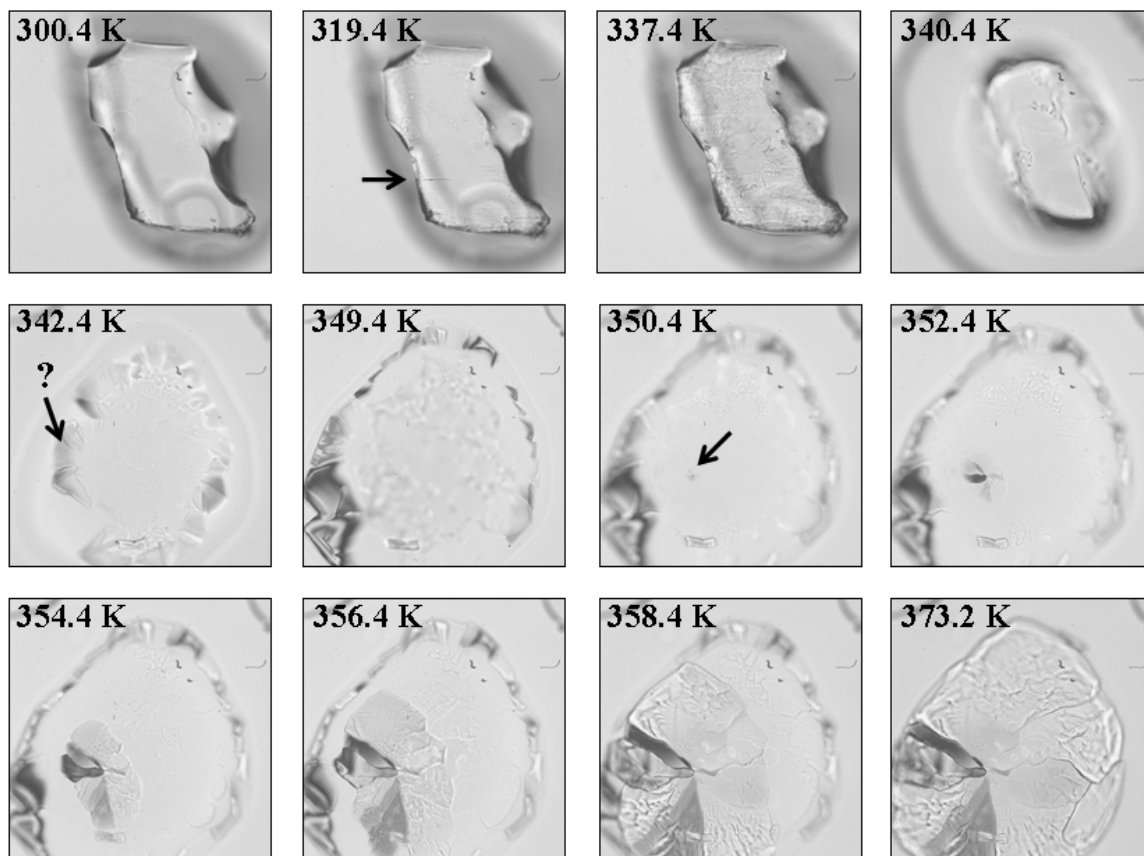


Figure 3.4. Digital frames (10x magnification) obtained from hot-stage microscopy experiments. Crystals of the starting material $[\text{Ni}(\text{H}_2\text{O})_6](\text{NO}_3)_2 \cdot (15\text{-crown-5}) \cdot 2\text{H}_2\text{O}$ are monitored by optical microscopy as the temperature increases. Crystals are found to be stable between 298 and 317 K. Near 317 K, cracks appear on the surface of the crystal. Above 318 K, cracks become larger and crystallites of an unknown phase become noticeable. The decomposition of the crystal is found to occur near 340-341 K. Crystals of an unknown compound can be observed between 341 and 350 K. Nucleation of crystals of the desired compound $[\text{Ni}(\text{H}_2\text{O})_2(15\text{-crown-5})](\text{NO}_3)_2$ occurs near 350 K.

X-ray crystallography

The general procedures for data collection and for the H-atoms treatment were given in the corresponding section of Chapter 2.

All data were collected using a Nonius KappaCCD diffractometer with graphite-monochromated Mo $K\alpha$ radiation ($\lambda = 0.71073 \text{ \AA}$) under the program *COLLECT* (Nonius, 1997).

The methoxy H-atoms of the methanol ligands in the compound $[\text{Ni}(\text{H}_2\text{O})_6](\text{NO}_3)_2 \cdot \text{trans-}[\text{Ni}(\text{H}_2\text{O})_4(\text{MeOH})_2](\text{NO}_3)_2 \cdot 2(15\text{-crown-5})$ were placed at calculated positions (*AFIX 137*) with isotropic displacement parameters having values 1.5 times U_{eq} of the attached C atom. The hydroxyl H-atoms of the methanol ligands in the previous compound were located in difference Fourier maps and restrained such that the O-H distances had values within accepted ranges [bond length $(\text{O-H})_{90\text{K}} = 0.840 (1) \text{ \AA}$]. The hydroxyl H-atoms have isotropic displacement parameters 1.5 times U_{eq} of the attached O atom.

Structures are given in the order of decreasing the ratio of water molecules to Ni^{2+} ions. For all structures cited below (except when specified), data were collected at 90 K^{43} after crystals had been flash-cooled from room temperature.

⁴³ 90 K is near the lower limit of stable temperature control when the cooling device is running with liquid nitrogen.

[Ni(H₂O)₆](NO₃)₂·(15-crown-5)·H₂O (second polymorph)

The structure of the second polymorph of [Ni(H₂O)₆](NO₃)₂·(15-crown-5)·H₂O was solved and refined in the space group $P\bar{1}$ with $Z' = 3$. The conventional cell was transformed so that H-bonded chains of the [Ni(H₂O)₆]²⁺ ions and the 15-crown-5 molecules are along the a axis. The transformation matrix is given by: $\mathbf{a}(P\bar{1}) = \begin{pmatrix} -1 & 1 & 0 \\ 0 & 1 & 0 \\ 0 & 1 & 0 \end{pmatrix} \mathbf{a}(P\bar{1})$. The cell constants of the conventional cell at 90 K are: $a = 10.163$ (1)Å, $b = 13.607$ (1)Å, $c = 24.765$ (2)Å, $\alpha = 82.21$ (1)°, $\beta = 89.71$ (1)°, $\gamma = 83.50$ (1)°.

The asymmetric unit contains three 15-crown-5 molecules, four [Ni(H₂O)₆]²⁺ ions, six nitrate ions and three lattice water molecules. Two [Ni(H₂O)₆]²⁺ cations are located at sites of inversion symmetry. The two other [Ni(H₂O)₆]²⁺ cations have no symmetry imposed.

The refinement was not completely satisfactory because several crystallographic problems were found. Although the R factor [$F^2 > 2\sigma(F^2)$] is not unusually high (~ 0.057), the final difference Fourier map showed peaks as large as $1.93 \text{ e } \text{Å}^{-3}$. The largest peaks (0.57 - $1.93 \text{ e } \text{Å}^{-3}$) were located at about 1 Å from the Ni²⁺ ions. One isolated peak ($1.38 \text{ e } \text{Å}^{-3}$) was located at about 2.5 Å from one oxygen atom of two nitrate ions and at about 2.6 Å from one oxygen atom of one [Ni(H₂O)₆]²⁺ cation. The latter peak was initially thought to be a partial occupancy lattice water molecule but the intermolecular distances between the lattice water molecule and its neighbors (*i.e.*, two nitrate ions and one [Ni(H₂O)₆]²⁺ cation) would then be too short. The existence of a partial occupancy lattice water molecule in the structure was then ruled out. Another problem was the existence of extra reflections found in the reconstructed reciprocal lattice slices. This may indicate the existence of twinning although the program suite *PLATON* (Spek, 2005) failed to identify any reasonable twin law. The problems observed in the refinement may result from the single crystals not being phase pure. Although there are some problems with the refinement, the overall structure is basically correct. Disorder of one nitrate ion is observed. The value of the occupancy factor given for the major component is 0.529 (6). The ellipsoids of all atoms in the asymmetric units are shown in Figure 3.5.

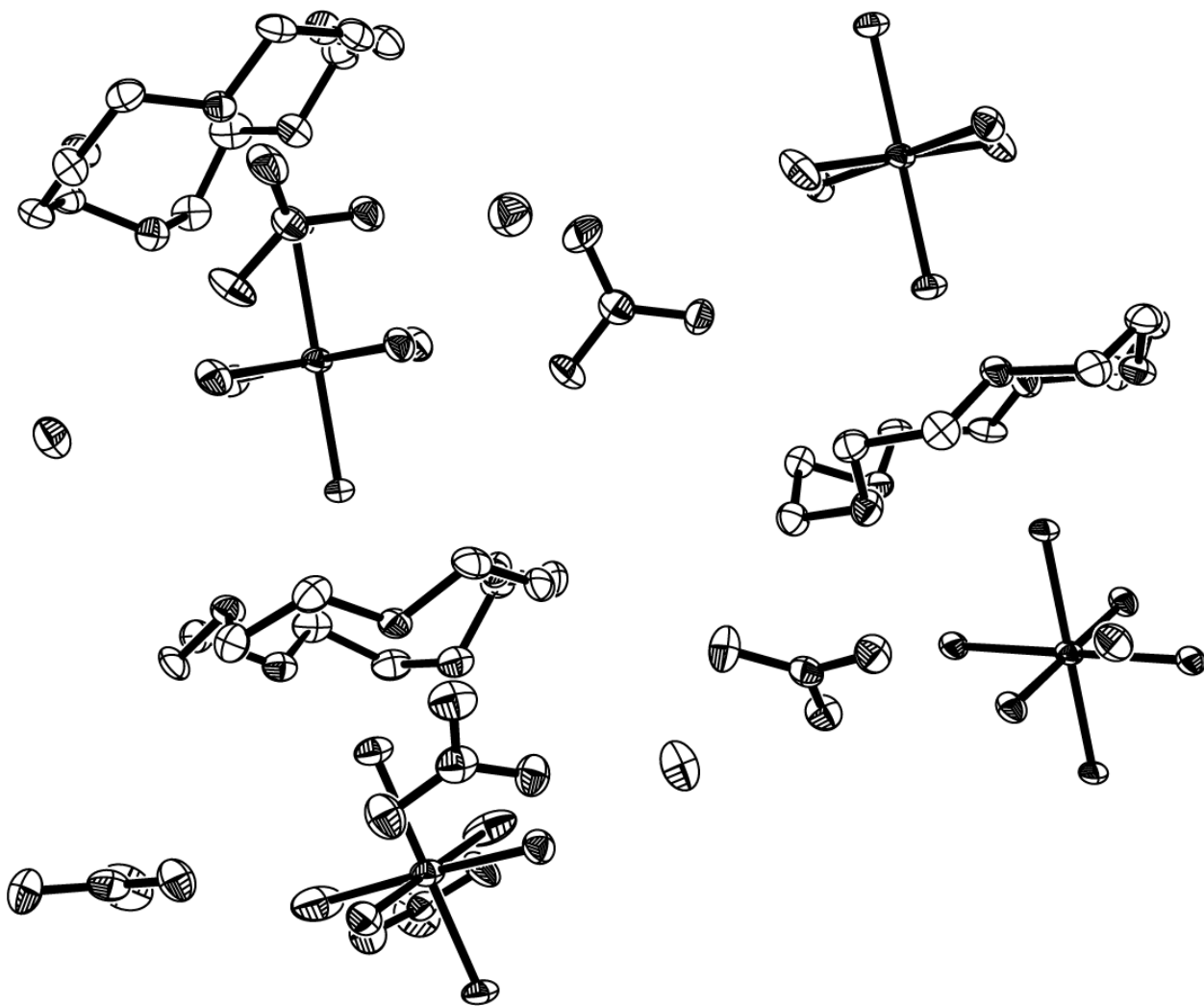


Figure 3.5. The displacement ellipsoids (50% probability level) of the asymmetric unit of the second polymorph of $[\text{Ni}(\text{H}_2\text{O})_6](\text{NO}_3)_2 \cdot (15\text{-crown-5}) \cdot \text{H}_2\text{O}$ at 90 K. The minor component of the disordered nitrate ion and H atoms are omitted for clarity.

[Ni(H₂O)₆](NO₃)₂·*trans*-[Ni(H₂O)₄(MeOH)₂](NO₃)₂·2(15-crown-5)

The structure of [Ni(H₂O)₆](NO₃)₂·*trans*-[Ni(H₂O)₄(MeOH)₂](NO₃)₂·2(15-crown-5) was solved and refined in the space group $P2_1/c$ with $Z' = \frac{1}{2}$. The alternative setting $P2_1/n$ was preferred so that H-bonded chains of the [Ni(H₂O)₆]²⁺, [Ni(H₂O)₄(MeOH)₂]²⁺ ions and 15-crown-5 molecules are along a crystallographic axis as they are in other structures⁴⁴. The transformation matrix is given by: $\mathbf{a}(P2_1/n) = (-1 \ 0 \ -1 / 0 \ 1 \ 0 / 1 \ 0 \ 0) \mathbf{a}(P2_1/c)$. The cell constants of the $P2_1/c$ cell at 90 K are: $a = 10.429 (1)\text{Å}$, $b = 15.481 (1)\text{Å}$, $c = 14.118 (1)\text{Å}$, $\beta = 98.66 (1)^\circ$.

The Ni²⁺ ions of [Ni(H₂O)₆]²⁺ and [Ni(H₂O)₄(MeOH)₂]²⁺ are located on inversion centers. The asymmetric unit contains one 15-crown-5 molecule, $\frac{1}{2}$ [Ni(H₂O)₆]²⁺, $\frac{1}{2}$ [Ni(H₂O)₄(MeOH)₂]²⁺ and two nitrate ions.

A first attempt to refine the structure was not satisfactory: the R factor [$F^2 > 2\sigma(F^2)$] was about 0.075 and the final difference Fourier map suggested high residual electron density with peaks ranging within 2.06-3.00 e Å⁻³. The largest peaks were located near O1 and O2 atoms of the crown-ether ligand. The ellipsoids of the O1 and O2 atoms were very eccentric and the ellipsoids of the C1, C2, C3 and C10 atoms of the 15-crown-5 molecule were also suspicious (see Figure 3.6). These observations were all warning signs suggesting disorder of the 15-crown-5 molecule. The disorder results from the non-superposition of the two conformational enantiomers (hereafter, R and S) of the crown ether. The disorder is found to be partial rather than full because some parts of the two enantiomers overlay well and some other parts of the two enantiomers cannot be superimposed [see the parts (a), (b) and (c) of Figure 3.7].

⁴⁴ [Ni(H₂O)₆](NO₃)₂·(15-crown-5)· n H₂O ($n = 1, 2$), *cis*-[Ni(H₂O)₄(NO₃)₂]·*trans*-[Ni(H₂O)₄(NO₃)₂]·2(15-crown-5) and [Ni(H₂O)₂(MeCN)(NO₃)₂]·(15-crown-5)·MeCN.

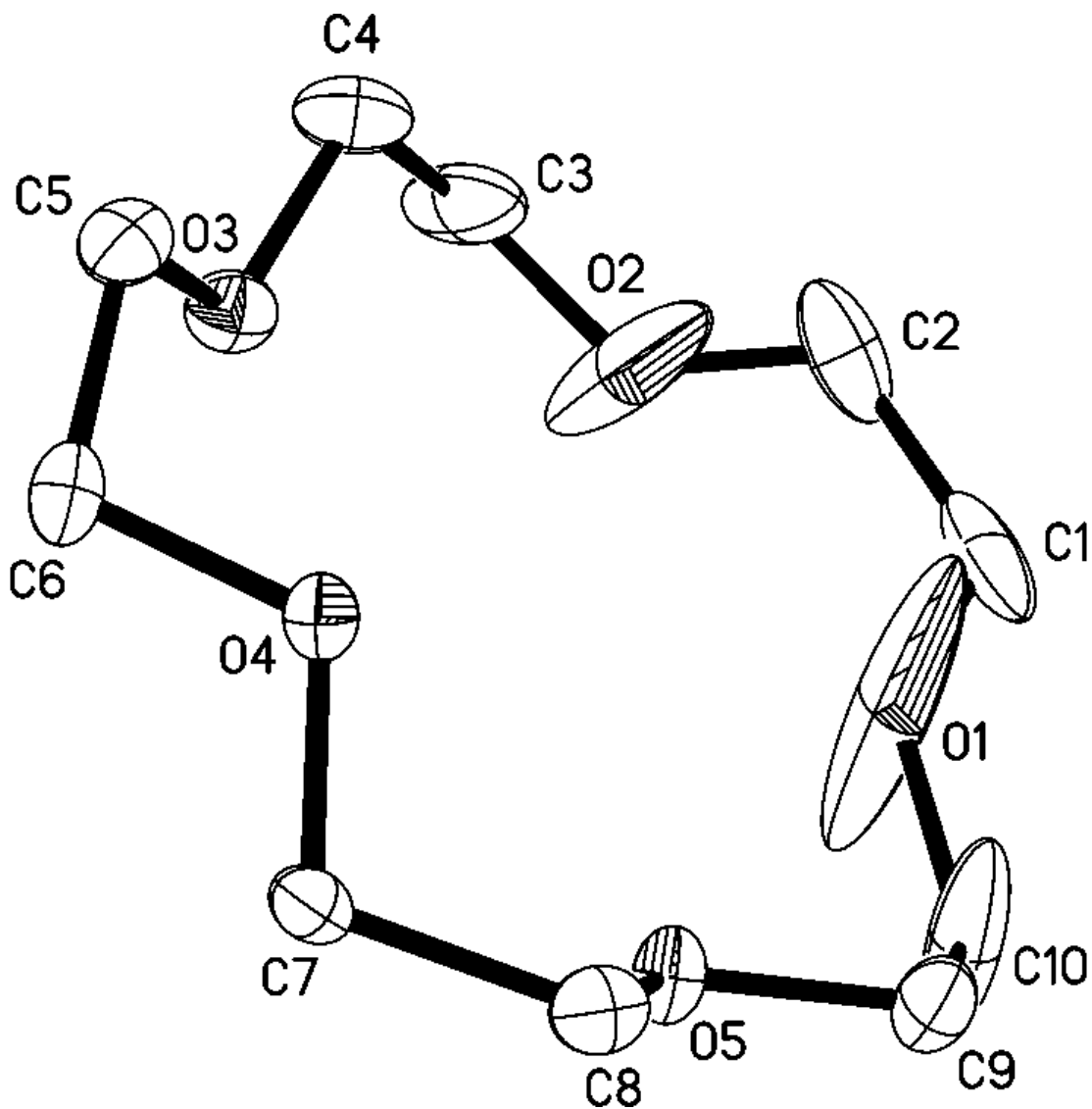


Figure 3.6. The displacement ellipsoids (50% probability level) of the 15-crown-5 molecule in the compound $[\text{Ni}(\text{H}_2\text{O})_6](\text{NO}_3)_2 \cdot \text{trans}-[\text{Ni}(\text{H}_2\text{O})_4(\text{MeOH})_2](\text{NO}_3)_2 \cdot 2(15\text{-crown-5})$ at 90 K. The ellipsoids of the O1 and O2 atoms are very eccentric. The ellipsoids of the C1, C2, C3 and C10 atoms are abnormally elongated. The ellipsoids of the other atoms look normal. H atoms are omitted for clarity.

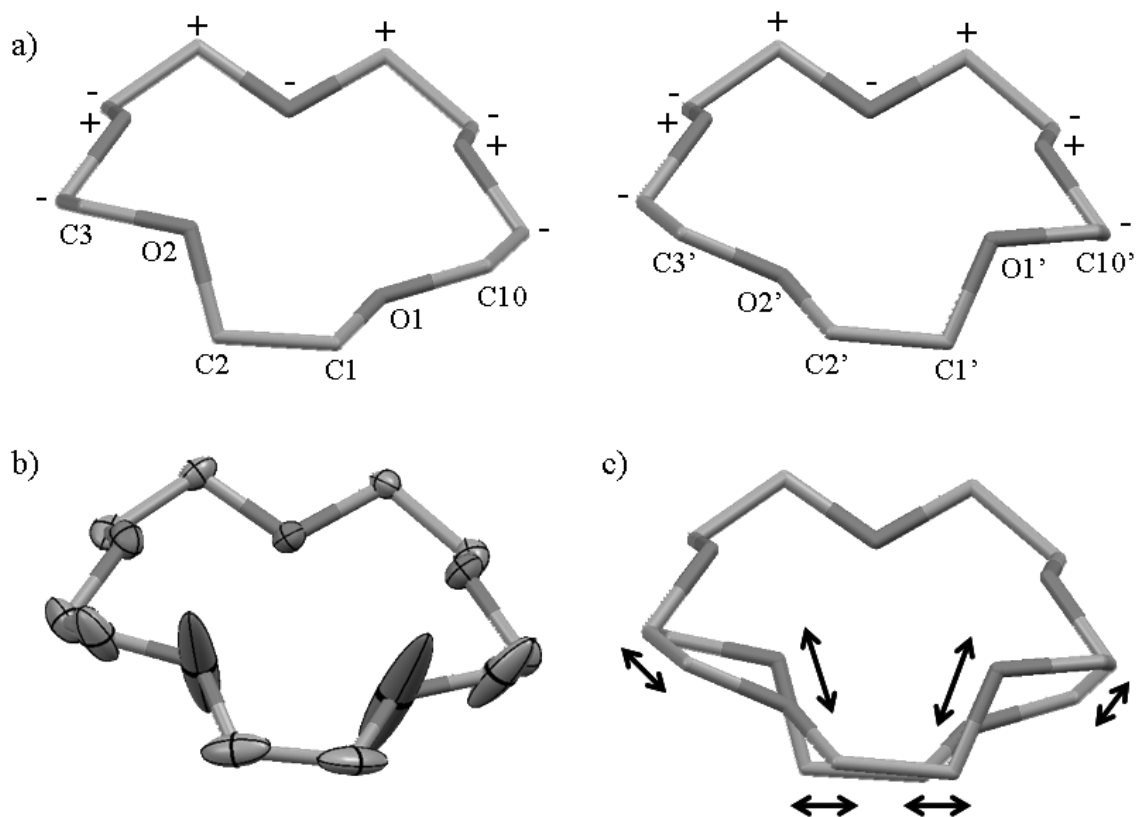


Figure 3.7. (a) Drawing showing the geometry of the two conformational enantiomers of the 15-crown-5 molecule. The + / - fragments of the two enantiomers overlay well, whereas the C3–O2–C2–C1–O1–C10 fragment of one enantiomer and the C3'–O2'–C2'–C1'–O1'–C10' fragment of the other enantiomer cannot be superimposed. (b) The displacement ellipsoids (50% probability level) of the 15-crown-5 molecule in the compound $[\text{Ni}(\text{H}_2\text{O})_6](\text{NO}_3)_2 \cdot \text{trans}-[\text{Ni}(\text{H}_2\text{O})_4(\text{MeOH})_2](\text{NO}_3)_2 \cdot 2(15\text{-crown-5})$ at 90 K. The eccentric ellipsoids for the C1, C2, C3, C10, O1 and O2 atoms are warning signs of partial disorder of the 15-crown-5 molecule. (c) Overlay of the two conformational enantiomers of the 15-crown-5 molecule. The partial disorder results from the non-superposition of the two enantiomers. The black arrows correspond to the directions of elongation of ellipsoids for the C1, C2, C3, C10, O1 and O2 atoms. H atoms are omitted for clarity.

The inclusion of the disorder improved the model greatly: the R factor [$F^2 > 2\sigma(F^2)$] dropped to 0.037, the ellipsoids of all atoms of the 15-crown-5 molecule looked normal (see Figure 3.8) and the final difference Fourier map showed no peak larger than 0.72 e \AA^{-3} (the largest peak was located less than 0.01 \AA from the Ni^{2+} ion). Other peaks that are not near the Ni^{2+} ion are within the range 0.39-0.61 e \AA^{-3} but have no physical meaning. The anisotropic displacement parameters (hereafter, ADPs) of the related disordered atoms C1, C1', C2, C2', C3, C3', C10 and C10' were constrained to be identical (*EADP* instruction). The ADPs of the related disordered atoms O1, O1', O2 and O2' were refined without constraints since their atomic coordinates are sufficiently different. The major and minor components of the disorder were restrained to have similar geometry (*SAME* instruction). The bond distances between atoms for each component of the disorder of the crown ether are given in Table 3.1. The value of the occupancy factor given for the major component is 0.575(3). The ellipsoids of all atoms in the asymmetric unit are shown in Figure 3.9.

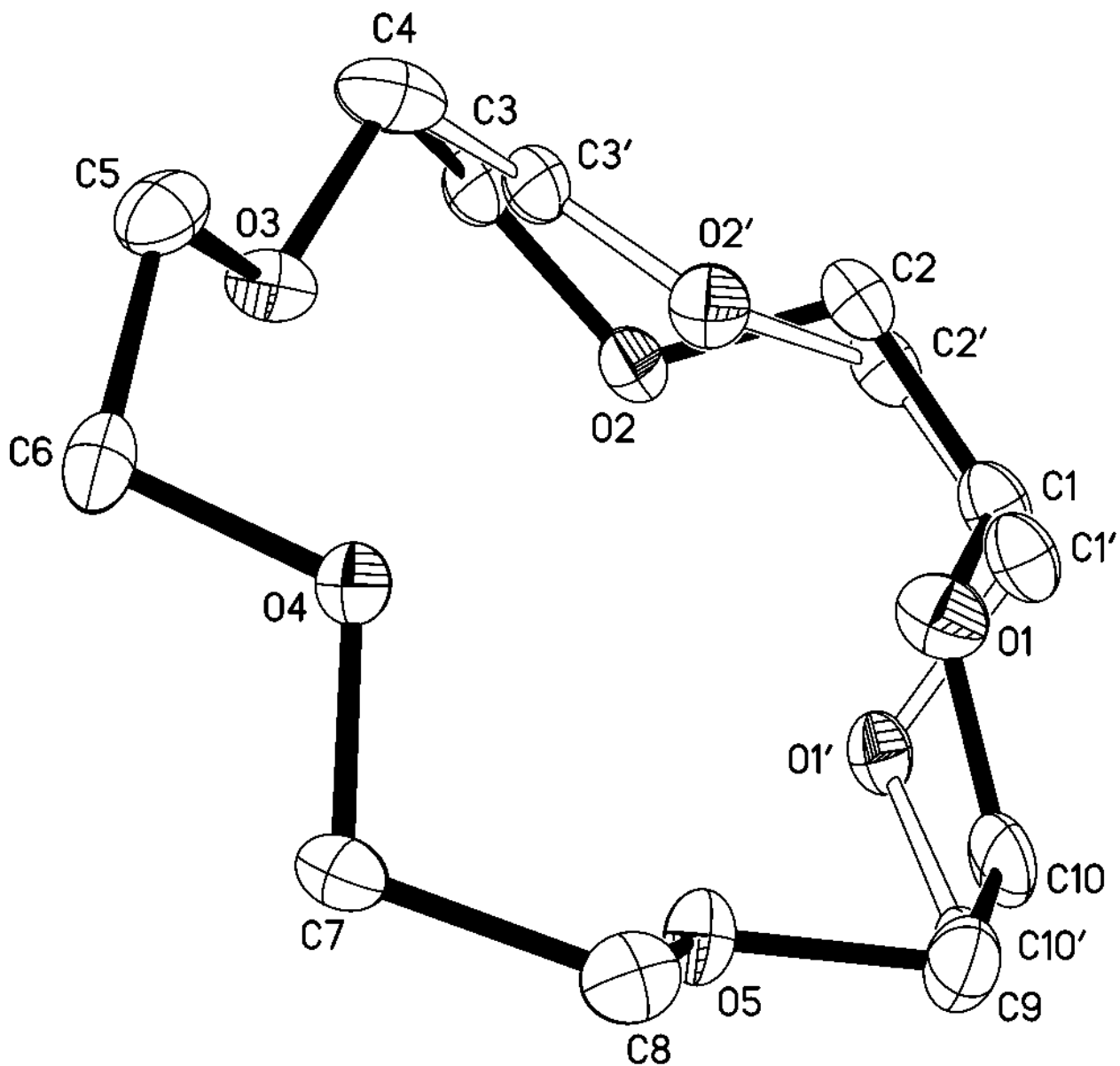


Figure 3.8. The displacement ellipsoids (50% probability level) of the disordered 15-crown-5 molecule in the compound $[\text{Ni}(\text{H}_2\text{O})_6](\text{NO}_3)_2 \cdot \text{trans-}[\text{Ni}(\text{H}_2\text{O})_4(\text{MeOH})_2](\text{NO}_3)_2 \cdot 2(15\text{-crown-5})$ at 90 K. The black solid lines indicate the major component of the disorder. The open lines indicate the minor component of the disorder. H atoms are omitted for clarity.

Table 3.1. Bond distances (Å) between atoms for each component of the disorder of the crown ether in the compound $[\text{Ni}(\text{H}_2\text{O})_6](\text{NO}_3)_2 \cdot \text{trans}-[\text{Ni}(\text{H}_2\text{O})_4(\text{MeOH})_2](\text{NO}_3)_2 \cdot 2(15\text{-crown-5})$.

major component of the disorder		minor component of the disorder	
C1–O1	1.439 (6)	C1'–O1'	1.434 (10)
C1–C2	1.500 (6)	C1'–C2'	1.506 (8)
C2–O2	1.423 (8)	C2'–O2'	1.446 (10)
C3–O2	1.442 (6)	C3'–O2'	1.444 (7)
C10–O1	1.419 (5)	C10'–O1'	1.440 (6)

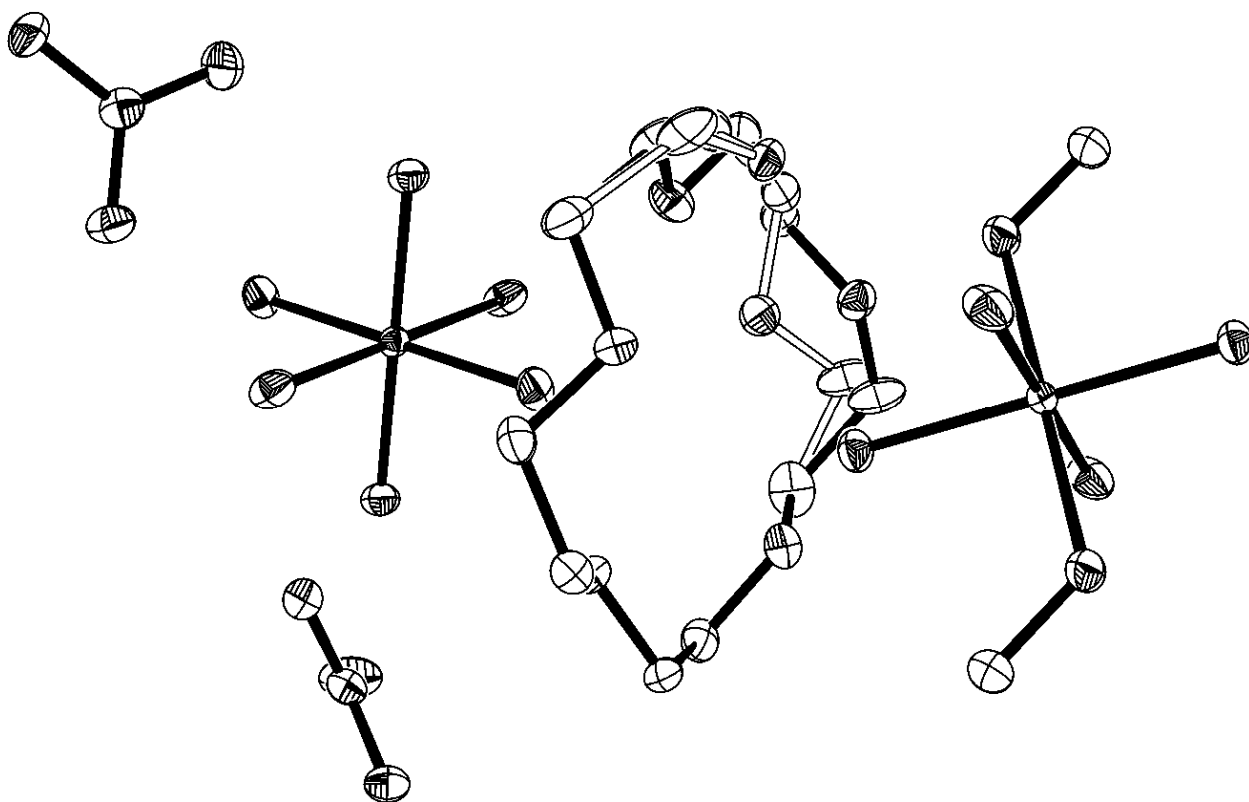


Figure 3.9. The displacement ellipsoids (50% probability level) of the asymmetric unit of the compound $[\text{Ni}(\text{H}_2\text{O})_6](\text{NO}_3)_2 \cdot \text{trans}-[\text{Ni}(\text{H}_2\text{O})_4(\text{MeOH})_2](\text{NO}_3)_2 \cdot 2(15\text{-crown-5})$ at 90 K. The asymmetric unit contains $\frac{1}{2} [\text{Ni}(\text{H}_2\text{O})_6]^{2+}$, $\frac{1}{2} [\text{Ni}(\text{H}_2\text{O})_4(\text{MeOH})_2]^{2+}$, one disordered 15-crown-5 molecule and two nitrate ions. One half of the $[\text{Ni}(\text{H}_2\text{O})_6]^{2+}$ and $[\text{Ni}(\text{H}_2\text{O})_4(\text{MeOH})_2]^{2+}$ ions are symmetry-generated. H atoms are omitted for clarity.

***cis*-[Ni(H₂O)₄(NO₃)₂]·*trans*-[Ni(H₂O)₄(NO₃)₂]·2(15-crown-5)**

The structure was solved and refined in the centrosymmetric space group *Pbca* with $Z' = 1$. The refinement was problem-free: all ellipsoids look normal (see Figure 3.10), the *R* factor [$F^2 > 2\sigma(F^2)$] is less than 0.040 and the final difference Fourier map suggests acceptable residual electron density with peaks no larger than 0.33 e Å⁻³.

The atom-numbering schemes for *trans*-[Ni(H₂O)₄(NO₃)₂] and *cis*-[Ni(H₂O)₄(NO₃)₂] are similar (see Figure 3.11).

[Ni(H₂O)₂(15-crown-5)](NO₃)₂ (phases I and II)

Two phases of [Ni(H₂O)₂(15-crown-5)](NO₃)₂ were isolated: a low-temperature phase with $Z' = 3$ and a high-temperature phase with $Z' = 2$. By convention, the two phases of [Ni(H₂O)₂(15-crown-5)](NO₃)₂ are numbered I and II, I for the high-temperature phase and II for the low-temperature phase.

The atom-numbering scheme is consistent for the two phases (see Figure 3.12).

The phase transition II → I was found in the range 284-288 K. Phase I was originally solved in the space group $P\bar{1}$ with two independent formula units ($Z' = 2$). The cell constants at 308 K of the standard primitive cell are: $a = 10.704(2)\text{Å}$, $b = 12.106(2)\text{Å}$, $c = 15.820(2)\text{Å}$, $\alpha = 108.95(1)^\circ$, $\beta = 105.64(1)^\circ$, $\gamma = 99.88(1)^\circ$. The non-standard space group $C\bar{1}$ was preferred because in this setting the α and γ angles are close to 90° and the H-bonded planes include the b axis, which makes comparisons with phase II easier. The transformation matrix is given by: $\mathbf{a}(C\bar{1}) = (-1 \ -1 \ 0 / -1 \ -1 \ -2 / 1 \ 0 \ 0)\mathbf{a}(P\bar{1})$.

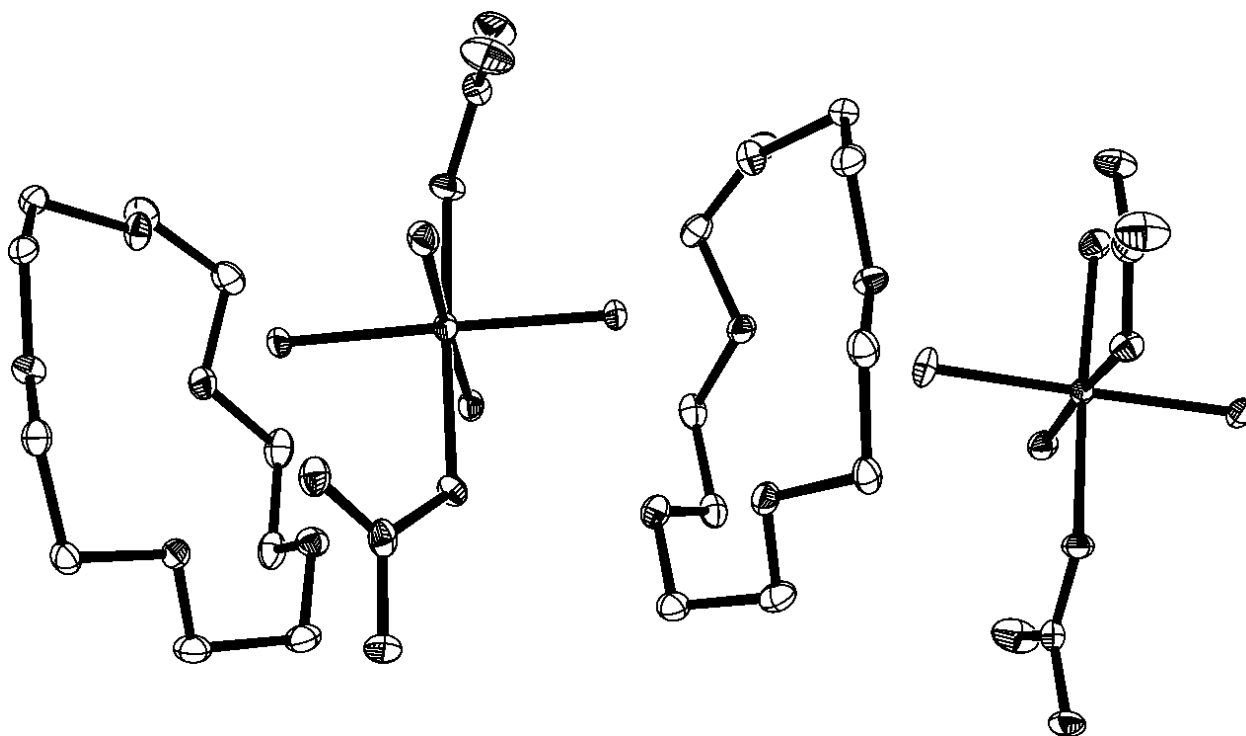


Figure 3.10. The displacement ellipsoids (50% probability level) of the two independent formula units in the asymmetric unit of *cis*-[Ni(H₂O)₄(NO₃)₂]·*trans*-[Ni(H₂O)₄(NO₃)₂]·2(15-crown-5) at 90 K. H atoms are omitted for clarity.

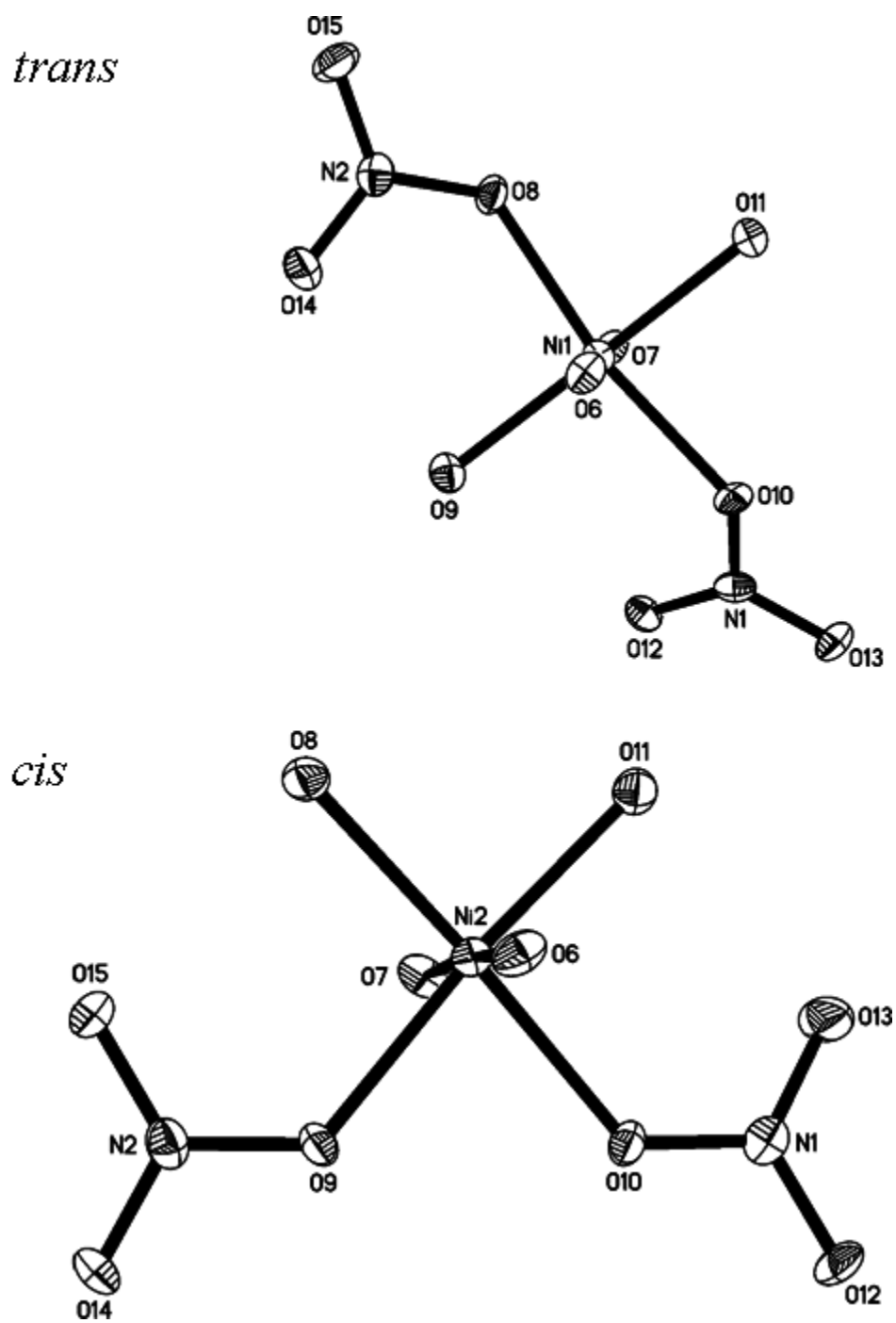


Figure 3.11. The displacement ellipsoids (50% probability level) of the two isomers of $[\text{Ni}(\text{H}_2\text{O})_4(\text{NO}_3)_2]$ at 90K. The atom-numbering scheme is consistent between the two isomers. H atoms are omitted for clarity.

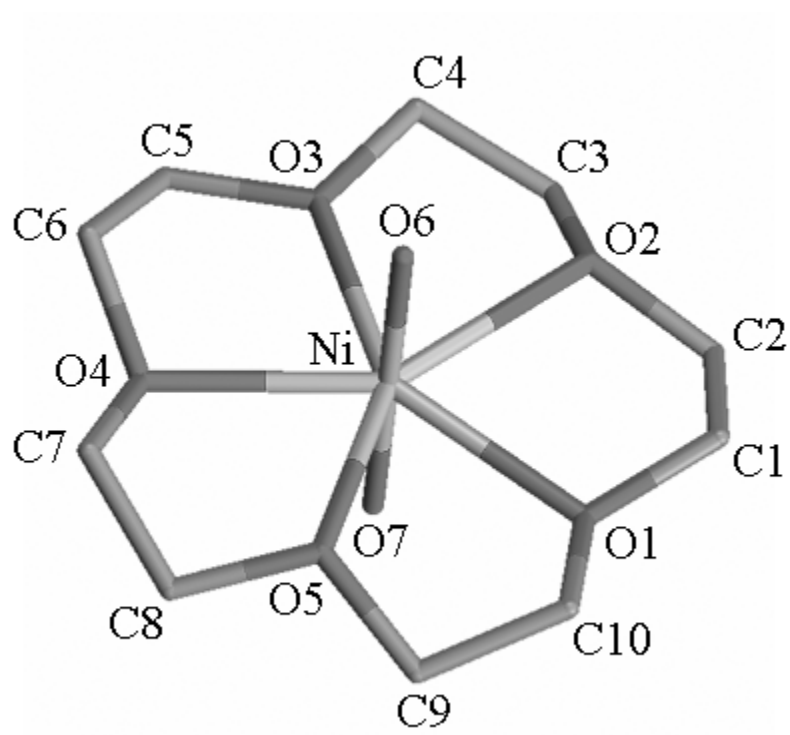


Figure 3.12. The atom-numbering scheme of one $[\text{Ni}(\text{H}_2\text{O})_2(15\text{-crown-5})]^{2+}$ ion in the two phases of $[\text{Ni}(\text{H}_2\text{O})_2(15\text{-crown-5})](\text{NO}_3)_2$. Nitrate ions and H atoms are omitted for clarity.

Phase II

Phase II is found to be isostructural with the low-temperature phases of $[M(\text{H}_2\text{O})_2(15\text{-crown-5})](\text{NO}_3)_2$, $M = \text{Mg, Mn, Fe, Zn}$, which were solved and refined in the space group $P2_1/c$ with $Z' = 3$ (Hao, Parkin & Brock, 2005; Hao, Siegler, Parkin & Brock, 2005). This phase is a commensurately modulated superstructure and the modulation is threefold along the c direction. A first attempt to refine the structure was successful and the R factor $[F^2 > 2\sigma(F^2)]$ is 0.049, but high residual electron density peaks ($0.95 \text{ e } \text{\AA}^{-3}$) and eccentric ellipsoids of the Ni^{2+} ion and O_{water} atoms were all warning signs suggesting disorder.

The inclusion of the disorder improved the model significantly: the ellipsoids of the Ni atoms looked normal, the R factor $[F^2 > 2\sigma(F^2)]$ dropped to 0.039, and the highest residual electron density peak was no more than $0.42 \text{ e } \text{\AA}^{-3}$ (the largest peak was located at 0.81 \AA from the Ni^{2+} ion). The anisotropic displacement parameters for related disordered nickel atoms were constrained to be identical (*EADP* instruction). The values of the occupancy factors given for the minor component of the three independent disordered nickel atoms are 0.333 (6), 0.435 (4) and 0.402 (5). The distances between the two nickel positions in each cation are 0.420 (3), 0.423 (2) and 0.413 (3) \AA . The disorder of the O_{water} atoms was not retained because the improvement was small when the disorder was included in the model. The ellipsoids of the independent ions in the asymmetric unit of phase II before and after treatment of the disorder are shown in Figure 3.13.

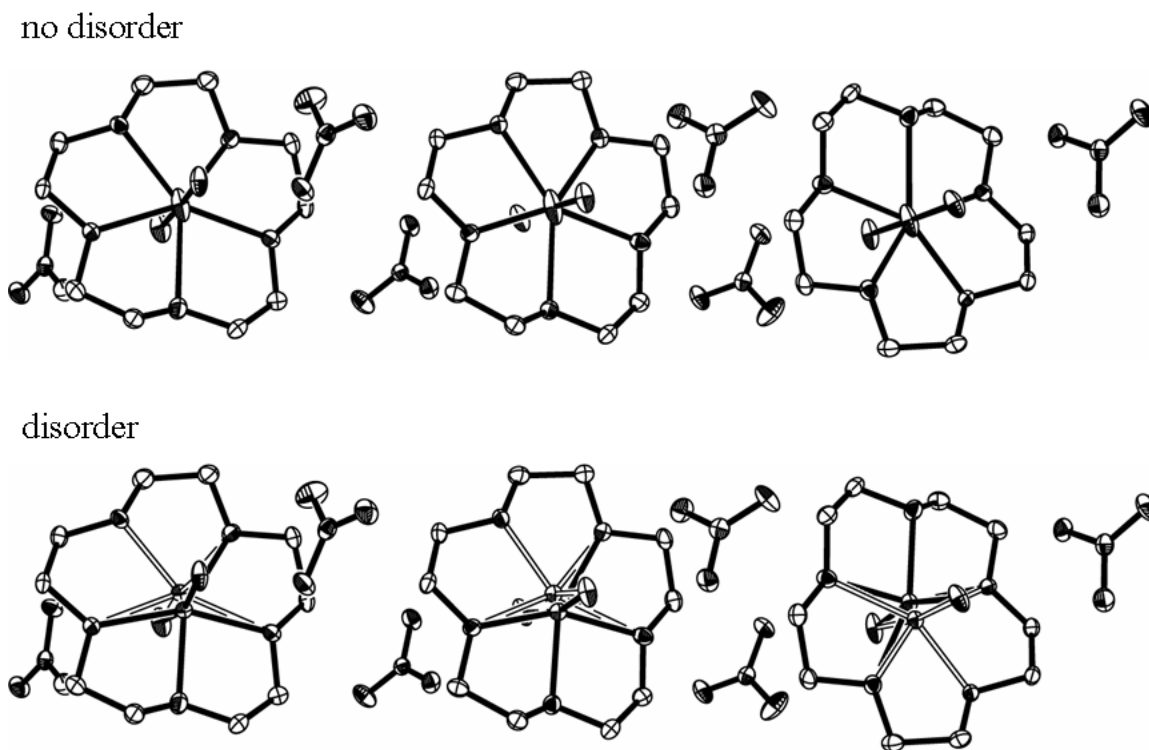


Figure 3.13. The displacement ellipsoids (50% probability level) of the independent ions (three cations and six nitrates) in the asymmetric units of phase II of $[\text{Ni}(\text{H}_2\text{O})_2(15\text{-crown-5})](\text{NO}_3)_2$ at 90 K before and after treatment of the metal-ion disorder. The eccentric ellipsoids of the nickel and O_{water} atoms are good evidence of disorder. The inclusion of the disorder of the nickel ions in the refinement significantly improves the model and the ellipsoids look normal. No disorder of the O_{water} atoms was included in the final refinement since the disorder did not improve the model significantly. H atoms are omitted from the drawing for clarity.

Phase I

Data for phase I were collected near 308 K. The high-temperature phases of $[M(\text{H}_2\text{O})_2(15\text{-crown-5})](\text{NO}_3)_2$, $M = \text{Mn, Ni and Cu}$, are found to be isostructural. Phase I is twinned pseudo-merohedrally (Hao, 2005) and the twinning was identified by using the program suite *PLATON*. The twin law is given by: $(-1\ 0\ 0 / 0\ 1\ 0 / 0\ 0\ -1)$, which corresponds to a twofold axis along the **b** direction. The refinement of the twin model in the space group $C\bar{1}$ was straightforward. The fractional contribution of the major twin component (*i.e.*, the *BASF* batch scale factor) refined to 0.690(1). The final difference Fourier map showed some residual electron density but the peaks were no larger than $0.65\ \text{e}\ \text{\AA}^{-3}$ (the largest peak was located at $0.44\ \text{\AA}$ from Ni^{2+} ion). Peaks that are not near the Ni^{2+} ion are no larger than $0.39\ \text{e}\ \text{\AA}^{-3}$. Near 308 K, the thermal motion is large so that the disorder is less noticeable than in the other phase and the ellipsoids of the Ni^{2+} ion and O_{water} atoms look fairly normal (see Figure 3.14). For these reasons, no disorder was included in the refinement process.

Crystallographic Data

The crystallographic data for the second polymorph of $[\text{Ni}(\text{H}_2\text{O})_6](\text{NO}_3)_2 \cdot (15\text{-crown-5}) \cdot \text{H}_2\text{O}$ are given in Table 3.2.

The crystallographic data for $[\text{Ni}(\text{H}_2\text{O})_6](\text{NO}_3)_2 \cdot \text{trans-}[\text{Ni}(\text{H}_2\text{O})_4(\text{MeOH})_2](\text{NO}_3)_2 \cdot 2(15\text{-crown-5})$ and $\text{cis-}[\text{Ni}(\text{H}_2\text{O})_4(\text{NO}_3)_2] \cdot \text{trans-}[\text{Ni}(\text{H}_2\text{O})_4(\text{NO}_3)_2] \cdot 2(15\text{-crown-5})$ are given in Table 3.3.

The crystallographic data for the two phases of $[\text{Ni}(\text{H}_2\text{O})_2(15\text{-crown-5})](\text{NO}_3)_2$ are given in Table 3.4.

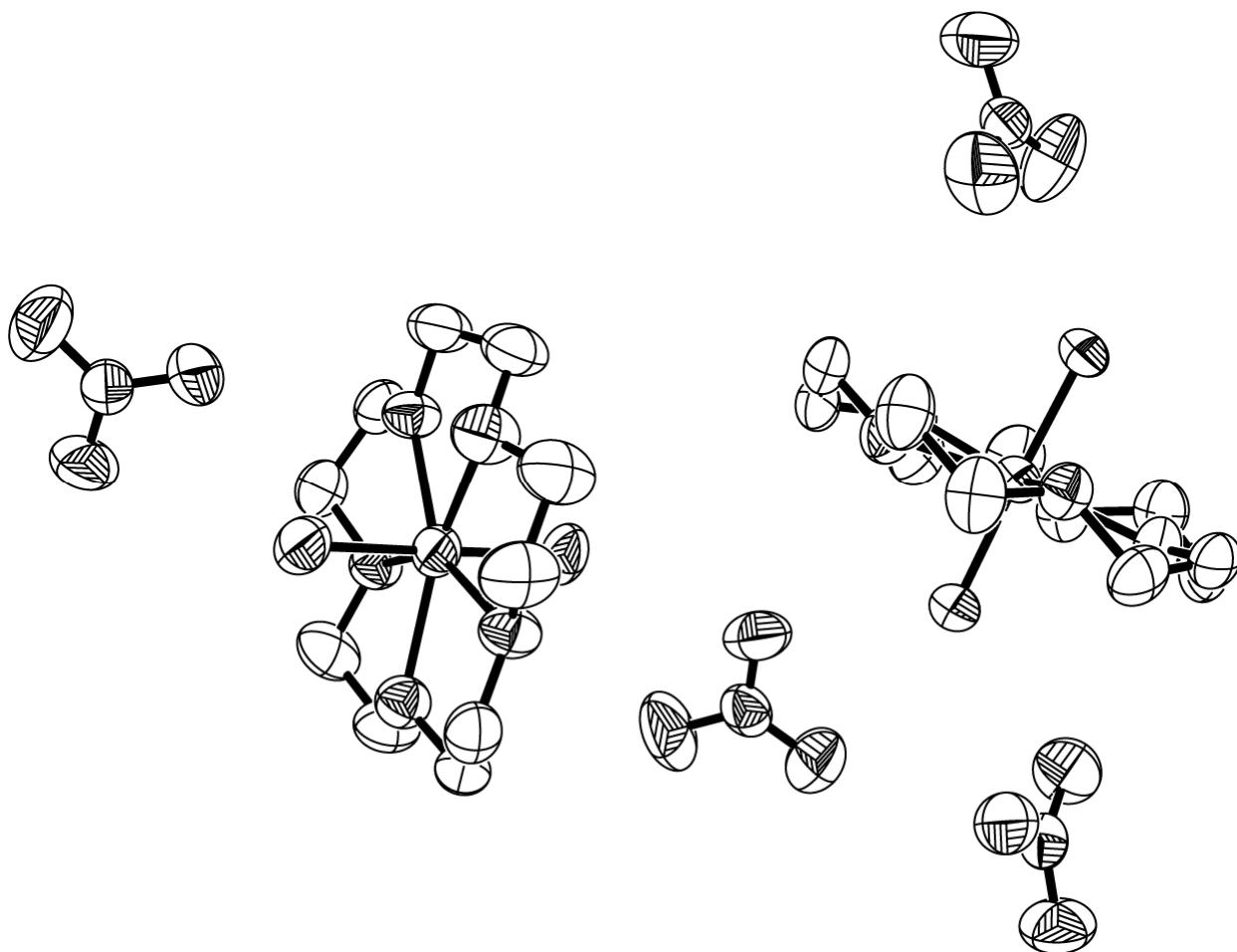


Figure 3.14. The displacement ellipsoids (50% probability level) of the independent ions (2 cations and 4 nitrate ions) in the asymmetric unit of phase I of $[\text{Ni}(\text{H}_2\text{O})_2(15\text{-crown-5})](\text{NO}_3)_2$ at 308 K. The thermal motion is significant and the disorder around the positions of the Ni^{2+} ions and O_{water} atoms is less obvious than in phase II. H atoms are omitted for clarity.

Table 3.2. Crystallographic data for the second polymorph of $[\text{Ni}(\text{H}_2\text{O})_6](\text{NO}_3)_2 \cdot (15\text{-crown-5}) \cdot \text{H}_2\text{O}$.

2nd polymorph of $[\text{Ni}(\text{H}_2\text{O})_6](\text{NO}_3)_2 \cdot (15\text{-crown-5}) \cdot \text{H}_2\text{O}$	
Crystal data	
Chemical formula	$\text{C}_{10}\text{H}_{34}\text{N}_2\text{NiO}_{18}$
M_r	529.10
Cell setting, space group	Triclinic, $P\bar{1}$
a, b, c (Å) ⁴⁵	16.036 (1) 24.765 (2) 10.163 (1)
α, β, γ (°)	89.71 (1) 122.53 (1) 83.58 (1)
V (Å ³)	3371.2 (5)
$Z; Z'$	6; 3
D_x (g cm ⁻³)	1.564
Radiation type	Mo $K\alpha$
No. of reflections for cell parameters	11233
θ range (°)	1.0–27.5
μ (mm ⁻¹)	0.95
Temperature (K)	90.0 (2)
Crystal form, colour	Irregular block, pale green
Crystal size (mm)	0.20 × 0.15 × 0.10
Data collection	
Diffractometer	Nonius KappaCCD
Data collection method	ω scans at fixed $\chi = 55^\circ$

⁴⁵ The estimated errors in the unit cell constants (a, b, c, α, β and γ) were modified by multiplying the experimental estimated standard uncertainties (*i.e.*, su's) by at least a factor of ~2.5 for a, b, c and by at least a factor of ~7 for α, β, γ . These factors were used in order to approximate the errors in the unit cell constants from one crystal to another (Herbstein, 2000).

Table 3.2. (continued)

Absorption correction	Multi-scan (based on symmetry-related measurements)
T_{\min}	0.833
T_{\max}	0.911
No. of measured, independent and observed parameters	11865, 11865, 7691
Criterion for observed reflections	$I > 2\sigma(I)$
R_{int}	0.103
θ_{max} (°)	25.0
Range of h, k, ℓ	$-18 < h < 19$ $0 < k < 29$ $-12 < \ell < 12$

Refinement

Refinement on	F^2
$R[F^2 > 2\sigma(F^2)], wR(F^2), S$	0.057, 0.137, 1.05
No. of reflections	11865 reflections
No. of parameters	980
H-atom treatment	Mixture of independent and constrained refinement
Weighting scheme	Calculated $w = 1/[\sigma^2(F_o^2) + (0.0448P)^2 + 8.9931P]$ where $P = (F_o^2 + 2F_c^2)/3$
$(\Delta/\sigma)_{\text{max}}$	0.001
$\Delta\rho_{\text{max}}, \Delta\rho_{\text{min}}$ (e Å ⁻³)	1.93, -0.56

Computer programs: *COLLECT* (Nonius, 1997); *DENZO-SMN* (Nonius, 1997); *SHELXS-97* (Sheldrick, 1990); *SHELXL-97* (Sheldrick, 1997); *XP in SHELXTL* (Bruker, 1995); *SHELX-97 and local procedures*.

Table 3.3. Crystallographic data for the compounds $[\text{Ni}(\text{H}_2\text{O})_6](\text{NO}_3)_2 \cdot \text{trans}-[\text{Ni}(\text{H}_2\text{O})_4(\text{MeOH})_2](\text{NO}_3)_2 \cdot 2(15\text{-crown-5})$ [4] and $\text{cis}-[\text{Ni}(\text{H}_2\text{O})_4(\text{NO}_3)_2] \cdot \text{trans}-[\text{Ni}(\text{H}_2\text{O})_4(\text{NO}_3)_2] \cdot 2(15\text{-crown-5})$ [5].

	4	5
Crystal data		
Chemical formula	$\text{C}_{20}\text{H}_{40}\text{O}_{10} \cdot (\text{C}_2\text{H}_{16}\text{NiO}_6) \cdot 2(\text{NO}_3) \cdot (\text{H}_{12}\text{NiO}_6) \cdot 2(\text{NO}_3)$	$\text{C}_{20}\text{H}_{40}\text{O}_{10} \cdot (\text{H}_8\text{NiN}_2\text{O}_{10}) \cdot (\text{H}_8\text{NiN}_2\text{O}_{10})$
M_r	1050.22	950.10
Cell setting, space group	Monoclinic, $P2_1/n$	Orthorhombic, $Pbca$
a, b, c (Å) ⁴⁶	16.241 (1) 15.481 (1) 10.429 (1)	15.352 (1) 16.278 (1) 30.716 (2)
β (°)	120.75 (1)	
V (Å ³)	2253.5 (4)	7675.9 (8)
$Z; Z'$	2; $\frac{1}{2}$	8; 1
D_x (g cm ⁻³)	1.548	1.644
Radiation type	Mo $K\alpha$	Mo $K\alpha$
No. of reflections for cell parameters	5368	9379
θ range (°)	1.0–27.5	1.0–27.5
μ (mm ⁻¹)	0.94	1.09
Temperature (K)	90.0 (2)	90.0 (2)
Crystal form, colour	Irregular block, pale green	Plate, pale green
Crystal size (mm)	0.20 × 0.15 × 0.11	0.50 × 0.40 × 0.05
Data collection		
Diffractometer	Nonius KappaCCD	Nonius KappaCCD
Data collection method	ω scans at fixed $\chi = 55^\circ$	ω scans at fixed $\chi = 55^\circ$
Absorption correction	Multi-scan (based on symmetry-related measurements)	

⁴⁶ The estimated errors in the unit cell constants (a , b , c and β) were modified by multiplying the experimental estimated standard uncertainties (*i.e.*, su's) by at least a factor of ~ 3 for a , b , c and by a factor of ~ 20 for β . These factors were used in order to approximate the errors in the unit cell constants from one crystal to another (Herbstein, 2000).

Table 3.3. (continued)

T_{\min}	0.834	0.612
T_{\max}	0.903	0.948
No. of measured, independent and observed parameters	10144, 5174, 3430	16396, 8782, 6081
Criterion for observed reflections	$I > 2\sigma(I)$	$I > 2\sigma(I)$
R_{int}	0.033	0.044
θ_{\max} (°)	27.5	27.5
Range of h, k, ℓ	$-21 < h < 21$ $-20 < k < 20$ $-13 < \ell < 13$	$-19 < h < 19$ $-21 < k < 21$ $-39 < \ell < 39$
Refinement		
Refinement on	F^2	F^2
$R[F^2 > 2\sigma(F^2)], wR(F^2), S$	0.037, 0.101, 1.03	0.036, 0.078, 1.01
No. of reflections	5174 reflections	8782 reflections
No. of parameters	348	553
H-atom treatment	Mixture of independent and constrained refinement	
Weighting scheme	Calculated $w = 1/[\sigma^2(F_o^2) + (0.054P)^2]$ where $P = (F_o^2 + 2F_c^2)/3$	Calculated $w = 1/[\sigma^2(F_o^2) + (0.0313P)^2 + 2.3161P]$ where $P = (F_o^2 + 2F_c^2)/3$
$(\Delta/\sigma)_{\max}$	0.001	0.002
$\Delta\rho_{\max}, \Delta\rho_{\min}$ (e Å ⁻³)	0.72, -0.53	0.33, -0.49

Computer programs: *COLLECT* (Nonius, 1997); *DENZO-SMN* (Nonius, 1997); *SHELXS-97* (Sheldrick, 1990); *SHELXL-97* (Sheldrick, 1997); *XP in SHELXTL* (Bruker, 1995); *SHELX-97 and local procedures*.

Table 3.4. Crystallographic data of the phases I and II of $[\text{Ni}(\text{H}_2\text{O})_2(15\text{-crown-5})](\text{NO}_3)_2$.

	I	II
Crystal data		
Chemical formula	$(\text{C}_{10}\text{H}_{24}\text{O}_7\text{Ni}^{2+}) \cdot 2(\text{NO}_3^{1-})$	$(\text{C}_{10}\text{H}_{24}\text{O}_7\text{Ni}^{2+}) \cdot 2(\text{NO}_3^{1-})$
M_r	439.02	439.02
Cell setting, space group	Triclinic, $C\bar{1}$	Monoclinic, $P2_1/c$
a, b, c (\AA) ⁴⁷	14.719 (2) 28.041 (3) 10.704 (2)	14.676 (1) 13.961 (1) 25.552 (2)
α, β, γ ($^\circ$)	90.20 (1) 125.88 (1) 89.87 (1)	90.00 96.56 (1) 90.00
V (\AA^3)	3574.6 (13)	5201.1 (7)
$Z; Z'$	8; 2	12; 3
D_x (g cm^{-3})	1.632	1.682
Radiation type	Mo $K\alpha$	Mo $K\alpha$
No. of reflections for cell parameters	8005	12375
θ range ($^\circ$)	1.0–27.5	1.0–27.5
μ (mm^{-1})	1.15	1.19
Temperature (K)	308 (2)	90.0 (2)
Crystal form, colour	Block, yellow	Block, yellow
Crystal size (mm)	$0.35 \times 0.15 \times 0.15$	$0.40 \times 0.15 \times 0.10$
Data collection		
Diffractometer	Nonius KappaCCD	Nonius KappaCCD
Data collection method	ω scans at fixed $\chi = 55^\circ$	ω scans at fixed $\chi = 55^\circ$

⁴⁷ The estimated errors in the unit cell constants (a, b, c, α, β and γ) were modified by multiplying the experimental estimated standard uncertainties (*i.e.*, su's) by at least a factor of ~ 5 for a, b, c and by at least a factor of ~ 16.5 for α, β, γ . These factors were used in order to approximate the errors in the unit cell constants from one crystal to another (Herbstein, 2000).

Table 3.4. (continued)

Absorption correction	Multi-scan (based on symmetry-related measurements)	Multi-scan (based on symmetry-related measurements)
T_{\min}	0.688	0.647
T_{\max}	0.846	0.890
No. of measured, independent and observed parameters	12132, 6301, 4268	23212, 11918, 6757
Criterion for observed reflections	$I > 2\sigma(I)$	$I > 2\sigma(I)$
R_{int}	0.037	0.038
θ_{\max} (°)	25.0	27.5
Range of h, k, ℓ	$-17 < h < 17$ $-33 < k < 32$ $-12 < \ell < 12$	$-19 < h < 19$ $-18 < k < 18$ $-33 < \ell < 33$
Refinement		
Refinement on	F^2	F^2
$R[F^2 > 2\sigma(F^2)], wR(F^2), S$	0.045, 0.125, 1.05	0.039, 0.102, 0.96
No. of reflections	6301 reflections	11918 reflections
No. of parameters	494	751
H-atom treatment	Constrained to parent site	Constrained to parent site
Weighting scheme	Calculated $w = 1/[\sigma^2(F_o^2) + (0.064P)^2]$ where $P = (F_o^2 + 2F_c^2)/3$	Calculated $w = 1/[\sigma^2(F_o^2) + (0.0457P)^2]$ where $P = (F_o^2 + 2F_c^2)/3$
$(\Delta/\sigma)_{\max}$	0.001	0.002
$\Delta\rho_{\max}, \Delta\rho_{\min}$ (e Å ⁻³)	0.65, -0.52	0.42, -0.56

Computer programs: *COLLECT* (Nonius, 1997); *DENZO-SMN* (Nonius, 1997); *SHELXS-97* (Sheldrick, 1990); *SHELXL-97* (Sheldrick, 1997); *XP in SHELXTL* (Bruker, 1995); *SHELX-97 and local procedures*.

Results and Discussion

[Ni(H₂O)₆](NO₃)₂·(15-crown-5)·H₂O (second polymorph)

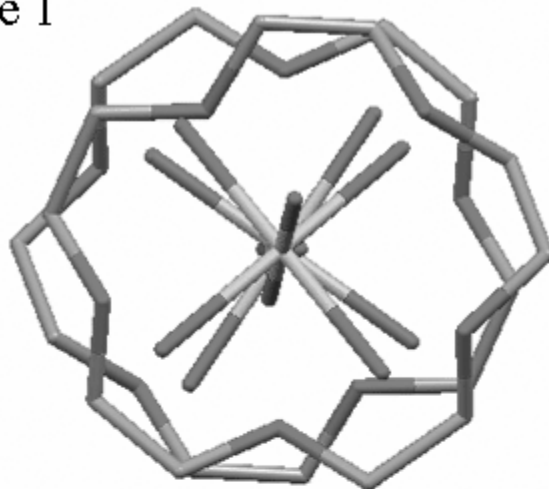
The three-dimensional (hereafter, 3-D) H-bonding network of the second polymorph of [Ni(H₂O)₆](NO₃)₂·(15-crown-5)·H₂O can be described as one-dimensional (hereafter, 1-D) chains of H-bonds and two-dimensional (hereafter, 2-D) planes of H-bonds.

Along the **a** direction, the H-bonded interactions between the 15-crown-5 molecules and the [Ni(H₂O)₆]²⁺ ions can be described as 1-D chains. Two types of 1-D chains are observed. The first type only contains the centrosymmetric [Ni(H₂O)₆]²⁺ ions. The second type only contains the [Ni(H₂O)₆]²⁺ ions that have no imposed symmetry. In the former type, the 15-crown-5 molecules are related by inversion centers (see Figure 3.15). The two types of 1-D chains are built via a set of hydrogen bonds between the five O_{ether} atoms (O1, O2, O3, O4 and O5) of the 15-crown-5 molecules, the O_{axial} atoms (O6 and O7) and the O_{equatorial} atoms (O8 and O9) of the [Ni(H₂O)₆]²⁺ ions (see Figure 3.16).

The hydrogen bond interactions between the four independent [Ni(H₂O)₆]²⁺ ions, the six independent nitrate ions and the three independent lattice water molecules correspond to 2-D planes of H-bonds parallel to (2 1 -1). The 2-D planes are complex because the hydrogen bond interactions around the four independent [Ni(H₂O)₆]²⁺ ions are different (see Figure 3.17).

Table 3.5 summarizes the O···O distances found in the 1-D chains and the O···O distances found around the four independent [Ni(H₂O)₆]²⁺ ions in the 2-D planes.

type 1



type 2

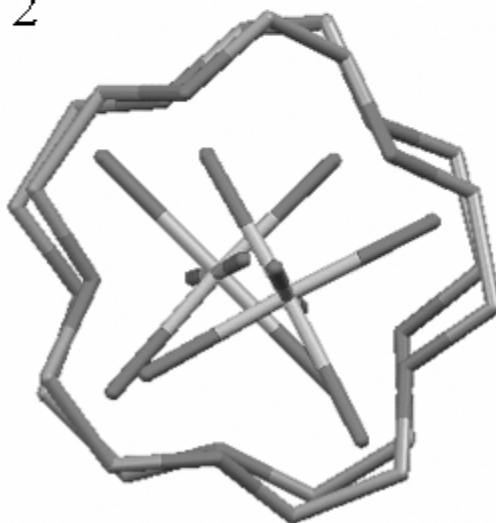


Figure 3.15. The two types of 1-D chains found in the second polymorph of $[\text{Ni}(\text{H}_2\text{O})_6](\text{NO}_3)_2 \cdot (15\text{-crown-5}) \cdot \text{H}_2\text{O}$ looking down the **a** direction. In the first type (type 1), the $[\text{Ni}(\text{H}_2\text{O})_6]^{2+}$ ions are centrosymmetric and the 15-crown-5 molecules are related by inversion centers. In the second type (type 2), the $[\text{Ni}(\text{H}_2\text{O})_6]^{2+}$ ions and the 15-crown-5 molecules have no symmetry imposed.

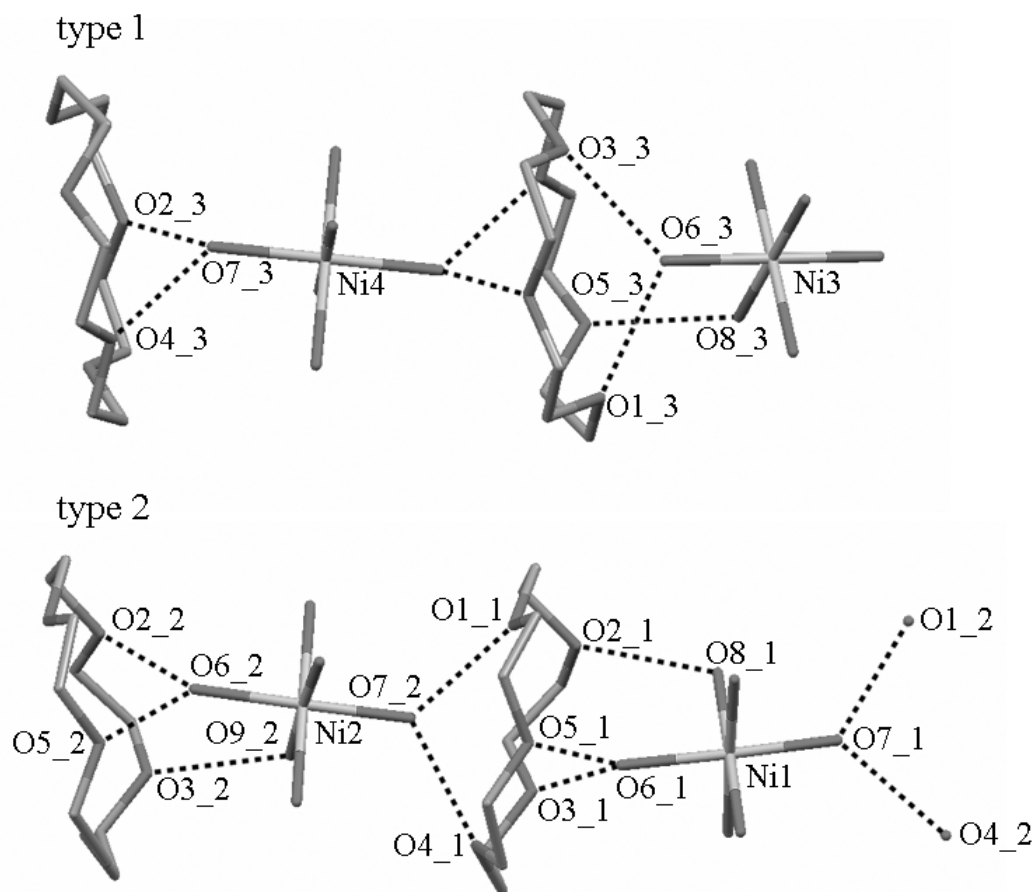


Figure 3.16. The set of hydrogen bonds found in the second polymorph of $[\text{Ni}(\text{H}_2\text{O})_6](\text{NO}_3)_2 \cdot (15\text{-crown-5}) \cdot \text{H}_2\text{O}$ along the **a** direction (*i.e.*, the direction of the 1-D chains). In type one of the 1-D chains, the two crystallographically independent Ni^{2+} ions (Ni3 and Ni4) are located at sites of inversion symmetry and the $[\text{Ni}(\text{H}_2\text{O})_6]^{2+}$ ions are centrosymmetric; the 15-crown-5 molecules are related by inversion centers and are symmetry equivalent. In type two of the 1-D chains, the two $[\text{Ni}(\text{H}_2\text{O})_6]^{2+}$ ions and the two 15-crown-5 molecules are crystallographically independent. H-bonds are shown as black dotted lines. In the former type of chains, one of the two centrosymmetric cations (Ni4) does not have any $\text{O}_{\text{equatorial}}$ atoms that are H-bond donors to the crown ether. In the other cation (Ni3), two $\text{O}_{\text{equatorial}}$ atoms make H bonds to two 15-crown-5 molecules (but only one of them is shown). The lattice water molecules, the nitrate ions and the H-atoms are omitted for clarity.

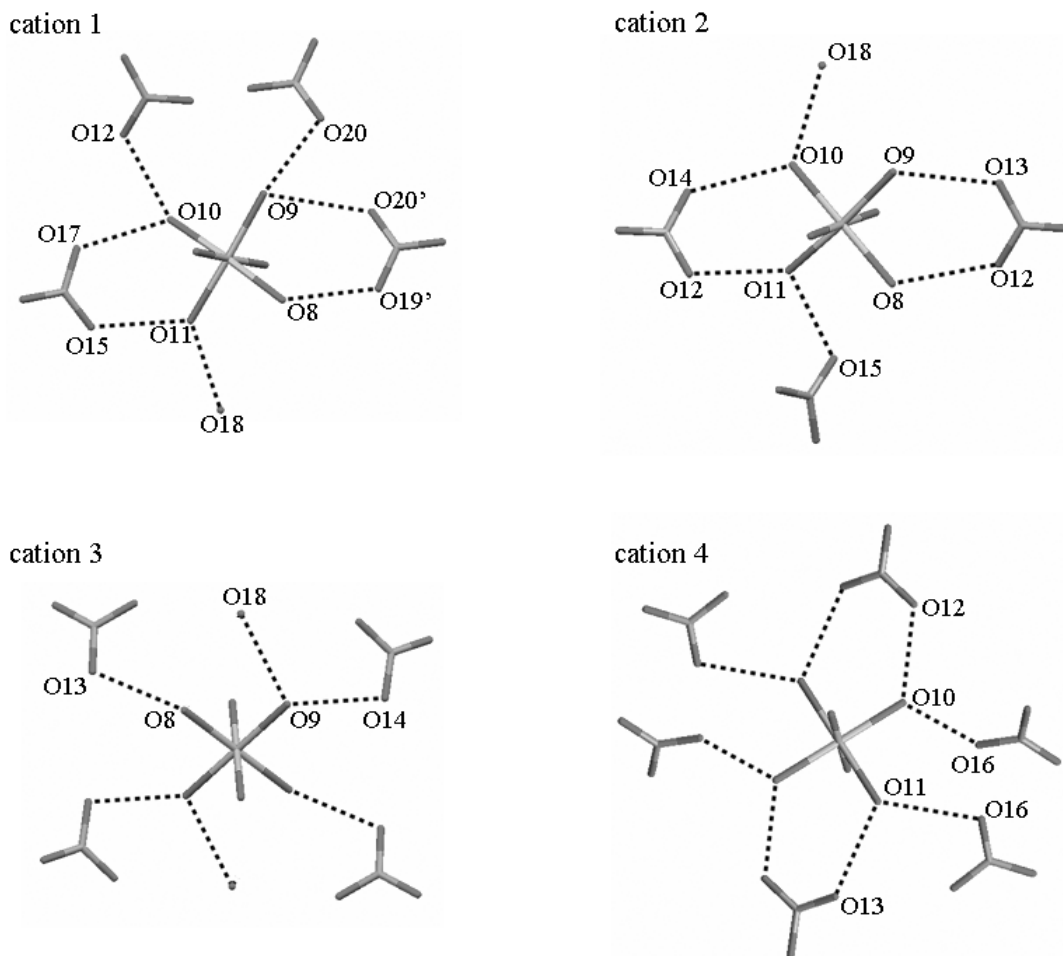


Figure 3.17. The set of hydrogen bonds observed around the four independent $[\text{Ni}(\text{H}_2\text{O})_6]^{2+}$ cations along the normal to the plane (2 1 -1). Two cations (cations 1 and 2) have no imposed symmetry; the remaining cations (cations 3 and 4) are centrosymmetric (because the Ni^{2+} ions are located at sites of inversion symmetry). The differences in hydrogen bonds, which involve the $\text{O}_{\text{equatorial}}$ atoms of the four $[\text{Ni}(\text{H}_2\text{O})_6]^{2+}$ cations, are noticeable. The H-bond donors (*i.e.*, the four $\text{O}_{\text{equatorial}}$ atoms) differ from one cation to another. One $\text{O}_{\text{equatorial}}$ atom can be an H-bond donor to two nitrate ions (O9 and O10 in cation 1, O11 in cation 2, O10 and O11 in cation 4), one nitrate ion and one 15-crown-5 molecule (O8 in cation 1, O9 in cation 2, O8 in cation 3), one nitrate ion and one lattice water molecule (O11 in cation 1, O10 in cation 2, O9 in cation 3) or one nitrate ion only (O8 in cation 2). In the latter case, the remaining H atom does not participate in H-bonds. H-bonds are shown as black dotted lines. The hydrogen bond interactions $\text{O}_{\text{equatorial}} \cdots \text{O}_{\text{ether}}$ (*i.e.*, interactions between the $[\text{Ni}(\text{H}_2\text{O})_6]^{2+}$ cations and the crown ether along the 1-D chains) and the H-atoms are omitted for clarity.

Table 3.5. Hydrogen bond distances D...A (Donor...Acceptor) for the second polymorph of $[\text{Ni}(\text{H}_2\text{O})_6](\text{NO}_3)_2 \cdot (15\text{-crown-5}) \cdot \text{H}_2\text{O}$ along the **a** direction (*i.e.*, the direction of the two types of 1-D H-bonded chains) and around the four independent $[\text{Ni}(\text{H}_2\text{O})_6]^{2+}$ cations in the 2-D planes of H-bonds.

D...A (Å)		along the a direction	
O6_1...O3_1	2.793 (5)	O7_2...O4_1	2.751 (5)
O6_1...O5_1	2.766 (5)	O9_2...O3_2	2.755 (5)
O7_1...O1_2	2.798 (5)	O6_3...O1_3	2.753 (5)
O7_1...O4_2	2.708 (5)	O6_3...O3_3	2.787 (4)
O8_1...O2_1	2.766 (5)	O7_3...O2_3	2.773 (5)
O6_2...O2_2	2.870 (5)	O7_3...O4_3	2.780 (5)
O6_2...O5_2	2.815 (5)	O8_3...O5_3	2.810 (4)
O7_2...O1_1	2.716 (5)		
D...A (Å)			
cation 1		cation 2	
O8...O19'	2.653 (10)	O8...O12	2.835 (5)
O9...O20	2.882 (10)	O9...O13	2.798 (5)
O9...O20'	2.764 (13)	O10...O14	2.838 (5)
O10...O12	2.868 (5)	O10...O18	2.727 (5)
O10...O17	2.745 (5)	O11...O12	2.746 (5)
O11...O15	2.746 (5)	O11...O15	2.694 (5)
O11...O18	2.690 (5)		
cation 3		cation 4	
O8...O13	2.771 (5)	O10...O12	2.703 (5)
O9...O14	2.777 (5)	O10...O16	2.668 (5)
O9...O18	2.766 (5)	O11...O13	2.822 (5)
		O11...O16	2.849 (5)

[Ni(H₂O)₆](NO₃)₂·*trans*-[Ni(H₂O)₄(MeOH)₂](NO₃)₂·2(15-crown-5)

The three-dimensional H-bonding network of the compound [Ni(H₂O)₆](NO₃)₂·*trans*-[Ni(H₂O)₄(MeOH)₂](NO₃)₂·2(15-crown-5) can be described as formed from one-dimensional (hereafter, 1-D) chains of H-bonds along the **a** direction and other hydrogen bond interactions along the [0 1 1], [0 1 -1] and [1 0 2] directions.

Along the **a** direction, the H-bond interactions between the 15-crown-5 molecule and the [Ni(H₂O)₆]²⁺ and [Ni(H₂O)₄(MeOH)₂]²⁺ ions are best described as 1-D chains. The crown ether is found to be H-bonded by the [Ni(H₂O)₆]²⁺ and [Ni(H₂O)₄(MeOH)₂]²⁺ ions (see Figure 3.18). The 1-D chains are built via a set of hydrogen bonds between the five O_{ether} atoms (O1/O1', O2/O2', O3, O4 and O5) of the crown ether, the O_{axial} and O_{methanol} atoms (respectively O6 and O11) of the [Ni(H₂O)₄(MeOH)₂]²⁺ ion and the O_{axial} atoms (O7) of the [Ni(H₂O)₆]²⁺ ion (see Figure 3.19). The partial disorder of the 15-crown-5 molecule affects the H-bonding pattern. The H-bond interactions O7–H··O2' and O11–H··O1' found in the minor component of the disorder replace in that order the H-bond interactions O11–H··O2 and O7–H··O1 found in the major component of the disorder.

The H-bond interactions between the [Ni(H₂O)₆]²⁺, [Ni(H₂O)₄(MeOH)₂]²⁺ and nitrate ions are three-dimensional. The [Ni(H₂O)₆]²⁺ and [Ni(H₂O)₄(MeOH)₂]²⁺ ions (H-bond donors) are bridged by nitrate ions (H-bond acceptors) along the [0 1 1], [0 1 -1] and [1 0 2] directions. Each nitrate ion makes a pair of O–H··O bonds (O12, O14, O15 and O17) to the O_{equatorial} atoms (O8 and O9) of the [Ni(H₂O)₆]²⁺ ions and a single O–H··H bond (O13, O16) to the O_{equatorial} atoms (O10) of the [Ni(H₂O)₄(MeOH)₂]²⁺ ions (see Figure 3.20).

Table 3.6 summarizes the O··O distances found in the three dimensional H-bonding network.

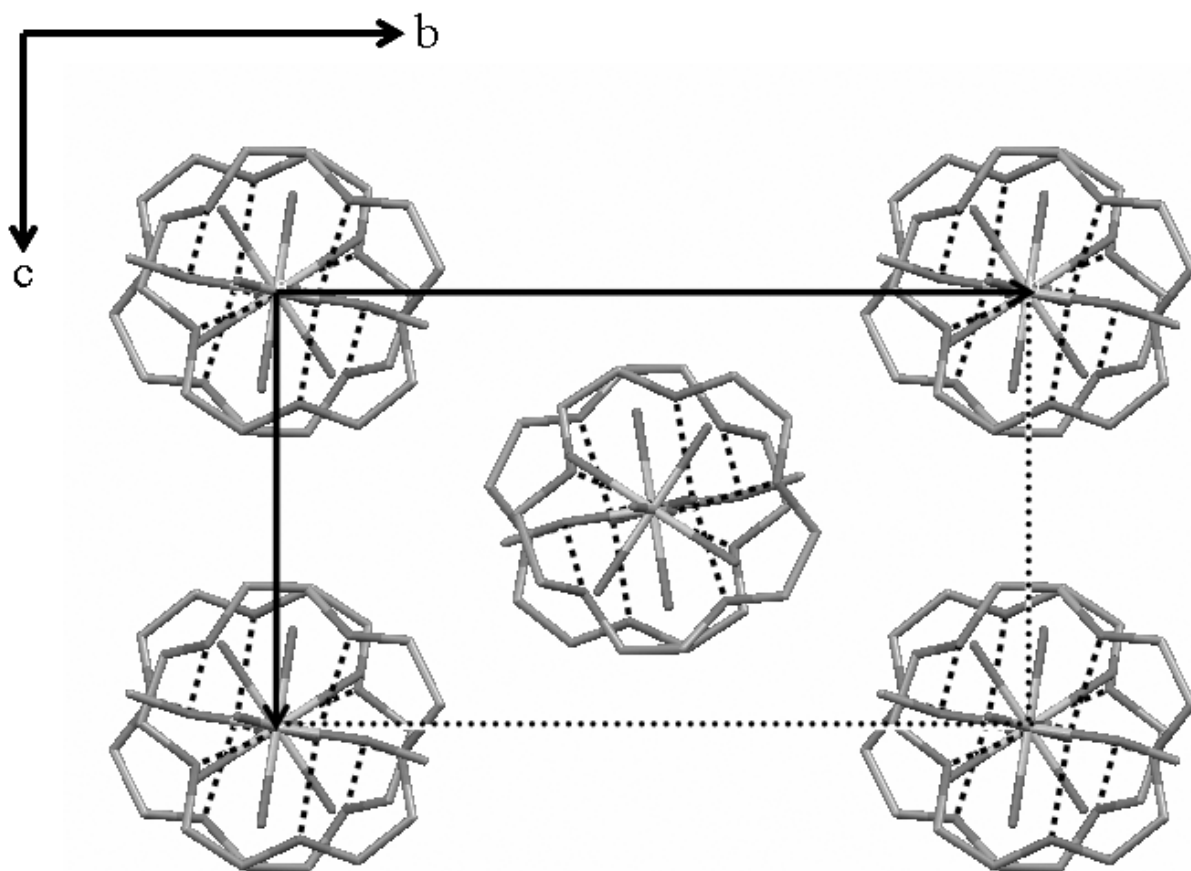


Figure 3.18. The packing of $[\text{Ni}(\text{H}_2\text{O})_6](\text{NO}_3)_2 \cdot \text{trans}-[\text{Ni}(\text{H}_2\text{O})_4(\text{MeOH})_2](\text{NO}_3)_2 \cdot 2(15\text{-crown-5})$ looking down the **a** direction. The drawing shows the out-of-plane 1-D chains, in which the 15-crown-5 molecules are H-bonded by the $[\text{Ni}(\text{H}_2\text{O})_6]^{2+}$ and $[\text{Ni}(\text{H}_2\text{O})_4(\text{MeOH})_2]^{2+}$ ions along the **a** direction. H-bonds are shown as black dotted lines. The **c** axis is not in the plane of the drawing. The disorder of the 15-crown-5 molecule, the nitrate ions and the H-atoms are omitted for clarity.

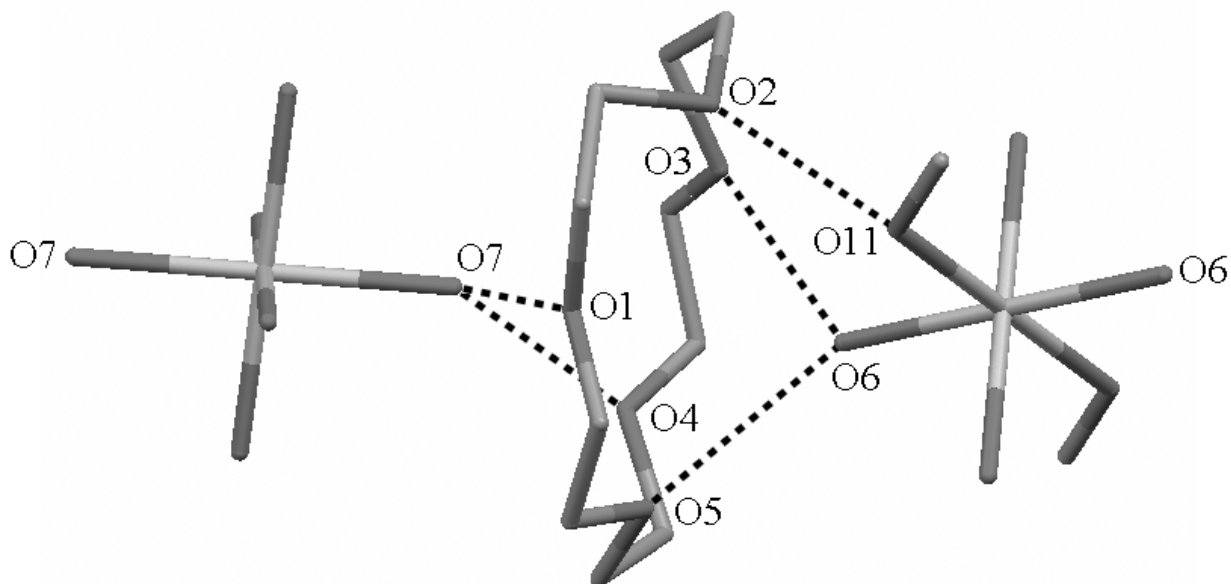


Figure 3.19. The set of hydrogen bonds in the asymmetric unit of the compound $[\text{Ni}(\text{H}_2\text{O})_6](\text{NO}_3)_2 \cdot \text{trans}-[\text{Ni}(\text{H}_2\text{O})_4(\text{MeOH})_2](\text{NO}_3)_2 \cdot 2(15\text{-crown-5})$ along the **a** direction (*i.e.*, along the 1-D H-bonded chains). One half of the $[\text{Ni}(\text{H}_2\text{O})_6]^{2+}$ and $[\text{Ni}(\text{H}_2\text{O})_4(\text{MeOH})_2]^{2+}$ ions are symmetry-generated. H-bonds are shown as black dotted lines. The disorder of the 15-crown-5 molecule, the nitrate ions and the H-atoms are omitted for clarity.

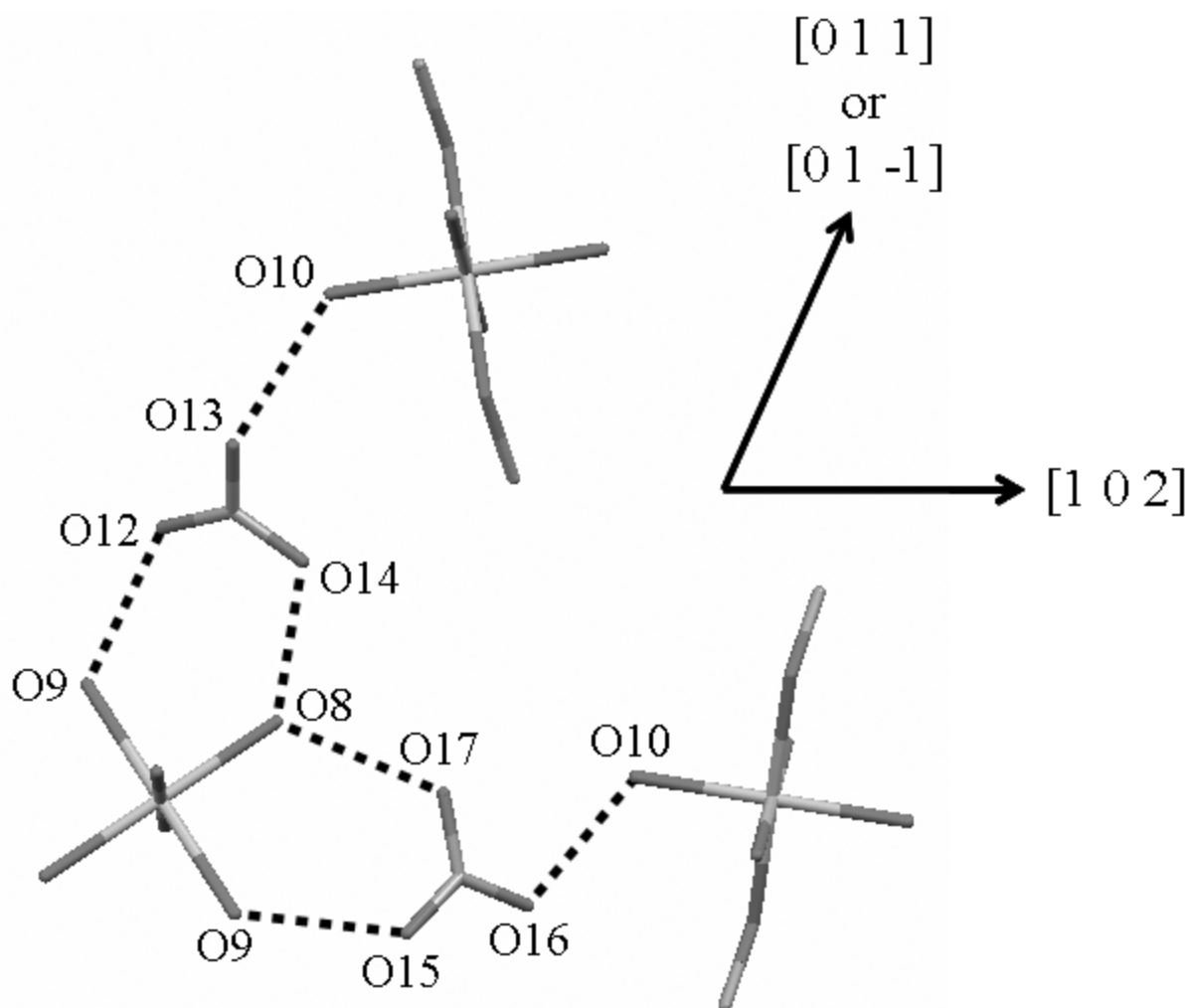


Figure 3.20. The set of hydrogen bonds along the $[0\ 1\ 1]$, $[0\ 1\ -1]$ and $[1\ 0\ 2]$ directions for the compound $[\text{Ni}(\text{H}_2\text{O})_6](\text{NO}_3)_2 \cdot \text{trans}-[\text{Ni}(\text{H}_2\text{O})_4(\text{MeOH})_2](\text{NO}_3)_2 \cdot 2(15\text{-crown-}5)$. One half of the $[\text{Ni}(\text{H}_2\text{O})_6]^{2+}$ and $[\text{Ni}(\text{H}_2\text{O})_4(\text{MeOH})_2]^{2+}$ ions are symmetry-generated. H-bonds are shown as black dotted lines. H-atoms are omitted for clarity.

Table 3.6. Hydrogen bond distances D...A (Donor...Acceptor) for the compound $[\text{Ni}(\text{H}_2\text{O})_6](\text{NO}_3)_2 \cdot \text{trans-}[\text{Ni}(\text{H}_2\text{O})_4(\text{MeOH})_2](\text{NO}_3)_2 \cdot 2(15\text{-crown-}5)$ along the **a** direction (*i.e.*, the direction of the 1-D H-bonded chains) and the $[0\ 1\ 1]$, $[0\ 1\ -1]$ and $[1\ 0\ 2]$ directions.

D...A (Å)	along the a direction
O6...O3	2.772 (2)
O6...O5	2.857 (3)
O7...O1	2.805 (3)
O7...O2'	2.765 (4)
O7...O4	2.769 (2)
O11...O1'	2.650 (4)
O11...O2	2.691 (3)
D...A (Å)	along the $[0\ 1\ 1]$ and $[0\ 1\ -1]$ directions
O8...O14	2.753 (2)
O9...O12	2.727 (2)
O10...O13	2.714 (2)
D...A (Å)	along the $[1\ 0\ 2]$ direction
O8...O17	2.773 (2)
O9...O15	2.722 (2)
O10...O16	2.717 (2)

***cis*-[Ni(H₂O)₄(NO₃)₂]·*trans*-[Ni(H₂O)₄(NO₃)₂]·2(15-crown-5)**

The H-bonding network of *cis*-[Ni(H₂O)₄(NO₃)₂]·*trans*-[Ni(H₂O)₄(NO₃)₂]·2(15-crown-5) is three-dimensional. The network can be described as a two-dimensional (hereafter, 2-D) plane of H-bonds along the **a** and **c** directions (1-D chains of H-bonds are found along the **c** direction) and a one-dimensional (hereafter, 1-D) ribbon of H-bonds along the **b** direction. The role of the crown-ether ligand along the **c** direction and the role of the two isomers of [Ni(H₂O)₄(NO₃)₂] along the **a**, **b** and **c** directions are described below.

Along the **c** direction, the H-bond interactions between the crown-ether ligand, *cis*- and *trans*-[Ni(H₂O)₄(NO₃)₂] are best described as 1-D wavy chains. The 15-crown-5 molecule, which is known to be a bifacial H-bond acceptor (Steed *et al.*, 2001), is found to be H-bonded by the *cis* and *trans* isomers of [Ni(H₂O)₄(NO₃)₂] (see Figure 3.21). The 1-D chains are built via a set of hydrogen bonds between the five O_{ether} atoms of the crown-ether ligand (O1, O2, O3, O4 and O5), O_{axial} of the *cis* and *trans* isomers (O6 and O7) and O_{equatorial} of the *trans* isomer (O11) (see Figure 3.22). The 1-D wavy chains are linked along the **a** direction by hydrogen-bond interactions found between the *cis* and *trans* isomers. The two equatorial water ligands (O8 and O11) of the *cis* isomer are H-bond donors to one nitrate (O12 and O13) of the *trans* isomer. Intramolecular hydrogen bonds are also found in the *cis* and *trans* isomers (see Figure 3.23). The 1-D chains found along the **c** direction and the hydrogen bond interactions *cis*···*trans* (D···A) found along the **a** direction form a 2-D plane of H-bonds parallel to (0 1 0) (see Figure 3.24).

Along the **b** direction, one layer of the *cis* isomers is found between two layers of the *trans* isomers and the hydrogen bond interactions can be described as 1-D ribbons (see Figure 3.25). Each isomer is found to be an H-bond donor and H-bond acceptor to two different isomers (*i.e.*, ···*cis*···*trans*···*cis*··· or ···*trans*···*cis*···*trans*···). The H-bond interactions *cis*···*trans* (D···A) are along the **a** direction and the H-bond interactions *trans*···*cis* (D···A) are along the **b** direction. In the latter type, one equatorial water ligand (O9) of the *trans* isomer is H-bond donor to one nitrate (O12) of the *cis* isomer. Table 3.7 summarizes the O···O distances found in the three dimensional H-bonding network.

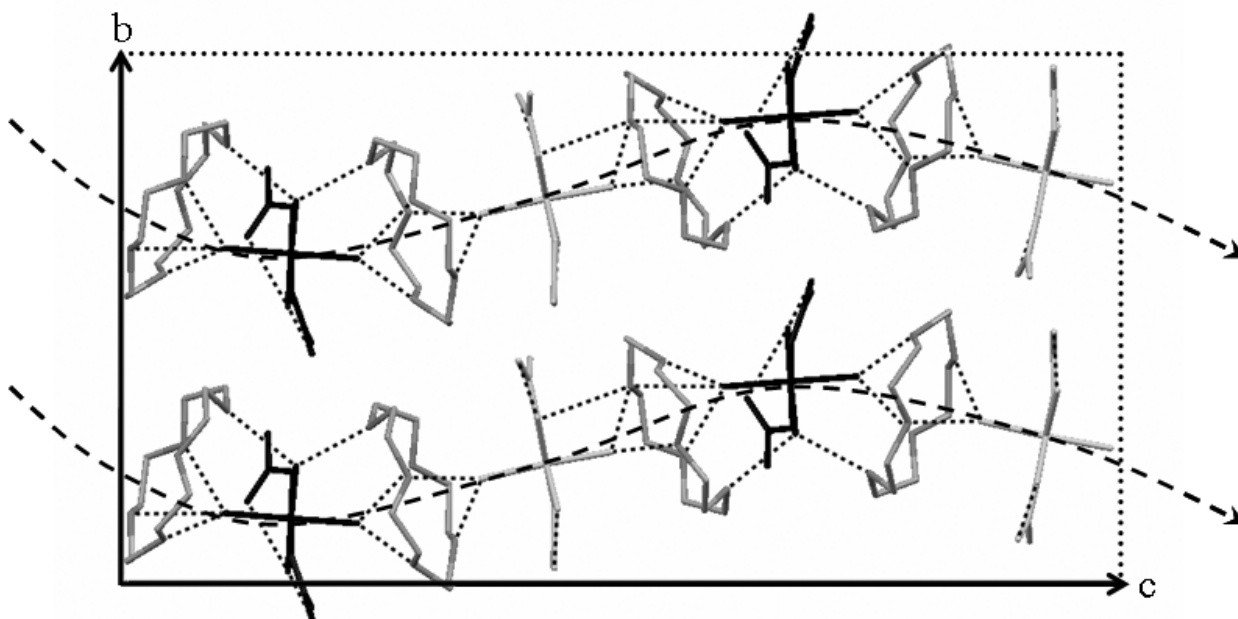


Figure 3.21. The packing of one layer of *cis*-[Ni(H₂O)₄(NO₃)₂]*·trans*-[Ni(H₂O)₄(NO₃)₂]*·2*(15-crown-5) looking down the **a** direction. The drawing illustrates the 1-D wavy chains (dashed curves), in which each 15-crown-5 molecule is H-bonded by the *trans* (black) and the *cis* (light gray) isomers of [Ni(H₂O)₄(NO₃)₂] along the **c** direction. H bonds are shown as black dotted lines. H atoms are omitted for clarity.

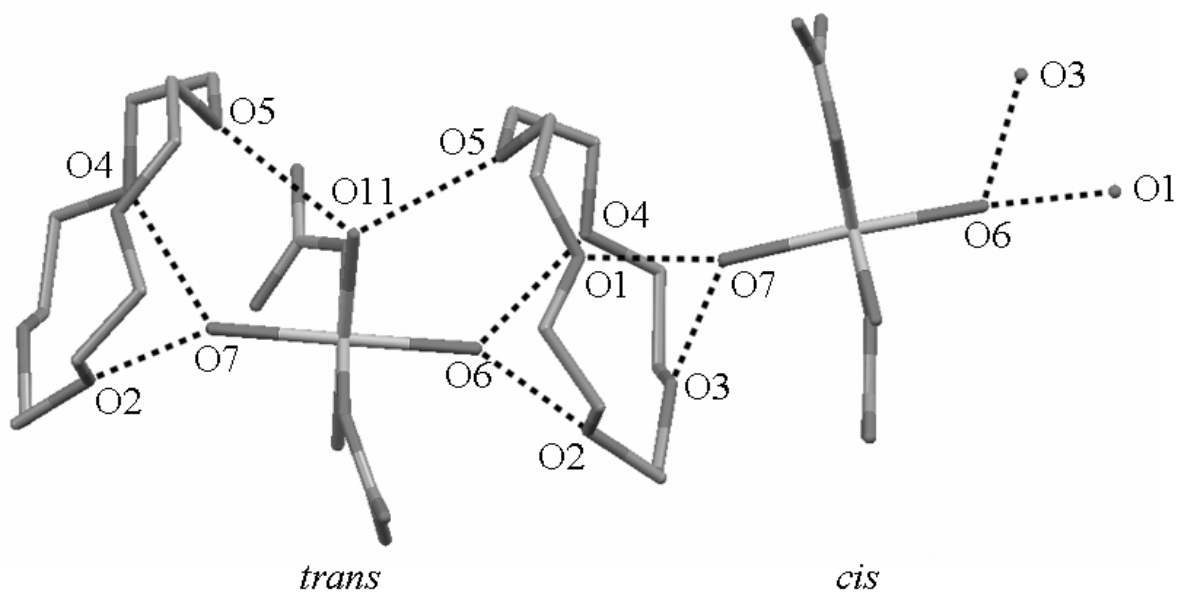


Figure 3.22. The set of hydrogen bonds in the asymmetric unit of *cis*-[Ni(H₂O)₄(NO₃)₂]*·trans*-[Ni(H₂O)₄(NO₃)₂]*·2*(15-crown-5) along the *c* direction. H-bonds are shown as black dotted lines. H atoms are omitted for clarity.

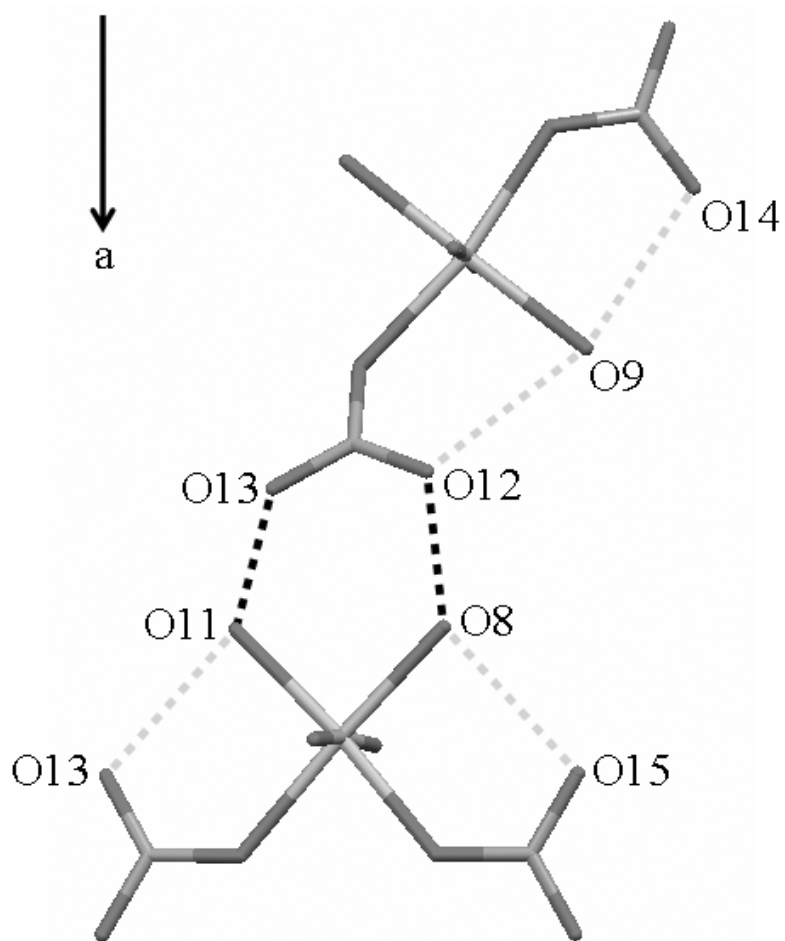


Figure 3.23. The H-bond interactions between the *cis* (H-bond donor) and the *trans* (H-bond acceptor) isomers of $[\text{Ni}(\text{H}_2\text{O})_4(\text{NO}_3)_2]$ found along the **a** direction. Intermolecular H-bonds are shown as black dotted lines. Intramolecular H-bonds are shown as light gray dotted lines. H atoms are omitted for clarity.

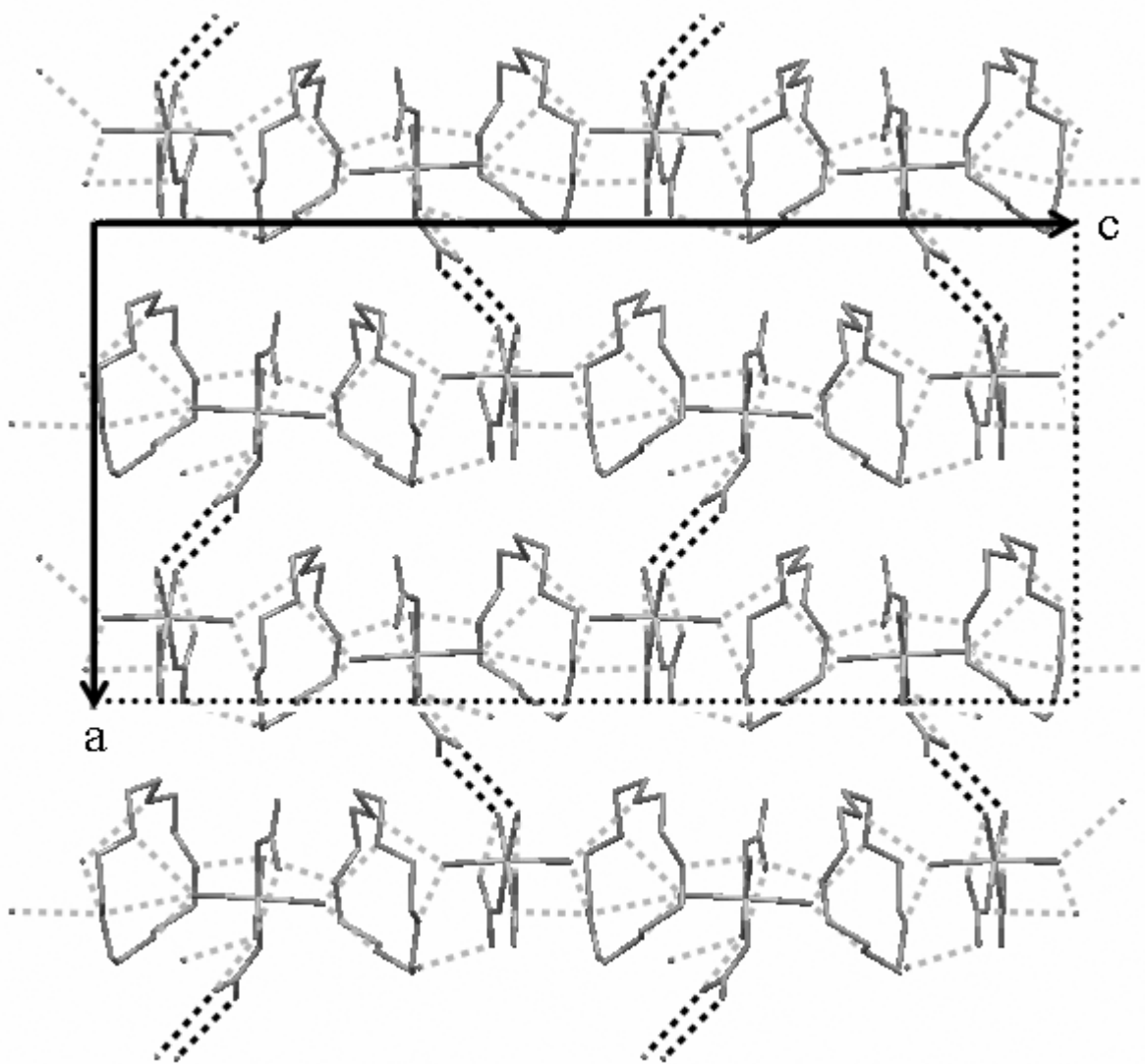


Figure 3.24. The packing of one layer of *cis*-[Ni(H₂O)₄(NO₃)₂]*·trans*-[Ni(H₂O)₄(NO₃)₂]*·2*(15-crown-5) looking down the **b** direction. The hydrogen bond interactions found along the **a** (black dotted lines) and **c** (light gray dotted lines) directions form 2-D planes of H-bonds parallel to (0 1 0). H atoms are omitted for clarity.

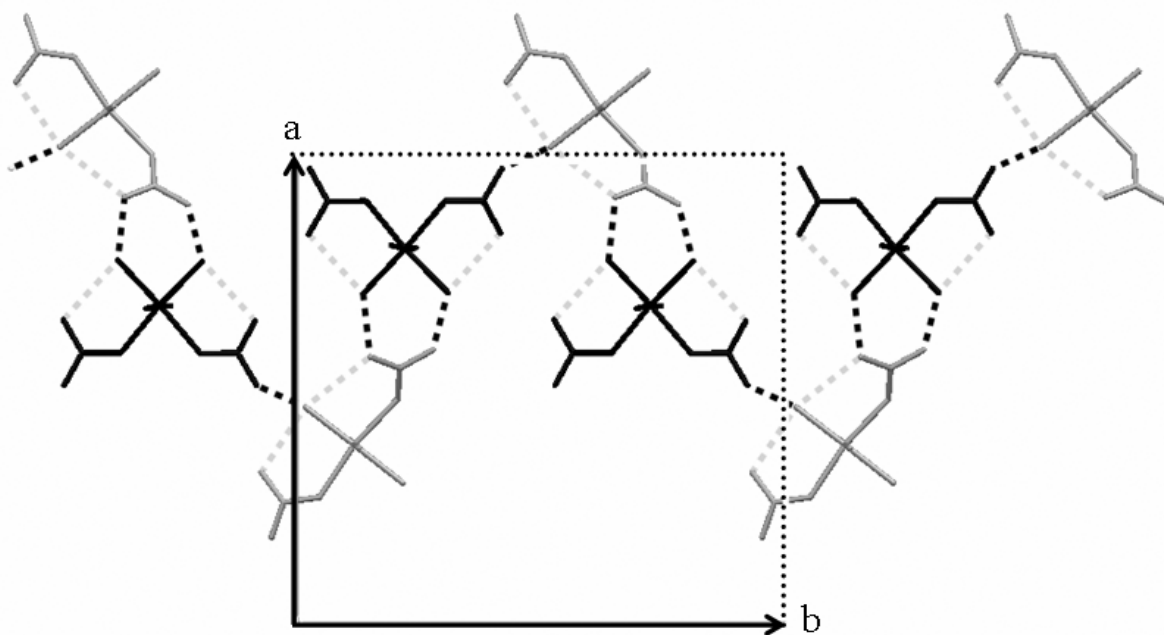


Figure 3.25. 1-D ribbon of *cis* (black) and *trans* (light grey) isomers of $[\text{Ni}(\text{H}_2\text{O})_4(\text{NO}_3)_2]$ down the *c* direction. The intermolecular H-bonds *cis*...*trans* ($\text{D}\cdots\text{A}$) and *trans*...*cis* ($\text{D}\cdots\text{A}$) are shown as black dotted lines. The intramolecular H-bonds *cis*...*cis* and *trans*...*trans* are shown as light gray dotted lines. The 15-crown-5 molecules and H atoms are omitted for clarity.

Table 3.7. Hydrogen bond distances D...A (Donor...Acceptor) for *cis*-[Ni(H₂O)₄(NO₃)₂]·*trans*-[Ni(H₂O)₄(NO₃)₂]·2(15-crown-5) along the **a**, **b** and **c** directions.

D...A (Å)	along the a direction		
O8 _{cis} ...O12 _{trans}	2.805 (2)		
O11 _{cis} ...O13 _{trans}	2.709 (2)		
D...A (Å)	along the b direction		
O9 _{trans} ...O12 _{cis}	2.868 (2)		
D...A (Å)	along the c direction		
O6 _{trans} ...O2 _{cis}	2.823 (2)	O6 _{cis} ...O1 _{trans}	2.780 (2)
O6 _{trans} ...O4 _{cis}	2.868 (2)	O6 _{cis} ...O3 _{trans}	2.676 (2)
O7 _{trans} ...O2 _{cis}	2.772 (2)	O7 _{cis} ...O1 _{trans}	2.703 (2)
O7 _{trans} ...O4 _{cis}	2.809 (2)	O7 _{cis} ...O3 _{trans}	2.754 (2)
O11 _{trans} ...O5 _{cis}	2.733 (2)		
O11 _{trans} ...O5 _{cis}	2.687 (2)		
D...A (Å)	intramolecular <i>cis</i>...<i>cis</i>		
O8...O15	2.679 (2)		
O11...O13	2.700 (2)		
D...A (Å)	intramolecular <i>trans</i>...<i>trans</i>		
O9...O14	2.707 (2)		



Cation Geometry

In the series of compounds $[\text{M}(\text{H}_2\text{O})_2(15\text{-crown-5})](\text{NO}_3)_2$, $M = \text{Mg, Mn, Fe, Co, Cu}$ and Zn , the cations $[\text{M}(\text{H}_2\text{O})_2(15\text{-crown-5})]^{2+}$ adopt the seven-coordinate pentagonal bipyramidal geometry (Hao, Parkin & Brock, 2005; Hao, Siegler, Parkin & Brock, 2005), but the compound $[\text{Ni}(\text{H}_2\text{O})_2(15\text{-crown-5})](\text{NO}_3)_2$ behaves differently. The geometry of the cations $[\text{Ni}(\text{H}_2\text{O})_2(15\text{-crown-5})]^{2+}$ was investigated and the study suggested that the coordination around the Ni^{2+} ion might be six rather than seven. The coordination environment around the Ni^{2+} ion is distorted.

Bond Lengths

In phase I, the Ni–O1 and Ni–O4 distances over the two independent cations $[\text{Ni}(\text{H}_2\text{O})_2(15\text{-crown-5})]^{2+}$ are the longest and their values vary within the ranges 2.26–2.30 Å. The Ni–O_{ether} distances are found to differ ($\Delta_{\text{max-min}} \sim 0.20$ Å) and the Ni^{2+} ion is disordered in the cation $[\text{Ni}(\text{H}_2\text{O})_2(15\text{-crown-5})]^{2+}$. At 308 K, the disorder of the metal ion is slight and has been mostly absorbed into the displacement parameters. In phase II, the discrepancy of the Ni–O_{ether} distances is larger ($\Delta_{\text{max-min}} \sim 0.30$ Å). The Ni–O4 distances over the three independent cations are by far the longest and their values vary within the range 2.35–2.42 Å. The suspicious elongation of the ellipsoids of the Ni^{2+} ions and O_{water} atoms results from disorder and is found along the approximate direction O1–O4 (see Figure 3.26). The Ni–O_{ether} distances found in the disordered model of phase II shows that some of the time the Ni^{2+} ion is more strongly coordinated by O1 than by O4 (major component), and the rest of the time the Ni^{2+} ion is more strongly coordinated by O4 than by O1 (minor component). All Ni–O_{water} distances found in the two phases of $[\text{Ni}(\text{H}_2\text{O})_2(15\text{-crown-5})](\text{NO}_3)_2$ are consistent with previous studies; the average Ni–O_{water} distance is 1.98 Å. Table 3.8 summarizes the deviations of the Ni–O_{ether} and Ni–O_{water} distances from the average Ni–O_{ether} and Ni–O_{water} distances found in the two phases.

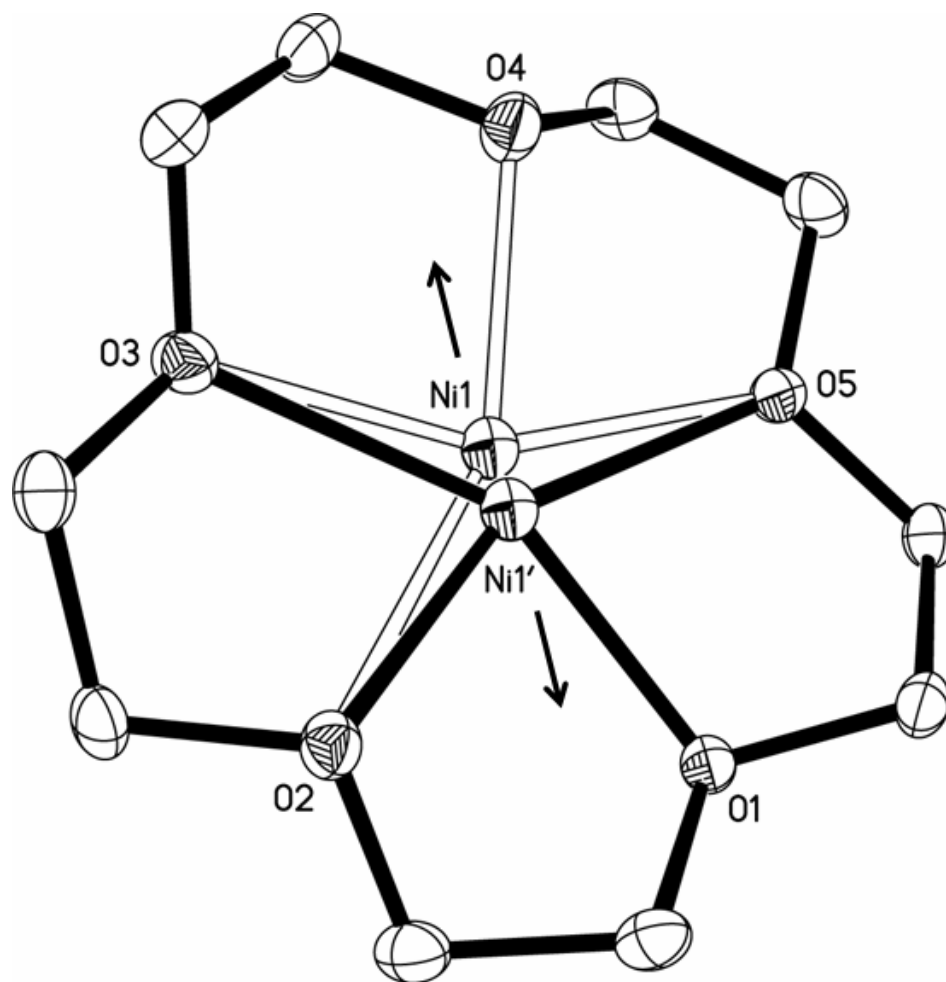


Figure 3.26. The displacement ellipsoids (50% probability level) of one disordered cation $[\text{Ni}(\text{H}_2\text{O})_2(15\text{-crown-5})]^{2+}$ of phase II at 90 K. The black solid lines indicate the major component of the disorder in which the $\text{Ni}1'^{2+}$ ion is coordinated by O1, O2, O3 and O5 atoms (the coordination by O4 is much weaker). The open lines correspond to the minor component of the disorder in which $\text{Ni}1^{2+}$ ion is coordinated by O2, O3, O4 and O5 atoms (the coordination by O1 is much weaker). The black arrows correspond to the direction of elongation of ellipsoids found around the positions of the Ni^{2+} ion and O_{water} atoms when no disorder has been included. The O_{water} and H atoms were omitted for clarity.

Table 3.8. Deviations (Å) of the Ni–O_{ether} (O1, O2, O3, O4, O5) and Ni–O_{water} (O6 and O7) distances from the average Ni–O_{ether} and Ni–O_{water} distances (Å) given for each residue in Ni I ($C\bar{1}$, $Z' = 2$) and Ni II ($P2_1/c$, $Z' = 3$) of $[\text{Ni}(\text{H}_2\text{O})_2(15\text{-crown-5})](\text{NO}_3)_2$.

Ni I $C\bar{1}, Z' = 2$	Residue 1	Residue 2	Average	
$\Delta_{\text{Ni-O1}}$	0.046 (3)	0.081 (3)	Ni–O _{ether}	2.216 (3)
$\Delta_{\text{Ni-O2}}$	-0.007 (3)	-0.052 (3)	Ni–O _{water}	1.982 (4)
$\Delta_{\text{Ni-O3}}$	0.013 (4)	-0.024 (3)		
$\Delta_{\text{Ni-O4}}$	0.087 (4)	0.054 (4)		
$\Delta_{\text{Ni-O5}}$	-0.104 (3)	-0.095 (3)		
$\Delta_{\text{Ni-O6}}$	-0.011 (3)	0.004 (3)		
$\Delta_{\text{Ni-O7}}$	-0.011 (4)	0.018 (4)		
Ni II $P2_1/c, Z' = 3$ no disorder	Residue 1	Residue 2	Residue 3	Average
$\Delta_{\text{Ni-O1}}$	0.007 (2)	0.035 (2)	0.054 (2)	Ni–O _{ether} 2.228 (2)
$\Delta_{\text{Ni-O2}}$	-0.099 (2)	-0.052 (2)	-0.103 (2)	Ni–O _{water} 1.979 (2)
$\Delta_{\text{Ni-O3}}$	-0.016 (2)	-0.016 (2)	-0.048 (2)	
$\Delta_{\text{Ni-O4}}$	0.189(2)	0.125 (2)	0.167 (2)	
$\Delta_{\text{Ni-O5}}$	-0.080 (2)	-0.095 (2)	0.070 (2)	
$\Delta_{\text{Ni-O6}}$	0.008 (2)	0.008 (2)	0.003 (2)	
$\Delta_{\text{Ni-O7}}$	0.005 (2)	0.004 (2)	0.006 (2)	

Table 3.8. (continued)

Ni II $P2_1/c, Z' = 3$ disorder	Residue 1	Residue 2	Residue 3	Average	
minor component					
$\Delta_{\text{Ni-O1}}$	0.276 (3)	0.262 (3)	0.283 (3)	Ni–O _{ether}	2.232 (3)
$\Delta_{\text{Ni-O2}}$	0.086 (3)	0.102 (3)	0.070 (3)	Ni–O _{water}	1.995 (4)
$\Delta_{\text{Ni-O3}}$	-0.182 (3)	-0.147 (4)	-0.180 (4)		
$\Delta_{\text{Ni-O4}}$	-0.091 (3)	-0.113 (3)	-0.083 (3)		
$\Delta_{\text{Ni-O5}}$	-0.090 (4)	-0.105 (4)	-0.091 (4)		
$\Delta_{\text{Ni-O6}}$	-0.006 (4)	-0.002 (3)	-0.005 (4)		
$\Delta_{\text{Ni-O7}}$	0.016 (4)	0.000 (3)	-0.006 (4)		
major component					
$\Delta_{\text{Ni-O1}}$	-0.113 (3)	-0.131 (3)	-0.090 (3)	Ni–O _{ether}	2.232 (3)
$\Delta_{\text{Ni-O2}}$	-0.177 (3)	-0.163 (3)	-0.207 (3)	Ni–O _{water}	1.986 (3)
$\Delta_{\text{Ni-O3}}$	0.058 (3)	0.085 (3)	0.037 (3)		
$\Delta_{\text{Ni-O4}}$	0.305 (3)	0.292 (3)	0.316 (3)		
$\Delta_{\text{Ni-O5}}$	-0.072 (2)	-0.080 (3)	-0.052 (3)		
$\Delta_{\text{Ni-O6}}$	0.013 (2)	0.016 (3)	-0.003 (3)		
$\Delta_{\text{Ni-O7}}$	-0.015 (2)	-0.006 (3)	-0.008 (3)		

Disorder of [Ni(H₂O)₂(15-crown-5)](NO₃)₂, why?

The series of compounds [M(H₂O)₂(15-crown-5)](NO₃)₂, M = Mg, Mn, Fe, Co, Ni, Cu and Zn, exists because the M²⁺ ion can fit inside the cavity of the 15-crown-5 molecule (cavity size: 1.7-2.2 Å). The effective ionic radius of M²⁺ varies within the range 0.61-0.74 Å (Shannon, 1976). The disorder is only found in the Ni compound although the ionic radius of the Ni²⁺ ion is intermediate (0.69 Å). The size effect clearly can restrict the insertion of divalent metal ions into the cavity of the crown ether [*i.e.*, Ca²⁺ does not fit inside the 15-crown-5 molecule, IR (Ca²⁺) = 1.06 Å] but can be ruled out as a cause for disorder found in [Ni(H₂O)₂(15-crown-5)](NO₃)₂.

In this research, the target compound [Ni(H₂O)₂(15-crown-5)](NO₃)₂ and several other complexes containing Ni²⁺, NO₃⁻, 15-crown-5 and water, and sometimes other solvents (*e.g.*, acetonitrile and methanol) were investigated. In all structures, six-coordinate Ni(II) complexes were found. In [Ni(H₂O)₂(15-crown-5)](NO₃)₂, the seven coordination of the Ni²⁺ ion is not certain because the metal ion might be coordinated by four rather than five crown-ether O atoms. The disorder around the metal position is likely to occur because there are several ways for Ni²⁺ ion to be coordinated by four crown-ether O atoms (see Figure 3.27). The single-crystal X-ray experiment suggests that the Ni²⁺ ion might not be coordinated by O1 and O4 atoms simultaneously⁴⁸. As a result, there are only two ways the Ni²⁺ ion is coordinated and twofold disorder occurs along the approximate O1-O4 direction. Previous studies (Simonsen *et al.*, 1982) suggested also that the Ni²⁺ ion might not be coordinated by all crown-ether O atoms⁴⁹. The disorder makes the nickel compound distinct from the series of isostructures (Mg, Mn, Fe, Zn LTP and Mn, Cu HTP) found in previous studies (Hao, Parkin & Brock, 2005; Hao, Siegler, Parkin & Brock, 2005).

⁴⁸ The ellipsoids of the Ni²⁺ ions and the water molecules were found to be elongated nearly along the O1-O4 direction.

⁴⁹ In one structure of Ni(II) complex of 18-crown-6, Larson *et al.* found that the Ni²⁺ ion is not coordinated by all six crown-ether O atoms: 'The Ni²⁺ ion is coordinated to three adjacent O atoms of the crown (O1, O4, O7) and to the O atoms of three ethanol solvate molecules, the O atoms forming a distorted octahedron' (Larson *et al.*, 1989).

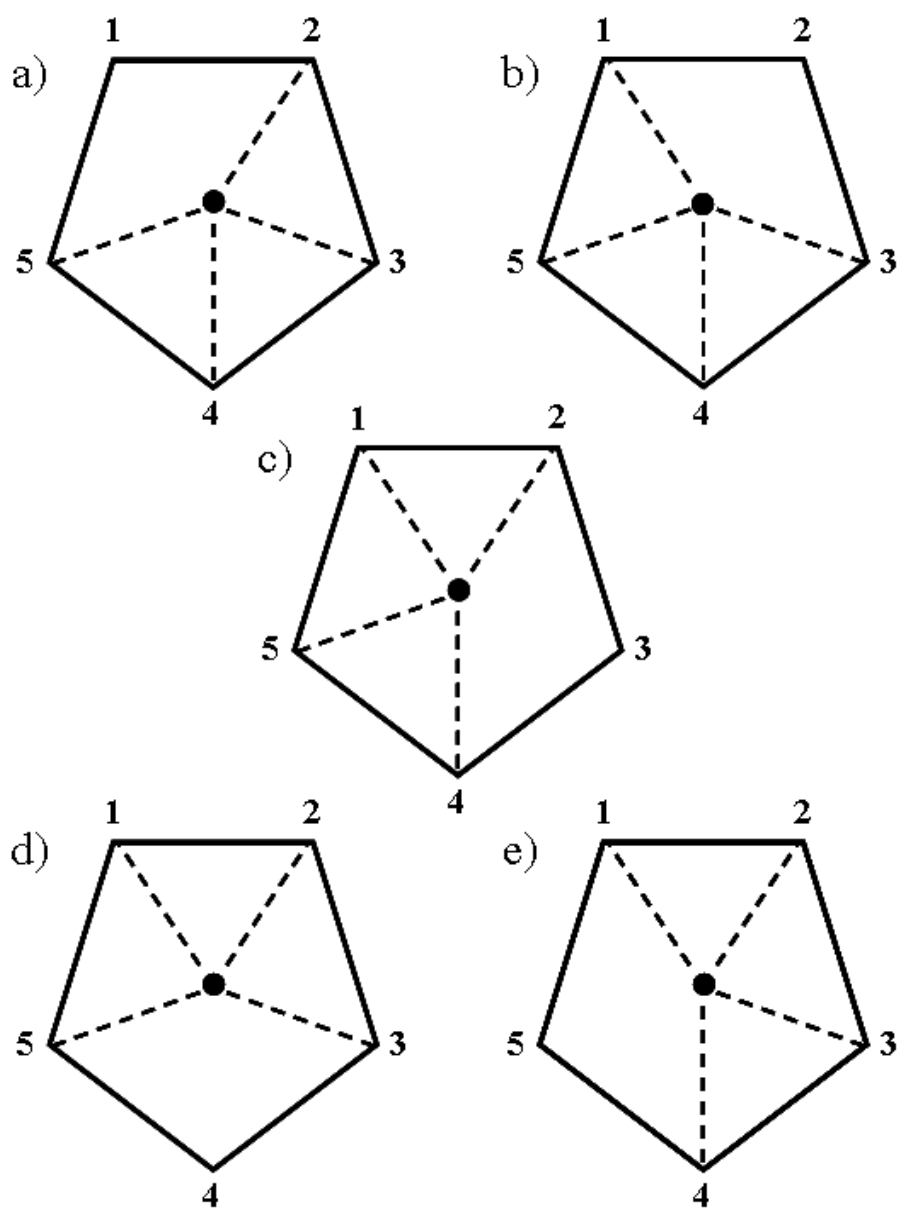
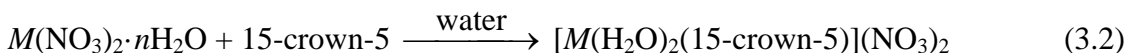


Figure 3.27. Drawing showing the five possibilities (a \rightarrow e) for the Ni^{2+} ion to be coordinated by the O atoms of the crown ether in $[\text{Ni}(\text{H}_2\text{O})_2(15\text{-crown-5})](\text{NO}_3)_2$. For clarity, the 15-crown-5 molecule is symbolized by a pentagon in which the edges correspond to the positions of the five O atoms. The numbers 1 \rightarrow 5 correspond to the atoms O1 \rightarrow O5 respectively. The dots correspond to the nickel position in the crown ether. The dashed lines indicate the coordination between the Ni^{2+} and O_{ether} atoms.

Synthesis of [Ni(H₂O)₂(15-crown-5)](NO₃)₂, why is it not straightforward?

Crystals of the compounds [M(H₂O)₂(15-crown-5)](NO₃)₂, M = Mg, Mn, Co, Cu and Zn, were grown at room temperature by evaporation from a water solution equimolar in 15-crown-5 and M(NO₃)₂·nH₂O, n = 3 for M = Cu, n = 4 for M = Mn, n = 6 for M = Mg, Co and Zn (see the chemical equation 3.2). The synthesis of the Fe compound is slightly different and is given in detail in Chapter 2.



For M = Ni, only green crystals of [Ni(H₂O)₆](NO₃)₂·(15-crown)·2H₂O were obtained and the Ni²⁺ ions were found to be coordinated by six water molecules rather than the five crown-ether O atoms. The partial exclusion of water from the structure was achieved by changing the solvent and other Ni(II) complexes were synthesized: [Ni(H₂O)₆](NO₃)₂·(15-crown-5)·H₂O from acetone, [Ni(H₂O)₆](NO₃)₂·*trans*-[Ni(H₂O)₄(MeOH)₂](NO₃)₂·2(15-crown-5) from methanol, *cis*-[Ni(H₂O)₄(NO₃)₂]·*trans*-[Ni(H₂O)₄(NO₃)₂]·2(15-crown-5) from acetone, 2-butanol, ethanol, THF and [Ni(H₂O)₂(MeCN)(NO₃)₂]·(15-crown-5)·MeCN from acetonitrile. However, the Ni²⁺ ion was not coordinated by the crown ligand in any of these compounds. The present research has thus far concluded that the amount of water available may have an important impact on the synthesis of [Ni(H₂O)₂(15-crown-5)](NO₃)₂, which is not straightforward because six-coordinate Ni(II) complexes seem to be more favorable than seven-coordinate Ni(II) complexes (Giordano *et al.*, 1979; Pelizzi *et al.*, 1986). Eventually, crystals of [Ni(H₂O)₂(15-crown-5)](NO₃)₂ were obtained from another route (see the 'Experimental' section for further details) but distorted pseudoseven-coordinate Ni(II) complexes are likely to occur.

One study of the systems [Ni(L¹)](NO₃)₂·H₂O and [Ni(L¹)](ClO₄)₂ [L¹ = *N,N'*-bis(2-aminobenzyl)-1, 10-diaza-15-crown-5] suggested that the distortion of the seven coordination environment around the Ni²⁺ ion was consistent with the Jahn-Teller effect (Platas-Iglesias *et al.*, 2005).

Analysis of the Packing in $[\text{Ni}(\text{H}_2\text{O})_2(15\text{-crown-5})](\text{NO}_3)_2$

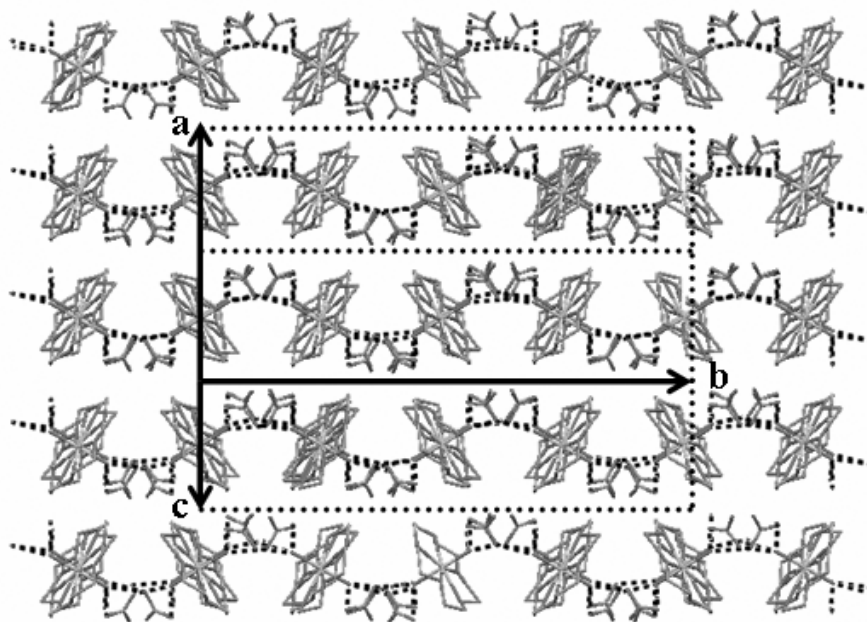
In the two phases of $[\text{Ni}(\text{H}_2\text{O})_2(15\text{-crown-5})](\text{NO}_3)_2$, the packing is found to be very similar. The H-bonding network is two dimensional (hereafter, 2-D) and is found along the **b** and $[1\ 0\ 2]$ directions in phase I or the **b** and **c** directions in phase II. The water ligands form hydrogen bonds to two distinct nitrate ions; and nitrate ions are H-bonded to two different cations. The 2-D H-bonding network can be described as corrugated sheets parallel to $(-2\ 0\ 1)$ in phase I and parallel to $(1\ 0\ 0)$ in phase II (see Figure 3.28).

Enantiomeric Alternation

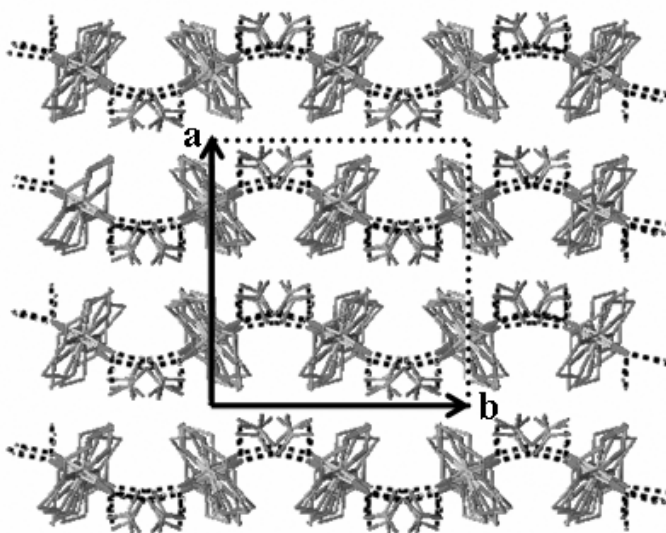
The cations $[\text{Ni}(\text{H}_2\text{O})_2(15\text{-crown-5})]^{2+}$ have nearly C_2 symmetry and have two conformational enantiomers (here designated as R and S; Hao, Parkin & Brock, 2005; Hao, Siegler, Parkin & Brock, 2005). In crystals of $[\text{Ni}(\text{H}_2\text{O})_2(15\text{-crown-5})](\text{NO}_3)_2$, the two conformational enantiomers are present in a ratio 1:1. Rows of cations along the $[1\ 0\ 2]$ and **c** directions in phase I and phase II differ in their enantiomeric alternation pattern (see Figure 3.29).

Along the $[1\ 0\ 2]$ direction of phase I, conformational enantiomers of the same independent cation (either residue 1 or 2) are related by inversion centers. The alternation pattern is found to be perfect: one cation R is adjacent to two cations S (or one cation S is adjacent to two cations R). The perfect alternation pattern along the $[1\ 0\ 2]$ direction is given by: R S (or S R).

Along the **c** direction of phase II, conformational enantiomers are related by either pseudoinversion or pseudotranslation. Enantiomers fail to alternate once every three contacts within a row of cations. The alternation pattern along the **c** direction is given by: R S S (or S R R).



Ni I



Ni II

Figure 3.28. The similar packing of phase I and phase II of $[\text{Ni}(\text{H}_2\text{O})_2(15\text{-crown-5})](\text{NO}_3)_2$ down the $[1\ 0\ 2]$ and c directions. The drawing illustrates the corrugation of the H-bonded sheets parallel to $(-2\ 0\ 1)$ in phase I and parallel to $(1\ 0\ 0)$ in phase II. For phase I, neither the a axis, nor the c axis is in the plane of the drawing. For phase II, the a axis is not in the plane of the drawing. H atoms are omitted for clarity. H bonds are shown as black dotted lines.

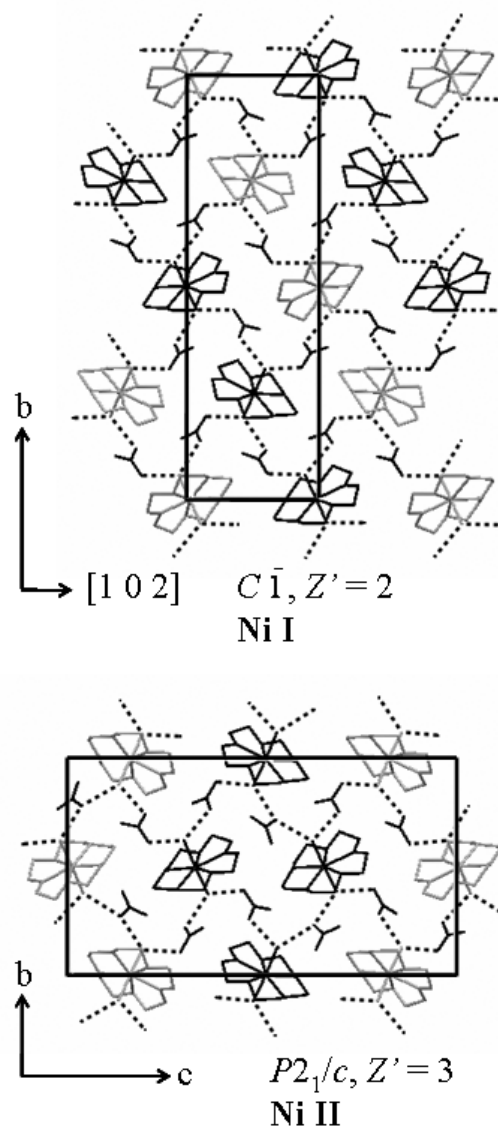


Figure 3.29. Drawing of a layer of the two phases of $[\text{Ni}(\text{H}_2\text{O})_2(15\text{-crown-5})](\text{NO}_3)_2$ down the \mathbf{a} direction. The rows of cations along the $[1\ 0\ 2]$ and \mathbf{c} directions in phase I and phase II are comparable but differ in their alternation pattern. In the triclinic structure ($C\bar{1}$, $Z' = 2$), cations within a row parallel to $[1\ 0\ 2]$ are related by inversion centers. In the monoclinic structure ($P2_1/c$, $Z' = 3$), cations within a row parallel to the \mathbf{c} direction are related by either pseudoinversion or pseudotranslation. For phase I, neither the b axis, nor $[1\ 0\ 2]$ is in the plane of the drawing. For phase II, the c axis is not in the plane of the drawing. The black and gray cations correspond to conformational enantiomers. H atoms are omitted for clarity. H bonds are shown as black dotted lines.

Phase Transition

The phase transition for the compound $[\text{Ni}(\text{H}_2\text{O})_2(15\text{-crown-5})](\text{NO}_3)_2$ is found to be reversible. No significant crystal damage is detectable as the system passes through the transition. The temperature of the phase transition $\text{LTP} \rightarrow \text{HTP}$ (*i.e.*, II \rightarrow I) is found to be near 288 K. The phase transition is first-order because hysteresis occurs.

Below the phase transition, there is one alternation fault over three contacts within a row of cations parallel to the **c** direction. Above the phase transition, there is no alternation fault found along the $[1\ 0\ 2]$ direction and the enantiomeric alternation pattern is perfect. The solid-solid phase transition is possible because enantiomers R/S can interconvert in the solid state. The two compounds $[\text{M}(\text{H}_2\text{O})_2(15\text{-crown-5})](\text{NO}_3)_2$, $M = \text{Mn}, \text{Ni}$ have analogous phase transitions (see Chapter 2 for further details).

Conclusions

The synthesis of the target compound $[\text{Ni}(\text{H}_2\text{O})_2(15\text{-crown-5})](\text{NO}_3)_2$ was difficult to work out. The general route (see the chemical equation 3.2) does not give the target compound and the Ni^{2+} ion, unlike M^{2+} ($M = \text{Mg}, \text{Mn}, \text{Fe}, \text{Co}, \text{Cu}$ and Zn), is coordinated by water molecules rather than the crown ligand. The compound $[\text{Ni}(\text{H}_2\text{O})_6](\text{NO}_3)_2 \cdot (15\text{-crown-5}) \cdot 2\text{H}_2\text{O}$ was always synthesized instead. Several other attempts aimed at limiting the amount of water that could be incorporated into the structure (*e.g.*, the use of other solvents such as acetone, acetonitrile, ethanol and methanol instead of water) were carried out but turned out to be unsuccessful. In the attempts, six Ni(II) complexes were obtained and the Ni^{2+} ion was always found to be coordinated by water molecules only⁵⁰ or by water molecules and other solvent molecules⁵¹ or by water molecules and nitrate ions⁵² or by water molecules, nitrate ions and other solvent molecules⁵³. Three of the compounds have been discussed in this chapter. These Ni(II) complexes are similar in that six coordination (octahedral geometry) is found around the Ni^{2+} ion. The 1-D H-bonded chains between the 15-crown-5 molecules and the Ni cations are also found in all Ni(II) complexes. The geometries of the 15-crown-5 molecule, which is known to be a bifacial H-bond acceptor (Steed *et al.*, 2001), and the six-coordinate Ni(II) cation may be conducive to that type of hydrogen interactions in the solid state. This requires that the six-coordinate Ni(II) cation must have, at least, two H-bond donors (*e.g.*, two water molecules acting as H-bond donors) along one direction, which is the approximate normal to the best molecular plane of the 15-crown-5 molecule.

Further efforts for making the target compound were carried out by removing some water from the samples. The synthesis of the target compound turned out to be successful and reproducible if crystals of $[\text{Ni}(\text{H}_2\text{O})_6](\text{NO}_3)_2 \cdot (15\text{-crown-5}) \cdot 2\text{H}_2\text{O}$ were heated from room temperature to 373 K.

⁵⁰ $[\text{Ni}(\text{H}_2\text{O})_6](\text{NO}_3)_2 \cdot (15\text{-crown-5}) \cdot n\text{H}_2\text{O}$ ($n = 1, 2$)

⁵¹ $[\text{Ni}(\text{H}_2\text{O})_6](\text{NO}_3)_2 \cdot \text{trans-}[\text{Ni}(\text{H}_2\text{O})_4(\text{MeOH})_2](\text{NO}_3)_2 \cdot 2(15\text{-crown-5})$

⁵² $\text{cis-}[\text{Ni}(\text{H}_2\text{O})_4(\text{NO}_3)_2] \cdot \text{trans-}[\text{Ni}(\text{H}_2\text{O})_4(\text{NO}_3)_2] \cdot 2(15\text{-crown-5})$

⁵³ $[\text{Ni}(\text{H}_2\text{O})_2(\text{MeCN})(\text{NO}_3)_2] \cdot (15\text{-crown-5}) \cdot \text{MeCN}$

The compound $[\text{Ni}(\text{H}_2\text{O})_2(15\text{-crown-5})](\text{NO}_3)_2$ has one solid-solid phase transition that takes place at about 284-288 K. The low-temperature phases of $[M(\text{H}_2\text{O})_2(15\text{-crown-5})](\text{NO}_3)_2$, $M = \text{Mg}, \text{Mn}, \text{Fe}, \text{Ni}$ and Zn (II, $P2_1/c$, $Z' = 3$) are isostructural. The high-temperature phases of $[M(\text{H}_2\text{O})_2(15\text{-crown-5})](\text{NO}_3)_2$, $M = \text{Mn}, \text{Ni}$ and Cu (I, $C\bar{1}$, $Z' = 2$) are isostructural. The phase transitions observed for $[M(\text{H}_2\text{O})_2(15\text{-crown-5})](\text{NO}_3)_2$, $M = \text{Mn}$ and Ni are analogous. The single-crystal X-ray experiments showed that the Ni^{2+} ions in the two phases of $[\text{Ni}(\text{H}_2\text{O})_2(15\text{-crown-5})](\text{NO}_3)_2$ might not be coordinated by all five O_{ether} atoms of the 15-crown-5 molecule. Disorder of the Ni^{2+} ion takes place inside the cavity of the crown ether and has been observed, thus far, for the compound $[\text{Ni}(\text{H}_2\text{O})_2(15\text{-crown-5})](\text{NO}_3)_2$ only.

Chapter Four

-

The First Polymorph of $[\text{Ni}(\text{H}_2\text{O})_6](\text{NO}_3)_2 \cdot (15\text{-crown-5}) \cdot \text{H}_2\text{O}$: a Two-Phase System

Introduction

Several attempts to synthesize the compound $[\text{Ni}(\text{H}_2\text{O})_2(15\text{-crown-5})](\text{NO}_3)_2$ were presented previously in Chapter 3. In all syntheses, efforts were made to reduce the number of water ligands coordinated to the Ni^{2+} ion by excluding water. Eight phases containing Ni^{2+} , 2NO_3^- , 15-crown-5 and water (as ligands and solvent molecules) were found. Among these phases, the first polymorph of $[\text{Ni}(\text{H}_2\text{O})_6](\text{NO}_3)_2 \cdot (15\text{-crown-5}) \cdot \text{H}_2\text{O}$ was isolated. No structure of this latter compound has been reported in the literature. Two other solvates, the second polymorph of $[\text{Ni}(\text{H}_2\text{O})_6](\text{NO}_3)_2 \cdot (15\text{-crown-5}) \cdot \text{H}_2\text{O}$ (discussed in the previous chapter) and the compound $[\text{Ni}(\text{H}_2\text{O})_6](\text{NO}_3)_2 \cdot (15\text{-crown-5}) \cdot 2\text{H}_2\text{O}$ were also found in the course of this research. The latter compound is subject to further discussions in Chapter 5.

The research demonstrates that the first polymorph of $[\text{Ni}(\text{H}_2\text{O})_6](\text{NO}_3)_2 \cdot (15\text{-crown-5}) \cdot \text{H}_2\text{O}$ is a two-phase system. One solid-solid phase transition and two phases were found between 90 and 295 K. This system was investigated methodically *via* DSC measurements and single-crystal X-ray diffraction experiments. The low-temperature phase (phase II, $Z' = 2$) is mostly ordered. The room-temperature phase (phase I, $Z' = 1$) is disordered. The temperature at which the low-temperature phase completely disappears was found to be between 195 and 200 K. The two phases are solved in the same noncentrosymmetric space group $P2_1$. Only one of the two conformational enantiomers (R or S) of the 15-crown-5 molecule is present in any individual crystal of either of the two crystal structures. The packing remains very similar in the two phases and one-dimensional H-bonded chains of the 15-crown-5 molecules and the $[\text{Ni}(\text{H}_2\text{O})_6]^{2+}$ ions are found along the **a** direction. There is no apparent loss of crystallinity as single crystals undergo the phase transition II \rightarrow I (heating).

The occurrence of hysteresis indicates that the phase transition II \rightarrow I is first-order. The temperature dependence of the cell dimensions shows that the phase transition may be more complicated to understand at intermediate temperatures (*i.e.*, between 150 and 200 K). Changes in the structure were observed at intermediate temperatures and an approach to the mechanism of the phase transition is described. The temperature at which phase II completely disappears was located by inspection of the reciprocal lattice slices between 190 and 200 K and by plotting the integrated intensities of specific classes of reflections between 90 and 200 K.

Experimental

Crystal Growth

Details of the crystal growth were given in Chapter 3.

Crystal Habit

Crystals are parallelepipeds that are somewhat elongated along one direction [see part (a) of Figure 4.1]. The favored direction for crystal growth corresponds to the direction of the one-dimensional H-bonded chains of the 15-crown-5 molecules and the $[\text{Ni}(\text{H}_2\text{O})_6]^{2+}$ ions (*i.e.*, the **a** direction). The most prominent faces of the crystal belong to the forms $\{0\ 1\ 0\}$ and $\{0\ 0\ 1\}$ [see part (b) of Figure 4.1]. The indices are given for the cell of the room temperature phase ($P2_1$, $Z' = 1$). The angles between two non-parallel faces [*i.e.*, the angles between the set of planes of the forms $\{0\ 1\ 0\}$ and $\{0\ 0\ 1\}$] are 90° . The crystal cross-section is often found to be approximately similar along the **b*** and **c*** directions. The faces found at the boundaries of the crystal were not indexed since their indices seemed to vary.

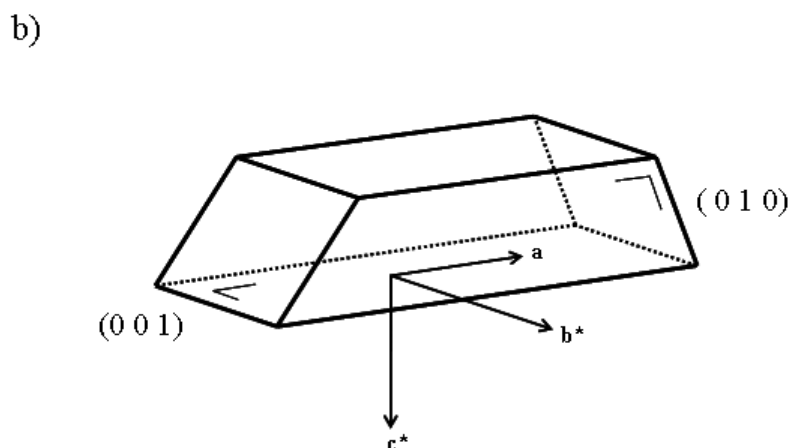
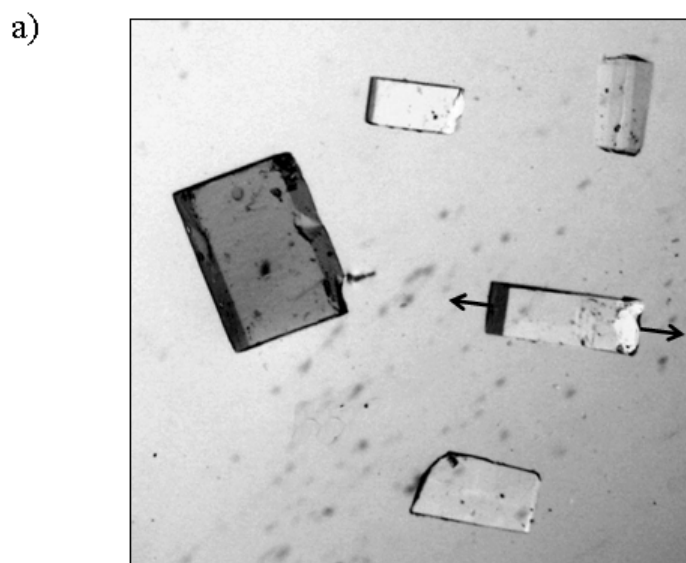


Figure 4.1. (a) A photograph of single crystals of the first polymorph of $[\text{Ni}(\text{H}_2\text{O})_6](\text{NO}_3)_2 \cdot (15\text{-crown-5}) \cdot \text{H}_2\text{O}$. Crystals are parallelepipeds elongated along one direction (the black arrows show the direction of elongation). (b) Drawing describing the crystal habit of the first polymorph of $[\text{Ni}(\text{H}_2\text{O})_6](\text{NO}_3)_2 \cdot (15\text{-crown-5}) \cdot \text{H}_2\text{O}$. The crystal growth is favored along the **a** direction and the most important faces of the crystal belong to the form $\{0\ 1\ 0\}$ and $\{0\ 0\ 1\}$. The planes $(0\ \bar{1}\ 0)$ and $(0\ 0\ \bar{1})$ (not shown in the picture) are respectively equivalent to the planes $(0\ 1\ 0)$ and $(0\ 0\ 1)$. The crystal growth was usually found to be similar along the **b*** and **c*** directions.

Differential Scanning Calorimetry Measurements

The first polymorph of $[\text{Ni}(\text{H}_2\text{O})_6](\text{NO}_3)_2 \cdot (15\text{-crown-5}) \cdot \text{H}_2\text{O}$ was investigated using the DSC 822^e apparatus and the controlling software STARe (version 8.10) manufactured by *METTLER TOLEDO*. One set of DSC measurements was collected between 173 and 298 K. The DSC sample was prepared from fine powder and contained in aluminum sealed pans. The amount of powdered sample was 1.95 mg. The cooling and heating rates were -10 and 10 K/min. Between 173 and 298 K, one solid-solid phase transition was found at $T_{\text{onset}} = 190$ K (given for heating). The small peak heights in the DSC traces prevent a good estimation of ΔH_{tr} . The solid-solid phase transition is first-order because hysteresis occurs. Enthalpy is associated with such a transition. The DSC traces are shown in Figure 4.2.

X-ray Crystallography

The general procedures for data collection and for the H-atoms treatment were given in the corresponding section of Chapter 2.

All data were collected using a Nonius KappaCCD diffractometer with graphite-monochromated Mo $K\alpha$ radiation ($\lambda = 0.71073$ Å) under the program *COLLECT* (Nonius, 1997).

Two phases of $[\text{Ni}(\text{H}_2\text{O})_6](\text{NO}_3)_2 \cdot (15\text{-crown-5}) \cdot \text{H}_2\text{O}$ were isolated: a low-temperature phase with $Z' = 2$ and a room temperature phase with $Z' = 1$. The two phases were solved and refined in the noncentrosymmetric space groups $P2_1$. By convention, the two phases of $[\text{Ni}(\text{H}_2\text{O})_6](\text{NO}_3)_2 \cdot (15\text{-crown-5}) \cdot \text{H}_2\text{O}$ are numbered I and II, I for the room temperature phase and II for the low-temperature phase.

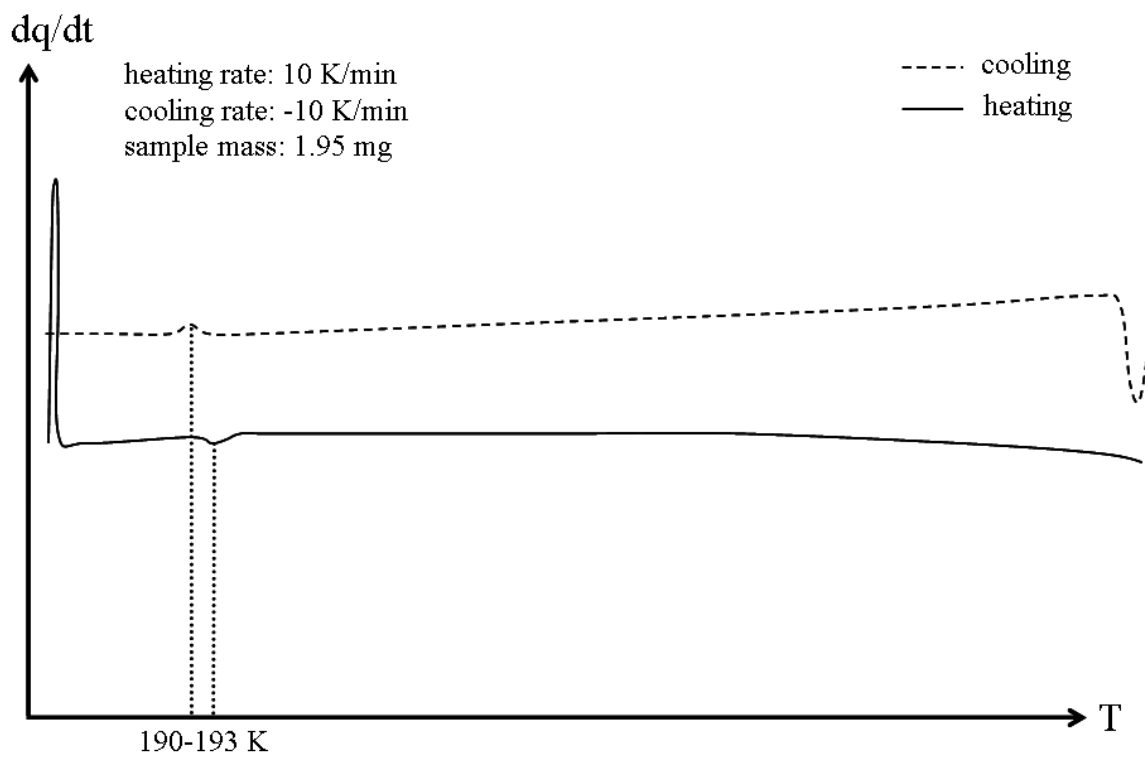


Figure 4.2. DSC traces of the first polymorph of $[\text{Ni}(\text{H}_2\text{O})_6](\text{NO}_3)_2 \cdot (15\text{-crown-5}) \cdot \text{H}_2\text{O}$ collected between 173 and 298 K at 10 K/min and between 298 and 173 K at -10 K/min. The two traces show one solid-solid phase transition between 190 and 193 K.

Generalities

The two phases of the first polymorph $[\text{Ni}(\text{H}_2\text{O})_6](\text{NO}_3)_2 \cdot (15\text{-crown-5}) \cdot \text{H}_2\text{O}$ were solved and refined in the noncentrosymmetric space group $P2_1$. The cell for phase II was transformed in ways that maximized the similarities with phase I (*i.e.*, the two phases have the one-dimensional H-bonded chains of the 15-crown-5 molecules and the $[\text{Ni}(\text{H}_2\text{O})_6]^{2+}$ ions along the **a** direction). Figure 4.3 shows that the two phases are very similar. The cell constants at 90 K of the standard primitive cell of phase II are: $a = 10.220$ (1)Å, $b = 16.514$ (2)Å, $c = 13.644$ (2)Å, $\beta = 95.96$ (1)°. The non-standard space group $B2_1$ was preferred for reasons explained above. The transformation matrix is given by: $\mathbf{a}(B2_1) = (1\ 0\ 1 / 0\ -1\ 0 / 1\ 0\ -1)\ \mathbf{a}(P2_1)$.

The atom-numbering scheme is consistent in the two phases.

Phases I and II

Data for phases I and II were collected near 295 and 90 K⁵⁴ using the same crystal.

The refinements of phase I ($P2_1$, $Z' = 1$) and phase II ($B2_1$, $Z' = 2$) were problem-free. The R factors [$F^2 > 2\sigma(F^2)$] are less than 0.035 for both phases. The final difference Fourier map suggested residual electron density with peaks no larger than $0.44 \text{ e } \text{\AA}^{-3}$ in phase I and $0.58 \text{ e } \text{\AA}^{-3}$ in phase II. The largest peaks were 0.86 - 1.16 \AA from one H atom of the crown ether but were not physically meaningful. The other peaks are no larger than $0.37 \text{ e } \text{\AA}^{-3}$. Phase I is disordered: libration of the 15-crown-5 molecule is significant. Phase II is mainly ordered. Disorder of the lattice water molecule in phase I and one of the two lattice water molecules in phase II is observed. The values of the occupancy factors given for the major components of the water disorder is 0.633 (6) in phase I and 0.809 (9) in phase II. An extinction correction was included in the model of the two structures. The extinction parameters $EXTI$ are 0.022 (2) for phase I and 0.00036 (6) for phase II. The absolute configuration was successfully determined in the two phases. The values of the Flack parameters x (Flack, 1983; Flack & Bernardinelli, 1999) are -0.013 (11) and -0.002 (7) respectively given for the phases I and II, so there is no inversion twinning. The ellipsoids of all atoms in the asymmetric units of the phases I and II are shown in Figure 4.4.

The crystallographic data for the two phases are given in Table 4.1.

⁵⁴ 90 K is near the lower limit of stable temperature control when the cooling device is running with liquid nitrogen.

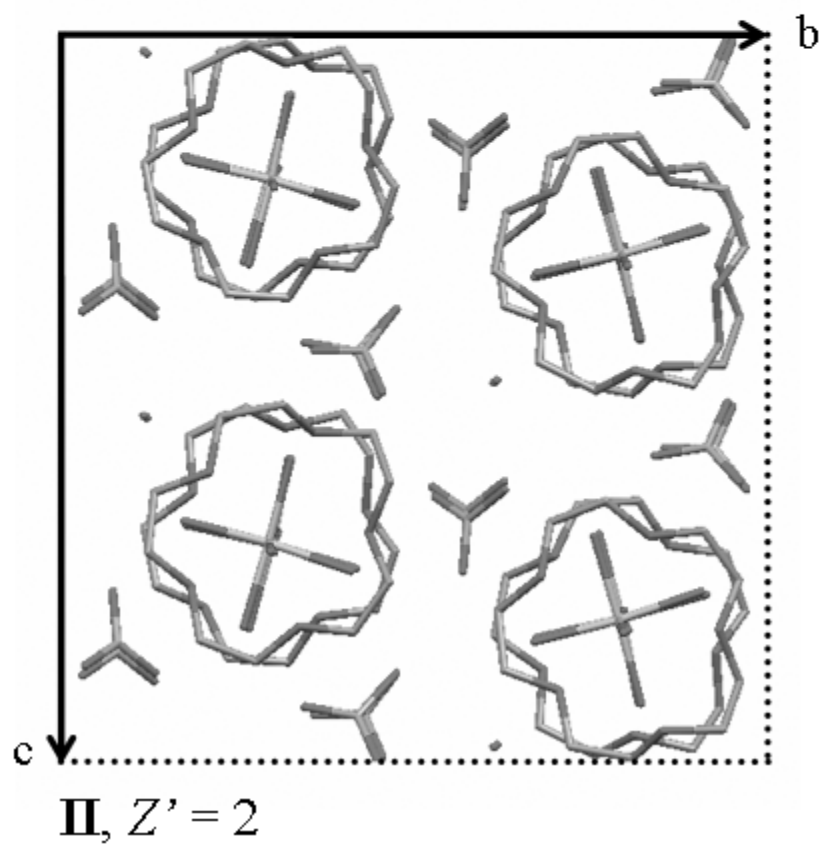
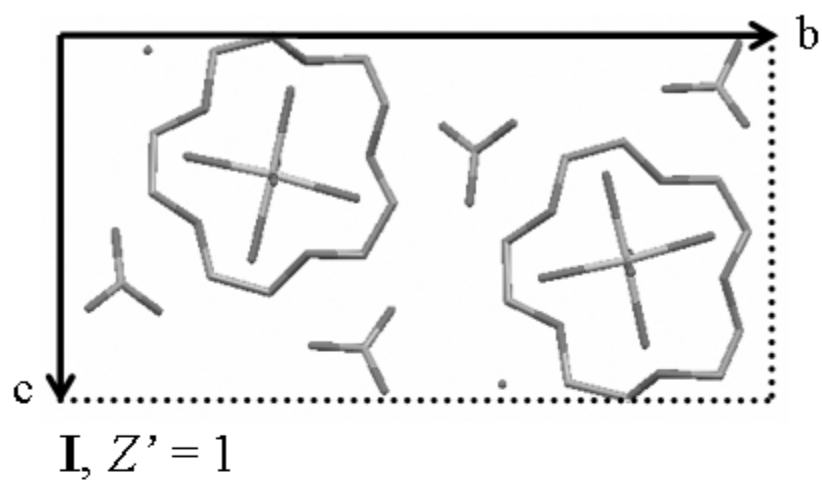
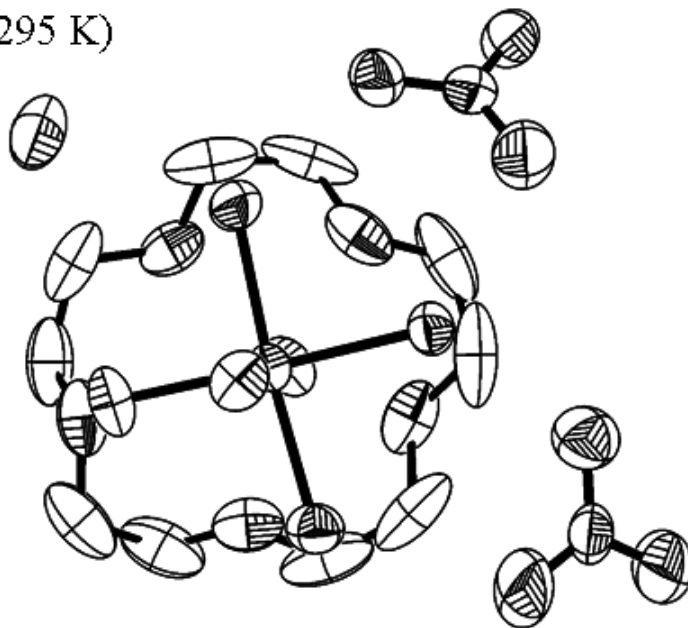


Figure 4.3. Projections of the two phases of the first polymorph of $[\text{Ni}(\text{H}_2\text{O})_6](\text{NO}_3)_2 \cdot (15\text{-crown-5}) \cdot \text{H}_2\text{O}$ down the **a** direction. For the two phases, the *c* axis is not in the plane of the drawing. The drawing shows that the packing is very similar in the two phases. The disorder of the lattice water molecules and the H atoms are omitted for clarity.

Phase I (295 K)



Phase II (90 K)

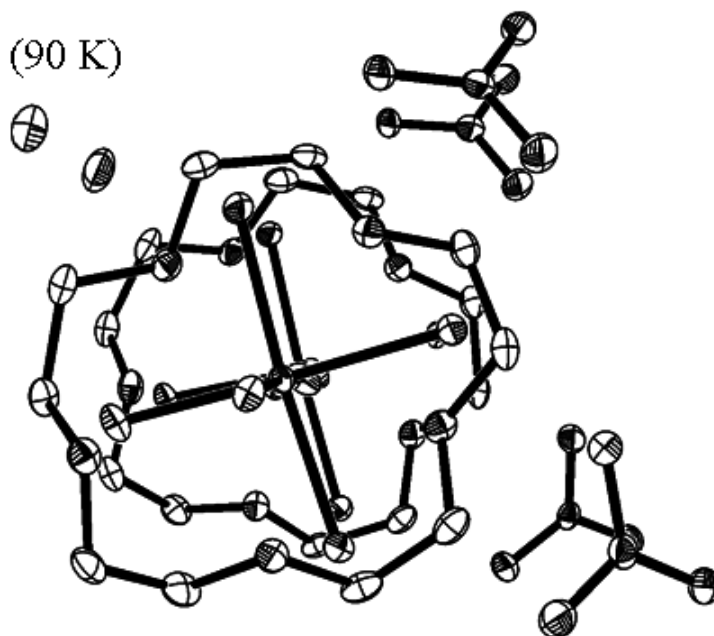


Figure 4.4. The displacement ellipsoids (50% probability level) of the asymmetric unit of the first polymorph of $[\text{Ni}(\text{H}_2\text{O})_6](\text{NO}_3)_2 \cdot (15\text{-crown-5}) \cdot 2\text{H}_2\text{O}$ in phase I at 295 K and in phase II at 90 K. The librational and/or disorder effects of the 15-crown-5 molecule are significant at 295 K. The disorder of the lattice water molecules and the H atoms are omitted for clarity.

Table 4.1. Crystallographic data for the two phases (I and II) of the first polymorph of $[\text{Ni}(\text{H}_2\text{O})_6](\text{NO}_3)_2 \cdot (15\text{-crown-5}) \cdot \text{H}_2\text{O}$.

	I	II
Crystal data		
Chemical formula	$(\text{C}_{10}\text{H}_{20}\text{O}_5) \cdot (\text{H}_{12}\text{NiO}_6^{2+}) \cdot 2(\text{NO}_3^{1-}) \cdot (\text{H}_2\text{O})$	
M_r	529.10	529.10
Cell setting, space group	Monoclinic, $P2_1$	Monoclinic, $B2_1$
a, b, c (Å) ⁵⁵	8.180 (2) 16.701 (4) 8.960 (2)	16.176 (2) 16.514 (2) 17.876 (2)
β (°)	105.96 (1)	106.42 (1)
V (Å ³)	1176.9 (5)	4590.5 (9)
$Z; Z'$	2; 1	8; 2
D_x (g cm ⁻³)	1.493	1.535
Radiation type	Mo $K\alpha$	Mo $K\alpha$
No. of reflections for cell parameters	2714	5425
θ range (°)	1.0–27.5	1.0–27.5
μ (mm ⁻¹)	0.91	0.93
Temperature (K)	295 (2)	90.0 (2)
Crystal form, colour	Parallelepiped, pale green	Parallelepiped, pale green
Crystal size (mm)	0.40 x 0.20 x 0.20	0.40 x 0.20 x 0.20
Data collection		
Diffractometer	Nonius KappaCCD	Nonius KappaCCD
Data collection method	ω scans at fixed $\chi = 55^\circ$	ω scans at fixed $\chi = 55^\circ$
Absorption correction	Multi-scan (based on symmetry-related measurements)	
T_{\min}	0.713	0.707

⁵⁵ The estimated errors in the unit cell constants (a , b , c and β) were modified by multiplying the experimental estimated standard uncertainties (*i.e.*, su's) by at least a factor of ~10 for a , b , c and by at least a factor of ~16.5 for β . These factors were used in order to approximate the errors in the unit cell constants from one crystal to another (Herbstein, 2000).

Table 4.1. (continued)

T_{\max}	0.840	0.836
No. of measured, independent and observed parameters	5045, 5045, 4593	10301, 10301, 8534
Criterion for observed reflections	$I > 2\sigma(I)$	$I > 2\sigma(I)$
R_{int}	0.044	0.049
θ_{\max} (°)	27.3	27.5
Range of h, k, ℓ	$-10 < h < 10$ $-21 < k < 21$ $-11 < \ell < 11$	$-20 < h < 20$ $-21 < k < 20$ $-23 < \ell < 23$
Refinement		
Refinement on	F^2	F^2
$R[F^2 > 2\sigma(F^2)], wR(F^2), S$	0.031, 0.076, 1.03	0.031, 0.069, 1.04
No. of reflections	5045 reflections	10301 reflections
No. of parameters	327	648
H-atom treatment	Mixture of independent and constrained refinement	
Weighting scheme	Calculated $w = 1/[\sigma^2(F_o^2) + (0.0346P)^2 + 0.3184P]$ where $P = (F_o^2 + 2F_c^2)/3$	Calculated $w = 1/[\sigma^2(F_o^2) + (0.0249P)^2 + 2.8514P]$ where $P = (F_o^2 + 2F_c^2)/3$
$(\Delta/\sigma)_{\max}$	0.001	0.001
$\Delta\rho_{\max}, \Delta\rho_{\min}$ (e Å ⁻³)	0.44, -0.24	0.58, -0.41
Extinction method	SHELXL	SHELXL
Extinction coefficient	0.022 (2)	0.00036 (6)
Absolute structure	Flack H D (1983), Acta Cryst. A39, 876-881	Flack H D (1983), Acta Cryst. A39, 876-881
Flack parameter	-0.013 (11)	-0.002 (7)

Computer programs: *COLLECT* (Nonius, 1997); *DENZO-SMN* (Nonius, 1997); *SHELXS-97* (Sheldrick, 1990); *SHELXL-97* (Sheldrick, 1997); *XP in SHELXTL* (Bruker, 1995); *SHELX-97 and local procedures*.

Temperature Dependence of the Cell Dimensions

The temperature dependence of the cell dimensions (*i.e.*, a , b , c and β) for the first polymorph of $[\text{Ni}(\text{H}_2\text{O})_6](\text{NO}_3)_2 \cdot (15\text{-crown-5}) \cdot \text{H}_2\text{O}$ was studied between 90 and 273 K. The cell dimensions were measured at 10 K intervals at temperatures away from the phase transition and at 5 K intervals at temperatures near the phase transition. Twenty-two full data sets were collected from one single crystal for consistency. There is no evidence of significant crystal damage or loss of crystallinity as crystals pass through the reversible phase transition.

Before plots were made, the cell dimensions were modified in a way that minimizes the effect of structural changes between the two phases. Phase II was chosen to be the cell of reference because the a and c axes are about twice as large in phase II as in phase I. As a result, the changes of the cell constants appear larger near the phase transition. The a and c axes of phase I were multiplied by a factor of two, the volume V of the same phase was multiplied by a factor of four. The temperature dependences of the cell dimensions a , b , c and β , V of the first polymorph of $[\text{Ni}(\text{H}_2\text{O})_6](\text{NO}_3)_2 \cdot (15\text{-crown-5}) \cdot \text{H}_2\text{O}$ are shown in Figures 4.5 and 4.6. Between 90 and 273 K, the thermal expansion of the b axis ($\Delta b \sim 0.19 \text{ \AA}$) and the change in β angle ($\Delta\beta \sim 0.40^\circ$) are the largest. The temperature dependences of the b axis and the β angle (and to a less extent, the c axis) show evidence of significant changes between 150 and 200 K. The phase transition cannot be located more precisely because the changes are diffuse⁵⁶ rather than abrupt. The other plots are less informative regarding the phase transition $\text{II} \rightarrow \text{I}$.

The agreement of this crystallographic study with the DSC measurements is good. The temperature at which the $Z' = 2$ phase completely disappears is found to be somewhere between 190 and 200 K. The phase transition $\text{II} \rightarrow \text{I}$ will be explored in more detail in the ‘Results and Discussion’ section.

⁵⁶ The term “diffuseness” is used in Mnyukh’s book (Fundamentals of Solid State Phase Transitions, Ferromagnetism and Ferroelectricity) to make reference to gradual changes as a given system passes through a solid-state phase transition.

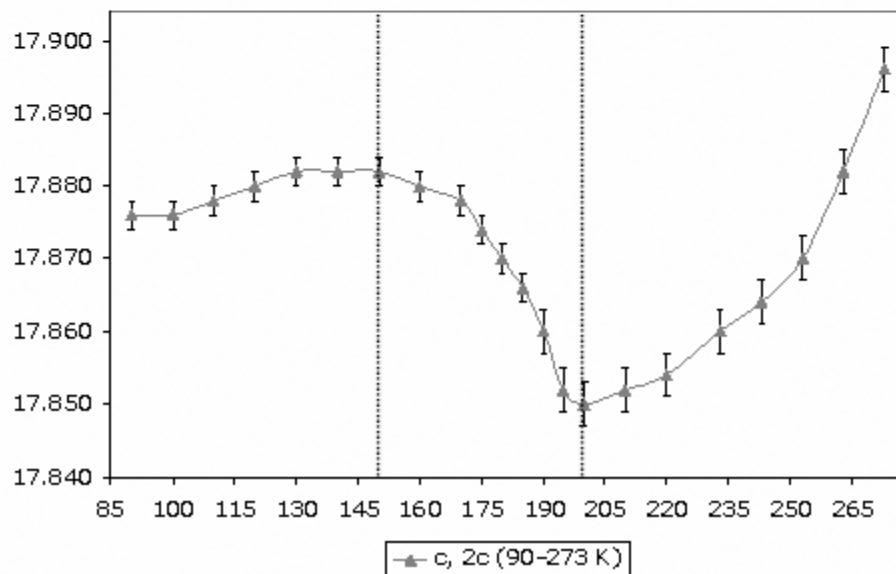
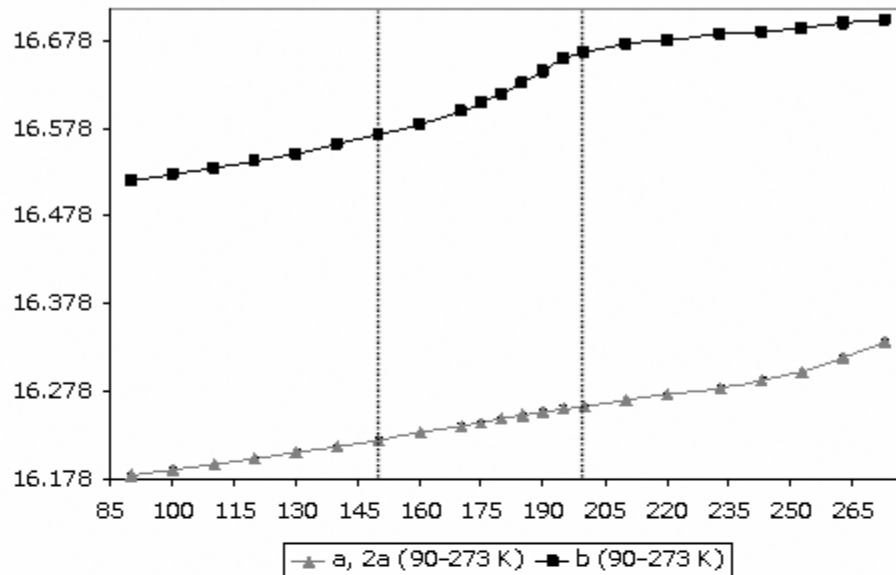


Figure 4.5. Plots of the cell dimensions a , b and c (Å) of the first polymorph of $[\text{Ni}(\text{H}_2\text{O})_6](\text{NO}_3)_2 \cdot (15\text{-crown-5}) \cdot \text{H}_2\text{O}$ versus T (K). The a and c cell dimensions for phase I were multiplied by two so that the cells of the two phases are very similar. Significant changes are found in the temperature dependence of the b axis (and to a lesser extent in that of the c axis) between 150 and 200 K. The positions of the vertical dotted lines are given at temperatures for which the changes occur. Error bars of the cell constants are shown. Error bars associated with the a and b dimensions are insignificant compared to the axis scale.

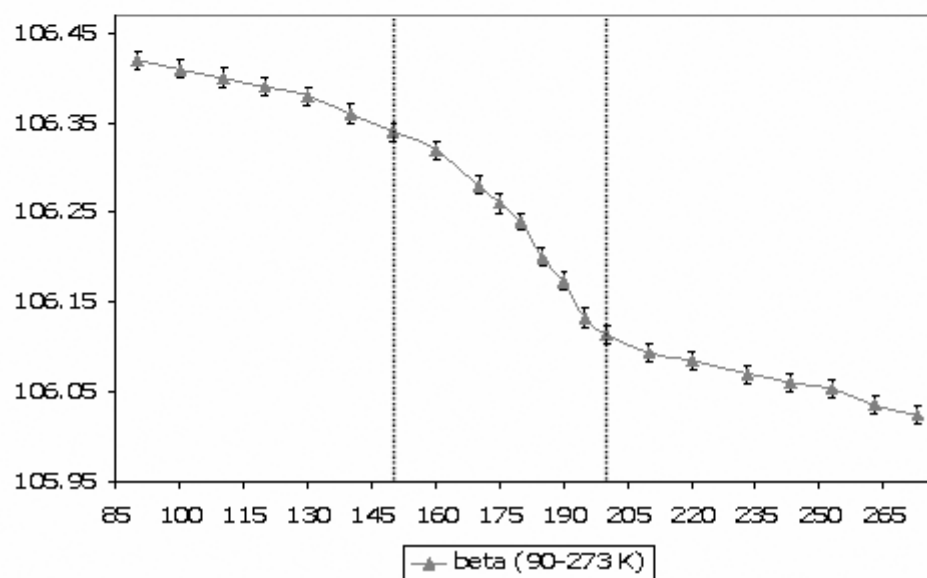
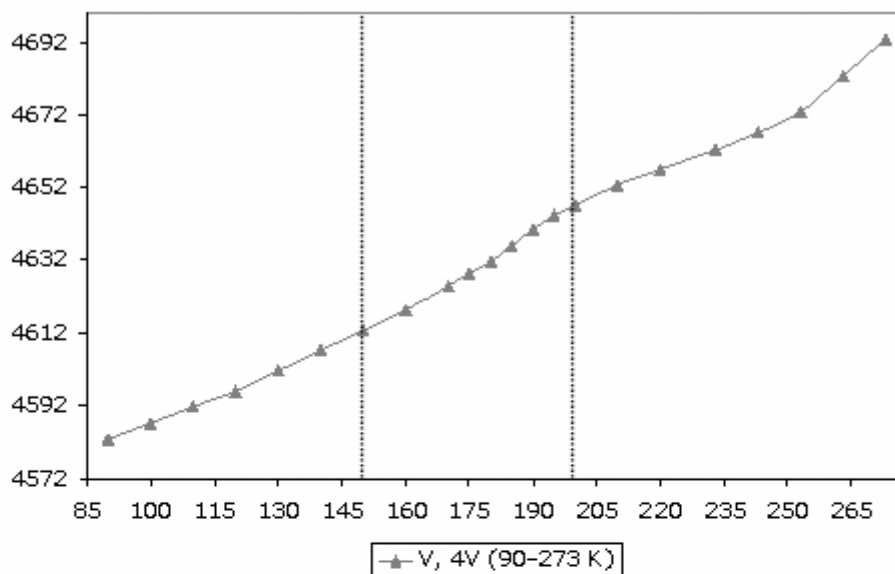


Figure 4.6. Plots of the cell dimensions β ($^\circ$) and V (\AA^3) of the first polymorph of $[\text{Ni}(\text{H}_2\text{O})_6](\text{NO}_3)_2 \cdot (15\text{-crown-5}) \cdot \text{H}_2\text{O}$ versus T (K). The volume V for phase I was multiplied by four so that the cells of the two phases are very similar. Significant changes are found in the temperature dependence of the β angle between 150 and 200 K. The positions of the vertical dotted lines are given at temperatures for which the changes occur. Error bars of the cell constants are shown. Error bars associated with the volume V are insignificant compared to the axis scale.

Results and Discussion

Analysis of the Packing

The H-bonded network of the two phases of the first polymorph of $[\text{Ni}(\text{H}_2\text{O})_6](\text{NO}_3)_2 \cdot (15\text{-crown-5}) \cdot \text{H}_2\text{O}$ is three-dimensional. The system is better depicted as one-dimensional (hereafter, 1-D) chains and two-dimensional (hereafter, 2-D) corrugated planes of H-bonds. There is no evidence that the hydrogen bond interactions are different in the two phases. The nature of the hydrogen bonds observed in the two phases is given in detail.

Along the **a** direction, the H-bond interactions between the 15-crown-5 molecules and the $[\text{Ni}(\text{H}_2\text{O})_6]^{2+}$ ions correspond to 1-D chains. In this system, the crown ether acts as a bifacial hydrogen bond acceptor (Steed *et al.*, 2001) and is found to be H-bonded by two $[\text{Ni}(\text{H}_2\text{O})_6]^{2+}$ ions. The 1-D chains are built *via* a set of hydrogen bonds between the five O_{ether} atoms (O1, O2, O3, O4 and O5) of the crown ether, one $\text{O}_{\text{equatorial}}$ (O8) and the two O_{axial} atoms (O6 and O7) of the $[\text{Ni}(\text{H}_2\text{O})_6]^{2+}$ ions [see the part (a) of Figure 4.7].

The interactions between the $[\text{Ni}(\text{H}_2\text{O})_6]^{2+}$ and nitrate ions and the lattice water molecules are two-dimensional and are found along the **b** and **c** directions. The 2-D planes are built *via* a set of H-bonds between the $\text{O}_{\text{equatorial}}$ atoms (O8, O9, O10 and O11) of the $[\text{Ni}(\text{H}_2\text{O})_6]^{2+}$ ion, O atoms (O12, O13, O14, O15, O16 and O17) of the nitrate ions and the lattice water molecules (O18). Along the 2-D planes, the O8 atom is an H-bond donor to one nitrate ion only, the O9 and O10 atoms are H-bond donors to two nitrate ions, and the O11 atom is an H-bond donor to one nitrate ion and one lattice water molecule [see the part (b) of Figure 4.7]. Along the **b** and **c** directions, the simplest hydrogen bond pattern is given by $\cdots\text{nitrate}\cdots[\text{Ni}(\text{H}_2\text{O})_6]^{2+}\cdots\text{nitrate}\cdots$. The 1-D H-bonded chains and the corrugation of the 2-D plane are shown in Figure 4.8. The role of the lattice water molecule is discussed in the next section. Table 4.2 summarizes the O \cdots O distances found in the 3-D H-bonded network of the two phases.

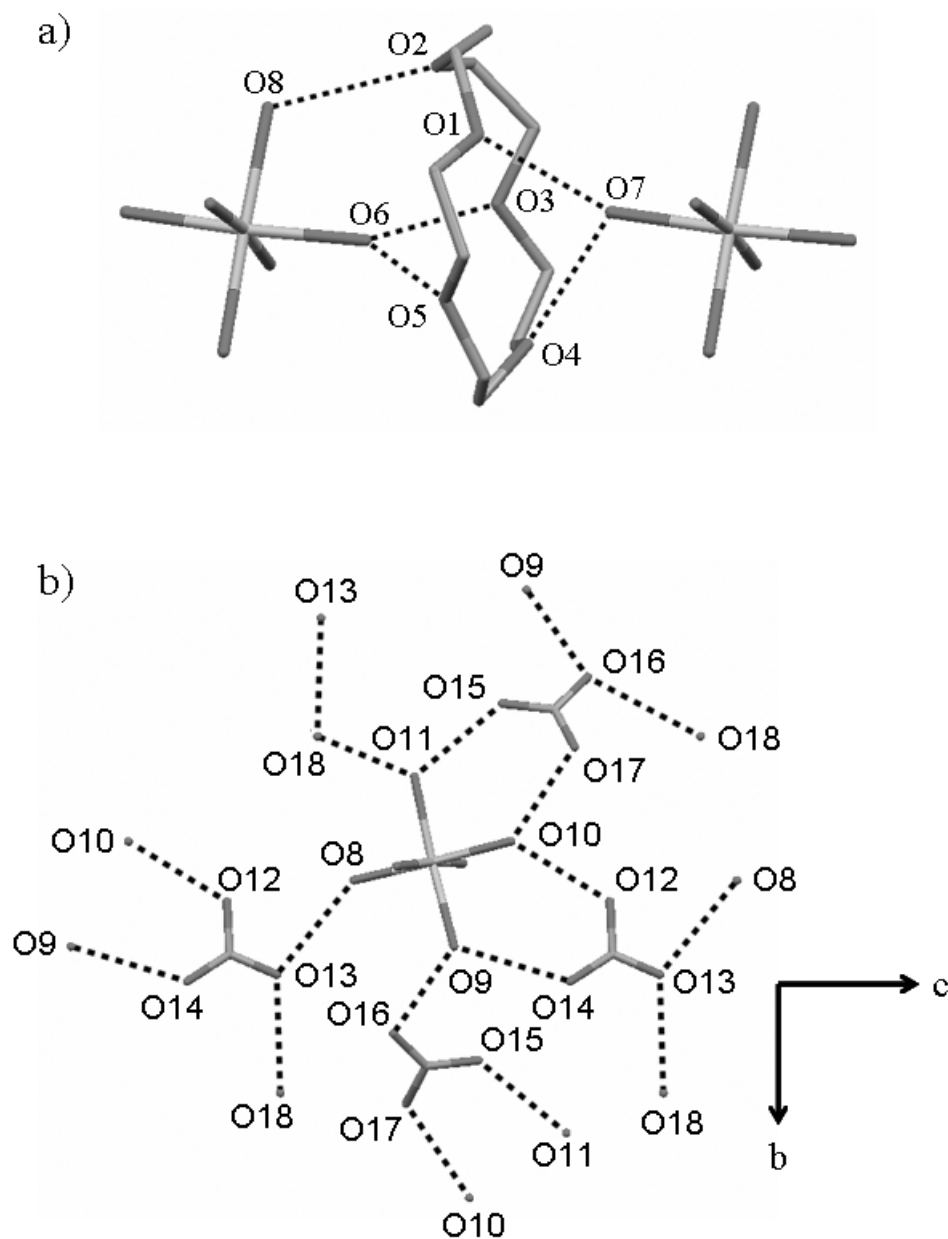


Figure 4.7. (a) The set of hydrogen bond interactions in the first polymorph of $[\text{Ni}(\text{H}_2\text{O})_6](\text{NO}_3)_2 \cdot (15\text{-crown-5}) \cdot \text{H}_2\text{O}$ along the **a** direction (*i.e.*, along the 1-D H-bonded chains). H-bonds are shown as black dotted lines. The nitrate ions, the lattice water molecule and the H-atoms are omitted for clarity. (b) The set of hydrogen bond interactions in the compound $[\text{Ni}(\text{H}_2\text{O})_6](\text{NO}_3)_2 \cdot (15\text{-crown-5}) \cdot \text{H}_2\text{O}$ along the **b** and **c** directions (*i.e.*, along the 2-D H-bonded planes). H-bonds are shown as black dotted lines. The 15-crown-5 molecule, the disorder of the lattice water molecule and the H atoms are omitted for clarity.

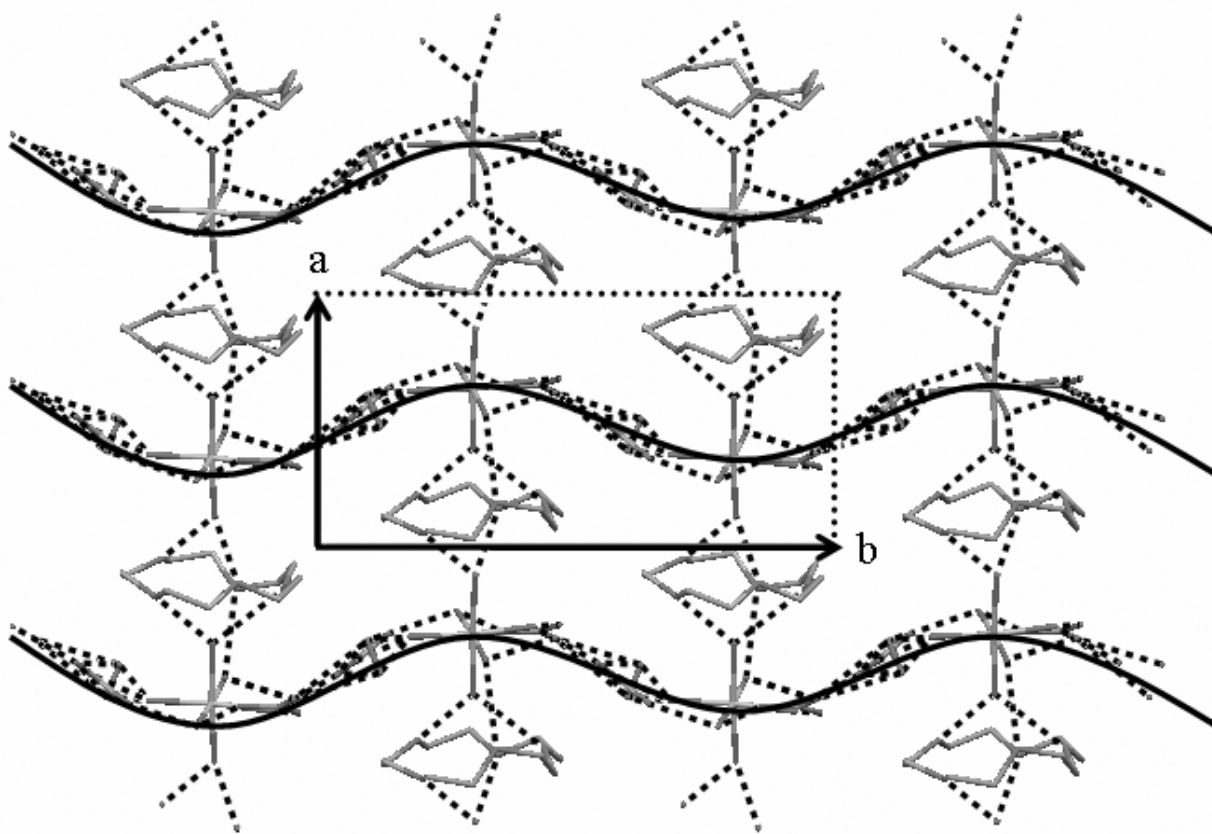


Figure 4.8. The packing of one layer in phase I of the first polymorph of $[\text{Ni}(\text{H}_2\text{O})_6](\text{NO}_3)_2 \cdot (15\text{-crown-5}) \cdot \text{H}_2\text{O}$ looking down the **c** direction. The drawing illustrates the 1-D chains found along the **a** direction and the corrugation of the 2-D planes observed along the **b** direction. The corrugation is symbolized by black thick lines. The *a* axis is not in the plane of the drawing. H-bonds are shown as black dotted lines. The disorder of the lattice water molecules and the H atoms are omitted for clarity.

Table 4.2. Hydrogen bond distances D···A (Donor···Acceptor) along the **a** direction (*i.e.*, the direction of the 1-D H-bonded chains) and along the **b** and **c** directions (*i.e.*, the directions found along the 2-D planes) for the phases I and II of the first polymorph of [Ni(H₂O)₆](NO₃)₂·(15-crown-5)·H₂O. The hydrogen bond interactions involving the minor component of the disorder of the lattice water molecule in phase I are not given.

D···A (Å)	1-D		2-D			
Phase I	O6···O3	2.831 (4)	O8···O13	2.930 (4)		
	O6···O5	2.744 (3)	O9···O14	2.839 (4)		
	O7···O1	2.762 (3)	O9···O16	2.749 (3)		
	O7···O4	2.790 (3)	O10···O12	2.790 (3)		
	O8···O2	2.861 (3)	O10···O17	2.758 (4)		
			O11···O15	2.781 (3)		
			O11···O18	2.700 (3)		
O18···O13			2.911 (6)			
Phase II	Residue 1		Residue 1		Residue 2	
	O6···O3	2.876 (2)	O8···O13	2.832 (2)	O8···O13	2.840 (2)
	O6···O5	2.730 (2)	O9···O14	2.860 (2)	O9···O14	2.819 (2)
	O7···O1	2.762 (2)	O9···O16	2.763 (2)	O9···O16	2.712 (2)
	O7···O4	2.757 (2)	O10···O12	2.741 (2)	O10···O12	2.742 (2)
	O8···O2	2.841 (2)	O10···O17	2.766 (2)	O10···O17	2.722 (2)
			O11···O15	2.781 (2)	O11···O15	2.764 (2)
			O11···O18	2.703 (3)	O11···O18	2.697 (2)
	Residue 2		O18···O13	2.884 (3)	O18···O13	2.930 (3)
	O6···O3	2.828 (2)				
	O6···O5	2.746 (2)				
	O7···O1	2.740 (2)				
	O7···O4	2.772 (2)				
	O8···O2	2.821 (2)				

Disordered Lattice Water Molecule and the Hydrogen Bond Pattern

In the two phases, the hydrogen atoms were located from the Fourier difference maps and their positions were refined without difficulty. Nevertheless, ambiguities may arise in the hydrogen bond interactions for which the disordered lattice water molecules are involved. It is clear that O8 atoms are H-bond donors to O18 atoms in the two phases ($D\cdots A$ are within 2.695-2.706 Å and $\angle DHA$ are within 173-181°). The single-crystal X-ray experiments suggest that the lattice water molecules are H-donors to one nitrate ion only. The hydrogen bond interactions O18 \cdots O13 ($D\cdots A$ are within 2.881-2.933 Å and $\angle DHA$ are within 169-183°) that involve the major component of the disorder in the two phases are unambiguous. A geometrical consideration of the lattice water molecule does not allow the extra hydrogen atom to be involved in any other hydrogen bond interactions. The O17 atoms of the nitrate ions are potential H-bond acceptors but the atoms O18 (major part of the disordered lattice water molecule) and O17 (nitrate ion) are always found to be too far away (O18 \cdots O17 = 3.206 (6) Å in phase I and O18 \cdots O17 are within 3.06-3.15 Å in phase II).

Disorder of the lattice water molecule might result from weak competitive hydrogen bond interactions because at least two potential H-bond acceptors (*i.e.*, O13 and O17 atoms) are close enough to the O18 atoms. As a result, O18 \cdots O17 interactions may also be important. The problem might even be more complicated because there are short contacts between O18 and O16 atoms (O18 \cdots O16 distances are within 2.96-3.16 Å). Another problem is that the single-crystal X-ray experiments fail to locate the hydrogen atoms of the minor component of the disorder.

The existence of short contacts between the disordered lattice water molecules and nitrate ions may indicate that bifurcated H-bonds can occur. Lattice water molecules may help the propagations of H-bonds along the **b** and **c** directions (see Figure 4.9).

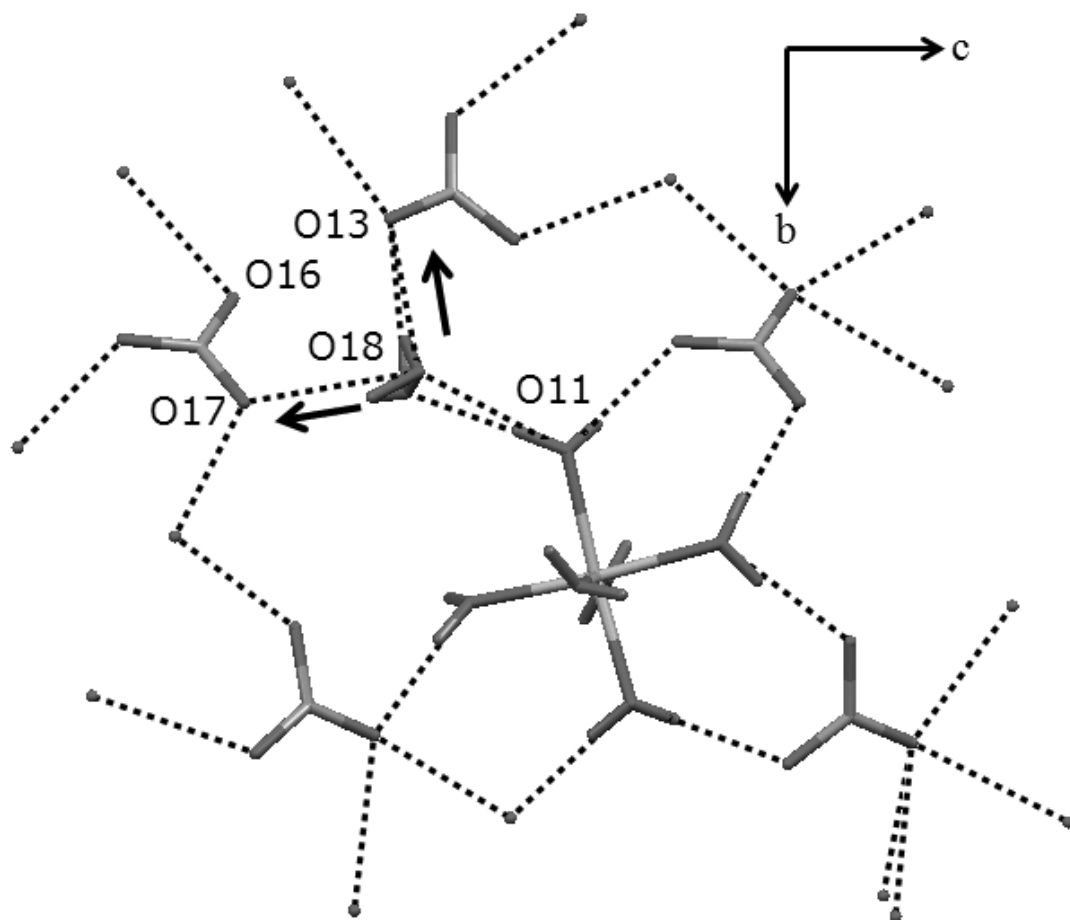


Figure 4.9. The set of hydrogen bond interactions as viewed down the **a** direction in the region where the lattice water molecules are disordered in phase II of the first polymorph of $[\text{Ni}(\text{H}_2\text{O})_6](\text{NO}_3)_2 \cdot (15\text{-crown-5}) \cdot \text{H}_2\text{O}$. Bifurcated H-bonds $\text{O18} \cdots \text{O17}$ (2.989 (4) Å) may occur between one disordered lattice water molecule and one nitrate ion. The black arrows indicate the direction of propagation of H-bonds *via* the lattice water molecule along the **b** and **c** directions.

Conformation of the 15-crown-5 Molecule

In crystals of the two phases of the first polymorph of $[\text{Ni}(\text{H}_2\text{O})_6](\text{NO}_3)_2 \cdot (15\text{-crown-5}) \cdot \text{H}_2\text{O}$, only one enantiomer (either R or S) of the 15-crown-5 molecule is present. As a result, the inversion symmetry is absent and the structure crystallizes in a noncentrosymmetric space group ($P2_1$). In phase II, the two crystallographically independent 15-crown-5 molecules are R R (or S S) and have almost the same conformation. A fit of the two independent crown-ether molecules was made by the program *XP-OFIT*; the overall root-mean-square deviation was less than 0.08 Å. The conformation of the 15-crown-5 remains nearly the same in the phases I and II. Fits of the crown-ether molecules of phases I and II was also made by the same program and the overall root-mean-square deviations were less than 0.07 Å.

Phase Transition II \rightarrow I

The phase transition II \rightarrow I was methodically investigated *via* several types of measurements. The methods included DSC measurements, measurements of the temperature dependence of the cell dimensions, inspection of the reconstructed reciprocal lattice slices near the temperature of the phase transition, and measurements of the temperature dependence of the integrated intensities of the strongest $h0\ell$ reflections with $h + \ell = 2n$. The transition II \rightarrow I is characterized by the change of lattice centerings B (II) $\rightarrow P$ (I). The temperature at which phase II disappears completely is defined by the temperature at which the intensities of the reflections $h + \ell = 2n$ (with h and ℓ odd) are zero. Above this temperature, the diffraction pattern changes: $\mathbf{a}^*_{\text{I}} = 2\mathbf{a}^*_{\text{II}}$, $\mathbf{b}^*_{\text{I}} = \mathbf{b}^*_{\text{II}}$, $\mathbf{c}^*_{\text{I}} = 2\mathbf{c}^*_{\text{II}}$.

The relationship between the phases I and II is obvious because the packing remains very similar. A reason for the existence of the phase transition II \rightarrow I has been identified.

Below 195 K, the space group is the noncentrosymmetric $B2_1$ with $Z' = 2$. Phase II is ordered (except for one of the two lattice water molecules that is found to be disordered). However, librational effects of one of the two independent 15-crown-5 molecules become significantly larger as the temperature increases between 150 and 195 K. This phenomenon is discussed in more detail in the next section. At 200 K and above, the space group is the noncentrosymmetric $P2_1$ with $Z' = 1$. Phase I is disordered.

The localization of the phase transition $\text{II} \rightarrow \text{I}$ was ambiguous because the results obtained from DSC measurements and single-crystal X-ray experiments did not completely agree. The DSC measurements suggested that the transition takes place near 193 K, whereas the temperature dependences of the b axis and β angle suggested that the transition is diffuse over a relatively large T -range (150-200 K) rather than abrupt. The observed diffuseness⁵⁷ was thought to be the result of a two-phase coexistence at intermediate temperatures. The two-phase coexistence was then ruled out because the two-phase refinements for data collected between 150 and 200 K were not conclusive. The problem was solved by inspection of the reciprocal lattice slices at 190, 195 and 200 K. Figure 4.10 shows that the diffraction pattern changes between 195 and 200 K over which phase II disappears completely. The plot of the integrated intensities of the strongest $h0\ell$ reflections with $h + \ell = 2n$ is consistent with the observations obtained from the reciprocal lattice slices. The intensities of the ten strongest $h0\ell$ reflections with $h + \ell = 2n$ (see Figure 4.11) were monitored between 90 and 200 K. The plot of the integrated intensities also indicates that phase II disappears completely between 195 and 200 K. These results suggest that the phase transition $\text{II} \rightarrow \text{I}$ takes place between 195 and 200 K.

The order-disorder transition $\text{II} \rightarrow \text{I}$ occurs because the increase in the $T\Delta S$ term ($\Delta S > 0$) outweighs the unfavorable ΔH term ($\Delta H > 0$). In phase I, the motion of the 15-crown-5 molecules is large. In phase II, the atoms are more localized.

⁵⁷ Mnyukh (2001) wrote: ‘The diffuseness is not the manifestation of a specific transition mechanism. It is a consequence of the non-simultaneous nucleation in different particles, or parts of the specimen...At intermediate temperatures T' , the sample is two-phase’.

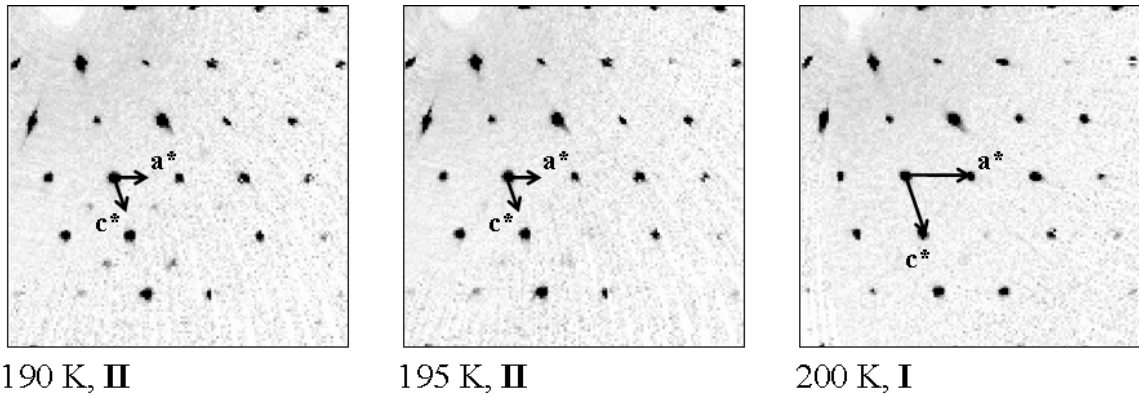


Figure 4.10. Parts of the reciprocal lattice slices $h0\ell$ digitally reconstructed directly from the measured frames given at 190 (phase II), 195 (phase II) and 200 K (phase I). At 190 K, the $h0\ell$ reflections with $h + \ell = 2n$ are not absent. The B -centered lattice ($B2_1, Z' = 2$) is a valid approximation because the $h + \ell = 2n + 1$ are systematically absent. This observation is still true at 195 K albeit the intensities of the $h0\ell$ reflections with $h + \ell = 2n$ are very weak. At 200 K, the intensities of the $h0\ell$ reflections with $h + \ell = 2n$ of phase II are zero, which indicate that phase II disappears completely. There is no condition for systematic absence of classes of reflections and the lattice is primitive ($P2_1, Z' = 1$). As a result, the phase transition $\text{II} \rightarrow \text{I}$ occurs between 195 and 200 K.

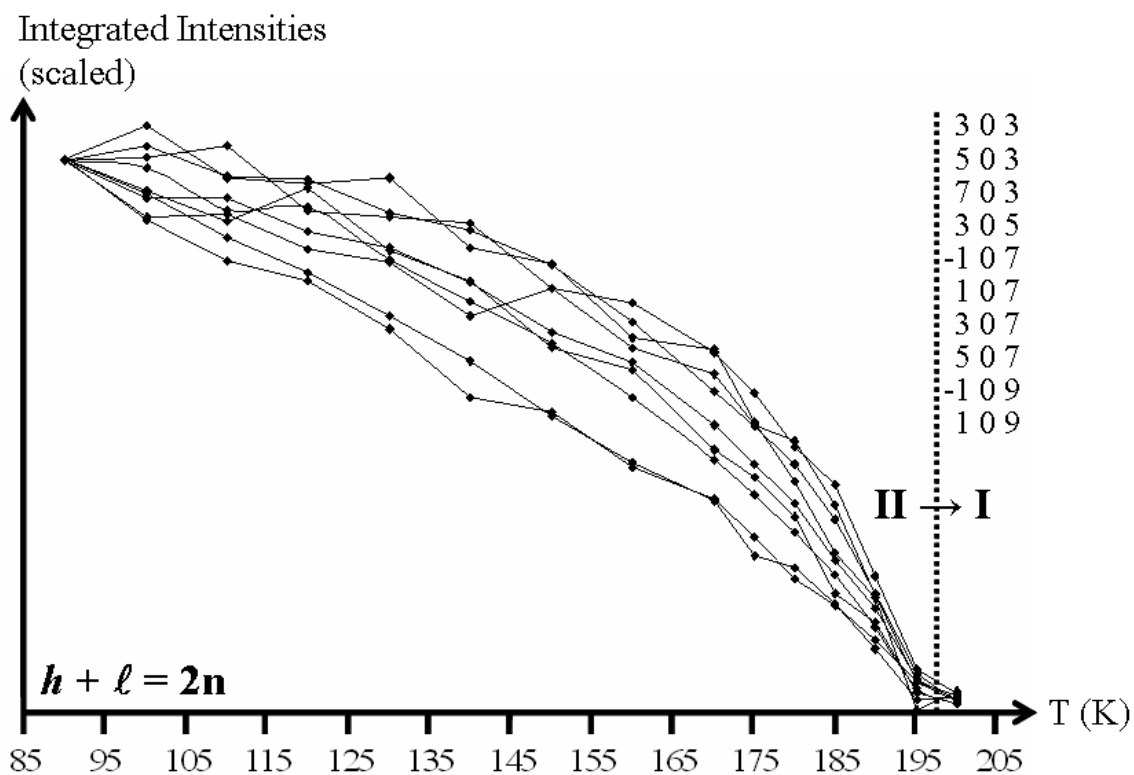


Figure 4.11. Temperature dependences of the integrated intensities of the 10 strongest $h0\ell$ reflections with $h + \ell = 2n$ monitored between 90 and 200 K. The plot shows that the integrated intensities go to zero between 195 and 200 K. As a result, the phase transition II \rightarrow I takes place between 195 and 200 K.

An Approach to the Mechanism of the Phase Transition II \rightarrow I

The temperature dependences of the cell dimensions show a change in the b and β dimensions and indicates the occurrence of a phase transition. These changes are observed over the T -range 150-200 K, which is surprisingly large. The temperature dependence of the intensities of the reflections $h + \ell = 2n$ leaves no doubt that phase II completely disappears between 195 and 200 K. However, the significant changes in the b and β dimensions observed between 150 and 200 K suggest some structural changes in the unit cell over a larger temperature range. A suggested mechanism for the phase transition II \rightarrow I is given and structural changes in the crystal are explored. The subsequent discussion is mainly concerned with the order/disorder of the 15-crown-5 molecule in phase II.

Between 90 and 150 K, phase II can be described as an ordered phase. The thermal motions of the two independent 15-crown-5 molecules are similar. At 150 K, the libration around the normal to the best molecular plane becomes slightly larger in one of the two 15-crown-5 molecules but the difference is not yet very significant. Between 170 and 190 K, the abnormal elongation of the atomic thermal displacements in one of the two 15-crown-5 molecules suggests that the libration becomes larger in one ring than the other. The ellipsoids of the other crown ether look fairly normal. In the latter T -range, disorder is significant in some regions of phase II and less significant in other regions of phase II. The Figures 4.12 and 4.13 show the ellipsoids of the two independent 15-crown-5 molecules in phase II between 90 and 170 K and between 170 and 190 K. Above 200 K, phase I is stable and atomic ellipsoids of the 15-crown-5 molecule are large. Above the phase transition, the potential energy function for libration around the normal to the best molecular plane probably has two minima separated by a low barrier. If this barrier is not large relative to kT then the system would be described as dynamically disordered (Shmueli & Goldberg, 1973).

Between 150 and 190 K, two different regions may coexist in phase II. The regions in which dynamic disorder is significant are similar to phase I and the regions in which dynamic disorder is less important are similar to phase II. The reciprocal lattice slices show that the intensities of the reflections $h + \ell = 2n$ decrease significantly in this T -range.

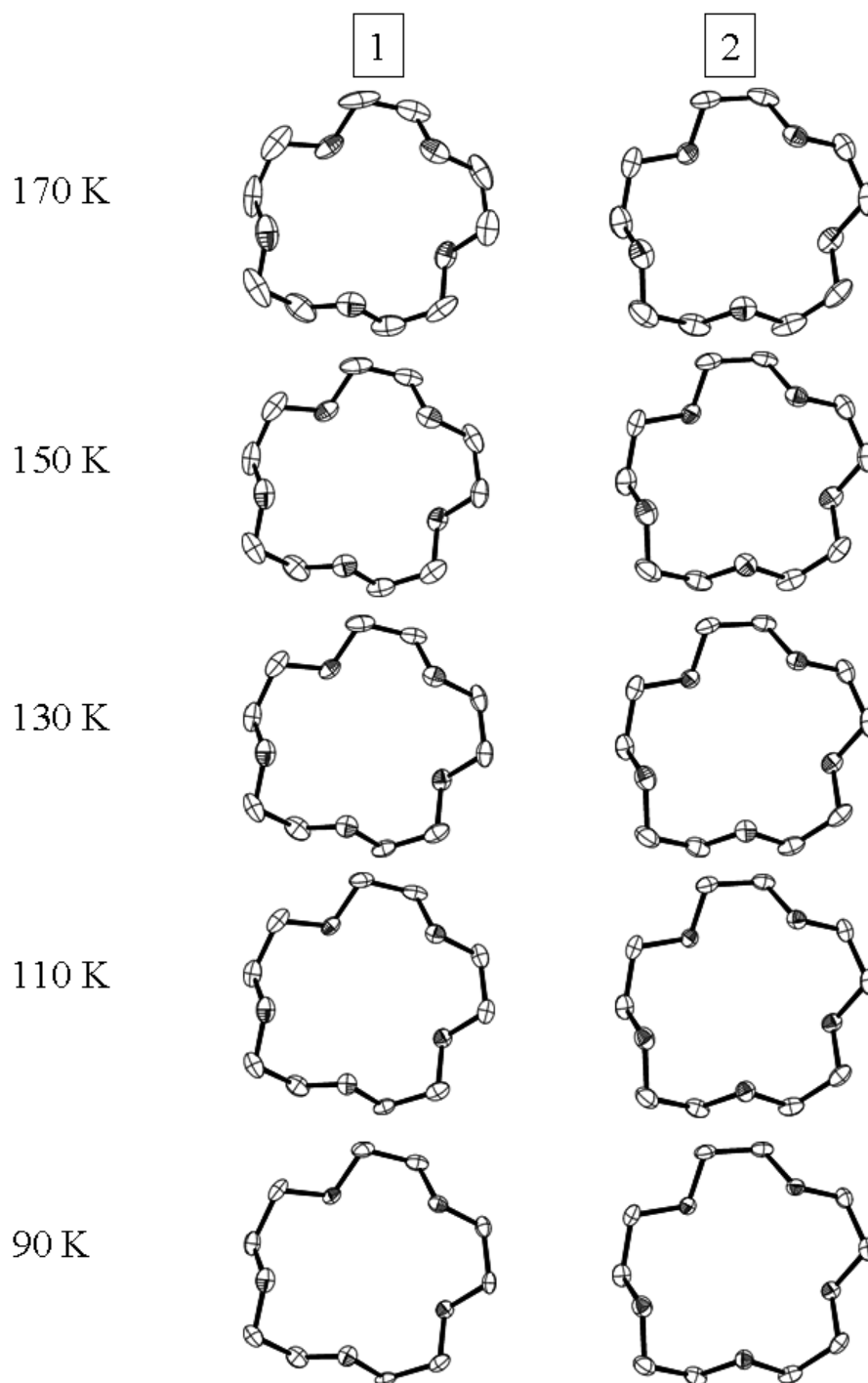


Figure 4.12. The displacement ellipsoids (50% probability level) of the two independent 15-crown-5 molecules in phase II of the first polymorph of $[\text{Ni}(\text{H}_2\text{O})_6](\text{NO}_3)_2 \cdot (15\text{-crown-5}) \cdot \text{H}_2\text{O}$ at 90, 110, 130, 150 and 170 K. At lower temperatures, the ellipsoids of the two independent 15-crown-5 molecules are similar. At 150 K and above, the atomic displacements in crown ether 1 are larger than in crown ether 2.

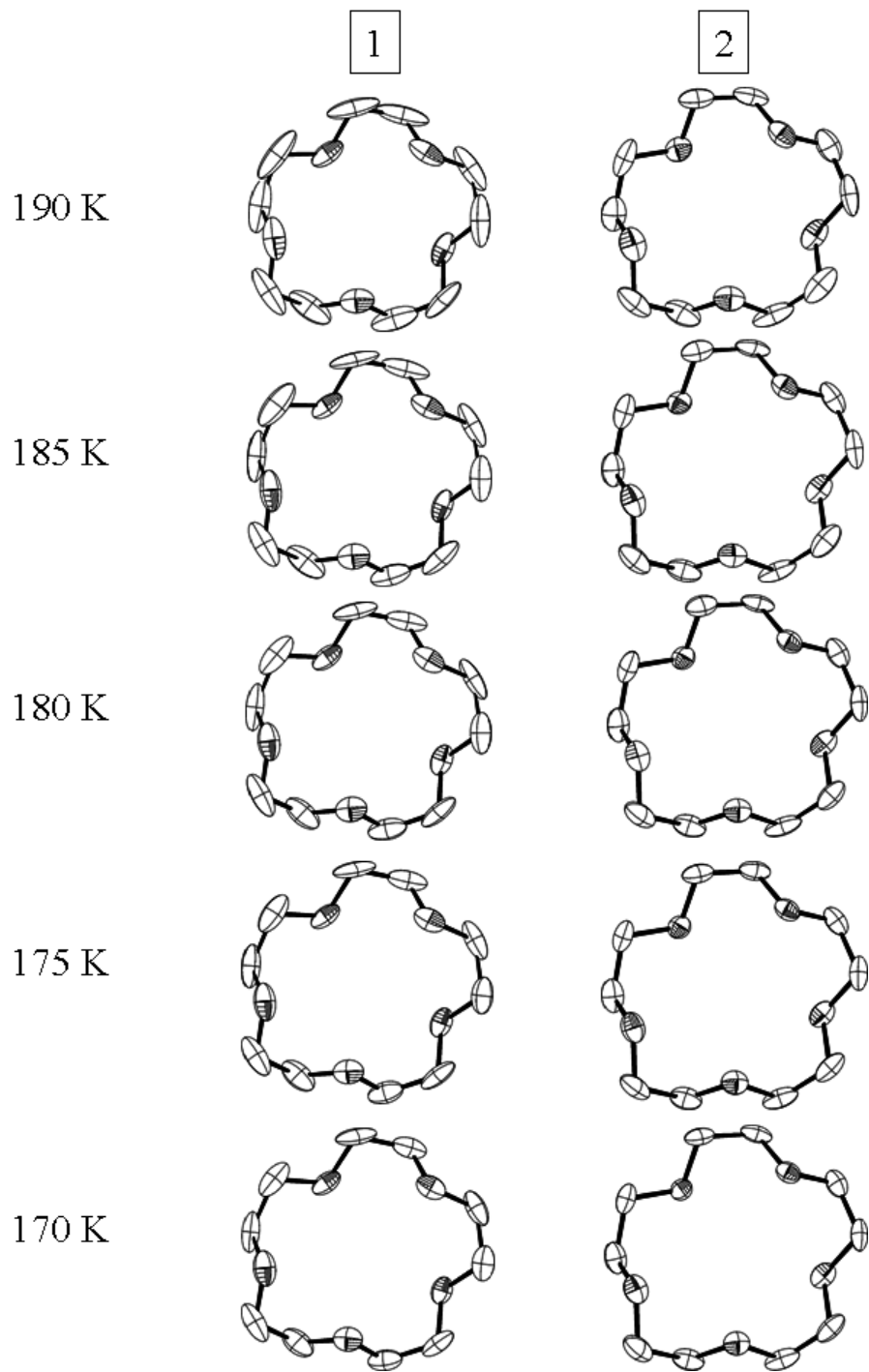


Figure 4.13. The displacement ellipsoids (50% probability level) of the two independent 15-crown-5 molecules in phase II of the first polymorph of $[\text{Ni}(\text{H}_2\text{O})_6](\text{NO}_3)_2 \cdot (15\text{-crown-5}) \cdot \text{H}_2\text{O}$ at 170, 175, 180, 185 and 190 K. Between 170 and 190 K, the displacements are significantly larger in crown ether 1 than in crown ether 2.

A projection of the crown-ether molecules of phase II down the **a** direction (see Figure 4.3) shows that the two formula units cannot be completely superimposed because the two crystallographically independent 15-crown-5 molecules are rotated by different amounts around the normal to the best molecular plane of the 15-crown-5 molecules (which is nearly the *a* axis). The temperature dependence of the fitted rotation angle ω (*i.e.*, the rotation angle needed to overlay the two independent 15-crown-5 molecules) was made with the program *PLATON - AutoMolFit* (Spek, 2003). The temperature dependence of the angle ω is given in Figures 4.14 and 4.15.

Comparisons of the first and second polymorphs of $[\text{Ni}(\text{H}_2\text{O})_6](\text{NO}_3)_2 \cdot (15\text{-crown-5}) \cdot \text{H}_2\text{O}$ ⁵⁸

The first and second polymorphs of $[\text{Ni}(\text{H}_2\text{O})_6](\text{NO}_3)_2 \cdot (15\text{-crown-5}) \cdot \text{H}_2\text{O}$ are different in various ways. The most important difference is the lack of any distinct crystallographic relationship between the two polymorphs, *i.e.* there is no orientation relationship because the packing of the two polymorphs are different (see Figure 4.16). In the first polymorph⁵⁹ of $[\text{Ni}(\text{H}_2\text{O})_6](\text{NO}_3)_2 \cdot (15\text{-crown-5}) \cdot \text{H}_2\text{O}$, only one of the two conformational enantiomers (R or S) of the crown ether is present; in the second polymorph of $[\text{Ni}(\text{H}_2\text{O})_6](\text{NO}_3)_2 \cdot (15\text{-crown-5}) \cdot \text{H}_2\text{O}$, the two conformational enantiomers (R and S) of the crown ether are present. The first polymorph crystallizes in a noncentrosymmetric space group ($P2_1$, $Z' = 1, 2$), whereas the second polymorph crystallizes in a centrosymmetric space group ($P\bar{1}$, $Z' = 3$).

In the two polymorphs, the hydrogen bond interactions between the $[\text{Ni}(\text{H}_2\text{O})_6]^{2+}$ ions and the 15-crown-5 molecules are best described as 1-D chains. The nature of the 1-D chains differs because the 15-crown-5 molecules are either R or S in the first polymorph and are R and S in the second polymorph.

⁵⁸ The crystallographic description of the second polymorph of $[\text{Ni}(\text{H}_2\text{O})_6](\text{NO}_3)_2 \cdot (15\text{-crown-5}) \cdot \text{H}_2\text{O}$ has been discussed in Chapter 3.

⁵⁹ The first polymorph of $[\text{Ni}(\text{H}_2\text{O})_6](\text{NO}_3)_2 \cdot (15\text{-crown-5}) \cdot \text{H}_2\text{O}$ has two phases (I and II).

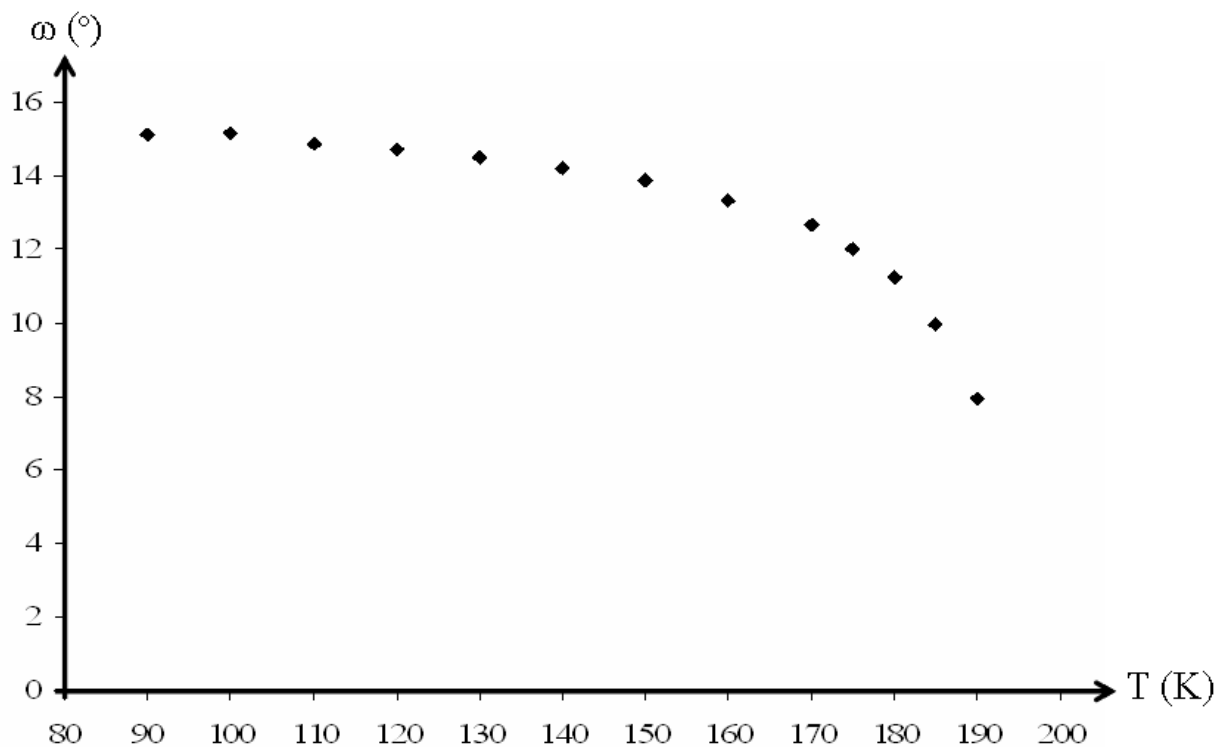
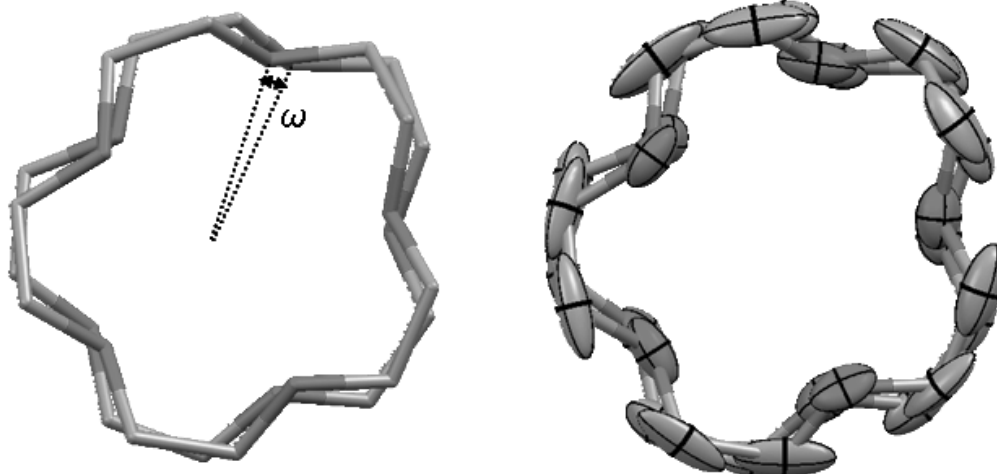


Figure 4.14. Plot of the fitted rotation angle ω (°) versus T (K). At 90 K, the fitted rotation angle ω is about 15.1°. Between 90 and 170 K, ω slightly decreases and $|\Delta\omega|_{90-170\text{K}}$ is estimated to be no larger than 2.5°. The decrease in ω is more significant between 170 and 190 K ($|\Delta\omega|_{170-190\text{K}} \sim 4.7^\circ$) and gets larger as the temperature increases. Near 190 K, the fit rotation angles ω is about 8°. Above 190 K, the large decrease in the rotation angle and the increase in dynamic disorder in phase II make the two independent 15-crown-5 molecules indistinguishable. As a result, the phase transition II \rightarrow I takes place.

190 K



90 K

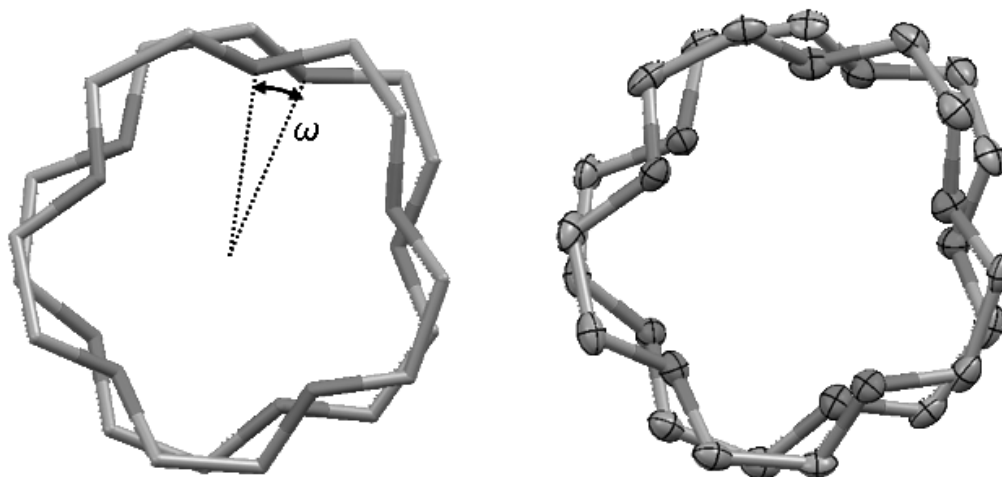
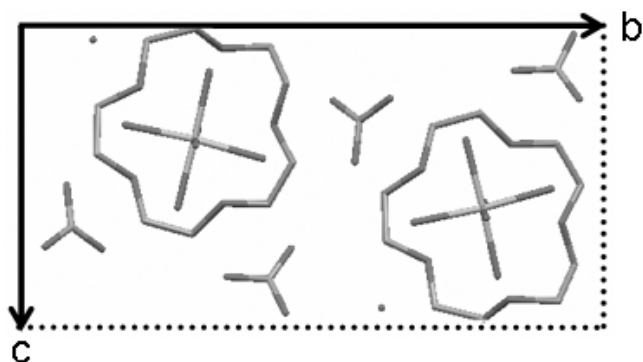


Figure 4.15. Projections of the two crystallographically independent 15-crown-5 molecules in phase II of the first polymorph of $[\text{Ni}(\text{H}_2\text{O})_6](\text{NO}_3)_2 \cdot (15\text{-crown-5}) \cdot \text{H}_2\text{O}$ at 90 and 190 K viewed down the **a** direction. In phase II, the two 15-crown-5 molecules (given in capped stick representation) are rotated around the **a** direction by the angle ω . The angle ω is temperature dependent and is found to decrease as the temperature increases. At 90 and 190 K, the angles ω are about 15 and 8°. The ellipsoid plots (50 % probability) are also given at 90 and 190 K. At 90 K, the thermal motion is small and the two 15-crown-5 molecules are distinguishable. Near 190 K, the two 15-crown-5 molecules are nearly indistinguishable because the angle ω is small and the atomic displacements are large.

first polymorph (phase I, $P2_1$, $Z' = 1$)



second polymorph ($P\bar{1}$, $Z' = 3$)

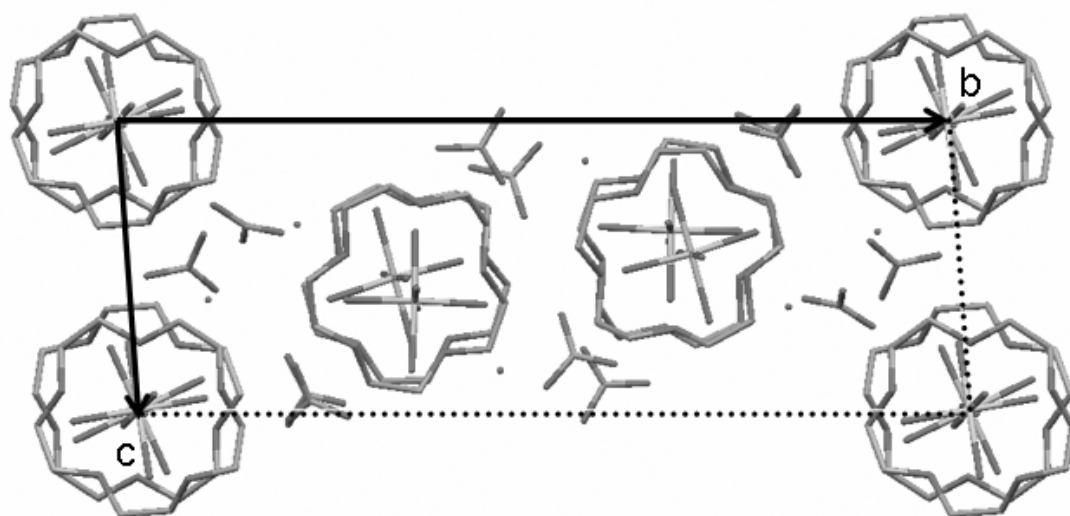


Figure 4.16. Projections of the first (only phase I is shown) and second polymorphs of $[\text{Ni}(\text{H}_2\text{O})_6](\text{NO}_3)_2 \cdot (15\text{-crown-5}) \cdot \text{H}_2\text{O}$ down the a direction (the direction of the 1-D H-bonded chains). The conformational enantiomers of the 15-crown-5 molecule are either R or S in the first polymorph and R and S in the second polymorph. For the first polymorph, the c axis is not in the plane of the drawing. For the second polymorph, neither the b axis, nor the c axis is in the plane of the drawing. There is no obvious relationship between the two polymorphs because their modes of packing are very different.

Conclusions

The first polymorph of $[\text{Ni}(\text{H}_2\text{O})_6](\text{NO}_3)_2 \cdot (15\text{-crown-5}) \cdot \text{H}_2\text{O}$ has one solid-solid phase transition that takes place between 195 and 200 K with no loss of crystallinity. Phase I ($P2_1$, $Z' = 1$) is disordered. The two disorder sites are separated by a small rotation around the **a** direction; it is likely that librational motion around the normal to the best molecular plane can take a molecule from one site to the other (dynamic disorder). Phase II ($B2_1$, $Z' = 2$) is mostly ordered although one of the two lattice water molecules is disordered. The latter disorder is also found in phase I.

The temperature dependence of the cell dimensions shows significant changes within the T -range 150-200 K. Structural changes in phase II are observed between 150 and 190 K. Librational effects of the crown ether are significant in some regions of phase II and less significant in other regions of phase II. The regions where dynamic disorder is significant are similar to phase I and the regions where dynamic disorder is less obvious are similar to phase II. The latter observation suggests that a more ordered region and a less ordered region may coexist in phase II at intermediate temperatures.

The rotation that relates the two independent 15-crown-5 molecules in the crystal lattice is temperature dependent. As the temperature increases, the fitted rotation angle decreases, thermal motion increases and librational effects gets larger. Between 195 and 200 K, the two independent 15-crown-5 molecules are indistinguishable and the phase transition II \rightarrow I takes place.

Chapter Five

-

[Ni(H₂O)₆](NO₃)₂·(15-crown-5)·2H₂O: an Uncommon Polymorphic System

Introduction

Previous studies of the series of the compounds $[M(\text{H}_2\text{O})_2(15\text{-crown-5})](\text{NO}_3)_2$, $M = \text{Mg}$, Mn, Fe Co, Cu and Zn describe a rich polymorphic system (Hao, Parkin & Brock, 2005; Hao, Siegler, Parkin & Brock, 2005). Attempts to synthesize the analogous Ni complex were carried out *via* the same synthesis (see Chapter 3 for further details) but turned out to be unsuccessful. The compound $[\text{Ni}(\text{H}_2\text{O})_6](\text{NO}_3)_2 \cdot (15\text{-crown-5}) \cdot 2\text{H}_2\text{O}$ was always produced instead. One phase of the latter compound had already been reported in the literature (Steed *et al.*, 2001).

Further efforts showed that the compound $[\text{Ni}(\text{H}_2\text{O})_6](\text{NO}_3)_2 \cdot (15\text{-crown-5}) \cdot 2\text{H}_2\text{O}$ is a polymorphic system. Three reversible solid-solid phase transitions and four phases were found between 90 and 308 K. The phase sequence was investigated using DSC measurements and single-crystal X-ray diffraction experiments. In this study, the phase reported earlier (phase IV) is ordered and has $Z' = 1$. The phases I and II are disordered in several ways and have respectively $Z' = \frac{1}{4}$ and $\frac{1}{2}$. Phase III is a modulated superstructure with $Z' = 7$ and has a complicated modulation that appears to be commensurate. The last phase (III) is best described as an intermediate phase that is similar to phase IV in some regions and similar to phase II in other regions. The packing remains very similar in the four phases and one-dimensional H-bonded chains of the 15-crown-5 molecules and the $[\text{Ni}(\text{H}_2\text{O})_6]^{2+}$ ions are found along the *c* direction. The phase sequence, during which there is no significant loss of crystallinity, is defined in the order of increasing temperature by $\text{IV} \rightarrow \text{III} \rightarrow \text{II} \rightarrow \text{I}$.

The three solid-solid phase transitions observed in this polymorphic system are first-order. The temperatures of the three solid-solid phase transitions were carefully examined by looking at the temperature dependence of the cell dimensions. The reciprocal lattice slices were also informative for locating the temperatures of the phase transitions. The phase transitions IV \rightarrow III, III \rightarrow II and II \rightarrow I take place, in that order, within the ranges 205-210, 242-253 and 290-295 K.

Experimental

Crystal Growth

Details of the crystal growth were given in Chapter 3.

Crystal Habit

Crystals are parallelepipeds that are very elongated along one direction [see the part (a) of Figure 5.1]. The favored direction for crystal growth corresponds to the direction of the one-dimensional H-bonded chains of the 15-crown-5 molecules and the $[\text{Ni}(\text{H}_2\text{O})_6]^{2+}$ ions (*i.e.*, the **c** direction). The most important faces of the crystal belong to the form $\{1\ 1\ 0\}$, which is the family of planes $(1\ 1\ 0)$, $(\bar{1}\ \bar{1}\ 0)$, $(1\ \bar{1}\ 0)$ and $(\bar{1}\ 1\ 0)$ that are equivalent if the point-group symmetry is $2/m$. The indices are given for the cell of the near-room-temperature phase ($P2_1/m$, $Z' = \frac{1}{2}$), which has the a dimension approximately equal to the b dimension (the ratio a/b is about 0.98). The angles between two non-parallel faces [*i.e.*, the angle between the planes $(1\ 1\ 0)$ and $(1\ \bar{1}\ 0)$] deviate from 90° by only 2.1° because the a and b dimensions are very similar. The crystal cross-section is found to be about twice as large in one direction as in the other direction, the reason being that crystals lying on a surface of the evaporation dish can grow only along one of the two directions perpendicular to the parallel faces $\{1\ 1\ 0\}$ but can grow along the two opposite directions perpendicular to the two other parallel faces $\{1\ 1\ 0\}$ [see the part (b) of Figure 5.1]. The smaller faces found at the boundaries of the crystal were not indexed since their indices seemed to vary.

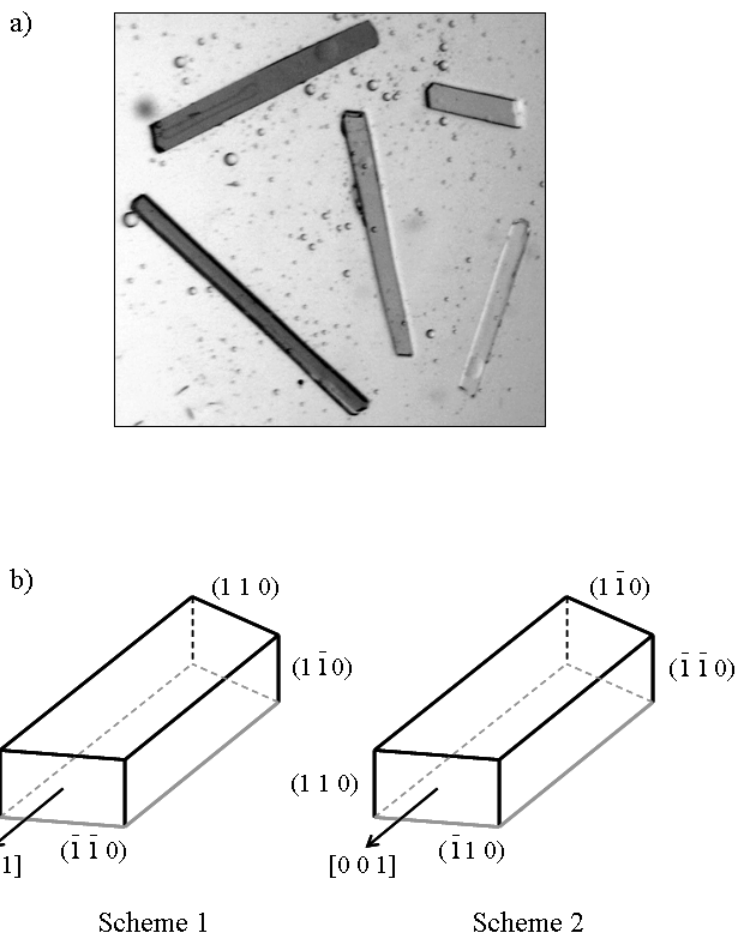


Figure 5.1. (a) A photograph of single crystals of $[\text{Ni}(\text{H}_2\text{O})_6](\text{NO}_3)_2 \cdot (15\text{-crown-5}) \cdot 2\text{H}_2\text{O}$. Crystals are parallelepipeds very elongated along the c direction (*i.e.*, the direction of the one-dimensional H-bonded chains). (b) Drawings describing the crystal habit of $[\text{Ni}(\text{H}_2\text{O})_6](\text{NO}_3)_2 \cdot (15\text{-crown-5}) \cdot 2\text{H}_2\text{O}$. The crystal growth is favored along $[0\ 0\ 1]$ and the most important faces of the crystal belong to the form $\{1\ 1\ 0\}$. The crystal growth takes place along the directions perpendicular to the faces $\{1\ 1\ 0\}$ that are directly in contact with the solution but cannot take place along the direction perpendicular to one face $\{1\ 1\ 0\}$ that is in contact with the glass surface of the vial [*i.e.*, $(\bar{1}\ \bar{1}\ 0)$ in scheme 1 and $(\bar{1}\ 1\ 0)$ in scheme 2]. The glass surface is shown as light gray lines in the schemes 1 and 2. In scheme 1, the crystal growth is more favored along the directions perpendicular to the faces $(1\ 1\ 0)$, $(1\ \bar{1}\ 0)$ and $(\bar{1}\ 1\ 0)$ and is less favored along the direction perpendicular to face $(\bar{1}\ \bar{1}\ 0)$. In scheme 2, the crystal growth is more favored along the directions perpendicular to the faces $(1\ 1\ 0)$, $(\bar{1}\ \bar{1}\ 0)$ and $(1\ \bar{1}\ 0)$ and is less favored along the direction perpendicular to face $(\bar{1}\ 1\ 0)$.

Differential Scanning Calorimetry Measurements

The compound $[\text{Ni}(\text{H}_2\text{O})_6](\text{NO}_3)_2 \cdot (15\text{-crown-5}) \cdot 2\text{H}_2\text{O}$ was investigated using the DSC 822^e apparatus and the controlling software STARe (version 8.10) manufactured by *METTLER TOLEDO*. Two sets of DSC measurements were made: the first set was carried out between 173 and 323 K and the second set was carried out between 298 and 373 K. All DSC samples were prepared from fine powders contained in pierced aluminum pans.

First Set of DSC Measurements (173-323 K)

In the first set of DSC measurements, the amount of powdered sample was 2.87 mg. The cooling and heating rates were -5 and 5 K/min. Between 173 and 323 K, three solid-solid phase transitions were found: $T_{\text{onset}} = 192, 233$ and 287 K and $\Delta H_{\text{tr}} = 0.47, 0.21$ & 0.38 $\text{kJ}\cdot\text{mol}^{-1}$ respectively (T_{onset} and ΔH_{tr} are given for heating). All solid-solid phase transitions are first-order because ΔH_{tr} are non-zero at the transition points. The lowest-temperature solid-solid phase transition showed significant hysteresis, which also suggests that the phase transition is first-order. The decomposition of $[\text{Ni}(\text{H}_2\text{O})_6](\text{NO}_3)_2 \cdot (15\text{-crown-5}) \cdot 2\text{H}_2\text{O}$ starts to take place above room temperature conditions (*i.e.*, near 300 K). The DSC traces are shown in Figure 5.2.

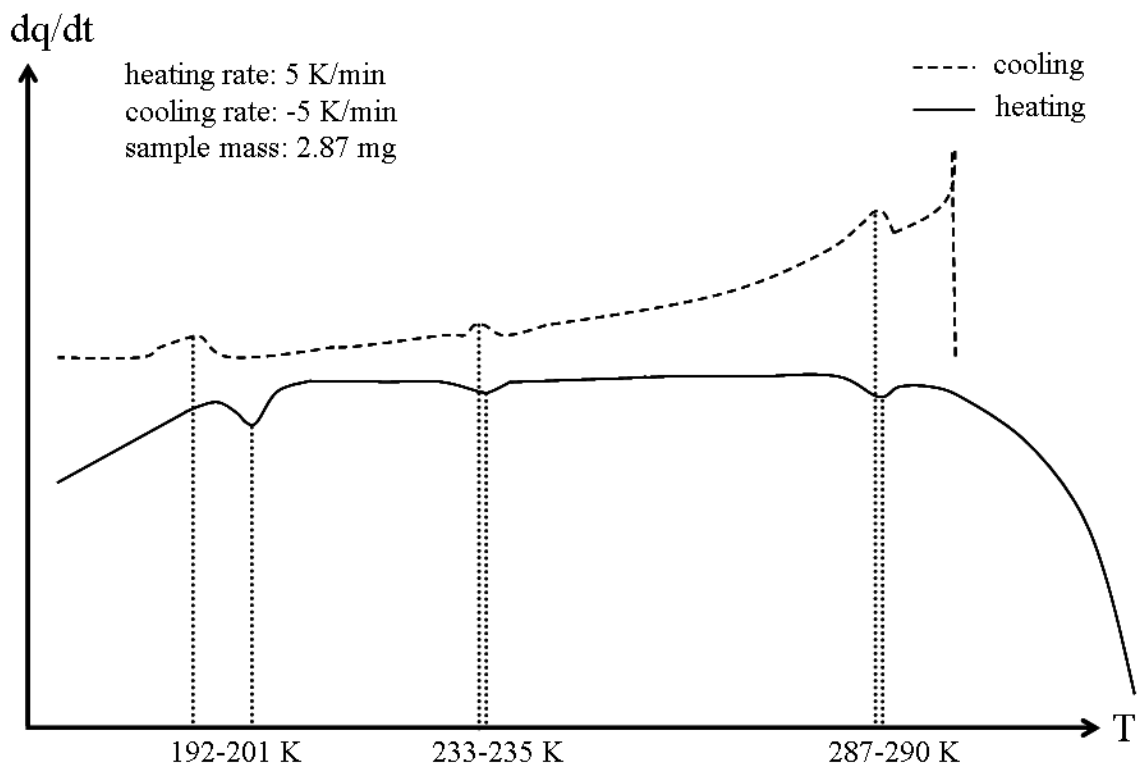


Figure 5.2. DSC traces of the compound $[\text{Ni}(\text{H}_2\text{O})_6](\text{NO}_3)_2 \cdot (15\text{-crown-5}) \cdot 2\text{H}_2\text{O}$ measured between 298 and 173 K at -5 K/min and between 173 and 323 K at 5 K/min. The two traces show three solid-solid phase transitions near 192, 233 and 287 K (given for heating). The lowest-temperature phase transition shows significant hysteresis. The heating trace shows that the compound $[\text{Ni}(\text{H}_2\text{O})_6](\text{NO}_3)_2 \cdot (15\text{-crown-5}) \cdot 2\text{H}_2\text{O}$ starts to decompose near 300 K.

Second Set of DSC Measurements (298-373 K)

The second set of DSC measurements aimed to explore the behavior of $[\text{Ni}(\text{H}_2\text{O})_6](\text{NO}_3)_2 \cdot (15\text{-crown-5}) \cdot 2\text{H}_2\text{O}$ between 298 and 373 K. Two series of DSC measurements were made.

The first series consisted of three DSC measurements (1) heating from 298 to 373 K (trace 1), (2) cooling from 373 to 298 K (trace 2) and (3) a second heating from 298 to 373 K (trace 3). Between each DSC measurement, the temperature was held at the initial temperature of the subsequent measurements for 10 minutes. The amount of powdered sample was 4.05 mg. The cooling and heating rates were -5 and 5 K/min. Trace 1 shows that the decomposition of the compound $[\text{Ni}(\text{H}_2\text{O})_6](\text{NO}_3)_2 \cdot (15\text{-crown-5}) \cdot 2\text{H}_2\text{O}$ is complete near 339 K. Another endothermic transition is found at about 363 K, which might correspond to the crystal formation of the phase $[\text{Ni}(\text{H}_2\text{O})_2(15\text{-crown-5})](\text{NO}_3)_2$. Trace 2 shows an exothermic transition near 313 K. This transition is not yet understood. Trace 3 is different from trace 1 and shows a set of peaks near the melting of $[\text{Ni}(\text{H}_2\text{O})_6](\text{NO}_3)_2 \cdot (15\text{-crown-5}) \cdot 2\text{H}_2\text{O}$. Trace 3 shows also a transition at 352 K, which might be where the nucleation of the phase $[\text{Ni}(\text{H}_2\text{O})_2(15\text{-crown-5})](\text{NO}_3)_2$ observed in the hot-stage microscopy occurs (see Chapter 3 for further details). The three DSC traces are shown in Figure 5.3.

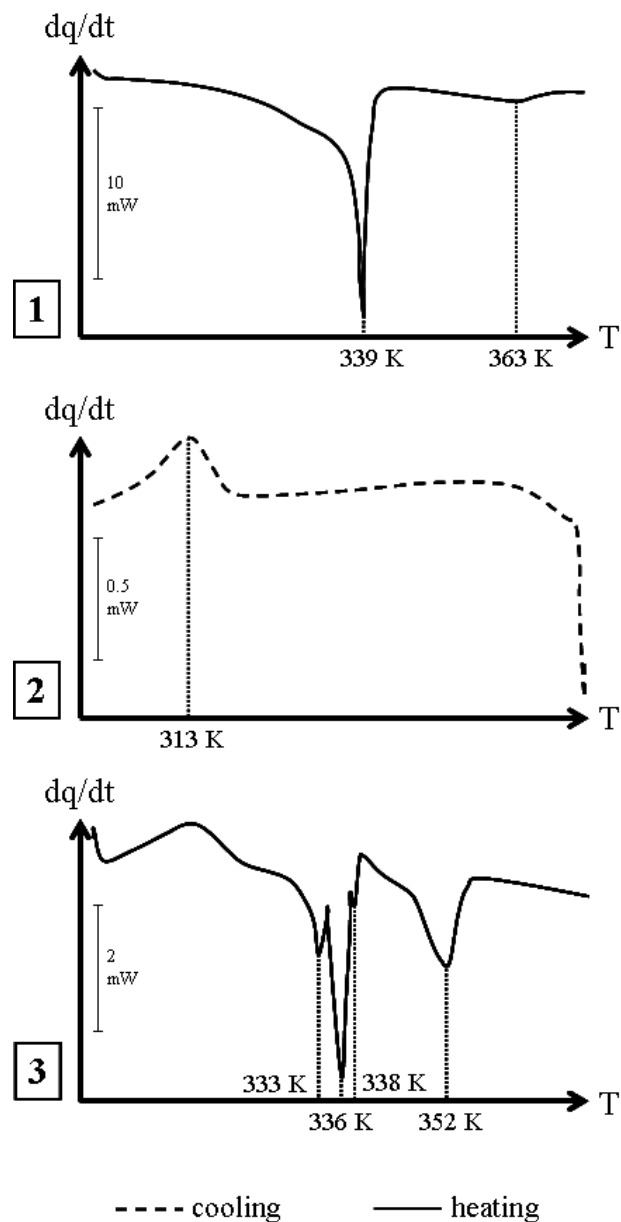


Figure 5.3. DSC traces of the compound $[\text{Ni}(\text{H}_2\text{O})_6](\text{NO}_3)_2 \cdot (15\text{-crown-5}) \cdot 2\text{H}_2\text{O}$ made from 298 to 373 K at 5 K/min (traces 1 and 3) and from 373 to 298 K at -5 K/min (trace 2). The melting of $[\text{Ni}(\text{H}_2\text{O})_6](\text{NO}_3)_2 \cdot (15\text{-crown-5}) \cdot 2\text{H}_2\text{O}$ is found near 339 K (see trace 1). Trace 1 shows another transition at 363 K, which might be associated with the crystal formation of the compound $[\text{Ni}(\text{H}_2\text{O})_2(15\text{-crown-5})](\text{NO}_3)_2$. Trace 2 shows a transition at 313 K. The nature of this transition remains unclear. The traces 1 and 3 are different. Trace 3 shows a series of transitions occurring near the melting point of $[\text{Ni}(\text{H}_2\text{O})_6](\text{NO}_3)_2 \cdot (15\text{-crown-5}) \cdot 2\text{H}_2\text{O}$ and another transition near 352 K. The latter transition is likely to correspond to the nucleation of the compound $[\text{Ni}(\text{H}_2\text{O})_2(15\text{-crown-5})](\text{NO}_3)_2$.

The second series consisted of five DSC measurements (1) heating from 298 to 348 K (trace 1), (2) cooling from 348 to 298 K (trace 2), (3) a second heating from 298 to 373 K (trace 3), (4) a second cooling from 373 to 298 K (trace 4) and (5) a third heating from 298 to 373 K (trace 5). Between each DSC measurement, the temperature was held at the initial temperature of the subsequent measurements for 10 minutes. The amount of powdered sample was 4.64 mg. The cooling and heating rates were -5 and 5 K/min. Trace 1 shows that the melting of the compound $[\text{Ni}(\text{H}_2\text{O})_6](\text{NO}_3)_2 \cdot (15\text{-crown-5}) \cdot 2\text{H}_2\text{O}$ takes place near 338 K, which is in good agreement with previous results. Trace 2 shows an exothermic transition near 317 K, which probably corresponds to the crystal formation of the compound $[\text{Ni}(\text{H}_2\text{O})_6](\text{NO}_3)_2 \cdot (15\text{-crown-5}) \cdot 2\text{H}_2\text{O}$. Trace 3 shows two peaks: the first peak corresponds to the melting of $[\text{Ni}(\text{H}_2\text{O})_6](\text{NO}_3)_2 \cdot (15\text{-crown-5}) \cdot 2\text{H}_2\text{O}$ at about 337 K and the second peak is found at 350 K, which might be where the nucleation of the phase $[\text{Ni}(\text{H}_2\text{O})_2(15\text{-crown-5})](\text{NO}_3)_2$ takes place. The traces 4 and 5 are very similar to the traces 2 and 3 of the first series of DSC measurements. The five DSC traces are shown in Figure 5.4.

The latter series of DSC measurements (traces 1, 2 and 3) shows that the decomposition of $[\text{Ni}(\text{H}_2\text{O})_6](\text{NO}_3)_2 \cdot (15\text{-crown-5}) \cdot 2\text{H}_2\text{O}$ is reversible. After melting (338 K), the compound $[\text{Ni}(\text{H}_2\text{O})_6](\text{NO}_3)_2 \cdot (15\text{-crown-5}) \cdot 2\text{H}_2\text{O}$ can recrystallize on cooling if and only if the preceding heating of the sample did not exceed 350 K.

Overall, the second set of DSC measurements shows that the compound $[\text{Ni}(\text{H}_2\text{O})_6](\text{NO}_3)_2 \cdot (15\text{-crown-5}) \cdot 2\text{H}_2\text{O}$ melts near 338 K and that at least one other compound that may contain less water is formed at about 350 K. One such compound is thought to be $[\text{Ni}(\text{H}_2\text{O})_2(15\text{-crown-5})](\text{NO}_3)_2$ (see Chapter 3 for a complete description).

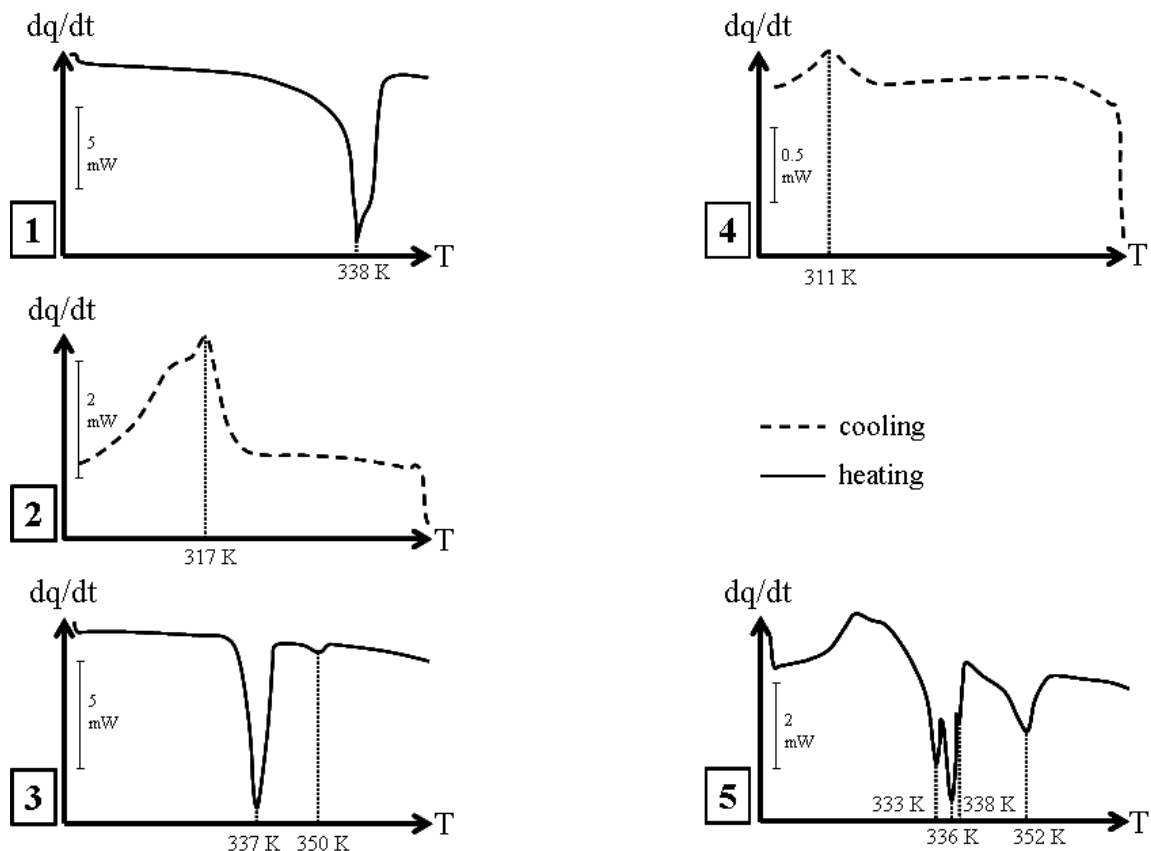


Figure 5.4. DSC traces of the compound $[\text{Ni}(\text{H}_2\text{O})_6](\text{NO}_3)_2 \cdot (15\text{-crown-5}) \cdot 2\text{H}_2\text{O}$ collected from 298 to 348 K at 5 K/min (trace 1), from 298 to 373 K at 5 K/min (traces 3 and 5), from 348 to 298 K at -5 K/min (trace 2) and from 373 and 298 K at -5 K/min (trace 4). Trace 1 shows that the melting of the compound $[\text{Ni}(\text{H}_2\text{O})_6](\text{NO}_3)_2 \cdot (15\text{-crown-5}) \cdot 2\text{H}_2\text{O}$ takes place near 338 K. Trace 2 shows an exothermic transition near 317 K, which might correspond to the crystal formation of the compound $[\text{Ni}(\text{H}_2\text{O})_6](\text{NO}_3)_2 \cdot (15\text{-crown-5}) \cdot 2\text{H}_2\text{O}$. Trace 3 shows two transitions. The first transition corresponds to the melting of the compound $[\text{Ni}(\text{H}_2\text{O})_6](\text{NO}_3)_2 \cdot (15\text{-crown-5}) \cdot 2\text{H}_2\text{O}$ observed at 337 K. The second transition is found at 350 K, which is where the nucleation of the phase $[\text{Ni}(\text{H}_2\text{O})_2(15\text{-crown-5})](\text{NO}_3)_2$ takes place. Trace 4 shows a transition at 311 K. The nature of this transition remains unclear. The traces 3 and 5 are different. Trace 5 shows a series of transitions occurring near the melting point of the compound $[\text{Ni}(\text{H}_2\text{O})_6](\text{NO}_3)_2 \cdot (15\text{-crown-5}) \cdot 2\text{H}_2\text{O}$ and another transition near 352 K. The latter transition is likely to correspond to the nucleation of the compound $[\text{Ni}(\text{H}_2\text{O})_2(15\text{-crown-5})](\text{NO}_3)_2$.

X-ray Crystallography

The general procedures for data collection and for the H-atoms treatment were given in the corresponding section of Chapter 2.

All data were collected using a Nonius KappaCCD diffractometer with graphite-monochromated Mo $K\alpha$ radiation ($\lambda = 0.71073 \text{ \AA}$) under the program *COLLECT* (Nonius, 1997).

Four phases of $[\text{Ni}(\text{H}_2\text{O})_6](\text{NO}_3)_2 \cdot (15\text{-crown-5}) \cdot 2\text{H}_2\text{O}$ were isolated: a low-temperature phase with $Z' = 1$, two intermediate temperature phases with $Z' = 7$ and $Z' = \frac{1}{2}$ and a room temperature phase with $Z' = \frac{1}{4}$. The phase with $Z' = 7$ is found to be a commensurately modulated superstructure and the modulations are sevenfold along the **c** direction. By convention, the four phases of $[\text{Ni}(\text{H}_2\text{O})_6](\text{NO}_3)_2 \cdot (15\text{-crown-5}) \cdot 2\text{H}_2\text{O}$ are numbered I to IV, I for the room temperature phase and IV for the lowest-temperature phase.

Generalities

In order to facilitate comparisons between the four phases (*i.e.*, the one-dimensional H-bonded chains are along the same direction for the four phases), the cells of the phases I, II and III were transformed in ways that maximized the similarities to the cell of phase IV (see Figure 5.5).

Phase I was described in the space group $I2/m$ with $Z' = \frac{1}{4}$ rather than the more conventional but equivalent (after transformation) space group $C2/m$ for consistency with the standard reduced cell for phase IV (Steed, 2001). The cell constants at 295 K of the C -centered cell are: $a = 13.375$ (2)Å, $b = 12.570$ (2)Å, $c = 8.114$ (1)Å, $\beta = 115.00$ (2)°. The corresponding cell constants for the I -centered cell are shown in Table 5.1. The transformation is given by: $\mathbf{a}(I2/m) = (1\ 0\ 1\ /\ 0\ -1\ 0\ /\ 0\ 0\ -1)\mathbf{a}(C2/m)$.

The structure of phase II was solved and refined in the relatively infrequent space group $P2_1/m$ (Brock & Dunitz, 1994) with $Z' = \frac{1}{2}$. The cell constants at 250 K of the standard primitive cell are: $a = 8.049$ (1)Å, $b = 12.543$ (2)Å, $c = 12.303$ (2)Å, $\beta = 100.65$ (2)°. The a and c axes were switched *via* the transformation matrix $(0\ 0\ 1\ /\ 0\ -1\ 0\ /\ 1\ 0\ 0)$ so that the new cell was similar to the cell of phase IV.

The structure of phase III was originally solved in the noncentrosymmetric space group $P2_1$ with seven independent formula units ($Z' = 7$). The cell constants at 90 K of the standard primitive cell are: $a = 21.740$ (2)Å, $b = 12.594$ (1)Å, $c = 30.632$ (3)Å, $\beta = 96.51$ (1)°. The non-standard space group $B2_1$ was preferred so that H-bonded chains of Ni cations and 15-crown-5 molecules are found along the c direction, which is the direction of the 1-D H-bonded chains in the other phases. The transformation matrix is given by: $\mathbf{a}(B2_1) = (0\ 0\ -1\ /\ 0\ -1\ 0\ /\ -2\ 0\ 1)\mathbf{a}(P2_1)$. The $Z' = 7$ phase is a racemic twin and the twinning was treated using the *TWIN* instruction (in *SHELXL97*) with the matrix $(-1\ 0\ 0\ /\ 0\ -1\ 0\ /\ 0\ 0\ -1)$.

The atom-numbering scheme is consistent for all four phases.

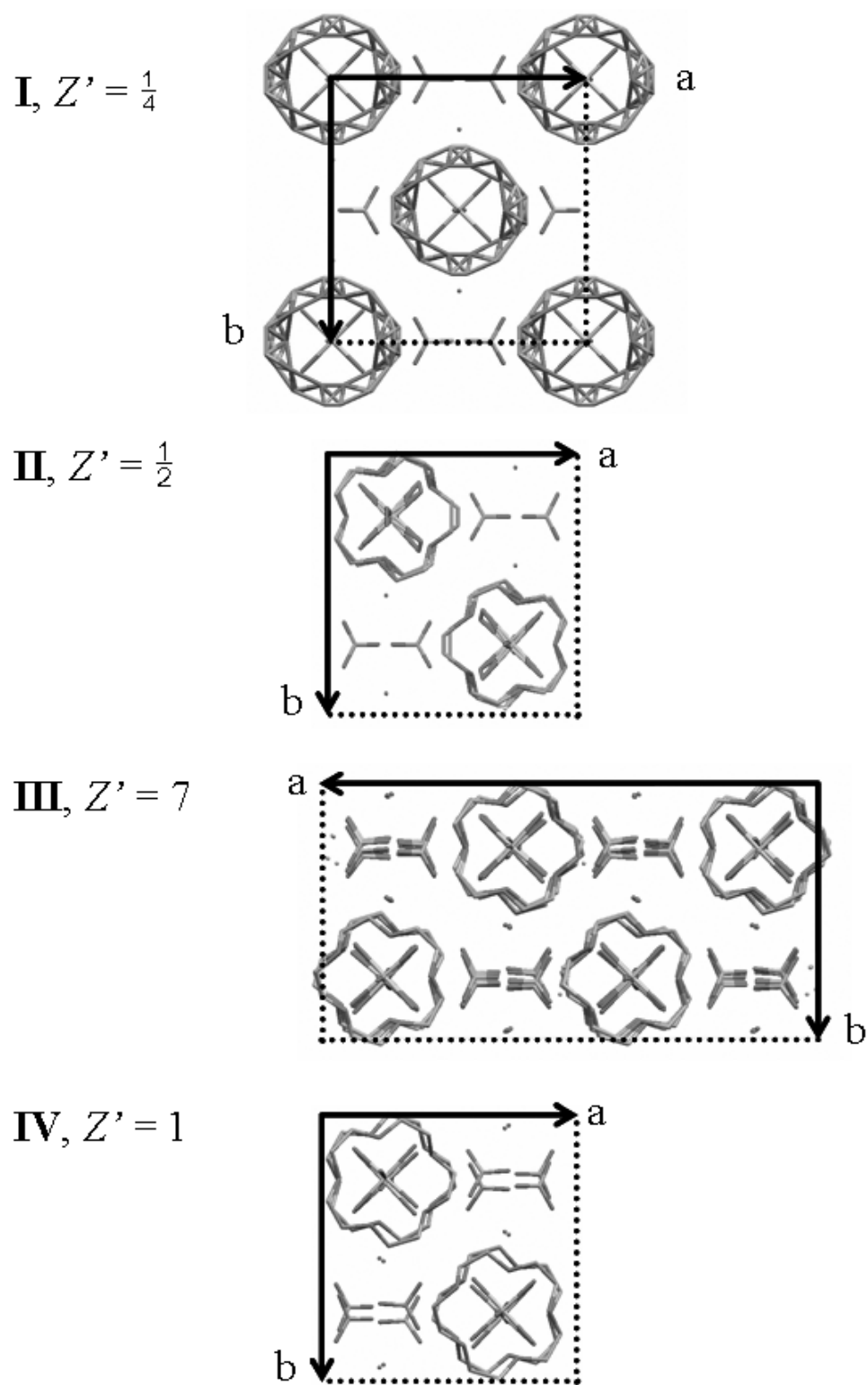


Figure 5.5. Projections of the four phases of $[\text{Ni}(\text{H}_2\text{O})_6](\text{NO}_3)_2 \cdot (15\text{-crown-5}) \cdot 2\text{H}_2\text{O}$ down the c direction. For the four phases, the a axis is not in the plane of the drawing. The drawing shows that the packing is very similar in the four phases.

Phase I

Data for the room temperature phase were collected near 295 K. The asymmetric unit contains $\frac{1}{4}$ 15-crown-5 molecule, $\frac{1}{4}$ $[\text{Ni}(\text{H}_2\text{O})_6]^{2+}$ ion, $\frac{1}{2}$ nitrate ion and $\frac{1}{2}$ lattice water molecule. The $[\text{Ni}(\text{H}_2\text{O})_6]^{2+}$ ion and the 15-crown-5 molecule lie on sites of $2/m$ symmetry, while the nitrate ions lie on sites with mirror symmetry and the lattice water molecules lie on sites with twofold rotational symmetry.

The twofold and mirror symmetries cause disorder in a complicated way. Because the 15-crown-5 molecule lies on a $2/m$ site but cannot have those symmetries, it is found to be highly disordered with at least four orientations [see the part (a) of Figure 5.6]. Near room temperature, the effects of the disorder of the $[\text{Ni}(\text{H}_2\text{O})_6]^{2+}$ ion were absorbed into the displacement parameters and so was not noticeable.

The refinement against F^2 was good. The R factor [$F^2 > 2\sigma(F^2)$] is less than 0.050, the ellipsoids showed no unusual signs and the highest residual electron density peak was no more than $0.44 \text{ e } \text{\AA}^{-3}$. The treatment of the disorder in the space group $I2/m$, however, was somewhat challenging because of the disorder. Some atoms of the crown ether were so close together (*e.g.*, the atoms C2 and C4C) that only one set of displacement parameters could be refined. The *DELU* instruction (*i.e.*, a rigid bond restraint) had to be applied to the atoms of the crown ether in order to get a satisfactory refinement [see the part (b) of Figure 5.6].

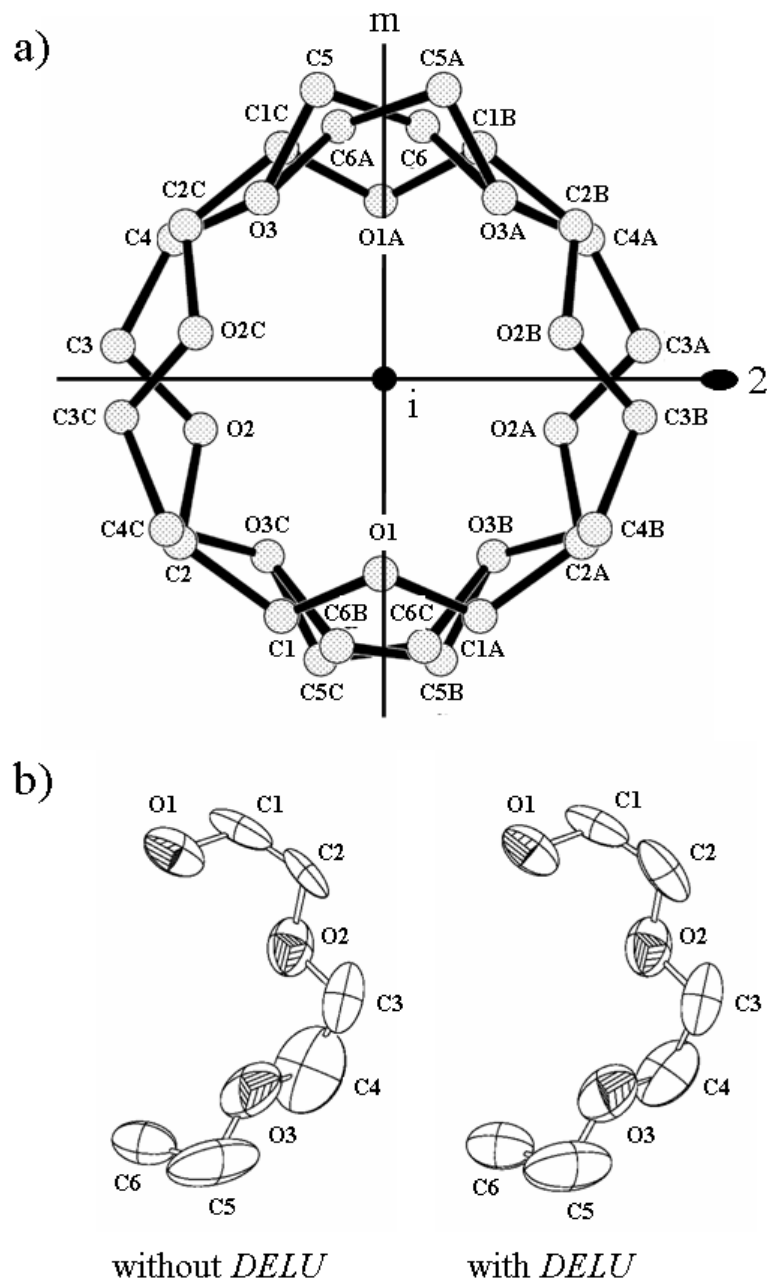


Figure 5.6. (a) Drawing showing the disordered 15-crown-5 molecule in phase IV (space group $I2/m$). The disorder of the crown is generated by the combination of a twofold axis and a mirror plane. The mirror plane forces the C5 and C6 atoms to be disordered. Because the positions of the atoms C2 / C4C and C2C / C4 are almost identical, the refinement of the displacement parameters for those atoms was problematic. (b) Drawing showing the displacement parameters of one half 15-crown-5 molecule in the space group $I2/m$. If the model includes no *DELU* restraints, the ellipsoids for atoms C2 and C4 are more eccentric.

Phase II

Data for phase II were collected near 250 K after crystals had been slowly cooled at -2 K/min from room temperature. The asymmetric unit contains $\frac{1}{2}$ 15-crown-5 molecule, $\frac{1}{2}$ $[\text{Ni}(\text{H}_2\text{O})_6]^{2+}$ ion, $2 \times \frac{1}{2}$ nitrate ions and one lattice water molecule. The $[\text{Ni}(\text{H}_2\text{O})_6]^{2+}$ ion, the nitrate ions and the 15-crown-5 molecule lie on sites with mirror symmetry. The crown ether lies on a mirror plane in a way that requires the molecule to conform to mirror symmetry.

The mirror plane found in phase II causes disorder in several ways. The disorder of the crown ether is symmetry generated because the 15-crown-5 molecule does not have the mirror symmetry. There are two possible orientations of the crown ether relative to the mirror.

A first refinement against F^2 was fair. The R factor [$F^2 > 2\sigma(F^2)$] was 0.054 and the final difference Fourier map showed no peak larger than $0.51 \text{ e } \text{\AA}^{-3}$ (the largest peak was located at 0.63 \AA from O7 atom). Eccentric ellipsoids of the O7 atoms were warning signs suggesting disorder of the $[\text{Ni}(\text{H}_2\text{O})_6]^{2+}$ ion. The disorder of the $[\text{Ni}(\text{H}_2\text{O})_6]^{2+}$ ion takes place because O6–Ni–O7 does not lie exactly on the mirror plane. Comparisons of the phases II and IV help to understand the nature of the disorder found in the former phase [see parts (a) and (b) of Figure 5.7].

The inclusion of the disorder of the $[\text{Ni}(\text{H}_2\text{O})_6]^{2+}$ ion makes the refinement against F^2 better. The R factor [$F^2 > 2\sigma(F^2)$] is 0.043 and the final difference Fourier map showed no peak larger than $0.40 \text{ e } \text{\AA}^{-3}$. The occupancy factors of all atoms of the 15-crown-5 molecule and the $[\text{Ni}(\text{H}_2\text{O})_6]^{2+}$ ion were 0.5 because of the requirements of the mirror symmetry.

The displacement ellipsoids of all atoms in the asymmetric unit of the phases I and II are shown in Figure 5.8. The crystallographic data for the phases I and II of the compound $[\text{Ni}(\text{H}_2\text{O})_6](\text{NO}_3)_2 \cdot (15\text{-crown-5}) \cdot 2\text{H}_2\text{O}$ are given in Table 5.1.

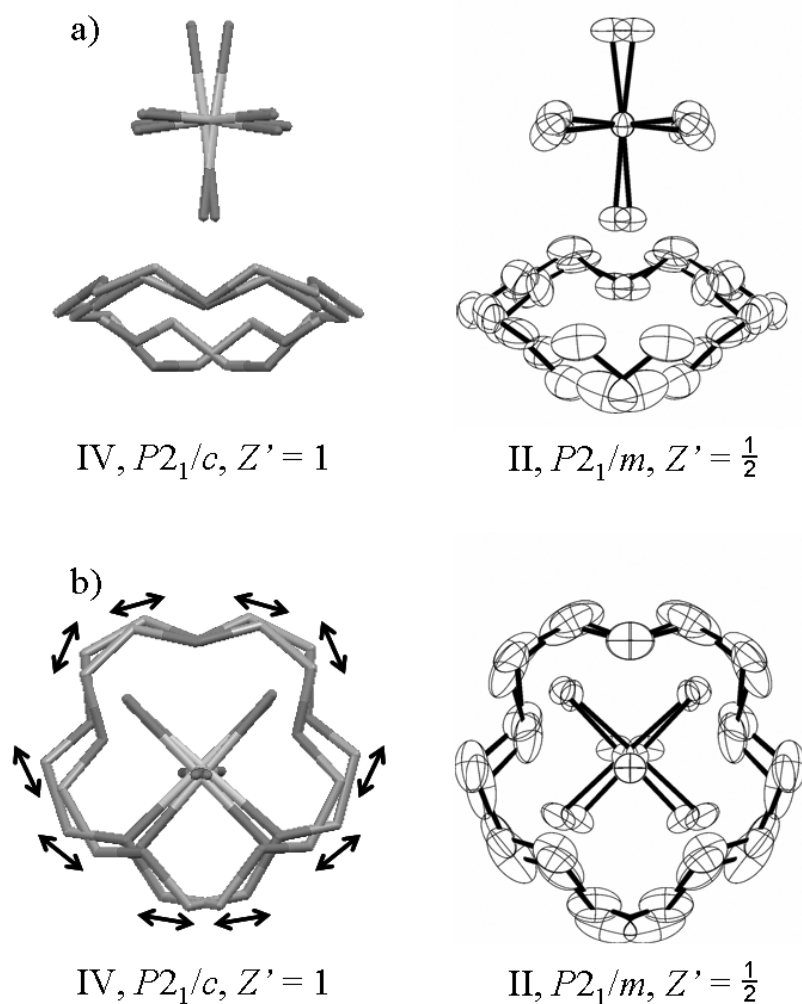
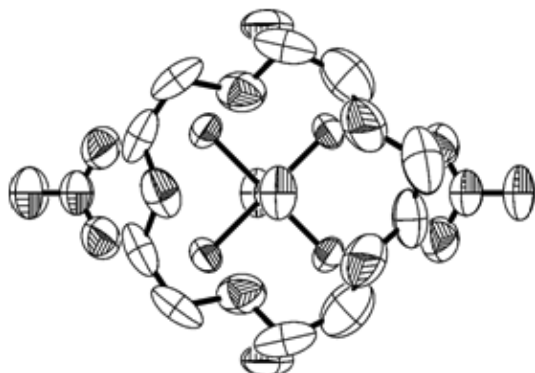
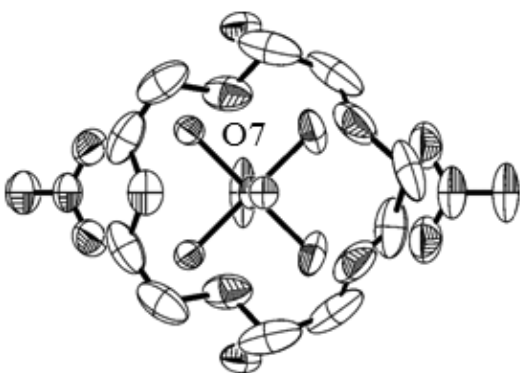


Figure 5.7. (a) Projections of the 15-crown-5 molecules and the $[\text{Ni}(\text{H}_2\text{O})_6]^{2+}$ ions in the phases II and IV down the **a** direction. The drawing of phase IV shows the superposition of two 15-crown-5 molecules and two $[\text{Ni}(\text{H}_2\text{O})_6]^{2+}$ ions (given in the capped stick representation) related by a *c* glide plane. The drawing of phase II shows the ellipsoid plot (50 % probability) of the disordered 15-crown-5 molecule and the $[\text{Ni}(\text{H}_2\text{O})_6]^{2+}$ ion at 250 K. The comparison of the two drawings shows the nature of the disorder found in phase II. The disorder of the 15-crown-5 molecule results from the non-superposition of the two enantiomers R and S (see Chapter 3 for further details). In phase II, the $[\text{Ni}(\text{H}_2\text{O})_6]^{2+}$ ion is also disordered because the cation does not lie absolutely on the mirror plane. (b) The projection of part (a) has been rotated by 90° around the horizontal so that the view is down the **c** direction. The black arrows correspond to the directions of elongation of ellipsoids of the 15-crown-5 molecules (not shown for the O_{ether} atoms) in phase II. H atoms are omitted for clarity.

Phase I (295 K)



Phase II (250 K),
without disorder



Phase II (250 K),
with disorder

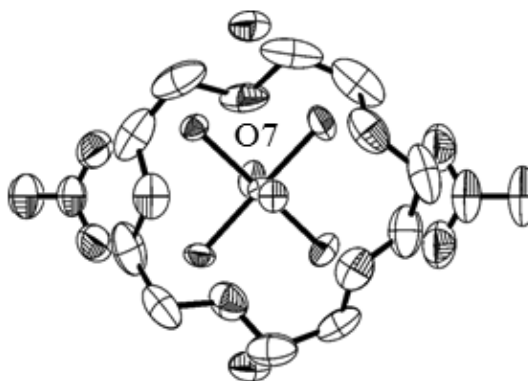


Figure 5.8. The displacement ellipsoids (50% probability level) of the asymmetric unit of the compound $[\text{Ni}(\text{H}_2\text{O})_6](\text{NO}_3)_2 \cdot (15\text{-crown-5}) \cdot 2\text{H}_2\text{O}$ in phase I at 295 K and in phase II at 250 K without and with the inclusion of disorder of the $[\text{Ni}(\text{H}_2\text{O})_6]^{2+}$ ion. In phase II, the displacement ellipsoid of the atom O7 looks very eccentric. All atoms of the asymmetric unit and their symmetry equivalents (*i.e.*, the atoms related by the twofold and mirror symmetries in phase I and the atoms related by the mirror symmetry in phase II) are shown. The disorder of the crown ether and the $[\text{Ni}(\text{H}_2\text{O})_6]^{2+}$ ion generated by symmetry and the H atoms are omitted for clarity.

Table 5.1. Crystallographic data for the phases I and II of $[\text{Ni}(\text{H}_2\text{O})_6](\text{NO}_3)_2 \cdot (15\text{-crown-5}) \cdot 2\text{H}_2\text{O}$.

	I	II
Crystal data		
Chemical formula	$(\text{C}_{10}\text{H}_{20}\text{O}_5) \cdot (\text{H}_{12}\text{NiO}_6^{2+}) \cdot 2(\text{NO}_3^{1-}) \cdot 2(\text{H}_2\text{O})$	
M_r	547.12	547.12
Cell setting, space group	Monoclinic, $I2/m$	Monoclinic, $P2_1/m$
a, b, c (Å) ⁶⁰	12.370 (2) 12.570 (2) 8.114 (1)	12.303 (2) 12.543 (2) 8.049 (1)
β (°)	101.48 (2)	100.65 (2)
V (Å ³)	1236.4 (3)	1220.7 (3)
$Z; Z'$	2; $\frac{1}{4}$	2; $\frac{1}{2}$
D_x (g cm ⁻³)	1.479	1.489
Radiation type	Mo $K\alpha$	Mo $K\alpha$
No. of reflections for cell parameters	1481	2934
θ range (°)	1.0–27.5	1.0–27.5
μ (mm ⁻¹)	0.87	0.88
Temperature (K)	295 (2)	250 (1)
Crystal form, colour	Parallelepiped, pale green	Parallelepiped, pale green
Crystal size (mm)	0.20 x 0.15 x 0.15	0.30 x 0.20 x 0.10
Data collection		
Diffractometer	Nonius KappaCCD	Nonius KappaCCD
Data collection method	ω scans at fixed $\chi = 55^\circ$	ω scans at fixed $\chi = 55^\circ$
Absorption correction	Multi-scan (based on symmetry-related measurements)	
T_{\min}	0.751	0.778

⁶⁰ The estimated errors in the unit cell constants (a , b , c and β) were modified by multiplying the experimental estimated standard uncertainties (*i.e.*, su's) by at least a factor of ~ 3 for a , b , c and by at least a factor of ~ 13 for β . These factors were used in order to approximate the errors in the unit cell constants from one crystal to another (Herbstein, 2000).

Table 5.1. (continued)

T_{\max}	0.958	0.917
No. of measured, independent and observed parameters	2838, 1487, 1162	4999, 2647, 1839
Criterion for observed reflections	$I > 2\sigma(I)$	$I > 2\sigma(I)$
R_{int}	0.037	0.035
θ_{\max} (°)	27.5	26.5
Range of h, k, ℓ	$-16 < h < 15$ $-16 < k < 16$ $-10 < \ell < 10$	$-15 < h < 15$ $-15 < k < 15$ $-10 < \ell < 10$
Refinement		
Refinement on	F^2	F^2
$R[F^2 > 2\sigma(F^2)], wR(F^2), S$	0.049, 0.132, 1.02	0.043, 0.118, 1.02
No. of reflections	1487 reflections	2647 reflections
No. of parameters	144	345
H-atom treatment	Constrained to parent site	Constrained to parent site
Weighting scheme	Calculated $w = 1/[\sigma^2(F_o^2) + (0.0848P)^2]$ where $P = (F_o^2 + 2F_c^2)/3$	Calculated $w = 1/[\sigma^2(F_o^2) + (0.0685P)^2]$ where $P = (F_o^2 + 2F_c^2)/3$
$(\Delta/\sigma)_{\max}$	<0.0001	<0.0001
$\Delta\rho_{\max}, \Delta\rho_{\min}$ (e Å ⁻³)	0.44, -0.33	0.40, -0.39

Computer programs: *COLLECT* (Nonius, 1997); *DENZO-SMN* (Nonius, 1997); *SHELXS-97* (Sheldrick, 1990); *SHELXL-97* (Sheldrick, 1997); *XP in SHELXTL* (Bruker, 1995); *SHELX-97 and local procedures*.

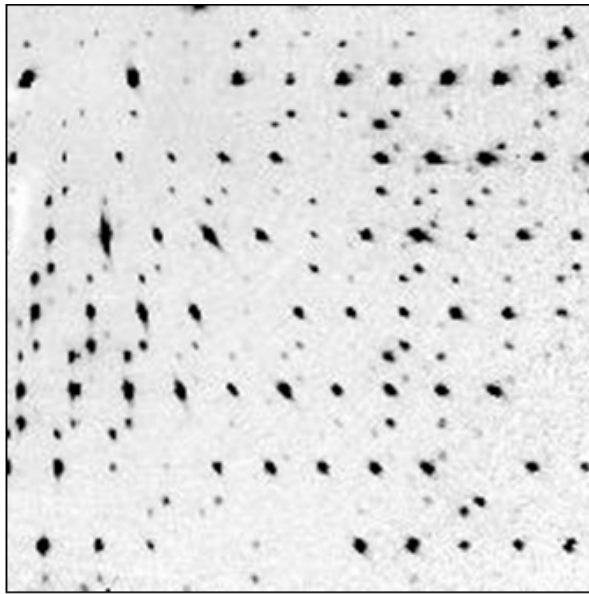
Phase III

Passing through the phase transition near 207 K revealed a very unusual superstructure with seven crystallographically independent formula units in the asymmetric unit ($Z' = 7$). A search on the Cambridge Structural Database (Allen, 2002) showed that only 5 structures with $Z' = 7$ (refcodes GEFXEV, GUFKEX, OLOGEB, SABPOB and VUKSAV01) are known to date. Data were collected at 213 K where the phase is stable. Data could also be obtained at 90 K⁶¹, where the phase is metastable⁶² if the crystal had been flash-cooled (*i.e.*, crystals had been cooled rapidly) from room temperature. In the latter case, the number of reflections having $I > 2\sigma(I)$ rises as a result of a decrease in thermal motion (see Figure 5.9). Near 90 K, 43.8% of the reflections have $I > 2\sigma(I)$; near 213 K, only 27.7 % of the reflections have $I > 2\sigma(I)$. Attempts to refine the structure of phase III at 213 K were not completely successful because the $I > 2\sigma(I)$ ratio was too low (*i.e.*, there was not enough information in the diffraction pattern).

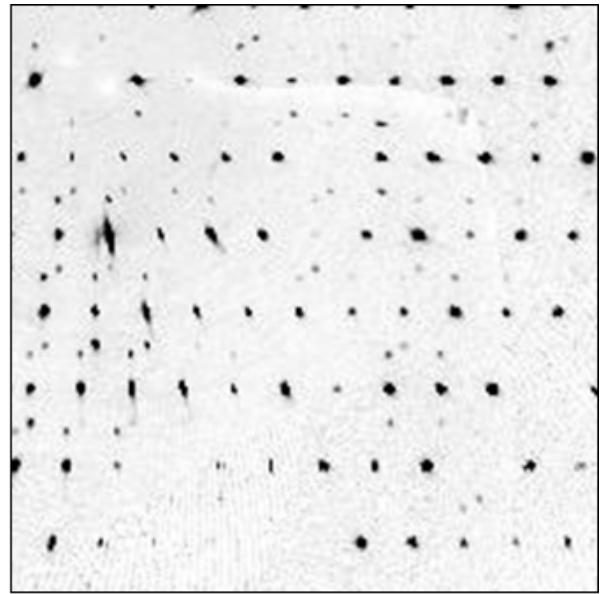
The refinement of phase III was challenging because of the high degree of pseudosymmetry in the structure. In phase III, the pseudosymmetry corresponds to pseudomirror planes in some regions of the structure and pseudoglide planes in other regions of the structure. The regions with the pseudomirror plane symmetry are disordered similarly to the structure of phase II (see phase II for further details). In the disordered regions of phase III, two 15-crown-5 molecules, two $[\text{Ni}(\text{H}_2\text{O})_6]^{2+}$ ions, two nitrate ions and four lattice water molecules are found to be disordered. The regions with the pseudoglide plane symmetry are ordered and are similar to the structure of phase IV.

⁶¹ 90 K is near the lower limit of stable temperature control when the cooling device is running with liquid nitrogen.

⁶² X-ray diffraction showed evidence that the structure of the $Z' = 7$ phase found at 90 K and the structure of phase III found at 213 K were the same.



90 K



213 K

Figure 5.9. Parts of the reciprocal lattice slices $h1\ell$ digitally reconstructed directly from the measured frames for phase III ($B2_1$, $Z' = 7$) at 90 and 213 K. At 90 K, the ratio of reflections having $I > 2\sigma(I)$ is significantly larger than that given at 213 K (see text).

The anisotropic displacement parameters (hereafter, ADPs) of all independent atoms related by pseudosymmetry (*i.e.*, pseudomirror and pseudoglide planes) could not be constrained to be identical using the *EADP* instruction because the pseudosymmetry requires a change in the orientation of the atomic displacement ellipsoids. The ADPs of all independent atoms related by pseudosymmetry were set as free variables (*FVAR* instruction). All independent atoms related by pseudosymmetry were constrained to have identical anisotropic components U_{11} , U_{22} , U_{33} and U_{13} but anisotropic components U_{23} and U_{12} opposite in sign⁶³ (*e.g.*, U_{23} and $-U_{23}$). Seven sets of ADPs for all independent atoms related by pseudosymmetry were used in the refinement process: one set (of 15*6 values) for the atoms of the seven independent 15-crown-5 molecules, one set (of 7*6 values) for the atoms of the seven independent $[\text{Ni}(\text{H}_2\text{O})_6]^{2+}$ ions, three sets⁶⁴ [of (4+4+3)*6 values] for the atoms of the fourteen independent nitrate ions and two sets [of (1+1)*6 values] for the fourteen independent lattice water molecules. The total number of free variables used to describe the atomic displacements was (15+7+4+4+3+1+1)*6 = 210.

The refinement against F^2 was good. The *R* factor [$F^2 > 2\sigma(F^2)$] is 0.047, the ellipsoids looked normal and the highest residual electron density peak was no more than 0.72 e Å⁻³. The largest peaks were located near some oxygen atoms of some nitrate ions. The geometries of all independent 15-crown-5 molecules, $[\text{Ni}(\text{H}_2\text{O})_6]^{2+}$ ions and nitrate ions which are related by pseudosymmetry were restrained to be similar using the *SAME* instruction. The consistency of chemically equivalent bond distances⁶⁵ for all 15-crown-5 molecules, $[\text{Ni}(\text{H}_2\text{O})_6]^{2+}$ ions and nitrate ions related by pseudosymmetry was good; the estimated standard deviations for the sets of chemically equivalent distances averaged about 1.8 times the average uncertainty of an individual measurement. The values of the occupancy factors given for the major components of the two disordered 15-crown-5 molecules are 0.566 (3) and 0.584 (4). The minor components of the disordered crown

⁶³ The relationship between the six displacement parameters for atoms related by pseudosymmetry is defined by the following transformation matrix: (-1 0 0 / 0 1 0 / 0 0 -1). The signs of the off-diagonal elements U_{12} and U_{23} are changed via this transformation. The other terms remain unchanged.

⁶⁴ The third set corresponds to the six parameters for 3 atoms of two independent nitrate ions. The displacement parameters of the two oxygen atoms related by pseudomirror symmetry were constrained to have correlated orientations via the transformation matrix (-1 0 0 / 0 1 0 / 0 0 -1).

⁶⁵ The analysis excludes the hydrogen atoms.

ether were treated as rigid groups to help the refinement of the low-occupancy atomic coordinates. The values of the occupancy factors given for the major components of the two disordered $[\text{Ni}(\text{H}_2\text{O})_6]^{2+}$ ions are 0.613 (7) and 0.577 (7). The values of the occupancy factors given for the major components of the two disordered nitrate ions are 0.699 (16) and 0.588 (9). The values of the occupancy factors given for the major components of the four disordered lattice water molecules are 0.574 (12), 0.684 (15), 0.555 (11) and 0.721 (18). The total number of occupancy factors refined was 10.

An examination of classes of reflections along the \mathbf{c}^* direction was done using separate Wilson plots. The systematic classes of strong and weak reflections are the following: the $\ell = 7n$ reflections (primary reflections) are the strongest, whereas the $\ell = 7n \pm 1$ and the $\ell = 7n \pm 2$ reflections are very weak; the $\ell = 7n \pm 3$ are intermediate (see Figure 5.10). Qualitative observations resulting from careful inspections of the reciprocal lattice slices are consistent with previous results (see Figure 5.11). The reconstructed reciprocal lattice slices were obtained using the program *PRECESSION* (Nonius, 1997).

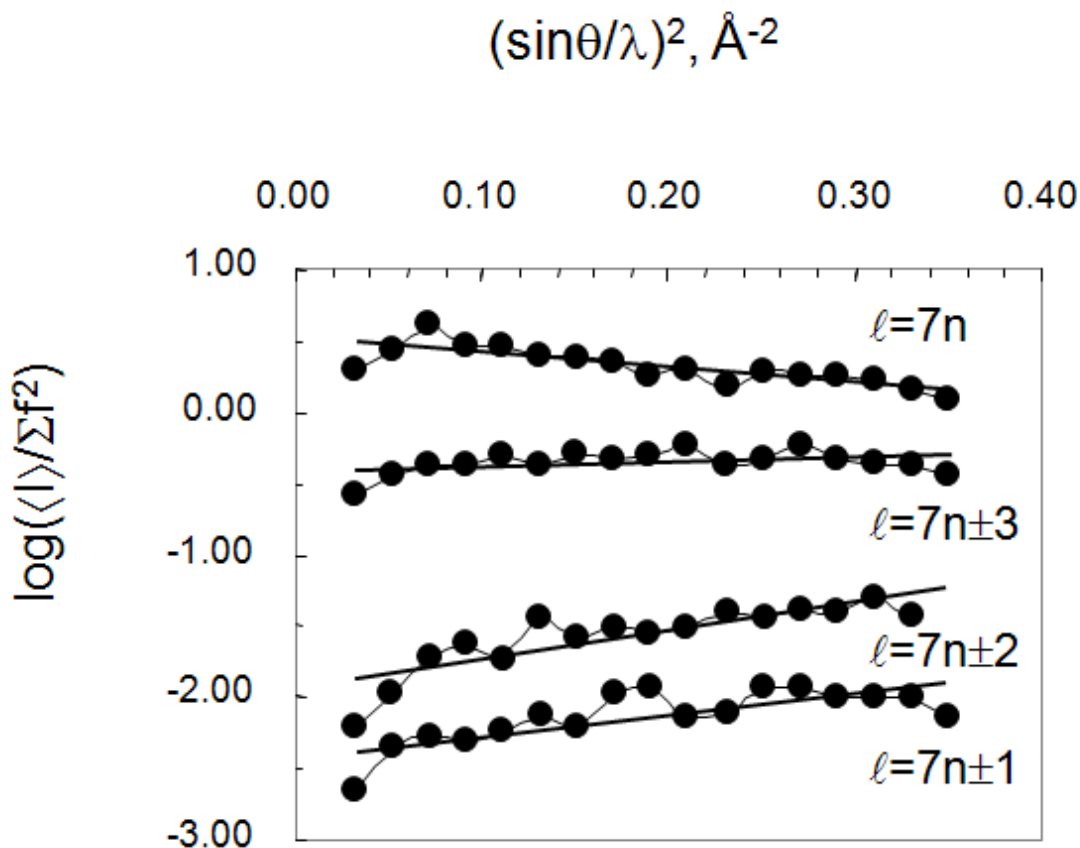


Figure 5.10. Separate Wilson plots for phase III ($B2_1$, $Z' = 7$) at 90 K. The reflections are divided into several classes with respect to the Miller index ℓ (i.e., $\ell = 7n$, $7n \pm 1$, etc.). The intensities of the primary reflections ($\ell = 7n$) are systematically stronger than the intensities of the superstructure reflections ($\ell = 7n \pm 1$, $7n \pm 2$, $7n \pm 3$). The $\ell = 7n \pm 1$ and $\ell = 7n \pm 2$ reflections are systematically the weakest superstructure reflections. The $\ell = 7n \pm 3$ reflections are intermediate.

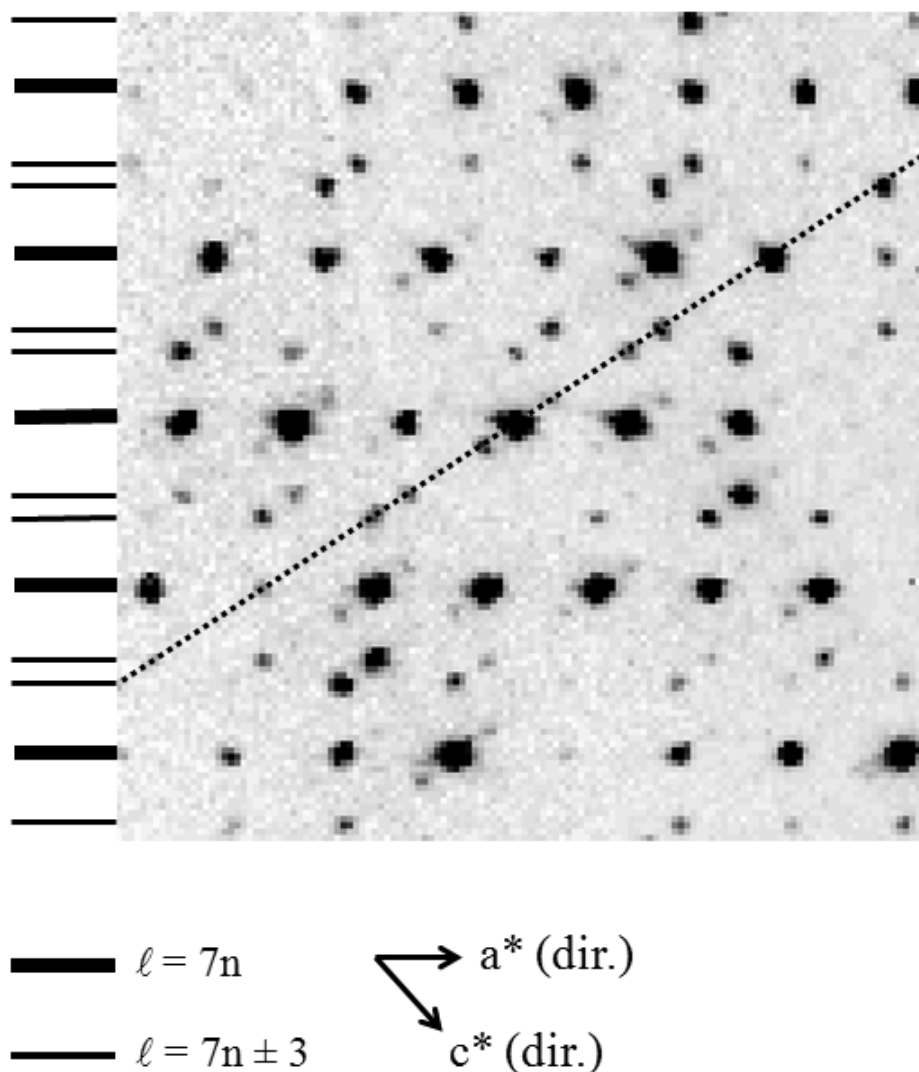


Figure 5.11. Parts of the reciprocal lattice slice $h1\ell$ (given at 90 K) digitally reconstructed directly from the measured frames for phase III ($B2_1$, $Z' = 7$). Systematic classes of strong and weak reflections are observed. The $\ell = 7n$ reflections are the strongest; the $\ell = 7n \pm 1$ and $\ell = 7n \pm 2$ reflections are very weak. The $\ell = 7n \pm 3$ reflections are intermediate. The satellite reflections (*i.e.*, reflections with $\ell = 7n \pm 1$, $\ell = 7n \pm 2$ and $\ell = 7n \pm 3$) are densest along the $a^* - c^*$ direction (shown as a black dotted line) in the $B2_1$ setting. The positions of the strongest class of reflections are indicated by thick solid lines. The positions of the intermediate class of reflections are shown by thinner solid lines. The positions of the two other classes of reflections are omitted for clarity.

Phase IV

The lowest-temperature phase of the compound $[\text{Ni}(\text{H}_2\text{O})_6](\text{NO}_3)_2 \cdot (15\text{-crown-5}) \cdot 2\text{H}_2\text{O}$ (IV, $P2_1/c$, $Z' = 1$) was initially found at 173 K (refcode XEMGIF) as part of a study in which the role of 15-crown-5 as a bifacial hydrogen-bond acceptor was examined in different metal complexes (Steed *et al.*, 2001). The phase was re-determined at 90 K (single crystals were slowly cooled from room temperature to 90 K at -2 K/min). The space group $P2_1/c$ used by Steed *et al.* was retained. The refinement was problem-free but the final difference Fourier map showed residual electron density with peaks as large as $0.85 \text{ e } \text{\AA}^{-3}$ (the largest peak was located at 0.05 \AA from Ni^{2+} ion). Peaks that are not near the metal-ion are within the range $0.35\text{-}0.60 \text{ e } \text{\AA}^{-3}$. The largest peak ($0.60 \text{ e } \text{\AA}^{-3}$), which is located at 0.91 \AA from one axial water molecule of $[\text{Ni}(\text{H}_2\text{O})_6]^{2+}$, may indicate slight disorder. The other peaks have no physical interpretation. This structure was treated as a completely ordered phase.

The ellipsoids of all atoms in the asymmetric unit of the phases III and IV are shown in Figure 5.12. The crystallographic data for the phases III and IV of the compound $[\text{Ni}(\text{H}_2\text{O})_6](\text{NO}_3)_2 \cdot (15\text{-crown-5}) \cdot 2\text{H}_2\text{O}$ are given in Table 5.2.

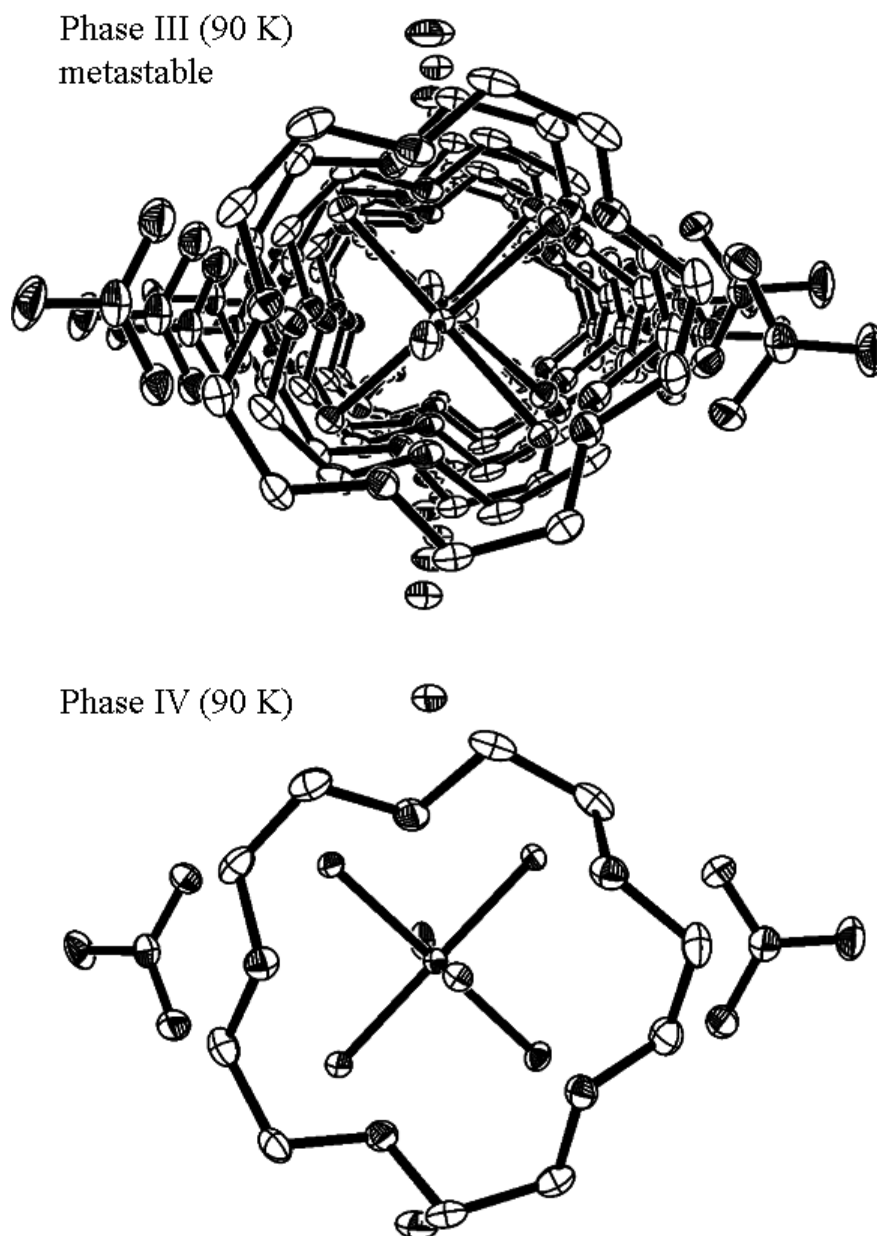


Figure 5.12. The displacement ellipsoids (50% probability level) of the asymmetric unit of the compound $[\text{Ni}(\text{H}_2\text{O})_6](\text{NO}_3)_2 \cdot (15\text{-crown-5}) \cdot 2\text{H}_2\text{O}$ in phase III and phase IV at 90 K. Phase III is found to be metastable at 90 K. The disorder found in phase III and the H atoms are omitted for clarity.

Table 5.2. Crystallographic data for the phases III and IV of $[\text{Ni}(\text{H}_2\text{O})_6](\text{NO}_3)_2 \cdot (15\text{-crown-5}) \cdot 2\text{H}_2\text{O}$.

	III	IV
Crystal data		
Chemical formula	$(\text{C}_{10}\text{H}_{20}\text{O}_5) \cdot (\text{H}_{12}\text{NiO}_6^{2+}) \cdot 2(\text{NO}_3^{1-}) \cdot 2(\text{H}_2\text{O})$	
M_r	547.12	547.12
Cell setting, space group	Monoclinic, $B2_1$	Monoclinic, $P2_1/c$
a, b, c (Å) ⁶⁶	30.632 (3)	11.950 (1)
	12.594 (1)	12.686 (1)
	55.955 (5)	15.988 (1)
β (°)	129.46 (1)	101.51 (1)
V (Å ³)	16666 (3)	2375.0 (3)
$Z; Z'$	28; 7	4; 1
D_x (g cm ⁻³)	1.526	1.530
Radiation type	Mo $K\alpha$	Mo $K\alpha$
No. of reflections for cell parameters	19869	5679
θ range (°)	1.0–27.5	1.0–27.5
μ (mm ⁻¹)	0.90	0.90
Temperature (K)	90.0 (2)	90.0 (2)
Crystal form, colour	Parallelepiped, pale green	Parallelepiped, pale green
Crystal size (mm)	0.60 x 0.25 x 0.20	0.30 x 0.25 x 0.20
Data collection		
Diffractometer	Nonius KappaCCD	Nonius KappaCCD
Data collection method	ω scans at fixed $\chi = 55^\circ$	ω scans at fixed $\chi = 55^\circ$
Absorption correction	Multi-scan (based on symmetry-related measurements)	
T_{\min}	0.614	0.773

⁶⁶ The estimated errors in the unit cell constants (a , b , c and β) were modified by multiplying the experimental estimated standard uncertainties (*i.e.*, su's) by at least a factor of ~ 5 for a , b , c and by at least a factor of ~ 16.5 for β . These factors were used in order to approximate the errors in the unit cell constants from one crystal to another (Herbstein, 2000).

Table 5.2. (continued)

T_{\max}	0.840	0.840
No. of measured, independent and observed parameters	37869, 37869, 16572	10666, 5463, 3979
Criterion for observed reflections	$I > 2\sigma(I)$	$I > 2\sigma(I)$
R_{int}	0.054	0.034
θ_{\max} (°)	27.5	27.5
Range of h, k, ℓ	$-39 < h < 39$ $-16 < k < 16$ $-72 < \ell < 72$	$-15 < h < 15$ $-16 < k < 16$ $-20 < \ell < 20$
Refinement		
Refinement on	F^2	F^2
$R[F^2 > 2\sigma(F^2)], wR(F^2), S$	0.047, 0.154, 1.23	0.040, 0.108, 1.06
No. of reflections	37869 reflections	5463 reflections
No. of parameters	1008	338
H-atom treatment	Constrained to parent site	Constrained to parent site
Weighting scheme	Calculated $w = 1/[\sigma^2(F_o^2) + (0.0500P)^2]$ where $P = (F_o^2 + 2F_c^2)/3$	Calculated $w = 1/[\sigma^2(F_o^2) + (0.0589P)^2 + 0.1330P]$ where $P = (F_o^2 + 2F_c^2)/3$
$(\Delta/\sigma)_{\max}$	0.010	<0.0001
$\Delta\rho_{\max}, \Delta\rho_{\min}$ (e Å ⁻³)	0.73, -0.59	0.85, -0.53
Absolute structure	Flack H D (1983), Acta Cryst. A39, 876-881	
Flack parameter	0.0 (7) – undetermined because racemic twin	

Computer programs: *COLLECT* (Nonius, 1997); *DENZO-SMN* (Nonius, 1997); *SHELXS-97* (Sheldrick, 1990); *SHELXL-97* (Sheldrick, 1997); *XP in SHELXTL* (Bruker, 1995); *SHELX-97* and local procedures.

Temperature Dependence of the Cell Dimensions

The variation of the cell dimensions (*i.e.*, a , b , c and β) with temperature was measured as single crystals of $[\text{Ni}(\text{H}_2\text{O})_6](\text{NO}_3)_2 \cdot (15\text{-crown-5}) \cdot 2\text{H}_2\text{O}$ were heated from 90 to 308 K. The measurements of the cell dimensions were performed at about 10 K intervals for temperatures away from the phase transitions and at about 5 K intervals for temperatures near the phase transitions. Overall, thirty full data sets were collected to examine the temperature dependence of the cell dimensions of $[\text{Ni}(\text{H}_2\text{O})_6](\text{NO}_3)_2 \cdot (15\text{-crown-5}) \cdot 2\text{H}_2\text{O}$. From 90 to 263 K, one single crystal was used during the experiment. A second series of measurements between 253 and 308 K using several crystals was made because crystals could not be heated without damage above 263 K.

The cell dimensions were presented in a way that minimizes the effect of structural changes between the four phases of $[\text{Ni}(\text{H}_2\text{O})_6](\text{NO}_3)_2 \cdot (15\text{-crown-5}) \cdot 2\text{H}_2\text{O}$. The cell of phase IV was chosen to be the cell of reference. Phase III was indexed in the pseudo-cell (*i.e.*, the cell which is very similar to the cell of phase II). The length of the c axis and V were multiplied by a factor of two for phases I, II and III. The temperature dependences of these modified cell dimensions a , b , c and β , V of the compound $[\text{Ni}(\text{H}_2\text{O})_6](\text{NO}_3)_2 \cdot (15\text{-crown-5}) \cdot 2\text{H}_2\text{O}$ are shown in Figures 5.13 and 5.14. The plots show a discontinuity near 207 K which corresponds to the phase transition IV \rightarrow III. There is no obvious discontinuity found for the two phase transitions III \rightarrow II and II \rightarrow I. The slopes of the plots of c and β against T change within the interval 242-253 K, in which the phase transition III \rightarrow II takes place. The plots are less informative about the phase transition II \rightarrow I⁶⁷.

The temperatures of the phase transitions IV \rightarrow III and III \rightarrow II are found to be higher by about 10 and 14 K in the analysis of the temperature dependence of the cell dimensions than in the DSC measurements. These results are not surprising because the DSC measurements were performed using fine powders, whereas single crystals were used in this analysis.

⁶⁷ The small changes in the plot of c against T might indicate the phase transition II \rightarrow I near 290 K.

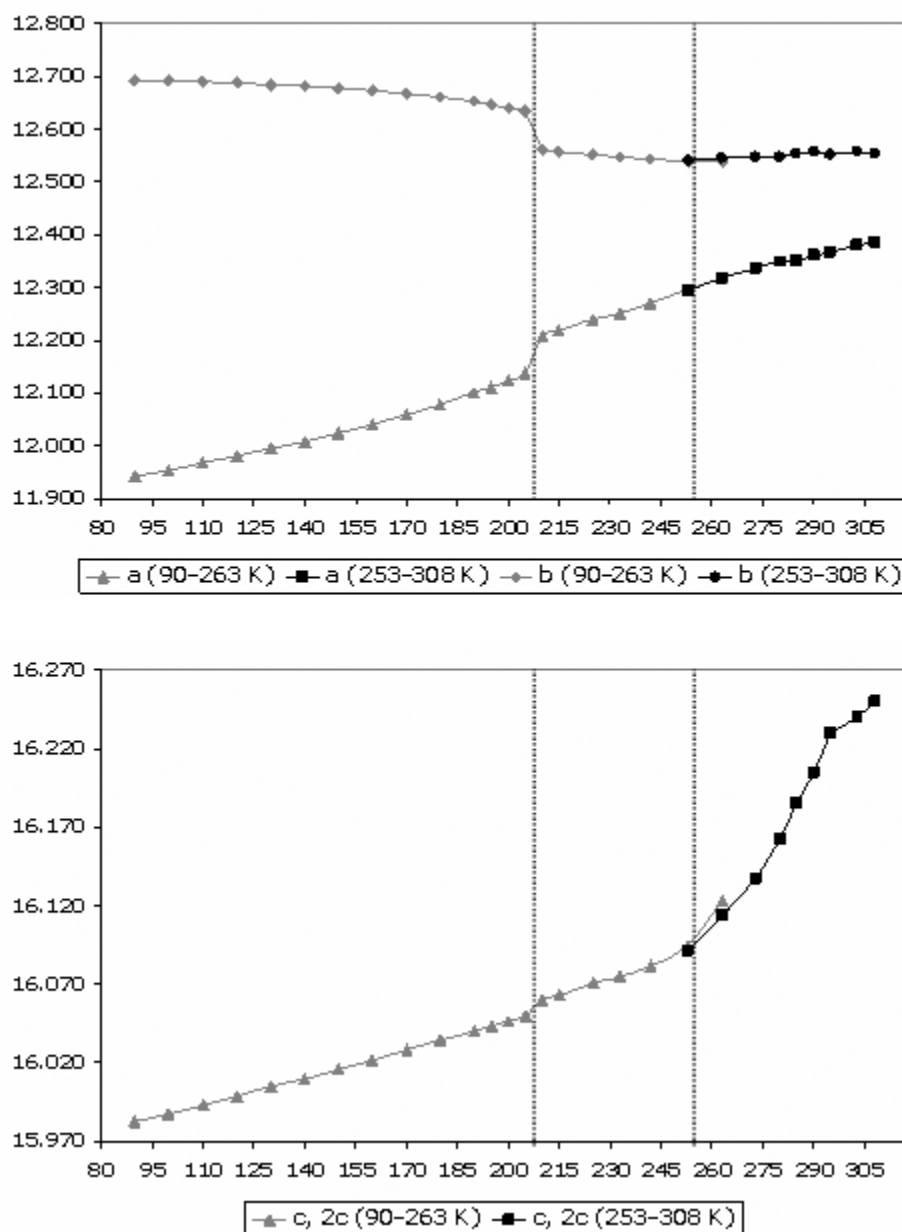


Figure 5.13. Plots of the modified cell dimensions a , b and c (Å) of $[\text{Ni}(\text{H}_2\text{O})_6](\text{NO}_3)_2 \cdot (15\text{-crown-5}) \cdot 2\text{H}_2\text{O}$ versus T (K). The first series of measurements between 90 and 263 K (light gray line) were done using one crystal. The second series of measurements between 253 and 308 K (black line) were done using several crystals. The c axis for the phases I, II and III were modified so that the cells of the four phases are analogous (see text). The phase transitions $\text{IV} \rightarrow \text{III}$ and $\text{III} \rightarrow \text{II}$ are found near 207 and 248 K and are shown as dotted lines. The plots are not as informative about the phase transition $\text{II} \rightarrow \text{I}$. Error bars associated with the a , b and c axes are insignificant compared to the axis scale.

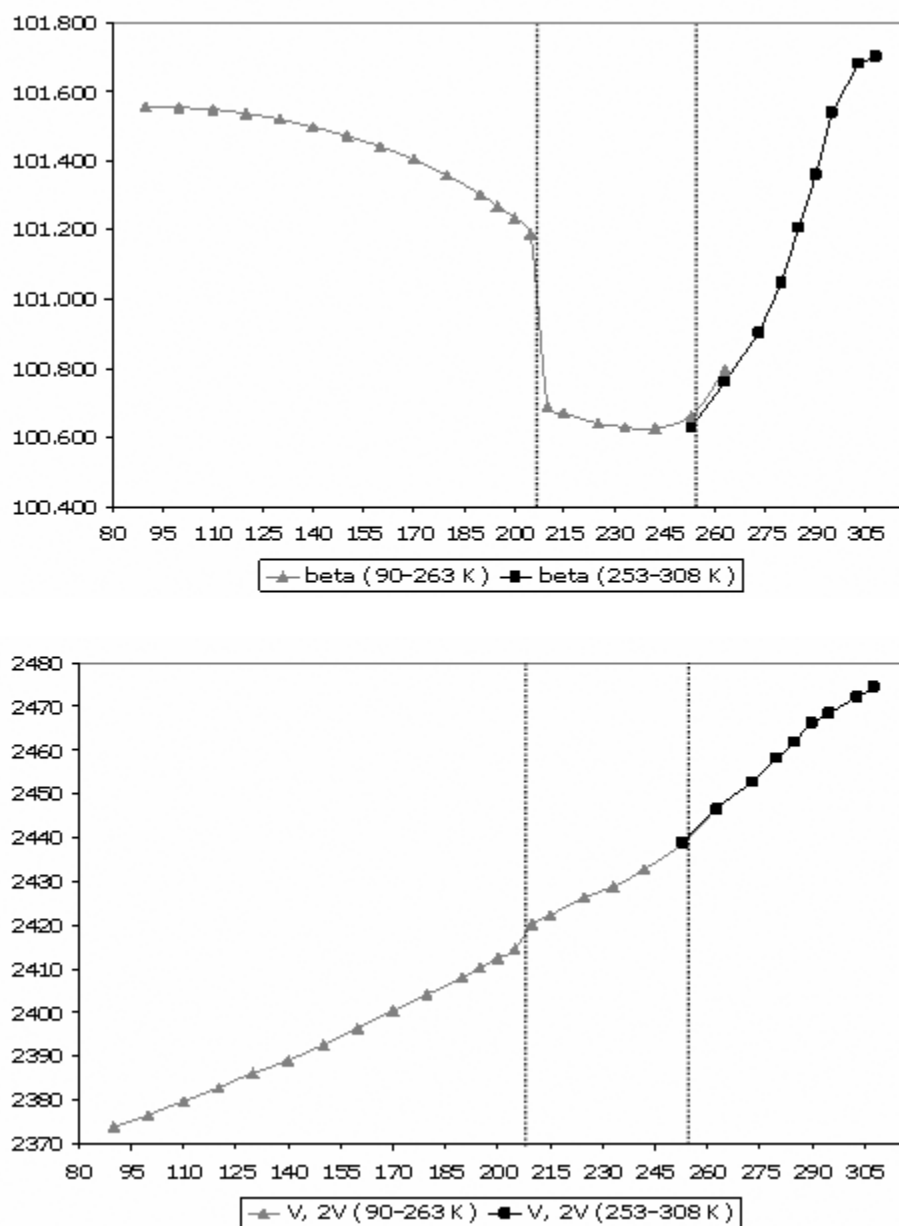


Figure 5.14. Plots of the modified cell dimensions β ($^\circ$) and V (\AA^3) of $[\text{Ni}(\text{H}_2\text{O})_6](\text{NO}_3)_2 \cdot (15\text{-crown-5}) \cdot 2\text{H}_2\text{O}$ versus T (K). The first series of measurements between 90 and 263 K (light gray line) were done using one crystal. The second series of measurements between 253 and 308 K (black line) were done using several crystals. The volume V for the phases I, II and III were modified so that the cells of the four phases are analogous (see text). The phase transitions $\text{IV} \rightarrow \text{III}$ and $\text{III} \rightarrow \text{II}$ are found near 207 and 248 K and are shown as dotted lines. The plots are less informative about the phase transition $\text{II} \rightarrow \text{I}$. Error bars associated with the β angle and the volume V are insignificant compared to the axis scale.

Results and Discussion

Analysis of the Packing

In the four phases of $[\text{Ni}(\text{H}_2\text{O})_6](\text{NO}_3)_2 \cdot (15\text{-crown-5}) \cdot 2\text{H}_2\text{O}$, the three-dimensional H-bonded network remains very similar and is best described as one-dimensional (hereafter, 1-D) chains and two-dimensional (hereafter, 2-D) planes of H-bonds. The nature of the hydrogen bonds observed in the four phases has been explored.

Along the **c** direction, the H-bond interactions between the 15-crown-5 molecules and the $[\text{Ni}(\text{H}_2\text{O})_6]^{2+}$ ions are best described as 1-D chains. The crown ether is found to be H-bonded by two $[\text{Ni}(\text{H}_2\text{O})_6]^{2+}$ ions. The 1-D chains are built *via* a set of hydrogen bonds between the five O_{ether} atoms (O1, O2, O3, O4 and O5) of the crown ether, one $\text{O}_{\text{equatorial}}$ (O10) and the two O_{axial} atoms (O6 and O7) of the $[\text{Ni}(\text{H}_2\text{O})_6]^{2+}$ ions [see the part (a) of Figure 5.15]. Table 5.3 summarizes the $\text{O} \cdots \text{O}$ distances found along the 1-D H-bonded chains of the four phases.

The interactions between the $[\text{Ni}(\text{H}_2\text{O})_6]^{2+}$ and nitrate ions and the lattice water molecules are two-dimensional. The 2-D planes are parallel to $(-1\ 0\ 1)$ for the phases I and II, parallel to $(-1\ 0\ 7)$ for phase III and parallel to $(-1\ 0\ 2)$ for phase IV. Each of three $\text{O}_{\text{equatorial}}$ atoms (O8, O9 and O11) of the $[\text{Ni}(\text{H}_2\text{O})_6]^{2+}$ ion are H-bond donors to one nitrate ion and one lattice water molecule. The remaining $\text{O}_{\text{equatorial}}$ atom (O10) of the $[\text{Ni}(\text{H}_2\text{O})_6]^{2+}$ ion is an H-bond donor to one nitrate only [see the part (b) of Figure 5.15]. Along the **b** direction, the hydrogen bond pattern is given by: $\cdots[\text{Ni}(\text{H}_2\text{O})_6]^{2+} \cdots \text{water} \cdots \text{nitrate} \cdots \text{water} \cdots [\text{Ni}(\text{H}_2\text{O})_6]^{2+} \cdots$. Along the $[1\ 0\ 1]$, $[1\ 0\ 1/7]$ or $[1\ 0\ \frac{1}{2}]$ directions (respectively given for phases I/II, III or IV), the hydrogen bond pattern is given by: $\cdots[\text{Ni}(\text{H}_2\text{O})_6]^{2+} \cdots \text{nitrate} \cdots \text{water} \cdots \text{nitrate} \cdots [\text{Ni}(\text{H}_2\text{O})_6]^{2+} \cdots$. Table 5.4 summarizes the $\text{O} \cdots \text{O}$ distances found in the 2-D H-bonded planes of the four phases.

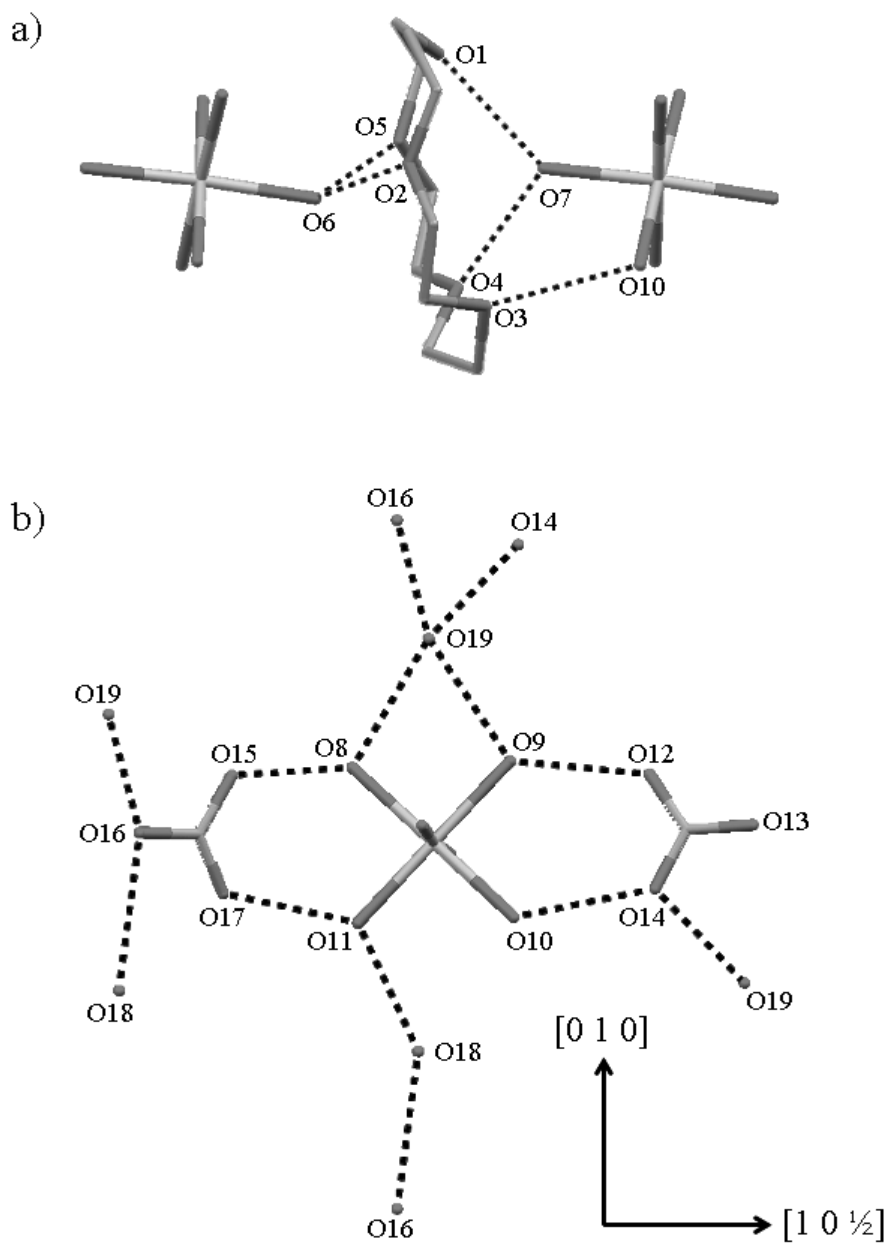


Figure 5.15. (a) The set of hydrogen bond interactions observed in phase IV of the compound $[\text{Ni}(\text{H}_2\text{O})_6](\text{NO}_3)_2 \cdot (15\text{-crown-5}) \cdot 2\text{H}_2\text{O}$ along the c direction (*i.e.*, along the 1-D H-bonded chains). H-bonds are shown as black dotted lines. The nitrate ions, the lattice water molecules and the H-atoms are omitted for clarity. (b) The set of hydrogen bond interactions given for phase IV of the compound $[\text{Ni}(\text{H}_2\text{O})_6](\text{NO}_3)_2 \cdot (15\text{-crown-5}) \cdot 2\text{H}_2\text{O}$ along the $[0\ 1\ 0]$ and $[1\ 0\ \frac{1}{2}]$ directions (*i.e.*, along the 2-D H-bonded planes). H-bonds are shown as black dotted lines. The 15-crown-5 molecule and the H-atoms are omitted for clarity.

Table 5.3. Hydrogen bond distances⁶⁸ D···A (Donor···Acceptor) along the **c** direction (*i.e.*, the direction of the 1-D H-bonded chains) for the phases I, II, III and IV of the compound [Ni(H₂O)₆](NO₃)₂·(15-crown-5)·2H₂O.

D···A (Å)	Phase IV (<i>P</i>2₁/<i>c</i>, <i>Z</i>' = 1)			
O6···O2	2.743 (2)			
O6···O5	2.729 (2)			
O7···O1	2.761 (2)			
O7···O4	2.810 (2)			
O10···O3	2.796 (2)			
D···A (Å)	Phase III (<i>B</i>2₁, <i>Z</i>' = 7)			
	Residues 1/7	Residues 2/1	Residues 3/2	Residues 4/3
O6···O2	2.821 (9)	2.627 (12)	2.770 (6)	2.756 (6)
O6···O5	2.717 (10)	2.907 (11)	2.787 (6)	2.708 (6)
O7···O1	2.782 (9)	2.777 (10)	2.748 (6)	2.770 (6)
O7···O4	2.807 (9)	2.822 (9)	2.841 (6)	2.797 (6)
O10···O3	2.751 (9)	2.687 (9)	2.841 (6)	2.777 (6)
	Residues 5/4	Residues 6/5	Residues 7/6	Average
O6···O2	2.724 (6)	2.759 (7)	2.717 (6)	2.739 (8)
O6···O5	2.756 (6)	2.725 (6)	2.755 (6)	2.765 (8)
O7···O1	2.762 (6)	2.778 (6)	2.756 (6)	2.768 (7)
O7···O4	2.805 (6)	2.797 (6)	2.819 (6)	2.813 (7)
O10···O3	2.759 (6)	2.779 (6)	2.809 (6)	2.771 (7)

⁶⁸ The hydrogen bond interactions involved with the minor component of the disorder (*i.e.*, the disorder of the 15-crown-5 molecule observed in phase I, the disorder of the 15-crown-5 molecule and the [Ni(H₂O)₆]²⁺ ion observed in phase II and in some residues of phase III) are not given in the table.

Table 5.3 (continued)

D···A (Å)	Phase II ($P2_1/m, Z' = \frac{1}{2}$)
-----------	---

O6···O2	2.689 (12)
---------	------------

O6···O5	2.825 (17)
---------	------------

O7···O1	2.765 (4)
---------	-----------

O7···O4	2.832 (9)
---------	-----------

O10···O3	2.799 (10)
----------	------------

D···A (Å)	Phase I ($I2/m, Z' = \frac{1}{4}$)
-----------	--

O6···O2	2.852 (5)
---------	-----------

O6···O5	2.852 (5)
---------	-----------

O7···O1	2.647 (5)
---------	-----------

O7···O4	2.923 (5)
---------	-----------

O10···O3	n/a
----------	-----

Table 5.4. Hydrogen bond distances⁶⁹ D...A (Donor...Acceptor) found in the 2-D H-bonded planes for the phases I, II, III and IV of the compound [Ni(H₂O)₆](NO₃)₂·(15-crown-5)·2H₂O.

D...A (Å)	Phase IV (<i>P</i>2₁/<i>c</i>, <i>Z</i>' = 1)			
O8...O15	2.734 (2)			
O8...O19	2.758 (2)			
O9...O12	2.775 (2)			
O9...O19	2.739 (2)			
O10...O14	2.759 (2)			
O11...O17	2.754 (2)			
O11...O18	2.700 (2)			
O18...O16	2.989 (2)			
O19...O14	2.841 (2)			
O19...O16	2.744 (2)			
D...A (Å)	Phase III (<i>B</i>2₁, <i>Z</i>' = 7)			
	Residues 1	Residues 2	Residues 3	Residues 4
O8...O15	2.846 (8)	2.782 (10)	2.719 (6)	2.769 (6)
O8...O19 (O18)	2.724 (11)	2.799 (10)	2.744 (7)	2.766 (7)
O9...O12	2.791 (10)	2.800 (12)	2.793 (6)	2.776 (6)
O9...O19 (O18)	2.766 (10)	2.718 (10)	2.741 (7)	2.735 (7)
O10...O14	2.725 (10)	2.698 (12)	2.724 (6)	2.763 (6)
O11...O17	2.790 (8)	2.757 (9)	2.742 (7)	2.755 (7)
O11...O18 (O19)	2.667 (13)	2.716 (14)	2.718 (6)	2.674 (7)
O18...O16	2.942 (9)	2.892 (10)	2.969 (8)	3.007 (8)

⁶⁹ The hydrogen bond interactions involved with the minor component of the disorder (*i.e.*, the disorder of the 15-crown-5 molecule observed in phase I, the disorder of the 15-crown-5 molecule and the [Ni(H₂O)₆]²⁺ ion observed in phase II and in some residues of phase III) are not given in the table.

Table 5.4 (continued)

O19···O14		2.864 (12)	2.833 (7)	2.854 (7)
O19···O16	2.677 (9)	2.812 (10)	2.732 (7)	2.734 (7)
	Residues 5	Residues 6	Residues 7	Average
O8···O15	2.738 (6)	2.740 (6)	2.720 (6)	2.759 (7)
O8···O19	2.740 (7)	2.787 (7)	2.727 (7)	2.755 (8)
O9···O12	2.776 (6)	2.789 (6)	2.776 (7)	2.785 (8)
O9···O19	2.712 (7)	2.711 (7)	2.745 (6)	2.732 (8)
O10···O14	2.749 (6)	2.740 (6)	2.765 (6)	2.738 (8)
O11···O17	2.759 (6)	2.733 (6)	2.738 (7)	2.753 (7)
(O15)				
O11···O18	2.717 (7)	2.673 (7)	2.702 (7)	2.695 (9)
O18···O16	2.947 (7)	2.955 (7)	3.015 (6)	2.961 (8)
O19···O14	2.896 (7)	2.862 (7)	2.837 (7)	2.858 (8)
O19···O16	2.744 (7)	2.752 (7)	2.744 (7)	2.742 (8)

D···A (Å) **Phase II ($P2_1/m$, $Z' = \frac{1}{2}$)**

O8···O15	2.747 (15)
O8···O19	2.666 (19)
O9···O12	2.777 (10)
O9···O19	2.717 (11)
O10···O14	2.730 (10)
O11···O17	2.692 (15)
O11···O18	2.763 (19)
O18···O16	2.816 (4)
O19···O14	3.007 (4)
O19···O16	2.816 (4)

Table 5.4 (continued)

D···A (Å)	Phase I ($I2/m, Z' = \frac{1}{4}$)
O8···O15	2.719 (3)
O8···O19	2.836 (3)
O9···O12	2.719 (3)
O9···O19	2.836 (3)
O10···O14	2.719 (3)
O11···O17	2.719 (3)
O11···O18	2.836 (3)
O18···O16	2.914 (5)
O19···O14	n/a
O19···O16	2.914 (5)

Are the Hydrogen Bond Interactions Different in the Four Phases?

It is important to understand the hydrogen bond interactions in the four phases because slight changes in these interactions may take place when single crystals undergo a solid-solid phase transition. That understanding requires locating the hydrogen atoms of all water molecules (*i.e.*, the ligand and lattice water molecules) in the structure for each phase.

In phase IV, all hydrogen atoms can be located from the difference Fourier map and their positions were refined with no difficulty. As a result, the hydrogen bond interactions are unambiguous. In the phases I and II, the increase of thermal motion and the disorder contribute to lower the peak densities of the hydrogen atoms. Thus, their positions are approximate rather than precise and the hydrogen bond interactions are more difficult to understand. In phase III, the case is intermediate to that observed in phases II and IV: the positions of the hydrogen atoms are well defined in some regions (*i.e.*, the ordered region of phase III) but are not well defined in other regions (*i.e.*, the disordered region of phase III). Some ambiguities remain in the ordered region of phase III because the positions of some hydrogen atoms of the $[\text{Ni}(\text{H}_2\text{O})_6]^{2+}$ ions and the lattice water molecules are unclear. Knowing the exact positions of the hydrogen atoms in phase III might be particularly useful to understand why such a phase can occur.

Are the hydrogen bond interactions different in the four phases? The question is still unanswered because single-crystal X-ray experiments cannot locate accurately the positions of all hydrogen atoms in the phases I, II and III. Neutron diffraction may help to solve this problem.

Phase III: an Intermediate Phase

In the polymorphic system $[\text{Ni}(\text{H}_2\text{O})_6](\text{NO}_3)_2 \cdot (15\text{-crown-5}) \cdot 2\text{H}_2\text{O}$, phase III is intermediate to the phases II and IV. Single-crystal X-ray experiments have shown that phase II is disordered and phase IV is ordered. The disorder found in phase II is symmetry imposed by a statistical mirror plane. In phase III, the presence of local pseudosymmetry makes some regions of this structure ordered and other regions of this structure disordered. The local disorder in phase III is generated by a pseudomirror plane. The pseudosymmetry of the ordered region corresponds to a pseudoglide plane with the translation component of $c/7$. The relationship between phase III and the two phases II and IV is clear: the disordered and ordered regions of phase III are similar respectively to the phases II and IV (see Figure 5.15). Phase III is best described as an intermediate phase. Nearly 30 % (two independent formula units) and 70% (five independent formula units) of the structure of phase III are similar respectively to the structures of phase II and IV.

The modulation of phase III can be examined by looking at the O6–Ni–O7 directions of the seven crystallographically independent $[\text{Ni}(\text{H}_2\text{O})_6]^{2+}$ ions. There are three possible orientations for the O6–Ni–O7 directions: one direction is parallel to the c direction, the two other directions are either up or down with respect to the c direction. The pseudomirror symmetry constrains the O6–Ni–O7 directions of the two $[\text{Ni}(\text{H}_2\text{O})_6]^{2+}$ ions in the disordered region to be parallel to c . The up and down alternation (see Figure 5.16) for the O6–Ni–O7 directions of the five $[\text{Ni}(\text{H}_2\text{O})_6]^{2+}$ ions in the ordered region is generated by the pseudoglide plane.

The directions O6–Ni–O7 of the $[\text{Ni}(\text{H}_2\text{O})_6]^{2+}$ ions in the phases II, III and IV are also compared in Figure 5.16. The fluctuations of the atomic positions of the independent units are remarkably low in the ordered region of phase III. The $\text{Ni} \cdots \text{O}_{\text{lattice_water}}$ (*i.e.*, O18 and O19) and the $\text{Ni} \cdots \text{Ni}$ distances are very similar for the phases III and IV (see Table 5.5). The pseudoglide plane observed in the ordered region of phase III is nearly exact.

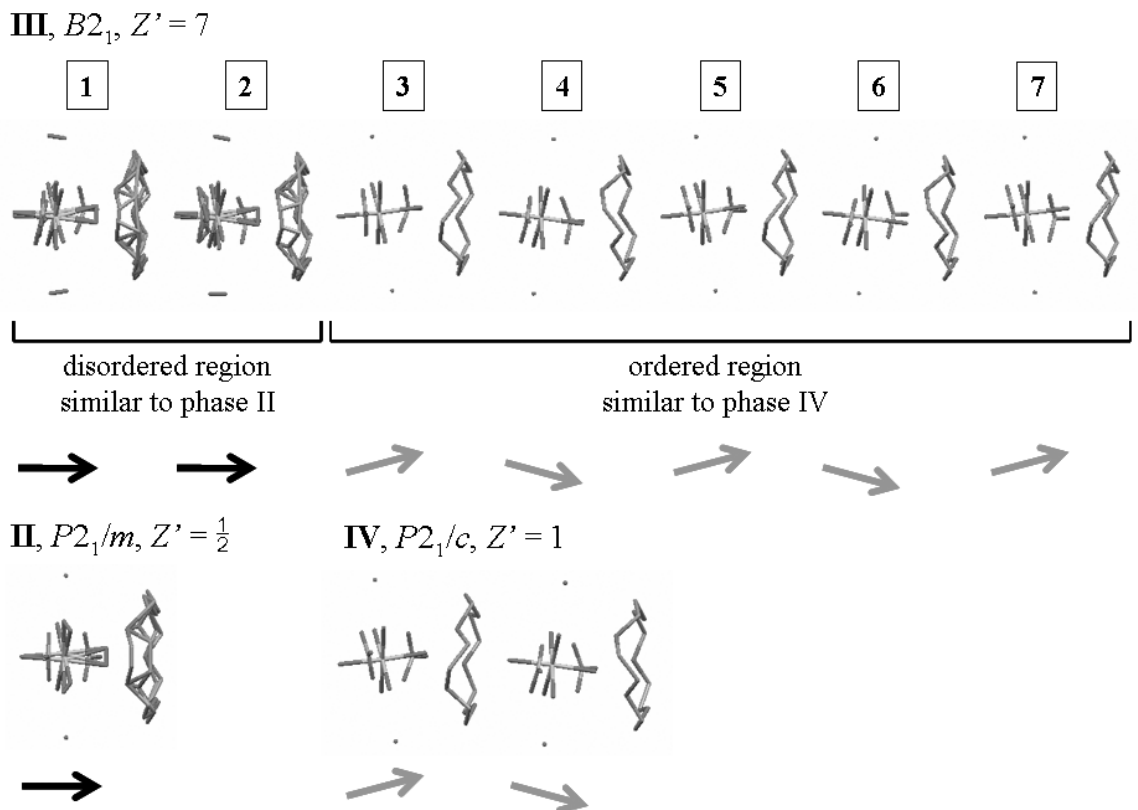


Figure 5.16. Projections of the asymmetric units of phases II, III and IV down the normal to the plane (1 0 0). The symmetry equivalent of the asymmetric unit for phase IV (*i.e.*, a second asymmetric unit generated by the c glide plane) is shown in order to make comparisons with phase III obvious. Phase III, which contains seven crystallographically independent formula units numbered from 1 to 7, is best described as an intermediate phase. Phase III contains a disordered region (formula units 1 and 2) similar to phase II and an ordered region (formula units 3 \rightarrow 7) similar to phase IV. The disorder in phase III is generated by a pseudomirror plane. The formula units 1 and 2 are very similar and are related by pseudotranslation of $c/7$. The formula units 3 \rightarrow 7 are ordered and are related by a pseudoglide plane with translation $c/7$. The arrows correspond to the directions O6–Ni–O7 of the $[\text{Ni}(\text{H}_2\text{O})_6]^{2+}$ ions with respect to the c direction in the phases II, III and IV. In phase II and in the disordered region of phase III (formula units 1 and 2), the directions are horizontal (black arrows) because the orientational disorder generated by mirror or pseudomirror symmetries is averaged over time and space. In phase IV and in the ordered region of phase III (formula units 3 \rightarrow 7), the up and down alternation is observed (gray arrows) because of the presence of a glide plane or a pseudoglide plane.

Table 5.5. Ni^{II}–O (O18 and O19) and Ni^{II}–Ni distances found in the ordered region of phase III and in phase IV of the compound [Ni(H₂O)₆](NO₃)₂·(15-crown-5)·2H₂O.

Ni ^{II} –O (Å)	Phase IV (<i>P2</i>₁/<i>c</i>, <i>Z'</i> = 1)				
Ni ^{II} –O18	3.916 (2)				
Ni ^{II} –O19	3.765 (2)				
Ni ^{II} –Ni (Å)					
Ni ^{II} –Ni	7.998 (1)				
Ni ^{II} –O (Å)	Phase III (<i>B2</i>₁, <i>Z'</i> = 7) - ordered region				
	Residue 3	Residue 4	Residue 5	Residue 6	Residue 7
Ni ^{II} –O18	3.909 (5)	3.913 (5)	3.917 (5)	3.920 (5)	3.919 (5)
Ni ^{II} –O19	3.762 (5)	3.755 (5)	3.740 (5)	3.760 (5)	3.753 (5)
	Average				
Ni ^{II} –O18	3.916 (5)				
Ni ^{II} –O19	3.754 (5)				
Ni ^{II} –Ni (Å)					
	Residues	Residues	Residues	Residues	Average
	3/4	4/5	5/6	6/7	
Ni ^{II} –Ni	8.008 (2)	8.002 (2)	7.994 (2)	7.984 (2)	7.997 (2)

Enantiomeric Alternation

Crystals of $[\text{Ni}(\text{H}_2\text{O})_6](\text{NO}_3)_2 \cdot (15\text{-crown-5}) \cdot 2\text{H}_2\text{O}$ are found to be racemic, the two conformational enantiomers R and S of the 15-crown-5 molecule are present in a ratio 1:1. The 15-crown-5 molecules are bridged by the $[\text{Ni}(\text{H}_2\text{O})_6]^{2+}$ ions along the *c* direction (*i.e.*, the direction of the 1-D H-bonded chains). The enantiomeric alternation pattern changes when single crystals of $[\text{Ni}(\text{H}_2\text{O})_6](\text{NO}_3)_2 \cdot (15\text{-crown-5}) \cdot 2\text{H}_2\text{O}$ pass through a phase transition.

In phase IV, the alternation pattern is found to be perfect: the enantiomers R and S are bridged by the $[\text{Ni}(\text{H}_2\text{O})_6]^{2+}$ ions along the *c* direction. The perfect alternation pattern is given by: R S R S R S. The repeated unit is R S or S R.

In phase III, the disorder of some 15-crown-5 molecules are observed locally (*i.e.*, in the disordered region). Disorder of the crown ether is observed when alternation faults (or non-alternations) occur (either R R or S S) within one 1-D H-bonded chain. In the disordered region, the alternation pattern is either R S or S R. In the ordered region, the alternation pattern is either R S R S R or S R S R S. Since there is an odd number of 15-crown-5 molecules in the asymmetric unit (7), enantiomers R/S fail to alternate once every seven contacts along the *c* direction. The alternation pattern observed in phase III is given by: R S R S R S R or S R R S R S R or S R S R S R S or R S S R S R S (see Figure 5.17)

In the phases I and II, there is no long-range enantiomeric alternation pattern because of the disorder of the crown ether generated by symmetry. In phase I, the disorder is caused by a twofold axis and a mirror plane. In phase II, the disorder is caused by a mirror plane.

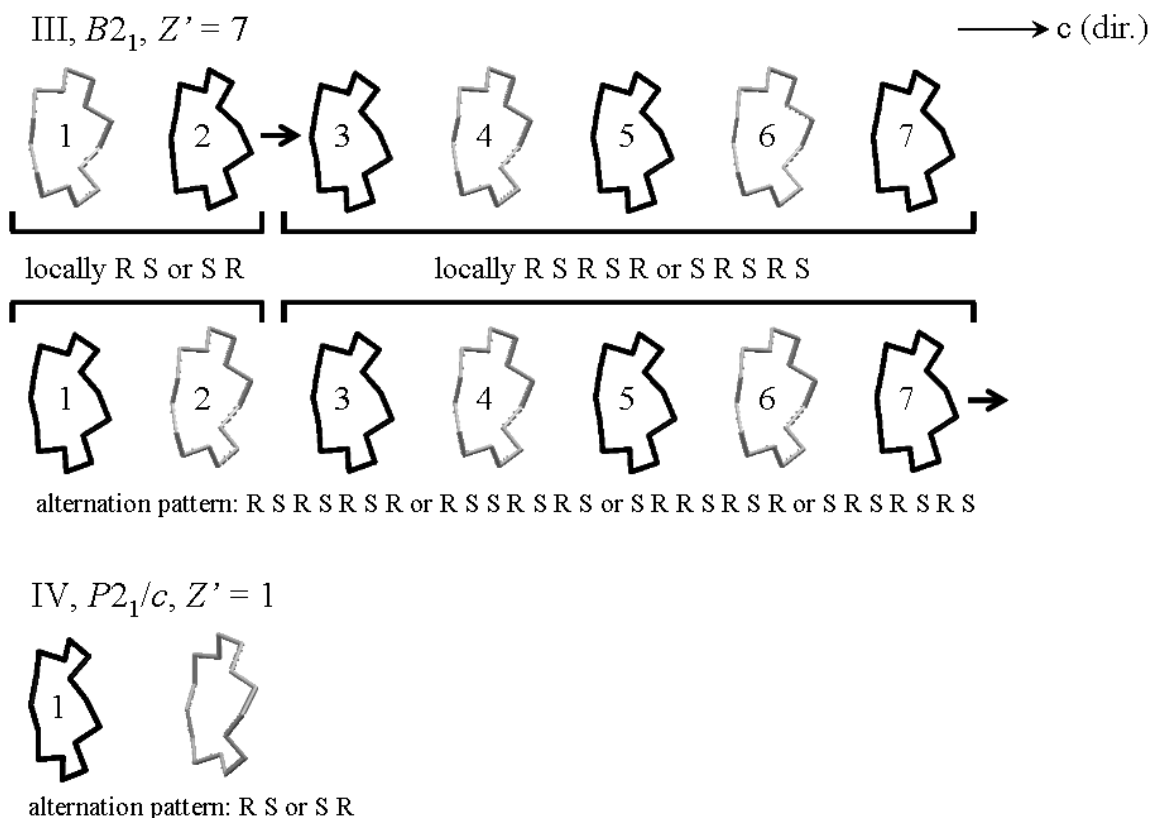


Figure 5.17. Projections of the crystallographically independent 15-crown-5 molecules down the **a** direction for phase III and down the normal to the plane (1 0 1) for phase IV. In the phases III and IV, there are respectively seven and one crystallographically independent 15-crown-5 molecules. The perfect enantiomeric alternation pattern R S (or S R) is observed in the ordered phase IV. The enantiomeric alternation pattern is more complicated in phase III: the alternation pattern R S R S R (or S R S R S) is found locally in one region (*i.e.*, the ordered region) and the alternation pattern R S (or S R) is found locally in another region (*i.e.*, the disordered region). In phase III, the enantiomers fail to alternate once every seven contacts along the **c** direction. The non-alternation (black arrows) occur either between the 15-crown-5 molecules 2 → 3 or 7 → 1. The alternation pattern is either R S R S R S R or S R R S R S R (or either S R S R S R S or R S S R S R S). The black and gray 15-crown-5 molecules correspond to the conformational enantiomers R/S. The $[\text{Ni}(\text{H}_2\text{O})_6]^{2+}$ ions, the nitrate ions and the lattice water molecules were omitted for clarity.

Phase Transitions

The three phase transitions of the polymorphic system $[\text{Ni}(\text{H}_2\text{O})_6](\text{NO}_3)_2 \cdot (15\text{-crown-5}) \cdot 2\text{H}_2\text{O}$ were studied by making DSC measurements, measuring the temperature dependence of the cell dimensions and inspecting the reciprocal lattice slices near the temperatures of the phase transitions. The phase transition $\text{II} \rightarrow \text{I}$ was also investigated by plotting the integrated intensities of the strongest $h0\ell$ reflections with $h + k + \ell = 2n + 1$ against temperature.

In this polymorphic system, the relationship between the four phases is obvious because the packing remains very similar.

IV \rightarrow III and III \rightarrow II

Below 207 K, the space group is the centrosymmetric $P2_1/c$ with $Z' = 1$ (phase IV). Phase IV is ordered. At temperatures between 207 and 247 K, the space group is the noncentrosymmetric $B2_1$ with $Z' = 7$ (phase III). Phase III is ordered in some regions and disordered in other regions. The presence of pseudomirror symmetry in the disordered region of phase III is responsible for generating disorder of two 15-crown-5 molecules and two $[\text{Ni}(\text{H}_2\text{O})_6]^{2+}$ ions. At temperatures between 247 and 292 K, the space group is the centrosymmetric $P2_1/m$ with $Z' = \frac{1}{2}$ (phase II). Phase II is disordered because the space group requires that the 15-crown-5 molecules have a statistically averaged mirror symmetry.

The temperatures of the phase transitions $\text{IV} \rightarrow \text{III}$ and $\text{III} \rightarrow \text{II}$ were checked by looking at the reciprocal lattice slices. Parts (a) and (b) of Figure 5.18 show that the diffraction pattern changes between 205 and 210 K and between 242 and 253 K, for which the phase transitions $\text{IV} \rightarrow \text{III}$ and $\text{III} \rightarrow \text{II}$ take place. These results are in good agreement with the study of the temperature dependence of the cell dimensions.

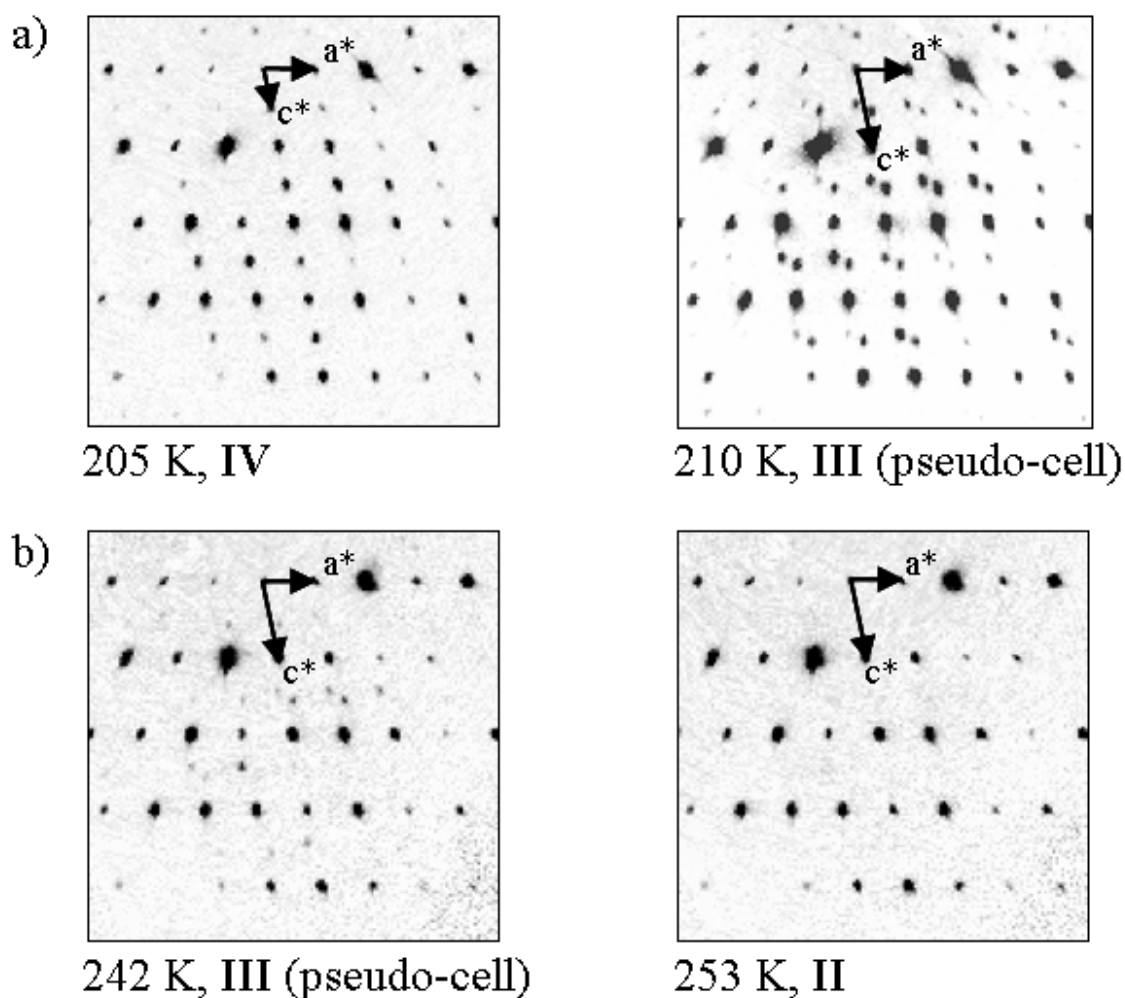


Figure 5.18. (a) Parts of the reciprocal lattice slices $h1\ell$ digitally reconstructed directly from the measured frames given for 205 K (phase IV) and 210 K (phase III). At 210 K, the less intense reflections (satellite reflections) appear to be split and are no longer indexed correctly in phase IV. The phase transition IV \rightarrow III occurs between 205 and 210 K. The indexing in the pseudo-cell (*i.e.*, the indexing for which the most intense reflections only are considered) was chosen so that the two frames are oriented similarly. (b) Parts of the reciprocal lattice slice $h1\ell$ digitally reconstructed directly from the measured frames given at 242 (phase III) and 253 K (phase II). At 253 K, the satellite reflections are no longer observable and the indexing in phase II is correct. The phase transition III \rightarrow II occurs between 242 and 253 K.

The phase sequence $IV \rightarrow III \rightarrow II$ is complicated to understand because of the occurrence of the intermediate $B2_1$ phase (phase III).

Phase III is stable over a surprisingly wide temperature range of about 40 K. The reason why phase III can exist over a large temperature range is not yet understood.

The c direction corresponds to the direction of change in the phase sequence $IV \rightarrow III \rightarrow II$: $c = 16.050$ (2), 56.246 (5) and 8.047 (1) Å respectively given at 205, 213 and 253 K (see Figure 5.19).

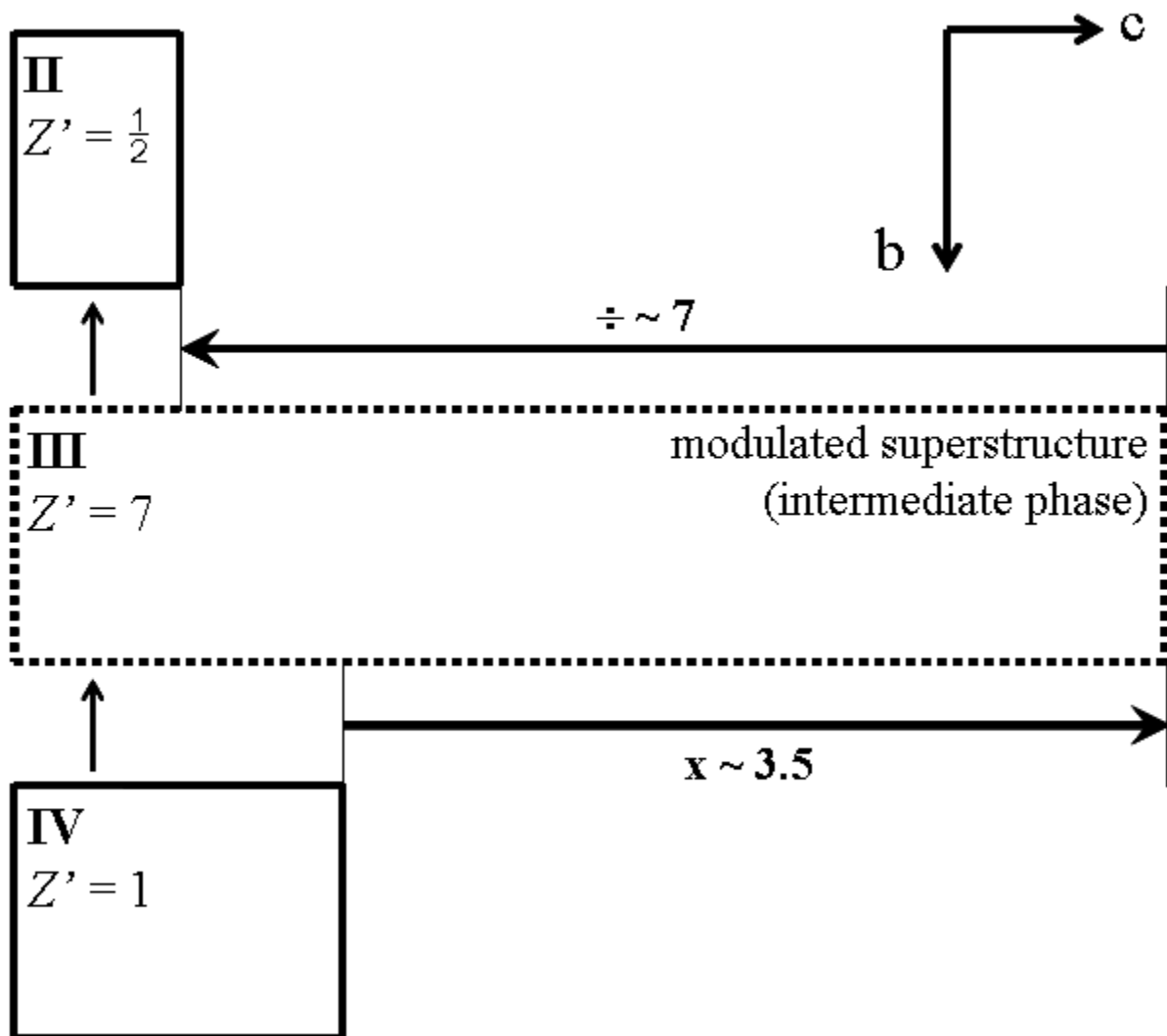


Figure 5.19. Projections of the unit cells down the *a* direction for phases II and IV and down the normal to the plane (1 0 0) for phase III. The drawing shows that the *c* direction corresponds to the direction of change in the phase sequence $\text{IV} \rightarrow \text{III} \rightarrow \text{II}$. At the phase transition $\text{IV} \rightarrow \text{III}$, the *c* dimension increases by a factor of approximately 3.5; at the phase transition $\text{III} \rightarrow \text{II}$, the *c* dimension shrinks by a factor of about 7.

II → I

At 295 K, the space group is the centrosymmetric $I2/m$ with $Z' = \frac{1}{4}$ (phase I). Phase I is disordered because the space group requires that the 15-crown-5 molecules have both the twofold and mirror symmetries. This phase was found to be stable between 295 and 308 K, and might be stable at temperatures slightly above 308 K.

The temperature of the phase transition II → I was checked by looking at the reciprocal lattice slices and by plotting the integrated intensities of the strongest $h0\ell$ reflections with $h + k + \ell = 2n + 1$ against the temperature. Part (a) of Figure 5.20 shows that the diffraction pattern changes in the T -range 290-295 K, in which the transition II → I takes place. At 290 K, the lattice is primitive (P) and there is no condition for systematic absences of reflections. At 295 K, the lattice is body-centered (I) and the $hk\ell$ reflections with $h + k + \ell = 2n + 1$ are systematically absent. The intensities of the ten strongest $h0\ell$ reflections with $h + k + \ell = 2n + 1$ were monitored between 250 and 303 K [see the part (b) of Figure 5.20]. The plot of the integrated intensities shows that the transition II → I takes place between 290 and 295 K, which is consistent with what it has been observed from the reciprocal lattice slices and, to a less extent, with the DSC measurements.

The order-disorder transition II → I occurs because the increase in $T\Delta S$ term ($\Delta S > 0$) outweighs the unfavorable ΔH term ($\Delta H > 0$). In phase I, the 15-crown-5 molecules can have four orientations. In phase II, the structure is less disordered although the 15-crown-5 molecules have two orientations. Disorder becomes larger as the temperature increases.

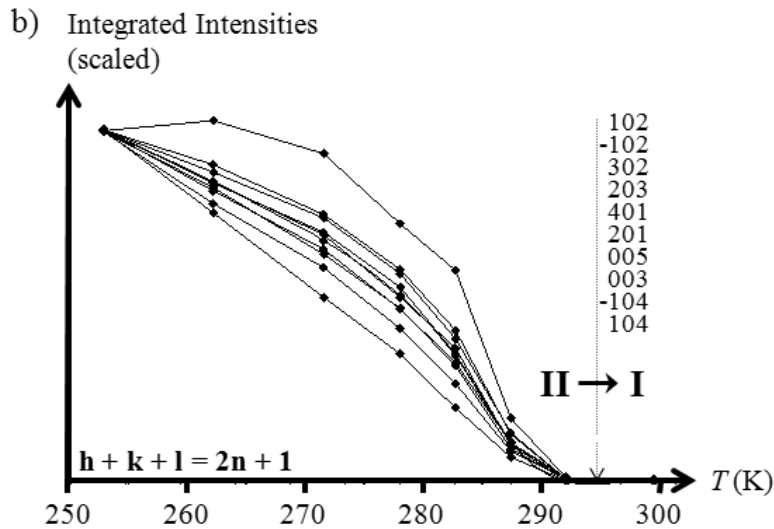
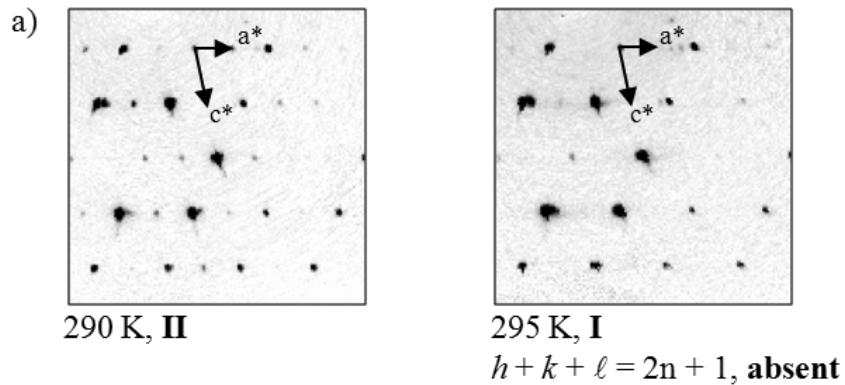


Figure 5.20. (a) Parts of the reciprocal lattice slices $h1\ell$ digitally reconstructed directly from the measured frames given at 290 (phase II) and 295 K (phase I). At 295 K, phase I is defined in the body-centered cell (*I*); as a result, the hkl reflections with $h + k + \ell = 2n + 1$ (*i.e.*, the $h1\ell$ reflections in the present case) are found to be absent from the diffraction pattern. The phase transition $\text{II} \rightarrow \text{I}$ occurs between 290 and 295 K. (b) Temperature dependence of the integrated intensities of the 10 strongest $h0\ell$ reflections with $h + k + \ell = 2n + 1$ monitored between 250 and 303 K. The plot shows that the integrated intensities are absent above 295 K, as a result, the phase transition $\text{II} \rightarrow \text{I}$ takes place between 290 and 295 K.

The Thermodynamics of the Phase Transitions

The three solid-solid phase transitions of the polymorphic system $[\text{Ni}(\text{H}_2\text{O})_6](\text{NO}_3)_2 \cdot (15\text{-crown-5}) \cdot 2\text{H}_2\text{O}$ are found to be first-order because of the occurrence of hysteresis (the hysteresis for the lowest-temperature phase transition is relatively large) and latent heat. At the transition points, ΔH_{tr} are non-zero (*i.e.*, there are discontinuities for the enthalpies at the phase transitions). In this study, one considers a system for which the temperature T can vary and the pressure P remains constant. The Gibbs free energy G is defined as a function of T . A phase transition takes place when ΔG_{tr} becomes negative (*i.e.*, the $T\Delta S_{\text{tr}}$ term outweighs the ΔH_{tr} term).

In this system, G_{I} , G_{II} , G_{III} and G_{IV} are the Gibbs free energies and H_{I} , H_{II} , H_{III} and H_{IV} are the enthalpies associated with the phases I, II, III and IV. When G_X ($X = \text{I, II, III}$ or IV) is the lowest at T , phase X is stable at T . As the crystals are heated, phase IV is stable below $T_{\text{IV} \rightarrow \text{III}}$, phase III is stable between $T_{\text{IV} \rightarrow \text{III}}$ and $T_{\text{III} \rightarrow \text{II}}$, phase II is stable between $T_{\text{III} \rightarrow \text{II}}$ and $T_{\text{II} \rightarrow \text{I}}$ and phase I is stable above $T_{\text{II} \rightarrow \text{I}}$ up to the temperature of decomposition of $[\text{Ni}(\text{H}_2\text{O})_6](\text{NO}_3)_2 \cdot (15\text{-crown-5}) \cdot 2\text{H}_2\text{O}$. The temperatures $T_{\text{IV} \rightarrow \text{III}}$, $T_{\text{III} \rightarrow \text{II}}$ and $T_{\text{II} \rightarrow \text{I}}$ are given when ΔG is zero (see Figure 5.21).

When crystals of $[\text{Ni}(\text{H}_2\text{O})_6](\text{NO}_3)_2 \cdot (15\text{-crown-5}) \cdot 2\text{H}_2\text{O}$ are flash-cooled, phase III is found to be metastable below $T_{\text{IV} \leftarrow \text{III}}$. In this case, the rate of reducing the thermal motion in the solid state must overcome the rate at which the molecules and ions can be rearranged from phase III to phase IV. This is an example where the kinetics overcomes the thermodynamics (Threlfall, 2003).

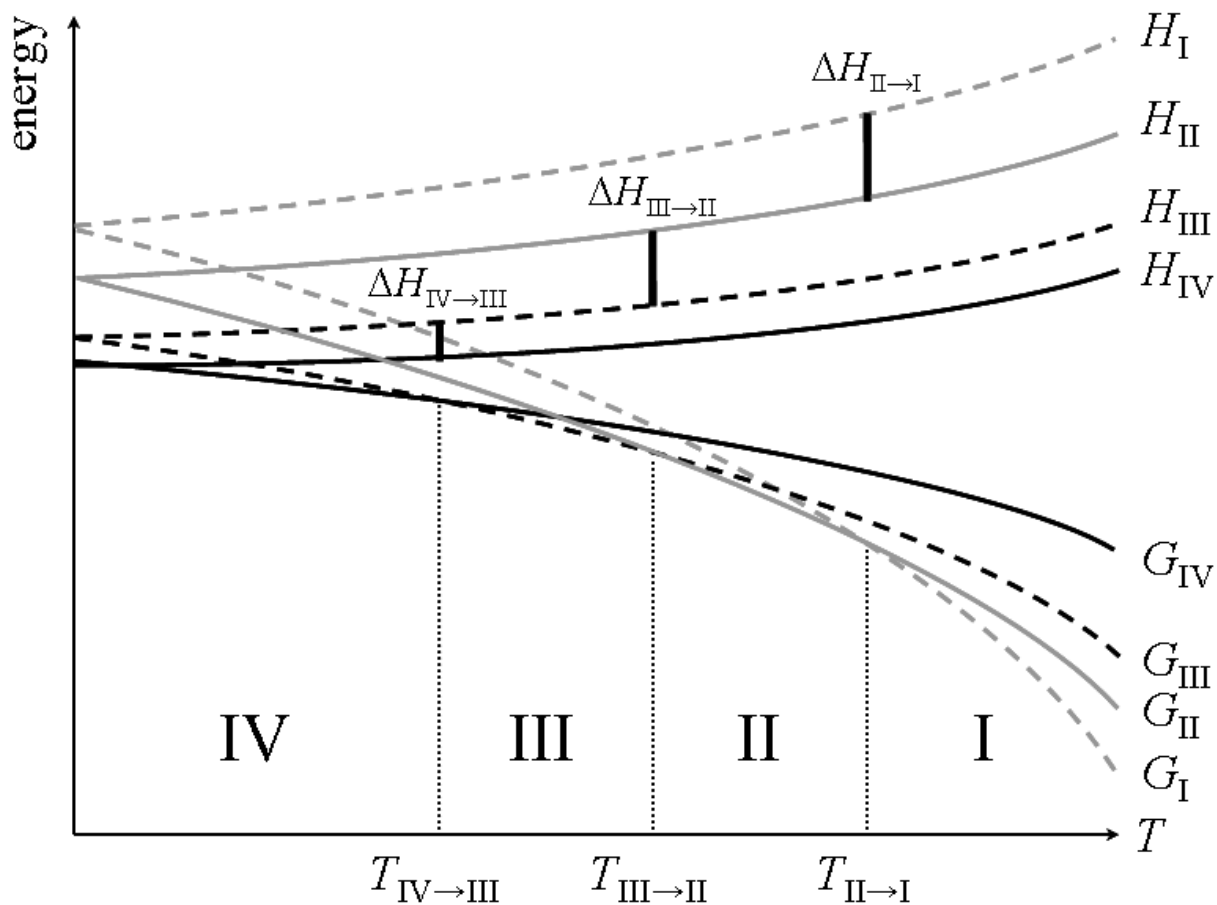


Figure 5.21. Schematic plots of the Gibbs free energy and enthalpy versus T in the polymorphic system $[\text{Ni}(\text{H}_2\text{O})_6](\text{NO}_3)_2 \cdot (15\text{-crown-5}) \cdot 2\text{H}_2\text{O}$. The Gibbs free energies G_{I} , G_{II} , G_{III} and G_{IV} and the enthalpies H_{I} , H_{II} , H_{III} and H_{IV} are defined for the phases I, II, III and IV. The phase X is stable at T when G_X is the lowest at T . The phase transitions $\text{IV} \rightarrow \text{III}$, $\text{III} \rightarrow \text{II}$ and $\text{II} \rightarrow \text{I}$ (shown as dotted lines) take place when $\Delta G_{\text{IV} \rightarrow \text{III}}$, $\Delta G_{\text{III} \rightarrow \text{II}}$ and $\Delta G_{\text{II} \rightarrow \text{I}}$ become negative. The temperatures $T_{\text{IV} \rightarrow \text{III}}$, $T_{\text{III} \rightarrow \text{II}}$ and $T_{\text{II} \rightarrow \text{I}}$ of the three phase transitions are given when $\Delta G_{\text{IV} \rightarrow \text{III}}$, $\Delta G_{\text{III} \rightarrow \text{II}}$ and $\Delta G_{\text{II} \rightarrow \text{I}}$ are zero. Discontinuities for the enthalpies are observed because the phase transitions of this system are first-order.

Conclusions

The existence of three solid-solid phase transitions occurring between 90 and 308 K makes the polymorphic system $[\text{Ni}(\text{H}_2\text{O})_6](\text{NO}_3)_2 \cdot (15\text{-crown-5}) \cdot 2\text{H}_2\text{O}$ very unusual. This system is remarkable because there is no major loss of crystallinity in the phase sequence. The phase sequence is described as a set of four phases (numbered as phases I, II, III and IV). Phase IV ($P2_1/c$, $Z' = 1$) is completely ordered and the two phases I ($I2/m$, $Z' = \frac{1}{4}$) and II ($P2_1/m$, $Z' = \frac{1}{2}$) are disordered because of symmetry constraints. Phase III ($B2_1$, $Z' = 7$), a commensurately modulated superstructure, is intermediate and the structure is ordered in some regions and disordered in other regions. This latter phase is best described as an intermediate structure because it contains regions of the two phases II and IV. This behavior is rare and poorly understood. The fact that phase III is stable over a relatively large range of temperature is very surprising.

The packing of the four phases remains surprisingly similar but structural changes occur along one direction (*i.e.*, the **c** direction) when thermal motion of the system decreases or increases.

The modulation in phase III may occur when competitive hydrogen bond interactions are present in the structure. However, this problem cannot be answered yet because the single-crystal X-ray experiments fail to locate the exact positions of some hydrogen atoms in phase III and in the disordered phases I and II. Location of all the H atoms may allow a better understanding of the phase transitions $\text{II} \leftrightarrow \text{III}$ and $\text{III} \leftrightarrow \text{IV}$.

Another result of this research involves locating with consistency the temperatures of the three solid-solid phase transitions. A method, which involves several techniques, has been described. DSC experiments and single-crystal X-ray experiments suggest that the phase transitions of this system are first-order. The temperature dependence of the cell dimensions, the examination of the reciprocal lattice slices near the transitions and the monitoring of the integrated intensities of some specific classes of reflections enable the finding of the transition temperatures within 5-10 K. Optical microscopy performed at low temperature may help to contribute a better understanding of the mechanisms of these transitions.

Chapter Six

-

[Ni(MeCN)(H₂O)₂(NO₃)₂](15-crown-5)·MeCN: An Analogous Polymorphic System to [Ni(H₂O)₆](NO₃)₂·(15-crown-5)·2H₂O

Introduction

Among the attempts to synthesize the target compound [Ni(H₂O)₂(15-crown-5)](NO₃)₂, the compound [Ni(H₂O)₂(MeCN)(NO₃)₂](15-crown-5)·MeCN was produced by replacing the water solution of 15-crown-5 and Ni(NO₃)₂·6H₂O by an acetonitrile solution in the original synthesis (see chemical equation 3.1 in Chapter 3). This compound belongs to a series of Ni(II) complexes (see Chapter 3) for which the Ni²⁺ ions are not coordinated by the 15-crown-5 molecule. In this series of Ni(II) complexes, the six ligands (*e.g.*, water, other solvent molecules and nitrate ions) are arranged around the Ni²⁺ ions in an octahedral geometry. No structure of the compound [Ni(H₂O)₂(MeCN)(NO₃)₂](15-crown-5)·MeCN has been reported in the literature.

The single-crystal X-ray experiments and the DSC measurements showed that the latter compound is a polymorphic system. Three reversible solid-solid phase transitions and four phases were found between 90 and 273 K. The phase sequence IV → III → II → I (defined in the order of increasing temperature), during which there is no significant loss of crystallinity, was investigated by a method aimed at characterizing two other polymorphic systems (see Chapters 4 and 5). The method is based on the analyses of the temperature dependences of the cell dimensions, careful inspection of the reciprocal lattice slices and plots of integrated intensities of specific classes of reflections as the system passes through a transition.

Phase IV is completely ordered and has $Z' = 2$. The amount of disorder observed in the system increases as the temperature rises. Phase III is partially disordered and has $Z' = 1$. Phase II is significantly disordered, has $Z' = 5$ and a commensurate modulation. Phase I is very disordered and has $Z' = \frac{1}{2}$. The high- Z' phase (*i.e.*, phase II) is an intermediate phase that is similar to phase III in some regions and similar to phase I in other regions. The packing remains very similar throughout the phase sequence and one-dimensional H-bonded chains of the 15-crown-5 molecules and the $[\text{Ni}(\text{MeCN})(\text{H}_2\text{O})_2(\text{NO}_3)_2]$ metal complexes are found along the *c* direction.

Analogies between the polymorphic systems $[\text{Ni}(\text{H}_2\text{O})_2(\text{MeCN})(\text{NO}_3)_2] \cdot (15\text{-crown-5}) \cdot \text{MeCN}$ and $[\text{Ni}(\text{H}_2\text{O})_6](\text{NO}_3)_2 \cdot (15\text{-crown-5}) \cdot 2\text{H}_2\text{O}$ (see Chapter 5) are also discussed.

Experimental

Crystal Growth

Details of the crystal growth were given in Chapter 3.

Differential Scanning Calorimetry Measurements

The compound $[\text{Ni}(\text{MeCN})(\text{H}_2\text{O})_2(\text{NO}_3)_2] \cdot (15\text{-crown-5}) \cdot \text{MeCN}$ was investigated using the DSC 822^e apparatus and the controlling software STARe (version 8.10) manufactured by *METTLER TOLEDO*. The sets of DSC measurements were made between 143 and 243 K. The DSC sample was prepared from fine powders contained in sealed aluminum crucibles. The amount of powdered sample was 3.89 mg. The cooling and heating rates were -5 or -10 K/min and 5 or 10 K/min. Between 143 and 243 K, one solid-solid phase transition was found: $T_{\text{onset}} = 219\text{-}220$ K (given for heating). The small peak heights in the DSC traces prevents a good estimation of ΔH_{tr} . The solid-solid phase transition is first-order because hysteresis occurs. Enthalpy is associated with such a transition. The DSC traces are shown in Figure 6.1.

X-ray Crystallography

The general procedures for data collection and for the H-atoms treatment were given in the corresponding section of Chapter 2.

All data were collected using a Nonius KappaCCD diffractometer with graphite-monochromated Mo $K\alpha$ radiation ($\lambda = 0.71073$ Å) under the program *COLLECT* (Nonius, 1997). The methoxy H-atoms of the acetonitrile ligands and of the acetonitrile lattice molecules were placed at calculated positions (*AFIX 137*) with isotropic displacement parameters having values 1.5 times U_{eq} of the attached C atom (see Chapter 2 for the other H-atoms treatment).

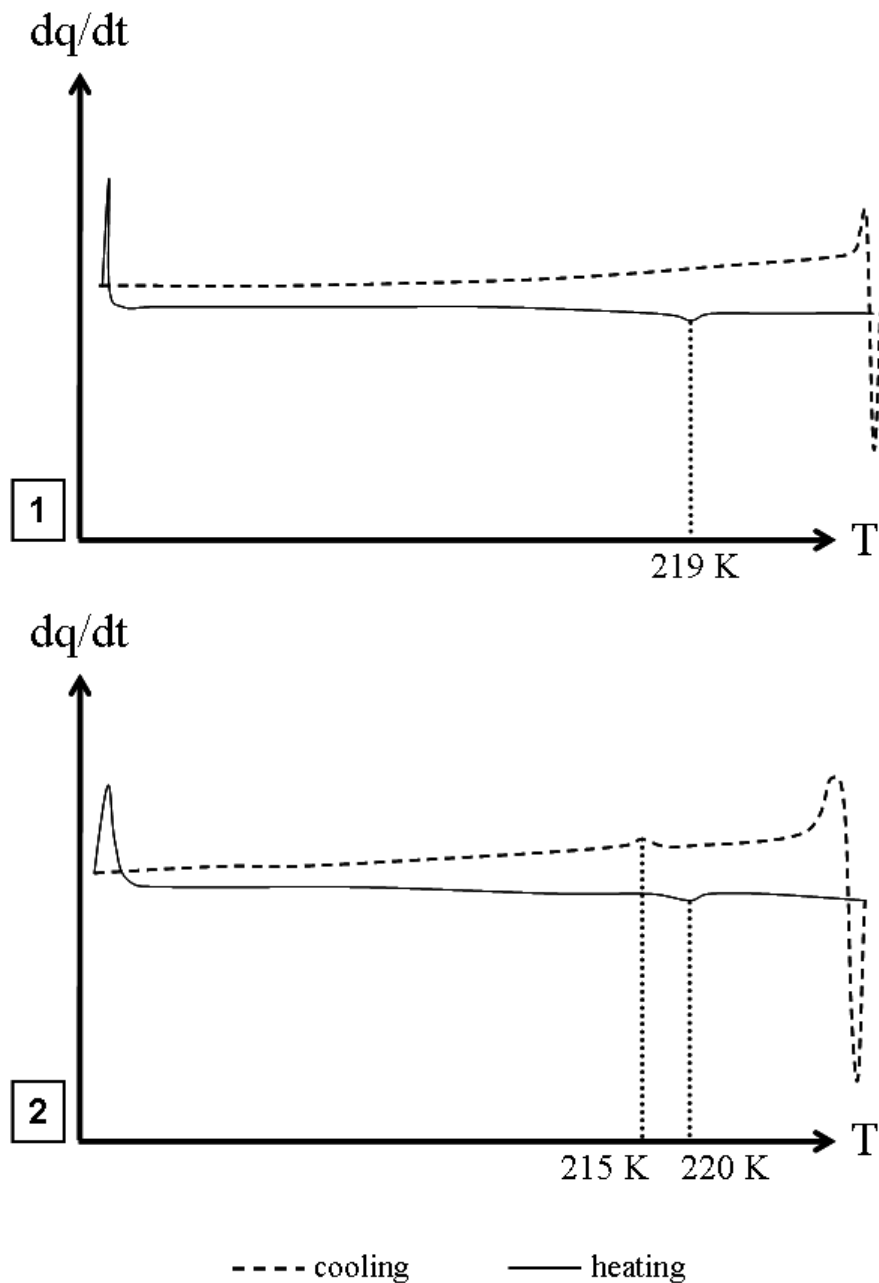


Figure 6.1. DSC traces of the compound $[\text{Ni}(\text{MeCN})(\text{H}_2\text{O})_2(\text{NO}_3)_2] \cdot (15\text{-crown-5}) \cdot \text{MeCN}$ made from 243 to 143 K at -5 K/min and from 143 to 243 K at 5 K/min (scheme 1). A second set of measurements was made using the cooling and heating rates -10 and 10 K/min (scheme 2). The measurements show one solid-solid phase transition near 217 K. The transition was not found as the sample was cooled at slower cooling rates (*i.e.*, at 5 K/min). The transition appears more obvious at faster cooling and heating rates. The solid-solid phase transition shows some hysteresis.

Generalities

In order to make comparisons between the four phases easier (*i.e.*, the one-dimensional H-bonded chains are along the same direction for the four phases), the cells of the phases I and II were reduced to the size of the smallest common cell (or pseudo-cell)⁷⁰ (see Figure 6.2). The atom-numbering scheme is consistent for all four phases.

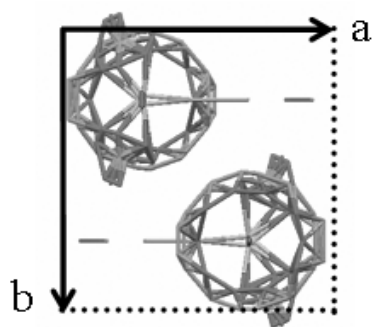
The structure of phase I was solved and refined in the relatively infrequent space group $P2_1/m$ (Brock & Dunitz, 1994) with $Z' = \frac{1}{2}$. The cell constants at 243 K of the standard primitive cell are: $a = 8.143$ (1)Å, $b = 12.339$ (2)Å, $c = 12.131$ (2)Å, $\beta = 105.51$ (1)°. The a and c axes were switched using the transformation matrix: $(0\ 0\ 1 / 0\ -1\ 0 / 1\ 0\ 0)$ so that the new cell was similar to the cell of phase III.

Phase II was originally described in the noncentrosymmetric space group $P2_1$ with five independent formula units ($Z' = 5$). The cell constants at 90 K of the standard primitive cell are: $a = 17.326$ (2)Å, $b = 12.185$ (1)Å, $c = 27.463$ (3)Å, $\beta = 100.19$ (1)°. The non-standard space group $B2_1$ was preferred so that H-bonded chains of Ni cations and 15-crown-5 molecules are found along the c direction, which is the direction of the chain in the other phases. The transformation matrix is given by: $\mathbf{a}(B2_1) = (0\ 0\ 1 / 0\ 1\ 0 / -2\ 0\ -1)\mathbf{a}(P2_1)$. The $Z' = 5$ phase is a racemic twin and the twinning was treated using the *TWIN* instruction with the matrix $(-1\ 0\ 0 / 0\ -1\ 0 / 0\ 0\ -1)$.

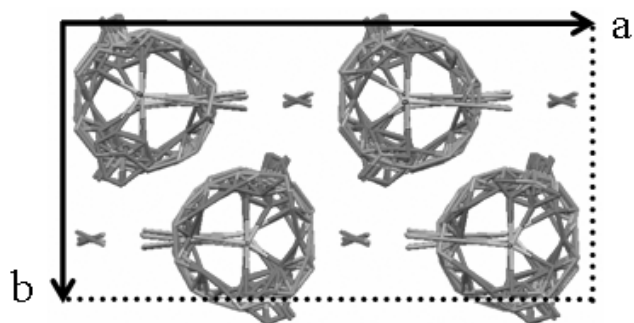
The structure of phase IV was solved and refined in the space group $P\bar{1}$ with two independent formula units ($Z' = 2$). Phase IV is a merohedral twin and the twinning was identified by using the program *PLATON* (Speck, 2005). The twin law is given by: $(-1\ 0\ 0 / 0\ 1\ 0 / 0\ 0\ -1)$, which corresponds to a twofold axis along the \mathbf{b} direction.

⁷⁰ The cell of phase III was chosen to be the cell of reference over the cell of phase IV because the structure of phase III is monoclinic (as the structures of the phases I and II) and the structure of phase IV is triclinic (but nearly monoclinic).

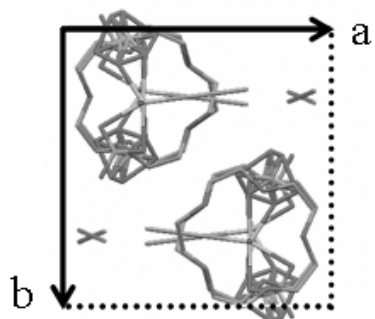
I, $Z' = \frac{1}{2}$



II, $Z' = 5$



III, $Z' = 1$



IV, $Z' = 2$

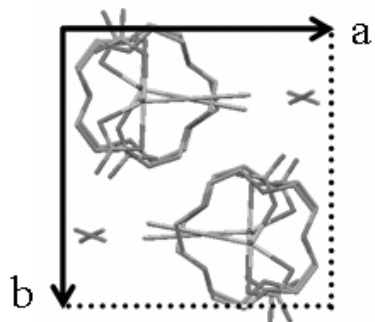


Figure 6.2. Projections of the four phases of $[\text{Ni}(\text{MeCN})(\text{H}_2\text{O})_2(\text{NO}_3)_2] \cdot (15\text{-crown-5}) \cdot \text{MeCN}$ down the c direction. For phases I, II and III, the a axis is not in the plane of the drawing. For phase IV, neither the a axis, nor the b axis is in the plane of the drawing, but the b axis is nearly in the plane. The drawing shows that the packing is very similar in the four phases.

Phase I

Data for phase I were collected near 243 K (see the section ‘Results and Discussion’ for further details). The asymmetric unit contains $\frac{1}{2}$ 15-crown-5 molecule, $\frac{1}{2}$ $[\text{Ni}(\text{MeCN})(\text{H}_2\text{O})_2(\text{NO}_3)_2]$ metal complex and $\frac{1}{2}$ lattice acetonitrile molecule.

The $[\text{Ni}(\text{MeCN})(\text{H}_2\text{O})_2(\text{NO}_3)_2]$ metal complex and the 15-crown-5 and the lattice acetonitrile molecules lie on sites with mirror symmetry. The crown ether is found to be very disordered. The partial disorder around the bond C5–C6 is forced by mirror symmetry. The 15-crown-5 molecule is also disordered around a pseudoinversion center [see part (a) of Figure 6.3].

In the six-coordinate metal complex $[\text{Ni}(\text{MeCN})(\text{H}_2\text{O})_2(\text{NO}_3)_2]$, one nitrate ion is monodentate and the other nitrate ion is bidentate. As a result of the mirror symmetry, the mono- and bidentate nitrate ions are disordered. Furthermore, two orientations are found for the monodentate nitrate ligand [see part (b) of Figure 6.3]. The metal complex $[\text{Ni}(\text{MeCN})(\text{H}_2\text{O})_2(\text{NO}_3)_2]$ is disordered because the axial ligands and the metal ion (O6–Ni–O7) do not lie exactly on the mirror plane. The effects of the disorder of the acetonitrile ligand and of the lattice acetonitrile molecule were absorbed into the displacement parameters.

The refinement against F^2 was good. The R factor [$F^2 > 2\sigma(F^2)$] is 0.040, the ellipsoids looked normal and the highest residual electron density peak is no more than $0.43 \text{ e } \text{\AA}^{-3}$. The treatment of the disorder in the space group $P2_1/m$ was challenging. The *DANG* instruction (*i.e.*, a bond distance restraint) was used as a geometric restraint for the disordered crown ether and the nitrate ligands. The *FLAT* instruction (*i.e.*, a geometric restraint for atoms that should lie on a common plane) was used for the nitrate ligands. The *DELU* instruction (*i.e.*, a rigid bond restraint) was applied to all atoms of the asymmetric unit to get a satisfactory refinement. The anisotropic displacement parameters (hereafter, ADPs) of the related disordered atoms of the crown ether and the nitrate ligands were constrained to be identical (*EADP* instruction). The value of the

occupancy factor given for the major component of the disorder of the crown ether is 0.667 (3). The occupancy factors of the C5 and C6 atoms of the 15-crown-5 molecule were 0.5 because of the requirements of the mirror symmetry. The values of the occupancy factors given for the disordered monodentate and bidentate nitrate ligands are respectively 0.221 (12), 0.279 (12) and 0.500 (the latter occupancy factor was fixed).

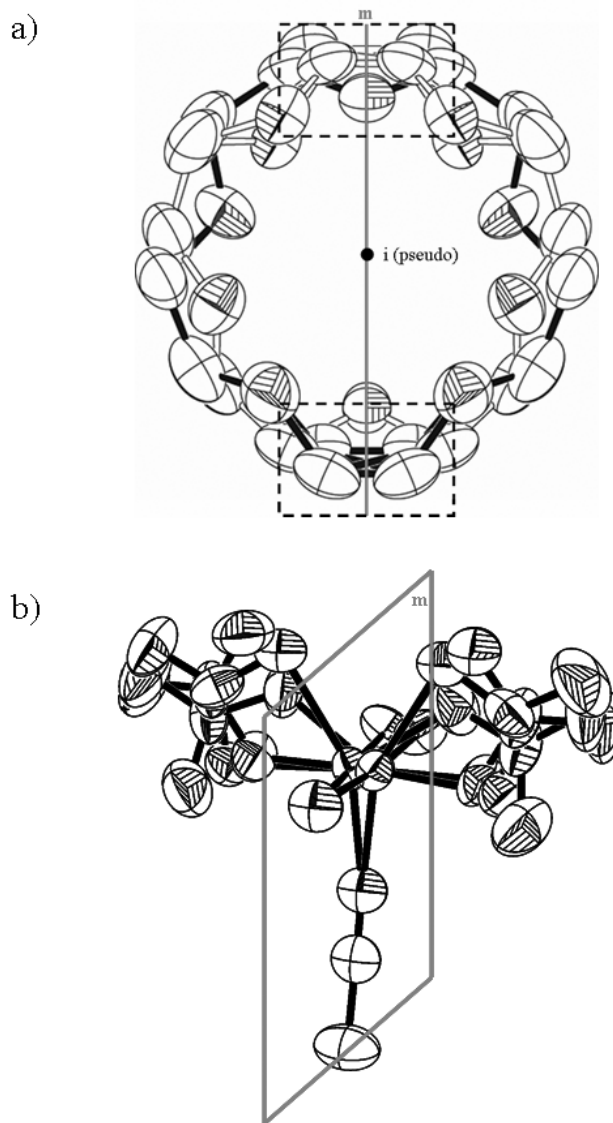


Figure 6.3. (a) Drawing showing the full disorder of the 15-crown-5 molecule in phase I. The major and minor components of the disorder are related by a pseudoinversion center (i). The two dashed boxes indicate the disorder imposed by mirror symmetry (m). The displacement ellipsoids are drawn at the 50 % probability level as determined at 243 K. The H atoms are omitted for clarity. (b) Drawing showing the disordered metal complex $[\text{Ni}(\text{MeCN})(\text{H}_2\text{O})_2(\text{NO}_3)_2]$ in phase I. Because of the mirror symmetry (m), the nitrate ions are found to be disordered in three orientations: one orientation for the bidentate nitrate ligand and two orientations for the monodentate nitrate ligand. The disorder of the acetonitrile ligand is absorbed into the displacement parameters. The displacement ellipsoids are drawn at the 50 % probability level as determined at 243 K. The H atoms are omitted for clarity.

Phase II

Phase II is an unusual superstructure with five crystallographically independent units (II, $B2_1$, $Z' = 5$). This phase was found to be metastable at 90 K⁷¹ after crystals had been flash-cooled from room temperature and was found to be stable between approximately 231 and 241 K (see the section ‘Results and Discussion’ for further details). Collecting data at lower temperatures presents the advantage of raising the number of reflections having $I > 2\sigma(I)$. Near 90 K, 47.6 % of the reflections have $I > 2\sigma(I)$. No data were collected between 231 and 241 K because the superstructures reflections were too weak to be correctly indexed (see Figure 6.4).

The refinement of phase II was complicated because of the large amount of disorder and the high degree of pseudosymmetry observed in the structure. The pseudosymmetries correspond to pseudoglide planes in some regions of the structure and pseudomirror planes and pseudoinversion centers in other regions of the structure. The regions with the pseudoglide plane symmetry are found to be slightly disordered because the monodentate nitrate ligands for three crystallographically independent $[\text{Ni}(\text{MeCN})(\text{H}_2\text{O})_2(\text{NO}_3)_2]$ metal complexes can take two orientations (see phase III for further details); these regions are similar to the structure of phase III. The regions with the pseudomirror plane and pseudoinversion symmetries are disordered in the same way as in phase I (see phase I for further details). In these regions, the major and minor components for two disordered $[\text{Ni}(\text{MeCN})(\text{H}_2\text{O})_2(\text{NO}_3)_2]$ metal complexes are related *via* pseudomirror symmetry; the major and minor components for three disordered 15-crown-5 molecules are related *via* pseudoinversion symmetry. The partial disorder required by pseudomirror symmetry around one C–C bond⁷² is also observed in one of the three disordered 15-crown-5 molecules.

⁷¹ 90 K is near the lower limit of stable temperature control when the cooling device is running with liquid nitrogen.

⁷² The corresponding carbon atoms are named C5 and C6. The atoms C5M and C6M are mirror images of the atoms C5 and C6.

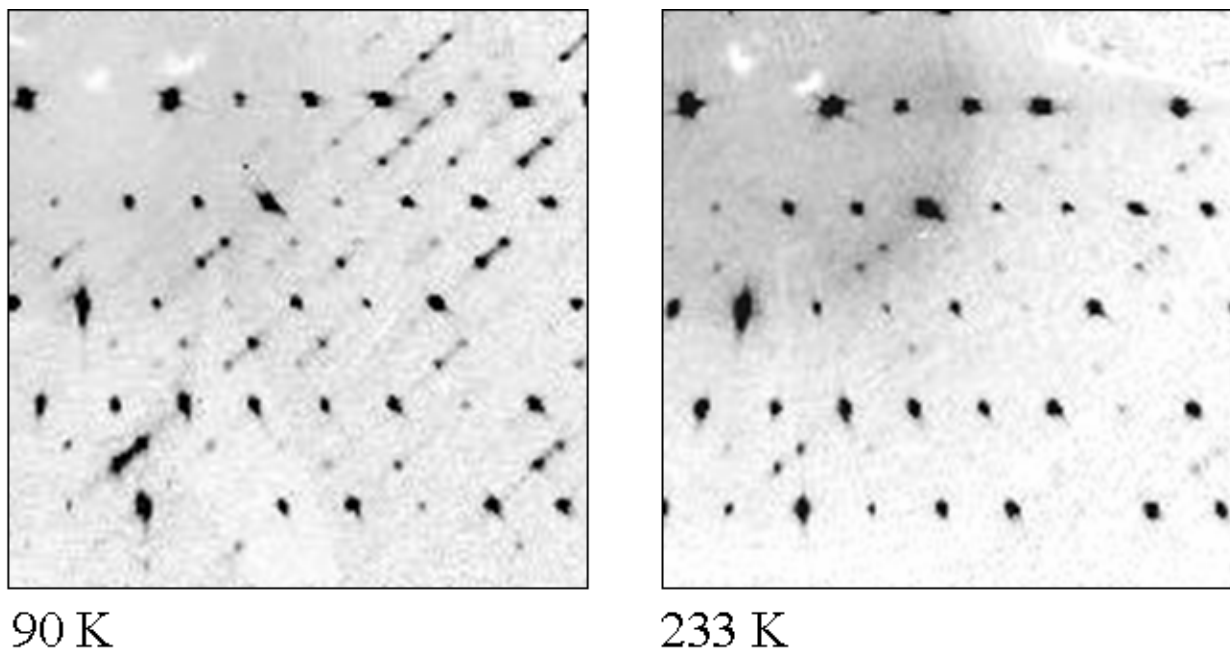


Figure 6.4. Parts of the reciprocal lattice slices $h1\ell$ digitally reconstructed directly from the measured frames for phase II ($B2_1, Z' = 5$) at 90 and 233 K. At 90 K, the ratio of reflections having $I > 2\sigma(I)$ is significantly larger than that given at 233 K (this ratio is undetermined at 233 K because the superstructures reflections were too weak to be correctly indexed). No quantitative comparison between the two data sets could be made because superstructures reflections at 233 K were not indexed. The indexing was done in the pseudocell (*i.e.*, only the most intense reflections were indexed). Diffuse scattering (or non-Bragg scattering) is only observed at 90 K between the most intense superstructure reflections.

The anisotropic displacement parameters (hereafter, ADPs) of all independent atoms related by pseudoglide and pseudomirror planes could not be constrained to be identical using the *EADP* instruction because the orientations of the displacement ellipsoids for atoms related by pseudoglide and pseudomirror planes are different. The ADPs of all independent atoms related by pseudosymmetry were set as free variables⁷³ (*FVAR* instruction). The relationship between the displacement parameters for atoms related by pseudoglide and pseudomirror planes is defined by the transformation matrix⁷⁴ $\begin{pmatrix} -1 & 0 & 0 & / & 0 & 1 & 0 & / & 0 & 0 & -1 \end{pmatrix}$. The displacement parameters for atoms related by pseudoinversion symmetry are the same. Three sets of ADPs for all independent atoms related by pseudosymmetry were used in the refinement process: one set⁷⁵ (of 14×6 values) for the atoms of the five independent 15-crown-5 molecules, one set (of 14×6) for the atoms of the five independent [Ni(MeCN)(H₂O)₂(NO₃)₂] metal complexes and one set (of 3×6 values) for the atoms of the five independent acetonitrile lattice molecules. The total number of free variables used to describe the atomic displacements was (14+14+3)*6 = 186. The displacement parameters of the Ni²⁺ ions of the ordered [Ni(MeCN)(H₂O)₂(NO₃)₂] metal complexes (*i.e.*, three out of the five metal complexes are ordered) were refined independently.

The refinement against F^2 was satisfactory. The *R* factor [$F^2 > 2\sigma(F^2)$] is 0.058, the ellipsoids look normal and the final difference Fourier map showed no peak larger than 0.70 e Å⁻³. The largest peaks were located near some oxygen atoms of some nitrate ligands. The geometries of all independent 15-crown-5 molecules, [Ni(MeCN)(H₂O)₂(NO₃)₂] metal complexes and lattice acetonitrile molecules were restrained to be similar using the *SAME* instruction. The consistency of chemically equivalent bond distances⁷⁶ for all 15-crown-5 molecules, [Ni(MeCN)(H₂O)₂(NO₃)₂] metal complexes and lattice acetonitrile molecules was good; the estimated standard

⁷³ The same method was used in the refinement of the structure of phase III of [Ni(H₂O)₆](NO₃)₂·(15-crown-5)·2H₂O (see Chapter 5 for further details).

⁷⁴ The signs of the off diagonal elements U_{12} and U_{23} are changed *via* the transformation matrix $\begin{pmatrix} -1 & 0 & 0 & / & 0 & 1 & 0 & / & 0 & 0 & -1 \end{pmatrix}$. The elements U_{11} , U_{22} , U_{33} and U_{13} remain unchanged.

⁷⁵ The set corresponds to the six displacement parameters for 14 atoms of the crown ether. The displacement parameters of the C5 and C6 atoms were constrained to be related via the transformation matrix $\begin{pmatrix} -1 & 0 & 0 & / & 0 & 1 & 0 & / & 0 & 0 & -1 \end{pmatrix}$.

⁷⁶ The analysis excludes the hydrogen atoms.

deviations for the sets of chemically equivalent distances averaged about 2.2 times the average uncertainty of an individual measurement. The *DANG* and *FLAT* instructions were used as geometric restraints for the nitrate ligands. The *DANG* instruction was also used to restrain the Ni–O distances to be within acceptable ranges⁷⁷; this helped the refinement of the atomic coordinates for disordered nitrate ligands. The values of the occupancy factors given for the major components of the three disordered 15-crown-5 molecules⁷⁸ are 0.853 (2), 0.812 (3) and 0.859 (3). The occupancy factor of the atoms C5, C6, C5M and C6M of the second disordered crown ether were approximated to be 0.406 (*i.e.*, 0.812/2) because of the requirements of the mirror symmetry. The values of the occupancy factors given for the major components of the three disordered monodentate nitrate ligands⁷⁹ are 0.707 (5), 0.541 (4) and 0.785 (4). The values of the occupancy factors given for the major components of the two disordered [Ni(MeCN)(H₂O)₂(NO₃)₂] metal complexes are 0.852 (3) and 0.573 (3). The occupancy factors of the acetonitrile ligands for the two disordered [Ni(MeCN)(H₂O)₂(NO₃)₂] metal complexes were approximated to be 1.0 since there was not enough information from the difference Fourier map to resolve the disorder of the acetonitrile ligand. The *SUMP* instruction was used to resolve the disorder of the monodentate nitrate ligand observed in the major component of the less disordered [Ni(MeCN)(H₂O)₂(NO₃)₂] metal complex (because there is partial overlap between the disordered monodentate nitrate ligand of the major component and the bidentate nitrate ligand of the minor component). The values of the occupancy factors given for the disordered monodentate nitrate ligands are 0.312 (3) and 0.559 (4). The value of the occupancy factor given for the bidentate nitrate ligand is 0.129 (4). No disorder of the monodentate nitrate ligands could be resolved for the major and minor components of the more disordered [Ni(MeCN)(H₂O)₂(NO₃)₂] metal complex. The total number of occupancy factors refined was 11.

⁷⁷ Most Ni–O distances in the $Z' = 5$ structure were found to vary between 2.00 and 2.10 Å.

⁷⁸ The minor and major components of the disordered 15-crown-5 molecules are related by pseudoinversion centers.

⁷⁹ This only concerns the monodentate nitrate ligands of the [Ni(MeCN)(H₂O)₂(NO₃)₂] metal complexes found in the regions that are similar to the structure of phase III.

An examination of classes of reflections along the \mathbf{c}^* direction was done using Wilson plots. The systematic classes of strong and weak reflections are the following: the $\ell = 5n$ reflections (primary reflections) are the strongest, whereas the $\ell = 5n \pm 1$ reflections are very weak; the $\ell = 5n \pm 2$ reflections are intermediate (see Figure 6.5). Qualitative observations obtained from a careful inspection of the reconstructed reciprocal lattice slices are consistent with previous results (see Figure 6.6). Because all primary and superstructure reflections were indexed without any problem at 90 K, there was no evidence of an incommensurate superstructure for phase II, but there are signs of significant diffuse scattering along the $\mathbf{a}^* - \mathbf{c}^*$ (or $-\mathbf{a}^* + \mathbf{c}^*$) direction. The reconstructed reciprocal lattice slices were obtained using the program *PRECESSION* (Nonius, 1997).

The displacement ellipsoids of all atoms in the asymmetric unit of phase I and one formula unit of phase II are shown in Figure 6.7. The crystallographic data for the phases I and II of the compound $[\text{Ni}(\text{H}_2\text{O})_2(\text{MeCN})(\text{NO}_3)_2] \cdot (15\text{-crown-5}) \cdot \text{MeCN}$ are given in Table 6.1.

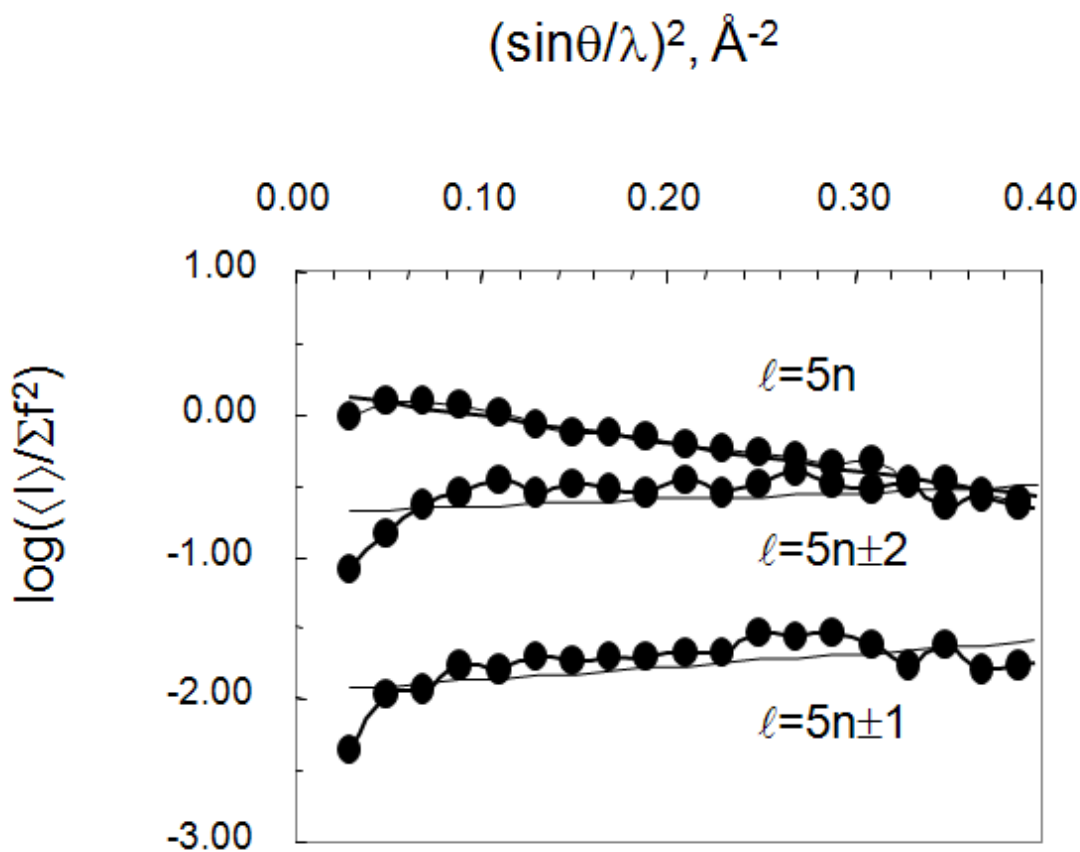


Figure 6.5. Separate Wilson plots for phase II ($B2_1$, $Z' = 5$) at 90 K. The reflections are divided into several classes with respect to the Miller index ℓ (i.e., $\ell = 5n$, $5n \pm 1$, etc.). The intensities of the primary reflections ($\ell = 5n$) are systematically stronger than the intensities of the superstructure reflections ($\ell = 5n \pm 1$, $5n \pm 2$). The $\ell = 5n \pm 1$ are systematically the weakest superstructure reflections. The $\ell = 5n \pm 2$ reflections are intermediate.

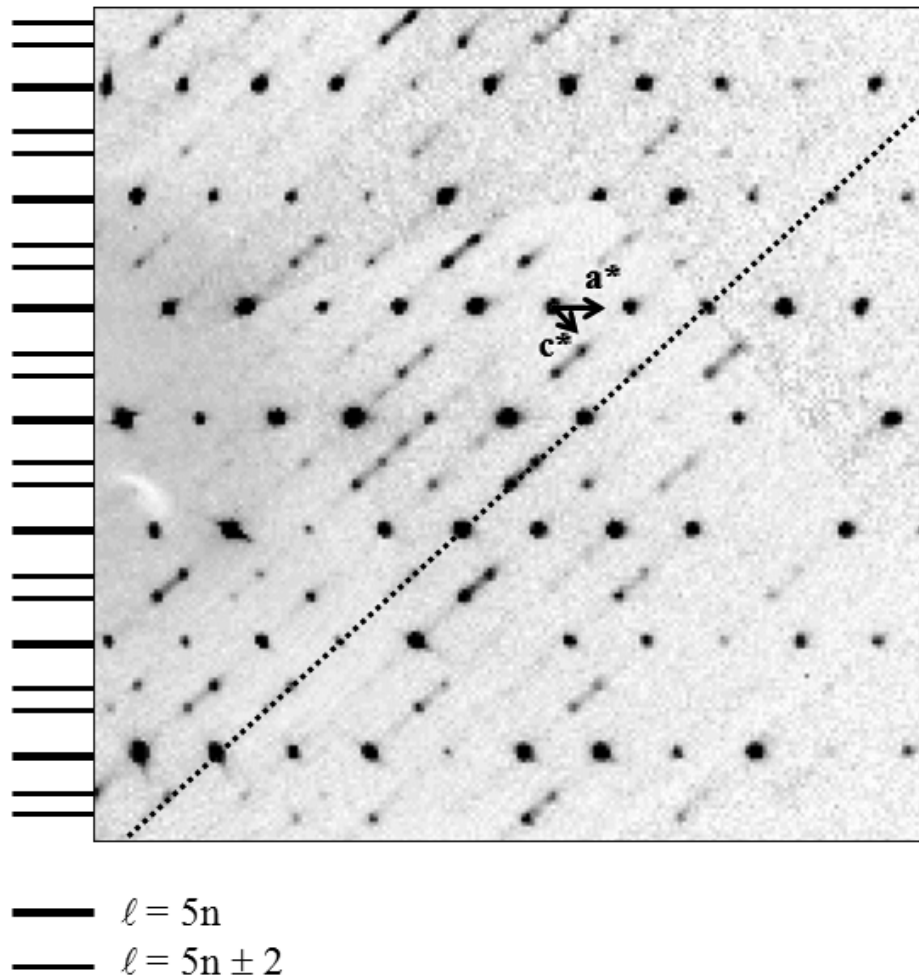
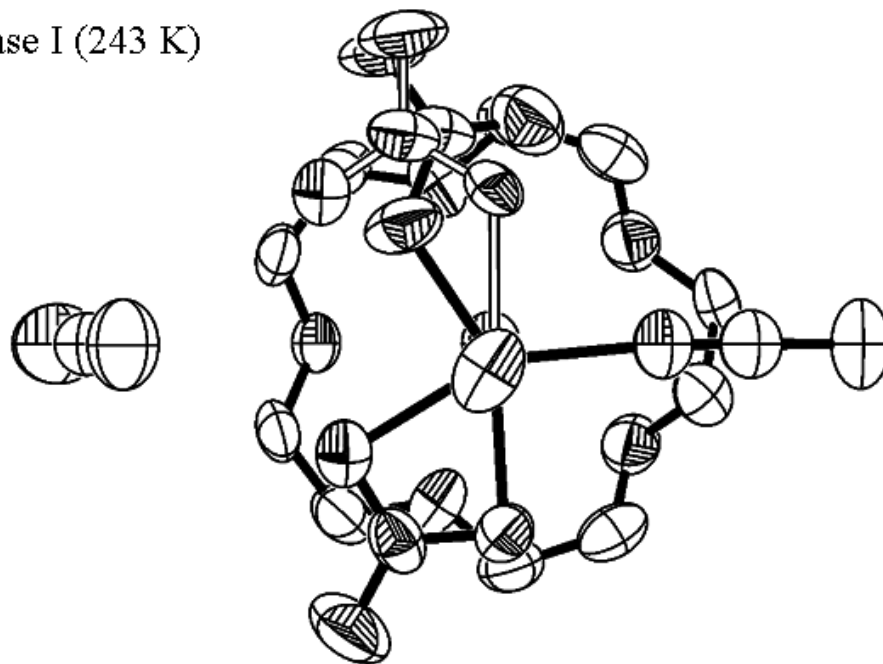


Figure 6.6. Part of the reciprocal lattice slice $h1 \ell$ digitally reconstructed directly from the measured frames for phase II ($B2_1$, $Z' = 5$). Systematic classes of strong and weak reflections are observed. The $\ell = 5n$ reflections are the strongest, the $\ell = 5n \pm 1$ reflections are very weak. The $\ell = 5n \pm 2$ reflections are intermediate. The satellite reflections (*i.e.*, the reflections with $\ell = 5n \pm 1$ and $\ell = 5n \pm 2$) are densest along the $\mathbf{a}^* - \mathbf{c}^*$ direction (shown as a black dotted line) in the $B2_1$ setting. The positions of the strongest class of reflections are indicated by thick solid lines. The positions of the intermediate class of reflections are shown by thinner solid lines. The positions of the weakest class of reflections are omitted for clarity. The diffuse scattering (non-Bragg scattering) may indicate short range order in phase II. The diffuse scattering is found along the $\mathbf{a}^* - \mathbf{c}^*$ (or $-\mathbf{a}^* + \mathbf{c}^*$) direction.

Phase I (243 K)



Phase II (90 K)
metastable

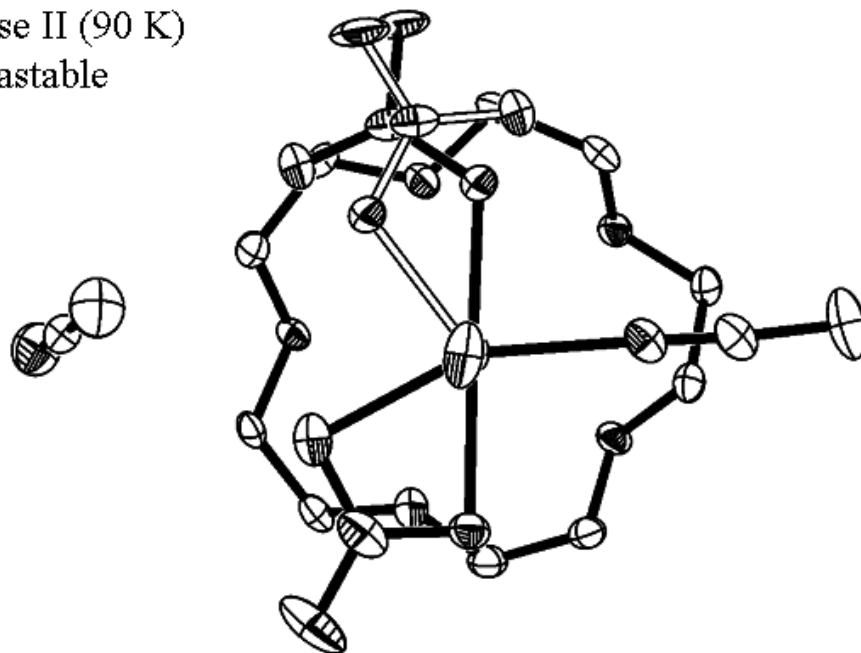


Figure 6.7. The displacement ellipsoids (50% probability level) of the asymmetric unit and one formula unit of the compound $[\text{Ni}(\text{H}_2\text{O})_2(\text{MeCN})(\text{NO}_3)_2] \cdot (15\text{-crown-5}) \cdot \text{MeCN}$ respectively in phase I at 243 K and in phase II at 90 K. Phase II is metastable at 90 K. Only the disorder of the monodentate nitrate ligands observed in the phases I and II are shown, the disorder of the crown molecules are not shown. H atoms are omitted for clarity.

Table 6.1. Crystallographic data for the phases I and II of $[\text{Ni}(\text{MeCN})(\text{H}_2\text{O})_2(\text{NO}_3)_2] \cdot (15\text{-crown-5}) \cdot \text{MeCN}$.

	I	II
Crystal data		
Chemical formula	$(\text{C}_{10}\text{H}_{20}\text{O}_5) \cdot (\text{C}_2\text{H}_7\text{N}_3\text{NiO}_8) \cdot (\text{C}_2\text{H}_3\text{N})$	
M_r	521.13	521.13
Cell setting, space group	Monoclinic, $P2_1/m$	Monoclinic, $B2_1$
a, b, c (Å) ⁸⁰	12.131 (2) 12.339 (2) 8.143 (1)	27.463 (2) 12.184 (1) 40.229 (3)
β (°)	105.51 (1)	122.03 (1)
V (Å ³)	1174.5 (3)	11411.8 (15)
$Z; Z'$	2; $\frac{1}{2}$	20; 5
D_x (g cm ⁻³)	1.474	1.515
Radiation type	Mo $K\alpha$	Mo $K\alpha$
No. of reflections for cell parameters	2826	13682
θ range (°)	1.0–27.5	1.0–27.5
μ (mm ⁻¹)	0.89	0.92
Temperature (K)	243 (1)	90.0 (2)
Crystal form, colour	parallelepiped, pale green	parallelepiped, pale green
Crystal size (mm)	0.25 × 0.12 × 0.10	0.30 × 0.20 × 0.18
Data collection		
Diffractometer	Nonius KappaCCD	Nonius KappaCCD
Data collection method	ω scans at fixed $\chi = 55^\circ$	ω scans at fixed $\chi = 55^\circ$
Absorption correction	Multi-scan (based on symmetry-related measurements)	
T_{\min}	0.807	0.770

⁸⁰ The estimated errors in the unit cell constants (a , b , c and β) were modified by multiplying the experimental estimated standard uncertainties (*i.e.*, su's) by at least a factor of ~5 for a , b , c and by at least a factor of ~12.5 for β . These factors were used in order to approximate the errors in the unit cell constants from one crystal to another (Herbstein, 2000).

Table 6.1. (continued)

T_{\max}	0.916	0.852
No. of measured, independent and observed parameters	5341, 2827, 1738	25889, 25889, 12328
Criterion for observed reflections	$I > 2\sigma(I)$	$I > 2\sigma(I)$
R_{int}	0.033	0.085
θ_{\max} (°)	27.5	27.5
Range of h, k, ℓ	$-15 < h < 15$ $-16 < k < 15$ $-10 < \ell < 10$	$-35 < h < 35$ $-15 < k < 15$ $-52 < \ell < 52$
Refinement		
Refinement on	F^2	F^2
$R[F^2 > 2\sigma(F^2)], wR(F^2), S$	0.040, 0.115, 1.02	0.058, 0.146, 1.01
No. of reflections	5341	25889
No. of parameters	321	962
H-atom treatment		Constrained to parent site
Weighting scheme	Calculated $w = 1/[\sigma^2(F_o^2) + (0.061P)^2 + 0.0469P]$ where $P = (F_o^2 + 2F_c^2)/3$	Calculated $w = 1/[\sigma^2(F_o^2) + (0.050P)^2]$ where $P = (F_o^2 + 2F_c^2)/3$
$(\Delta/\sigma)_{\max}$	0.001	0.002
$\Delta\rho_{\max}, \Delta\rho_{\min}$ (e Å ⁻³)	0.43, -0.25	0.70, -0.51
Absolute Structure		Flack H D (1983), Acta Cryst. A39, 876-881
Flack parameter		undetermined because racemic twin

Computer programs: *COLLECT* (Nonius, 1997); *DENZO-SMN* (Nonius, 1997); *SHELXS-97* (Sheldrick, 1990); *SHELXL-97* (Sheldrick, 1997); *XP in SHELXTL* (Bruker, 1995); *SHELX-97* and local procedures.

Phase III

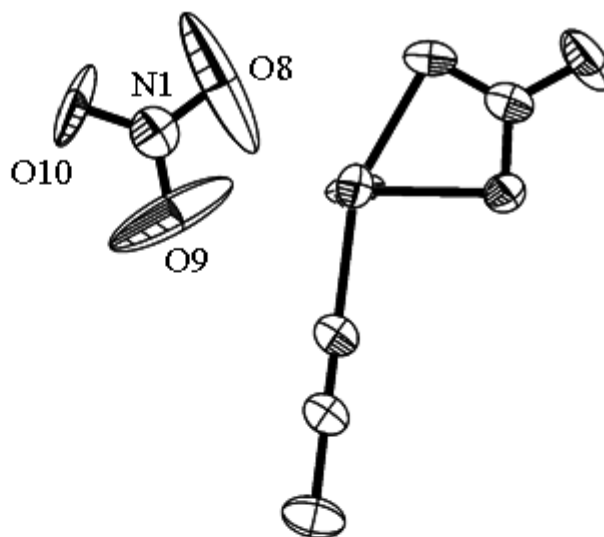
Data for phase III were collected near 150 K (see the section ‘Results and Discussion’ for further details) after the crystal had been slowly cooled from room temperature at -2 K/min. The structure of this phase was solved and refined in the space group $P2_1/c$ with $Z' = 1$. The asymmetric unit contains one 15-crown-5 molecule, one $[\text{Ni}(\text{MeCN})(\text{H}_2\text{O})_2(\text{NO}_3)_2]$ metal complex and one lattice acetonitrile molecule.

The structure is mostly ordered but the monodentate nitrate ligand was found to be disordered; either of the two oxygen atoms (O8 or O9) is a potential ligand donor. As a result, the monodentate nitrate ligand can take two different orientations.

A first refinement against F^2 of an ordered structure was not satisfactory. The R factor [$F^2 > 2\sigma(F^2)$] was 0.069 and the final Fourier map showed peaks as large as $2.21 \text{ e } \text{\AA}^{-3}$ (the two largest peaks were located at 0.71 \AA from the atom O9 and 0.59 \AA from the atom O8). Eccentric ellipsoids of the N1, O8, O9 and O10 atoms were warning signs suggesting disorder of the monodentate nitrate ligand.

The inclusion of the disorder makes the refinement against F^2 better. The R factor [$F^2 > 2\sigma(F^2)$] is less than 0.040, the ellipsoids looked normal and the highest residual electron density peak is no more than $0.60 \text{ e } \text{\AA}^{-3}$. The two largest peaks were located at 1.64 \AA from the O8 atom of the monodentate nitrate ligand and 0.96 \AA from Ni^{2+} ion but were not physically meaningful. Other peaks were found to be less than $0.30 \text{ e } \text{\AA}^{-3}$. The treatment of the disorder of the monodentate nitrate ligand was straightforward. The *FLAT* and *DANG* instructions were used as geometric restraints for the disordered monodentate nitrate ligand. The ADPs of the related disordered atoms N1/N1' and O10/O10' were constrained to be identical (*EADP* instruction) because they were very close together. The value of the occupancy factor given for the major component of the disorder is 0.525 (4). Figure 6.8 shows the ellipsoids of all atoms of the $[\text{Ni}(\text{MeCN})(\text{H}_2\text{O})_2(\text{NO}_3)_2]$ metal complex with and without the inclusion of the disorder.

Phase III (150 K),
without disorder



Phase III (150 K),
with disorder

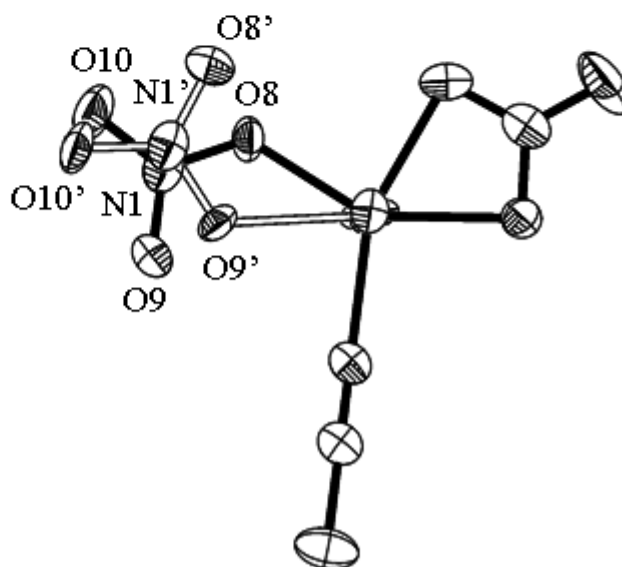


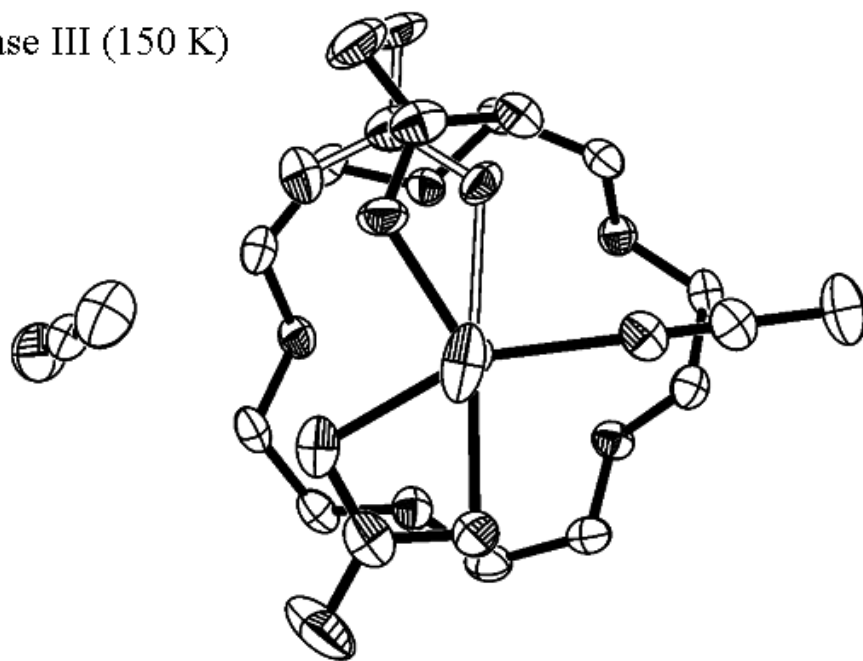
Figure 6.8. The displacement ellipsoids (50% probability level) of the $[\text{Ni}(\text{MeCN})(\text{H}_2\text{O})_2(\text{NO}_3)_2]$ metal complex in phase III at 150 K without and with the disorder of the monodentate nitrate ligand. The displacement ellipsoids of the N1, O8, O9 and O10 atoms are very eccentric without the inclusion of the disorder. The coordination of the monodentate nitrate ligand is not shown in the top drawing. The H atoms are omitted for clarity.

Phase IV

The lowest-temperature phase of the compound $[\text{Ni}(\text{MeCN})(\text{H}_2\text{O})_2(\text{NO}_3)_2] \cdot (15\text{-crown-5}) \cdot \text{MeCN}$ (IV, $P\bar{1}$, $Z' = 2$) was found at 90 K when the crystal had been slowly cooled from room temperature at -2 K/min. The structure at 90 K was treated as a completely ordered phase and the atomic displacement ellipsoids are small. Because of the pseudomerohedral twinning, phase IV is nearly monoclinic. The refinement was problem-free but the final difference Fourier map showed residual electron density with peaks as large as $0.77 \text{ e } \text{\AA}^{-3}$ (the three largest peaks were located at 0.96, 1.06 and 1.00 \AA from the two independent crystallographically independent Ni^{2+} ions). Peaks that are not near the metal-ions were less than $0.62 \text{ e } \text{\AA}^{-3}$ and are located at 1.23-1.37 \AA from the O8 and O9 atoms, but were not physically meaningful. The refinement of the twin model was also straightforward. The fractional contribution of the major twin component (or the *BASF* batch scale factor) refined to 0.429(1).

The ellipsoids of all atoms in the asymmetric unit of the phases III and IV are shown in Figure 6.9. The crystallographic data for the phases III and IV of the compound $[\text{Ni}(\text{MeCN})(\text{H}_2\text{O})_2(\text{NO}_3)_2] \cdot (15\text{-crown-5}) \cdot \text{MeCN}$ are given in Table 6.2.

Phase III (150 K)



Phase IV (90 K)

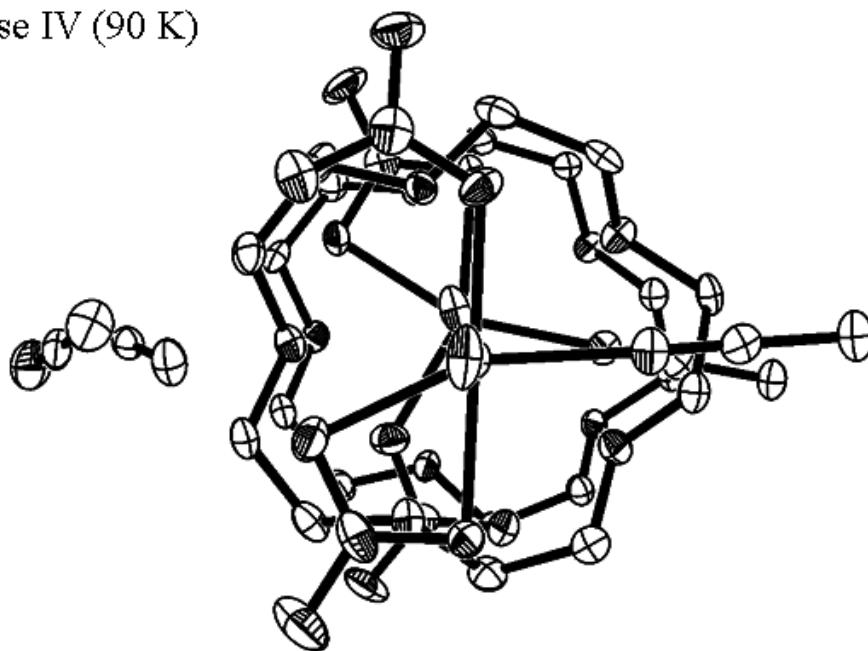


Figure 6.9. The displacement ellipsoids (50 % probability level) of the asymmetric units of phase III (at 150 K) and phase IV (at 90 K) of the compound $[\text{Ni}(\text{MeCN})(\text{H}_2\text{O})_2(\text{NO}_3)_2] \cdot (15\text{-crown-}5) \cdot \text{MeCN}$. The disorder of the monodentate nitrate ligand observed in phase III is shown. H atoms are omitted for clarity.

Table 6.2. Crystallographic data for the phases III and IV of [Ni(MeCN)(H₂O)₂(NO₃)₂]·(15-crown-5)·MeCN.

	III	IV
Crystal data		
Chemical formula	(C ₁₀ H ₂₀ O ₅). (C ₂ H ₇ N ₃ NiO ₈). (C ₂ H ₃ N)	
<i>M_r</i>	521.13	521.13
Cell setting, space group	Monoclinic, <i>P</i> 2 ₁ / <i>c</i>	Triclinic, <i>P</i> $\bar{1}$
<i>a</i> , <i>b</i> , <i>c</i> (Å) ⁸¹	12.164 (1) 12.183 (1) 16.089 (1)	12.144 (1) 12.137 (1) 16.039 (1)
α , β , γ (°)	90.00 105.46 (1) 90.00	90.12 (1) 105.47 (1) 90.04 (1)
<i>V</i> (Å ³)	2298.0 (3)	2278.4 (3)
<i>Z</i> ; <i>Z'</i>	4; 1	4; 2
<i>D_x</i> (g cm ⁻³)	1.506	1.519
Radiation type	Mo <i>K</i> α	Mo <i>K</i> α
No. of reflections for cell parameters	5528	9946
θ range (°)	1.0–27.5	1.0–27.5
μ (mm ⁻¹)	0.91	0.92
Temperature (K)	150.0 (5)	90.0 (2)
Crystal form, colour	parallelepiped, pale green	parallelepiped, pale green
Crystal size (mm)	0.25 x 0.12 x 0.10	0.20 x 0.10 x 0.08
Data collection		
Diffractometer	Nonius KappaCCD	Nonius KappaCCD
Data collection method	ω scans at fixed χ = 55°	ω scans at fixed χ = 55°

⁸¹ The estimated errors in the unit cell constants (*a*, *b*, *c*, α , β and γ) were modified by multiplying the experimental estimated standard uncertainties (*i.e.*, su's) by at least a factor of ~5 for *a*, *b*, *c* and by at least a factor of ~14 for α , β , γ . These factors were used in order to approximate the errors in the unit cell constants from one crystal to another (Herbstein, 2000).

Table 6.2. (continued)

Absorption correction	Multi-scan (based on symmetry-related measurements)	
T_{\min}	0.804	0.837
T_{\max}	0.914	0.930
No. of measured, independent and observed parameters	10251, 5276, 3606	19489, 10381, 7375
Criterion for observed reflections	$I > 2\sigma(I)$	$I > 2\sigma(I)$
R_{int}	0.038	0.051
θ_{\max} (°)	27.5	27.5
Range of h, k, ℓ	$-15 < h < 15$ $-15 < k < 15$ $-20 < \ell < 20$	$-15 < h < 15$ $-15 < k < 15$ $-20 < \ell < 20$
Refinement		
Refinement on	F^2	F^2
$R[F^2 > 2\sigma(F^2)], wR(F^2), S$	0.039, 0.097, 1.03	0.043, 0.095, 1.00
No. of reflections	5276 reflections	10381 reflections
No. of parameters	328	606
H-atom treatment	Mixture of independent and constrained refinement	
Weighting scheme	Calculated $w = 1/[\sigma^2(F_o^2) + (0.0472P)^2]$ where $P = (F_o^2 + 2F_c^2)/3$	Calculated $w = 1/[\sigma^2(F_o^2) + (0.0395P)^2]$ where $P = (F_o^2 + 2F_c^2)/3$
$(\Delta/\sigma)_{\max}$	0.001	<0.0001
$\Delta\rho_{\max}, \Delta\rho_{\min}$ (e Å ⁻³)	0.60, -0.40	0.77, -0.57

Computer programs: *COLLECT* (Nonius, 1997); *DENZO-SMN* (Nonius, 1997); *SHELXS-97* (Sheldrick, 1990); *SHELXL-97* (Sheldrick, 1997); *XP in SHELXTL* (Bruker, 1995); *SHELX-97 and local procedures*.

Temperature Dependence of the Cell Dimensions

The variations of the cell dimensions (*i.e.*, a , b , c and β) with temperature was measured as single crystals of $[\text{Ni}(\text{MeCN})(\text{H}_2\text{O})_2(\text{NO}_3)_2] \cdot (15\text{-crown-5}) \cdot \text{MeCN}$ were heated (1) from 90 to 273 K at about 10 K intervals and (2) from 210 to 243 K at about 3 K intervals. Overall, thirty full data sets were collected to examine the temperature dependences of the cell dimensions of the compound $[\text{Ni}(\text{MeCN})(\text{H}_2\text{O})_2(\text{NO}_3)_2] \cdot (15\text{-crown-5}) \cdot \text{MeCN}$. For each set of measurements, one single crystal was used. There was no significant damage as the crystals were heated.

The cell dimensions were presented in a way that minimizes the effect of structural changes between the four phases of $[\text{Ni}(\text{MeCN})(\text{H}_2\text{O})_2(\text{NO}_3)_2] \cdot (15\text{-crown-5}) \cdot \text{MeCN}$. The cell of phase III was chosen to be the cell of reference. Phase II was indexed in the pseudo-cell (*i.e.*, the cell which is very similar to the cell of phase I). The length of the c axis and V were multiplied by a factor of two for phases I and II. The temperature dependences of the modified cell dimensions a , b , c and β , V for the system $[\text{Ni}(\text{MeCN})(\text{H}_2\text{O})_2(\text{NO}_3)_2] \cdot (15\text{-crown-5}) \cdot \text{MeCN}$ are shown in Figures 6.10 and 6.11. The plots of the second set of measurements show a discontinuity near 231 K which corresponds to the phase transition III \rightarrow II. There is no obvious discontinuity found for the phase transitions IV \rightarrow III and II \rightarrow I. The plots of the first set of measurements show some significant changes in the cell dimensions within the interval 245-250 K, in which the phase transition II \rightarrow I is estimated to take place⁸². The plots are not informative about the phase transition IV \rightarrow III.

⁸² The temperature dependence of the cell dimensions gives actually a rough estimation for the temperature of the phase transition II \rightarrow I. The phase transition II \rightarrow I was in fact found to take place between 239 and 243 K (see the section 'Results and Discussion' for further details)

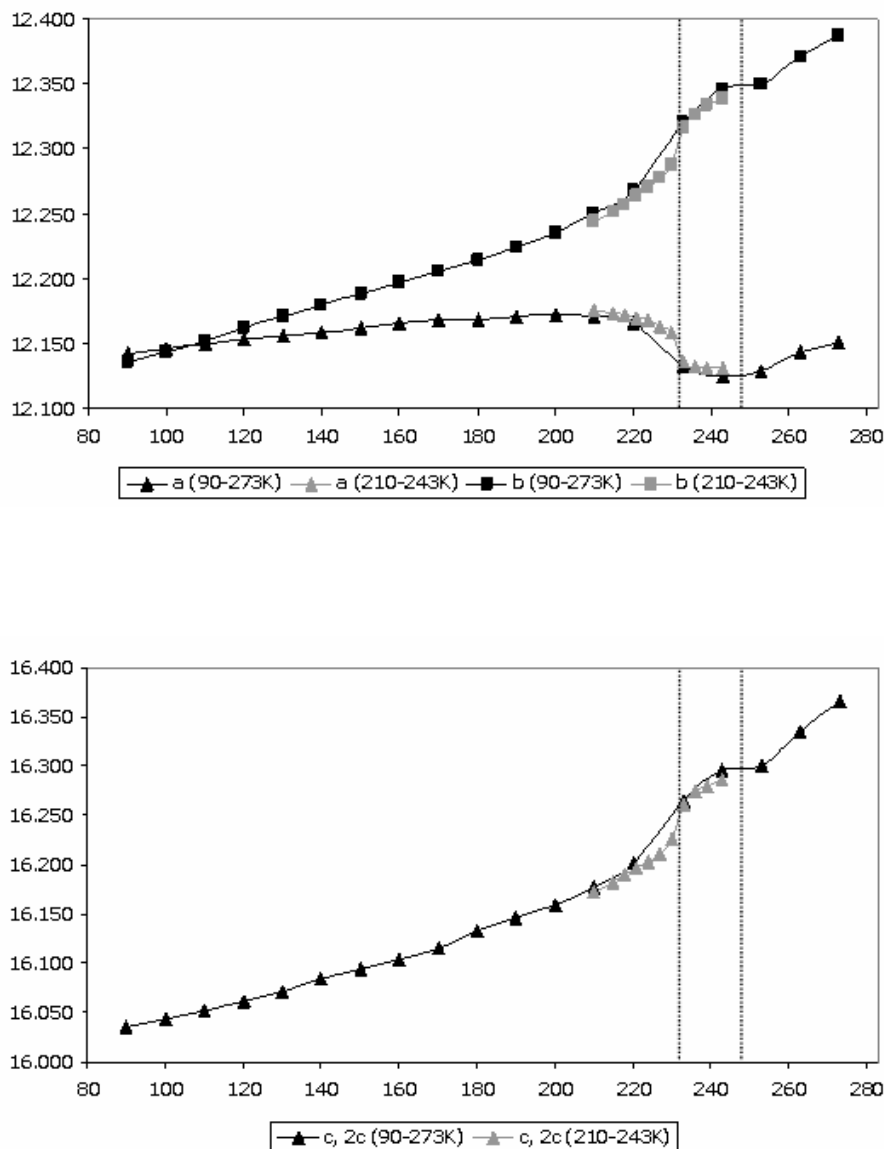


Figure 6.10. Plots of the modified cell dimensions a , b and c (Å) of the compound $[\text{Ni}(\text{MeCN})(\text{H}_2\text{O})_2(\text{NO}_3)_2] \cdot (15\text{-crown-5}) \cdot \text{MeCN}$ versus T (K). The first and second series of measurements were made respectively between 90 and 273 K (black line) and between 210 and 243 K (light gray line). The c axis for the phases I and II were modified so that the cells of the four phases are analogous (see text). The phase transitions III \rightarrow II and II \rightarrow I are estimated to take place near 231 and 247 K from the plots. The positions of the vertical dotted lines are given at temperatures for which the changes occur. The plots are not informative about the phase transition IV \rightarrow III. Error bars associated with the a , b and c dimensions are insignificant compared to the axis scale

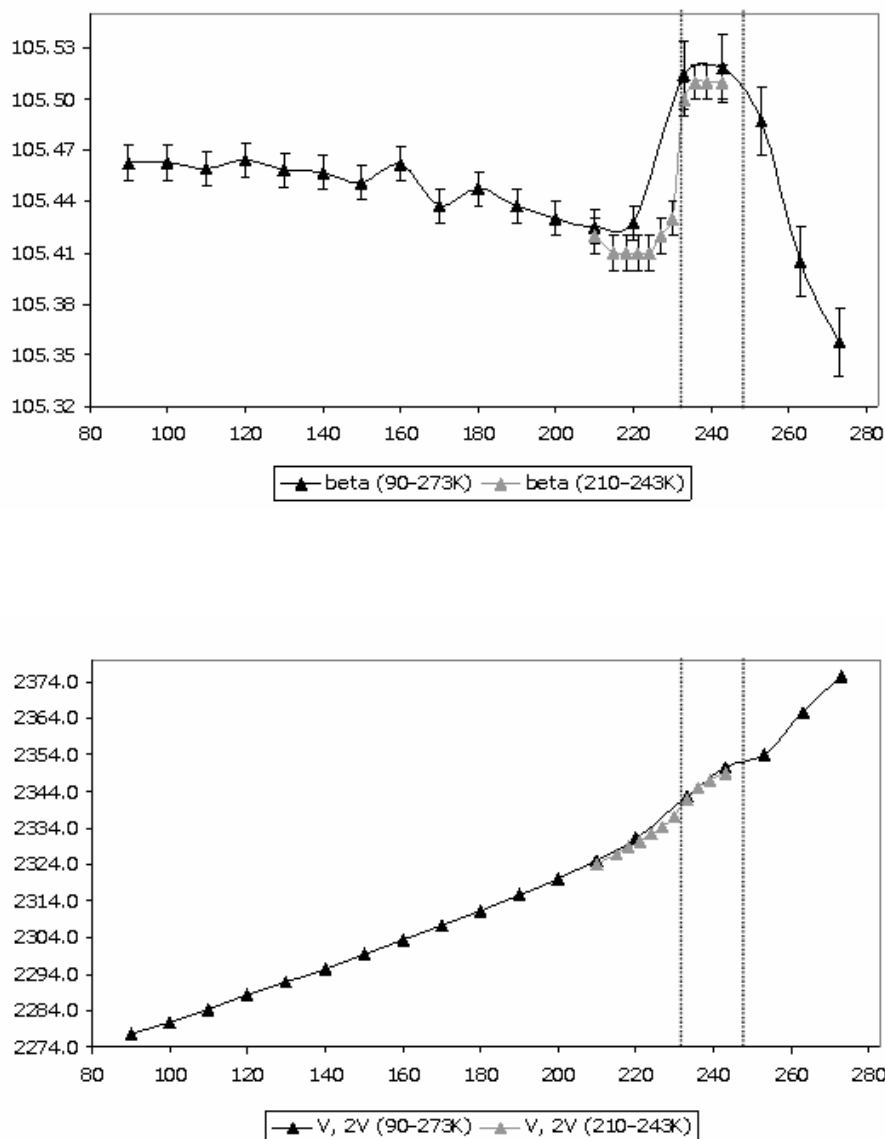


Figure 6.11. Plots of the modified cell dimensions β ($^\circ$) and V (\AA^3) of the compound $[\text{Ni}(\text{MeCN})(\text{H}_2\text{O})_2(\text{NO}_3)_2] \cdot (15\text{-crown-5}) \cdot \text{MeCN}$ versus T (K). The first and second series of measurements were made respectively between 90 and 273 K (black line) and between 210 and 243 K (light gray line). The volume V for the phases I and II were modified so that the cells of the four phases are analogous (see text). The phase transitions III \rightarrow II and II \rightarrow I are estimated to take place near 231 and 247 K from the plots. The positions of the vertical dotted lines are given at temperatures for which the changes occur. The plots are not informative about the phase transition IV \rightarrow III. Error bars of the cell constants are shown. Error bars associated with the volume V are insignificant compared to the axis scale.

Results and Discussion

Analysis of the Packing

The four phases of $[\text{Ni}(\text{MeCN})(\text{H}_2\text{O})_2(\text{NO}_3)_2] \cdot (15\text{-crown-5}) \cdot \text{MeCN}$ are built of one-dimensional (hereafter, 1-D) chains of H-bonds. The 1-D chains are found along the *c* direction where axial water ligands (O6 and O7) and 15-crown-5 molecules (O1, O2, O3 and O5) form hydrogen bonds (see Figure 6.12). The uncoordinated acetonitrile molecules form no strong H-bonds but rather fill otherwise empty spaces in the structure.

The H-bond pattern remains very similar between the phases III ($P2_1/c$, $Z' = 1$) and IV ($P\bar{1}$, $Z' = 2$). The disorder observed in the structure of phase I ($P2_1/m$, $Z' = \frac{1}{2}$) and in some regions of the structure of phase II ($B2_1$, $Z' = 5$) may or may not make little differences in the hydrogen bond interactions observed in the phase sequence IV \rightarrow I. Neutron diffraction might help to accurately locate the positions of all hydrogen atoms in the phases I and II. Table 6.3 summarizes the O \cdots O distances found in the 1-D H-bonded planes of the four phases.

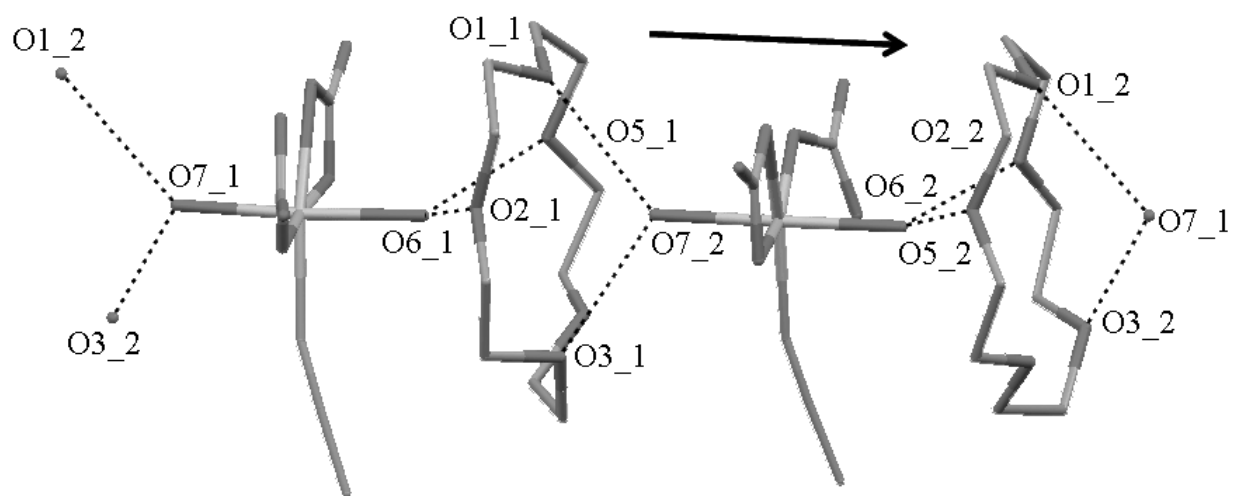


Figure 6.12. The set of hydrogen bond interactions observed in phase IV of the compound $[\text{Ni}(\text{MeCN})(\text{H}_2\text{O})_2(\text{NO}_3)_2] \cdot (15\text{-crown-5}) \cdot \text{MeCN}$ along the c direction (*i.e.*, along the 1-D H-bonded chains). The black arrow indicates the O7–Ni–O6 direction that roughly corresponds to the c direction. H-bonds are shown as black dotted lines. The lattice acetonitrile molecules and the H-atoms are omitted for clarity.

Table 6.3. Hydrogen bond distances D···A (Donor···Acceptor) along the **c** direction (*i.e.*, the direction of the 1-D H-bonded chains) for the phases I⁸³, II, III and IV of the compound [Ni(MeCN)(H₂O)₂(NO₃)₂]·(15-crown-5)·MeCN.

D···A (Å)	Phase I (<i>P2₁/m</i>, <i>Z'</i> = ½)			
O6···O2	2.773 (3)	O7···O4'	2.814 (11)	
O6···O4''	2.726 (11)			
O7···O1	2.914 (5)			
O7···O3	2.790 (5)			
D···A (Å)	Phase II (<i>B2₁</i>, <i>Z'</i> = 5)			
	Residues 1/5	Residues 2/1	Residues 3/2	Residues 4/3
O6···O2	2.666 (7)	2.718 (7)	2.699 (9)	2.871 (10)
O6···O5	2.788 (7)	2.730 (7)	2.788 (8)	2.611 (10)
O7···O1	2.841 (7)	2.823 (7)	2.834 (7)	2.892 (9)
O7···O3	2.817 (7)	2.766 (6)	2.799 (7)	2.931 (10)
	Residues 5/4	Average		
O6···O2	2.690 (7)	2.729 (8)		
O6···O5	2.775 (8)	2.738 (8)		
O7···O1	2.853 (7)	2.849 (7)		
O7···O3	2.850 (7)	2.832 (8)		
D···A (Å)	Phase III (<i>P2₁/c</i>, <i>Z'</i> = 1)			
O6···O2	2.704 (2)			
O6···O5	2.757 (2)			
O7···O1	2.839 (2)			
O7···O3	2.795 (2)			

⁸³ The hydrogen bond network observed in phase I is significantly more complicated than those observed in the other phases because of the whole-molecule disorder of the 15-crown-5 molecule. The atom-numbering scheme of the crown ether in phase I is slightly different.

Table 6.3(continued)

D ^{···} A (Å)	Phase IV ($P\bar{1}, Z' = 1$)		
	Residues 1/2	Residues 2/1	Average
O6 ^{···} O2	2.695 (4)	2.710 (4)	2.703 (3)
O6 ^{···} O5	2.756 (4)	2.752 (4)	2.754 (3)
O7 ^{···} O1	2.830 (3)	2.841 (3)	2.836 (2)
O7 ^{···} O3	2.810 (3)	2.758 (4)	2.784 (3)

Phase II: an Intermediate Phase⁸⁴

Phase II of the compound $[\text{Ni}(\text{MeCN})(\text{H}_2\text{O})_2(\text{NO}_3)_2] \cdot (15\text{-crown-5}) \cdot \text{MeCN}$ is found to be intermediate to the phases I and III. The single-crystal X-ray experiments have shown that phase I is very disordered and that phase III is slightly disordered. In phase I, the statistical mirror plane and the pseudoinversion symmetry cause disorder in a complicated way (see details of the refinement for phase I). In phase III, the monodentate nitrate ligand of the $[\text{Ni}(\text{MeCN})(\text{H}_2\text{O})_2(\text{NO}_3)_2]$ metal complex is found to have two orientations (see details of the refinement for phase III) because the coordination of the Ni^{2+} ion is six rather than seven^{85,86}. In phase II, the presence of local pseudosymmetry makes some regions of this structure slightly disordered and other regions of the structure very disordered. The pseudosymmetries of the more disordered regions correspond to a pseudomirror plane and pseudoinversion centers. The pseudosymmetry of the less disordered regions corresponds to a pseudoglide plane with the translation component of $c/5$. The relationship between phase II and the two phases I and III is obvious: the less and more disordered regions of phase II are similar respectively to the structures of phases III and I (see Figure 6.13). Phase II is best described as an intermediate phase. Nearly 40 % (two independent formula units) and 60% (three independent formula units) of the structure of phase II are similar respectively to the structures of phase I and III.

The positions of the O6–Ni–O7 fragments of the five crystallographically independent $[\text{Ni}(\text{MeCN})(\text{H}_2\text{O})_2(\text{NO}_3)_2]$ metal complexes with respect to the pseudoglide and pseudomirror planes emphasize the nature of the modulation observed in phase II. There are three possible positions for the O6–Ni–O7 fragments: two positions are found to be above or below the pseudoglide plane (*i.e.*, the O6–Ni–O7 fragments are ordered), the third position is found to be above and below the pseudomirror plane (*i.e.*, the O6–Ni–O7 fragments are disordered). The positions of the O6–Ni–O7 fragments of the

⁸⁴ Phase II of the compound $[\text{Ni}(\text{MeCN})(\text{H}_2\text{O})_2(\text{NO}_3)_2] \cdot (15\text{-crown-5}) \cdot \text{MeCN}$ presents similar characteristics with phase III of the compound $[\text{Ni}(\text{H}_2\text{O})_6](\text{NO}_3)_2 \cdot (15\text{-crown-5}) \cdot 2\text{H}_2\text{O}$, which is also an intermediate phase (see Chapter 5).

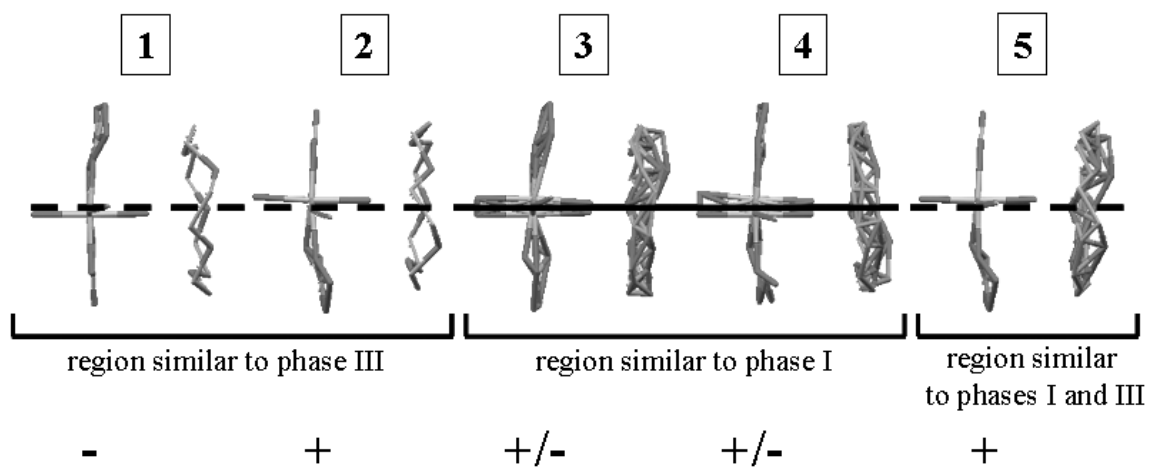
⁸⁵ In the $[\text{Ni}(\text{MeCN})(\text{H}_2\text{O})_2(\text{NO}_3)_2]$ metal complex, the Ni^{2+} ion is coordinated by one acetonitrile molecule, two water molecules, and two nitrates (one is bidentate and another is monodentate).

⁸⁶ See Chapter 3 for further details about the coordination of the Ni^{2+} ions in other Ni(II) complexes.

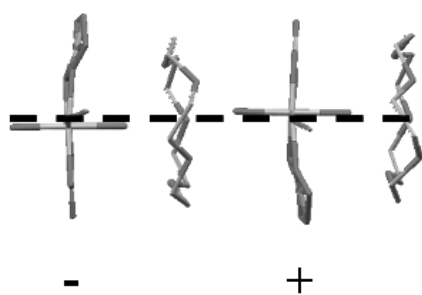
[Ni(MeCN)(H₂O)₂(NO₃)₂] metal complexes in the phases I, II and III are compared in Figure 6.13.

The modulation in phase II can be also examined by looking at the orientations of the five crystallographically independent lattice acetonitrile molecules with respect to the **c** direction. There are three possible orientations for the lattice acetonitrile molecules: two orientations are either up or down with respect to the **c** direction, the third orientation is parallel to the **c** direction (see Figure 6.14). The up and down alternation for the orientations of the lattice acetonitrile molecules is generated by a pseudoglide plane in the less disordered region of phase II. The pseudomirror symmetry constrains the orientations of the lattice acetonitrile molecules to be parallel to the **c** direction.

II, $B2_1$, $Z' = 5$



III, $P2_1/c$, $Z' = 1$

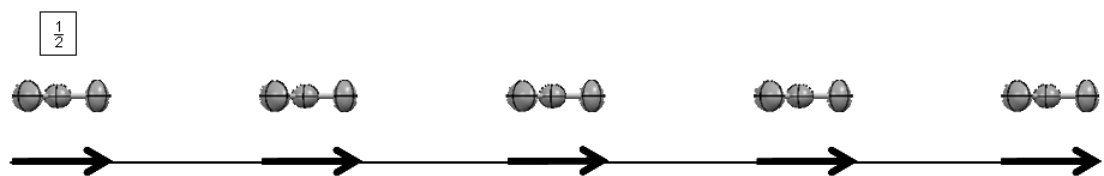


I, $P2_1/m$, $Z' = \frac{1}{2}$

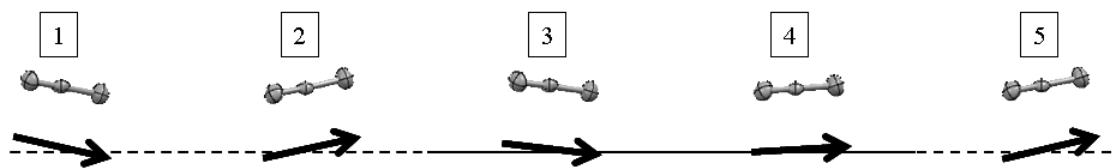


Figure 6.13. Projections of the asymmetric units of the phases I, II and III down the normal to the plane (1 0 0). Two asymmetric units for phase III (*i.e.*, the second formula unit is generated by the *c* glide plane) are shown in order to make comparisons with phase II obvious. Phase II, which contains five crystallographically independent formula units numbered from 1 to 5, is best described as an intermediate phase. Phase II contains a less disordered region (the formula units 1, 2 and some parts of the formula unit 5) similar to phase III and a more disordered region (the formula units 3, 4 and some parts of the formula unit 5) similar to phase I. The disorder of the $[\text{Ni}(\text{MeCN})(\text{H}_2\text{O})_2(\text{NO}_3)_2]$ metal complexes and the 15-crown-5 molecules (see the formula units 3, 4 and some parts of the formula unit 5) are generated respectively by a pseudomirror plane and pseudoinversions centers. The formula units 3 and 4 are related by a pseudotranslation of $c/5$. The formula units 1, 2 and 5 are slightly disordered and are related by a pseudoglide plane of $c/5$. The crown ether of formula unit 5 is found to be slightly disordered and the two components (*i.e.*, the minor and major components) of the disorder are related by a pseudoinversion center. The positions of the O6–Ni–O7 fragments of the $[\text{Ni}(\text{MeCN})(\text{H}_2\text{O})_2(\text{NO}_3)_2]$ metal complexes with respect to the glide and mirror planes (also pseudoglide and pseudomirror planes) are symbolized by ‘+’ (above), ‘-’ (below) and ‘+/-’ (above and below). The ‘+’ and ‘-’ positions are found in the regions similar to the structure of phase III (*i.e.*, when the pseudosymmetry corresponds to a pseudoglide plane). The ‘+/-’ position is found in the regions similar to the structure of phase I (*i.e.*, when the pseudosymmetries correspond to a pseudomirror plane and pseudoinversion centers). The pseudoglide and glide planes are shown as black dashed lines. The pseudomirror and mirror planes are shown as black lines. The lattice acetonitrile molecules are omitted for clarity.

I, $P2_1/m$, $Z' = \frac{1}{2}$ (243 K) → c (dir.)



II, $B2_1$, $Z' = 5$ (90 K, metastable)



III, $P2_1/c$, $Z' = 1$ (150 K)

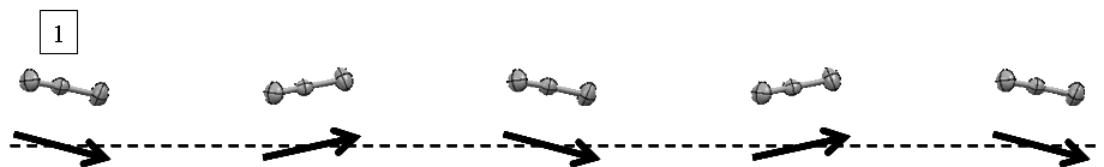


Figure 6.14. Projections of five lattice acetonitrile molecules found in the phases I, II and III down the normal to the plane (1 0 0). The displacement ellipsoids (50 % probability level) of the lattice acetonitrile molecules are given at 243, 90 and 150 K respectively for the phases I, II and III. In phase I, only one half of the lattice acetonitrile molecule (numbered $\frac{1}{2}$) is crystallographically independent (the other half is generated by symmetry) because each molecule lies statistically on sites with mirror symmetry. The other molecules are generated by a translation of c . In phase II, there are five crystallographically independent lattice acetonitrile molecules (numbered 1 \rightarrow 5). In phase III, there is only one crystallographically independent lattice acetonitrile molecule (numbered 1). The other molecules are symmetry generated by the c glide plane. The arrows correspond to the directions of the lattice acetonitrile molecules with respect to the positions of the glide and mirror planes (or pseudoglide and pseudomirror planes in phase II). In phase I and in some regions of phase II (*i.e.*, the molecules numbered as 3 and 4), the directions are horizontal and nearly horizontal because of the mirror or pseudomirror symmetries. In phase III and in some regions of phase II (*i.e.*, the molecules numbered as 1, 2 and 5), the up and down alternation is observed because of the presence of the glide or pseudoglide planes. The pseudoglide and glide planes are shown as black dashed lines. The pseudomirror and mirror planes are shown as black lines.

Enantiomeric Alternation

Crystals of the compound $[\text{Ni}(\text{MeCN})(\text{H}_2\text{O})_2(\text{NO}_3)_2] \cdot (15\text{-crown-5}) \cdot \text{MeCN}$ are found to be racemic because the conformational enantiomers (called here R and S for simplicity) of the crown ether are present in a ratio 1:1⁸⁷. The analysis of the structures of the four phases along the *c* direction shows evidence for a change in the enantiomeric alternation pattern when single crystals of $[\text{Ni}(\text{MeCN})(\text{H}_2\text{O})_2(\text{NO}_3)_2] \cdot (15\text{-crown-5}) \cdot \text{MeCN}$ pass through a phase transition.

In phase III and IV, the alternation pattern remains the same. The alternation is found to be perfect: the enantiomers R and S of the crown ether are bridged by the same $[\text{Ni}(\text{MeCN})(\text{H}_2\text{O})_2(\text{NO}_3)_2]$ metal complex along the *c* direction. The perfect alternation is given by R S (or S R).

In phase II, some 15-crown-5 molecules are disordered in some regions of the structure. The disorder of the 15-crown-5 molecules occurs because of the existence of pseudomirror planes and pseudoinversion centers⁸⁸. The disorder of the crown ether generated *via* pseudomirror planes is observed when alternation faults occur along the direction of the 1-D H-bonded chains. Enantiomers R/S fail to alternate once every five contacts. The alternation pattern observed in phase II is given by: R S R R S or R S R S S or S R S S R or S R S R R (see Figure 6.15).

In phase I, there is no long-range enantiomeric alternation pattern because the 15-crown-5 molecules are disordered. The disorder results from the non-superimposition of the enantiomers R/S of the crown ether because the 15-crown-5 molecules lie on sites with mirror symmetry. The 15-crown-5 molecules lie also on sites with pseudoinversion symmetry, which makes the disorder of the 15-crown-5 molecule complicated.

⁸⁷ This was also observed in the 'intermediate' phase III of the compound $[\text{Ni}(\text{H}_2\text{O})_6](\text{NO}_3)_2 \cdot (15\text{-crown-5}) \cdot 2\text{H}_2\text{O}$.

⁸⁸ The enantiomeric alternation pattern is not concerned with the minor component of the disorder of the 15-crown-5 molecule generated by pseudoinversion centers.

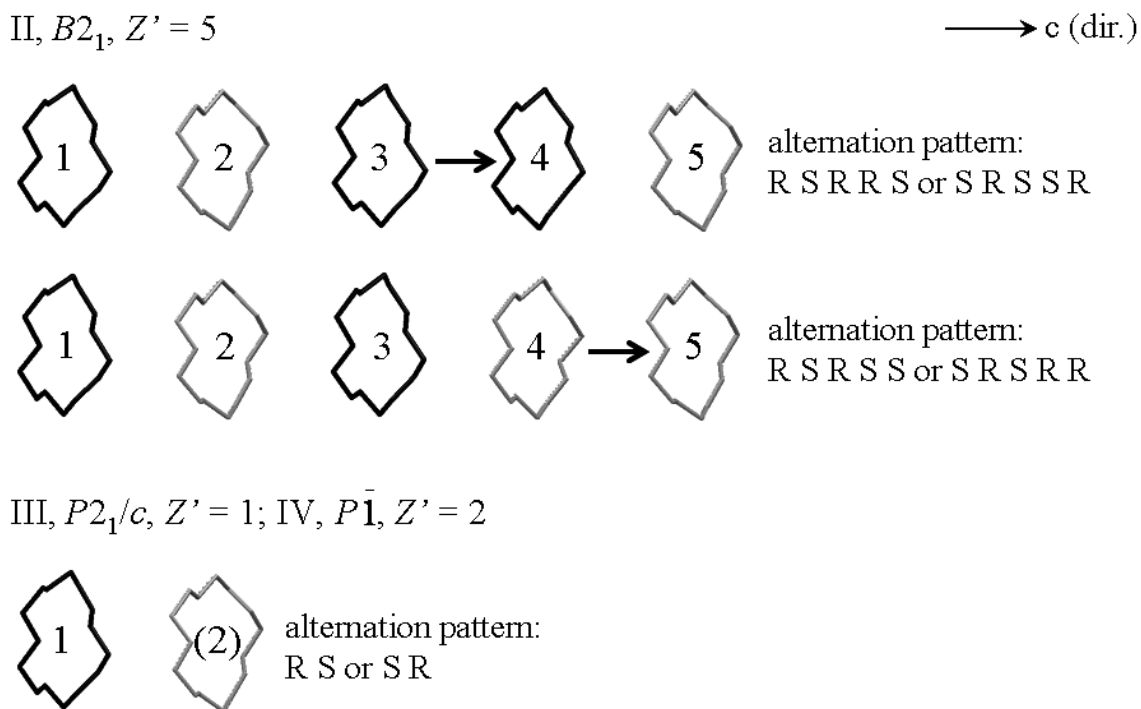


Figure 6.15. Projections of the crystallographically independent 15-crown-5 molecules down the **a** direction for phase II and down the normal to the plane (-4 0 3) for the phases III and IV. In the phases II, III and IV, there are respectively five, one and two crystallographically independent 15-crown-5 molecules. The enantiomeric alternation pattern is perfect in the phases III and IV. In phase II, the enantiomeric alternation pattern is more complicated because one 15-crown-5 molecule (*i.e.*, the crown ether numbered 4) is disordered. The disorder results from the non-superimposition of the enantiomers R/S of the 15-crown-5 molecule. In phase II, enantiomers fail to alternate once every 5 contacts along the **c** direction (*i.e.*, along the direction of the 1-D H-bonded chains). The non-alternation (black arrows) occurs either between the 15-crown-5 molecules 3 → 4 or 4 → 5. The alternation pattern is either R S R R S or R S R S S (or either S R S S R or S R S R R). The black and gray 15-crown-5 molecules correspond to the conformational enantiomers R/S. The minor components of the disorder of the 15-crown-5 molecules generated by pseudoinversion symmetry were omitted for clarity. The $[\text{Ni}(\text{MeCN})(\text{H}_2\text{O})_2(\text{NO}_3)_2]$ metal complexes and the lattice acetonitrile molecules were omitted for clarity.

Phase Transitions

The method for studying the phase transitions of the two polymorphic systems $[\text{Ni}(\text{H}_2\text{O})_6](\text{NO}_3)_2 \cdot (15\text{-crown-5}) \cdot n\text{H}_2\text{O}$, $n = 1, 2$ (see Chapters 4 and 5 for further details) was used to investigate the polymorphic system $[\text{Ni}(\text{MeCN})(\text{H}_2\text{O})_2(\text{NO}_3)_2] \cdot (15\text{-crown-5}) \cdot \text{MeCN}$. The three phase transitions of the latter compound were investigated making DSC measurements, measuring the temperature dependence of the cell dimensions and inspecting the reconstructed reciprocal lattice slices near the temperatures of the phase transitions. The phase transition $\text{IV} \rightarrow \text{III}$ was also investigated by plotting the integrated intensities of the strongest $h0\ell$ reflections with $\ell = 2n + 1$ against temperature. In this polymorphic system, the relationship between the four phases is obvious because the packing remains practically unchanged.

IV \rightarrow III

Below 145 K, the space group is the centrosymmetric $P\bar{1}$ with $Z' = 2$ (phase IV). Phase IV is a pseudomerohedral twin, which makes the unit cell nearly monoclinic. Phase IV is ordered. At temperatures between 145 and 231 K, the space group is the centrosymmetric $P2_1/c$ with $Z' = 1$ (phase III). Phase III is mostly ordered. The temperature of the phase transition $\text{IV} \rightarrow \text{III}$ was checked by looking at the reconstructed reciprocal lattice slices and by plotting the integrated intensities of the strongest $h0\ell$ reflections with $\ell = 2n + 1$ against T . At temperatures above the phase transition $\text{IV} \rightarrow \text{III}$, the $h0\ell$ reflections with $\ell = 2n + 1$ are systematically absent because of the existence of a c glide plane perpendicular to the b axis. Part (a) of Figure 6.16 shows that the $h0\ell$ reflections with $\ell = 2n + 1$ are absent at 140 K and above. The intensities of the ten strongest $h0\ell$ reflections with $\ell = 2n + 1$ were monitored between 90 and 150 K [see part (b) of Figure 6.16]. The plot of the integrated intensities shows that the transition $\text{IV} \rightarrow \text{III}$ takes place near 145 K. The temperatures of the transition observed by the two analyses are slightly different. At 140 K, the $h0\ell$ reflections with $\ell = 2n + 1$ are very weak but their intensities are not zero (the $h0\ell$ reflections with $\ell = 2n + 1$ are so weak that they are not observed on the reconstructed reciprocal lattice slices).

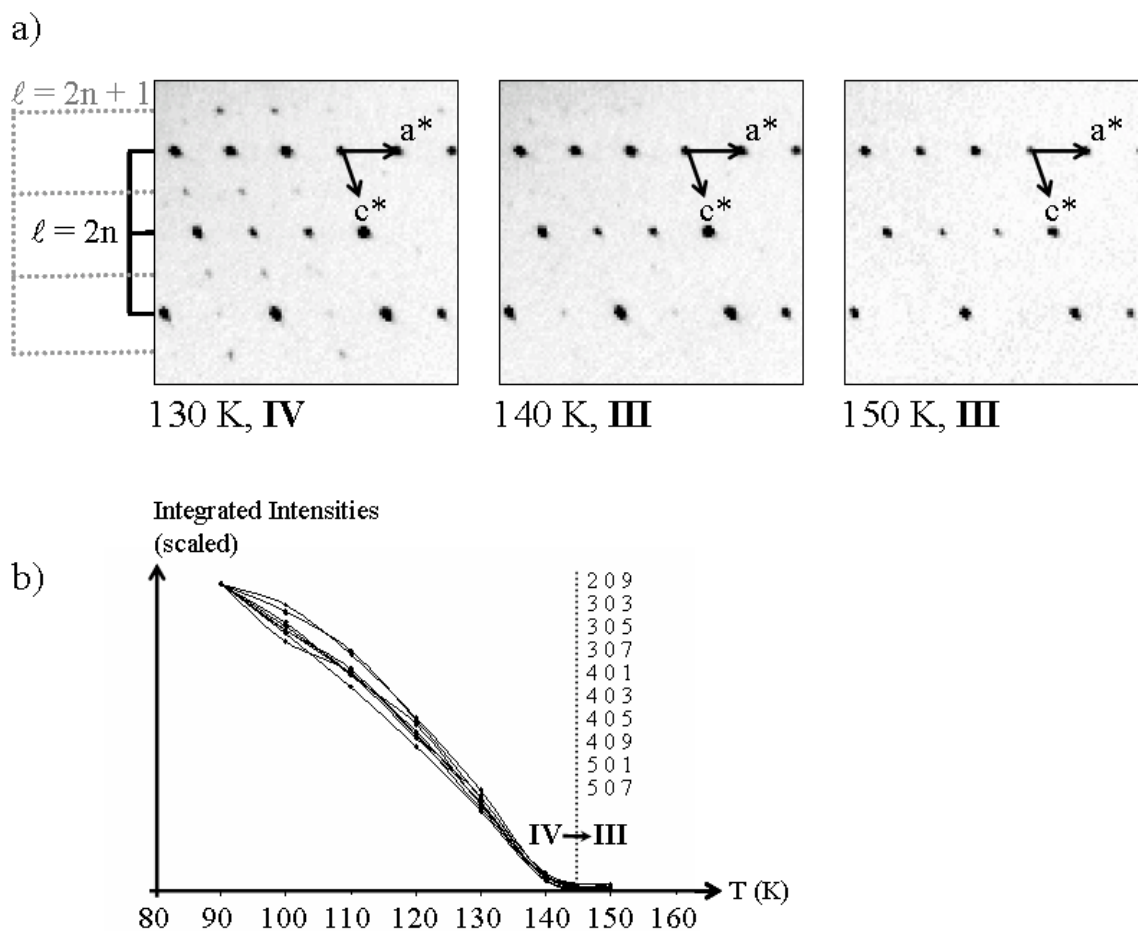


Figure 6.16. (a) Part of the reciprocal lattice slices $h0\ell$ digitally reconstructed from the measured frames at 130, 140 and 150 K. At 140 and 150 K, the $\ell = 2n + 1$ reflections are found to be absent from the diffraction pattern. From these observations, phase III is the stable phase at 140 K and above. (b) Temperature dependence of the integrated intensities of the 10 strongest $h0\ell$ reflections with $\ell = 2n + 1$ monitored between 90 and 150 K. The plot shows that the integrated intensities are absent near 145 K, so the phase transition IV \rightarrow III must take place near 145 K.

III → II and II → I

At temperatures between 231 and 241 K, the space group is the noncentrosymmetric space group $B2_1$ with $Z' = 5$ (phase II). Phase II is similar to phase III (mostly ordered) in some regions and similar to phase I (very disordered) in other regions. At temperatures above 241 K, the space group is the centrosymmetric $P2_1/m$ with $Z' = \frac{1}{2}$ (phase I). Phase I is very disordered because the space group requires that the 15-crown-5 molecules have mirror symmetry and because of the existence of pseudosymmetry (*i.e.*, pseudoinversion).

The temperatures of the phase transitions III → II and II → I were checked by looking at the reciprocal lattice slices. Parts (a) and (b) of Figure 6.17 show that the diffraction pattern changes between 230 and 233 K and between 239 and 243 K, for which the transitions III → II and II → I take place. The results for the transition III → II are in relatively good agreement with the study of the temperature dependence of the cell dimensions. In the latter study, the temperature of the transition II → I was estimated to take place slightly higher in temperature.

Phase II is stable over a relatively short temperature range of about 10 K.

The occurrence of hysteresis (see DSC measurements) and the existence of a discontinuity in the volume change near 231 K suggest that the phase transition III → II is first-order. The orders of the phase transitions IV → III and II → I are not known but the transitions might be second-order.

The *c* direction corresponds to the direction of greatest change in the phase sequence III → II → I: $c = 16.089$ (1), 40.229 (4) and value 8.143 (1) Å respectively given at 150, 90 and 243 K (see Figure 6.18).

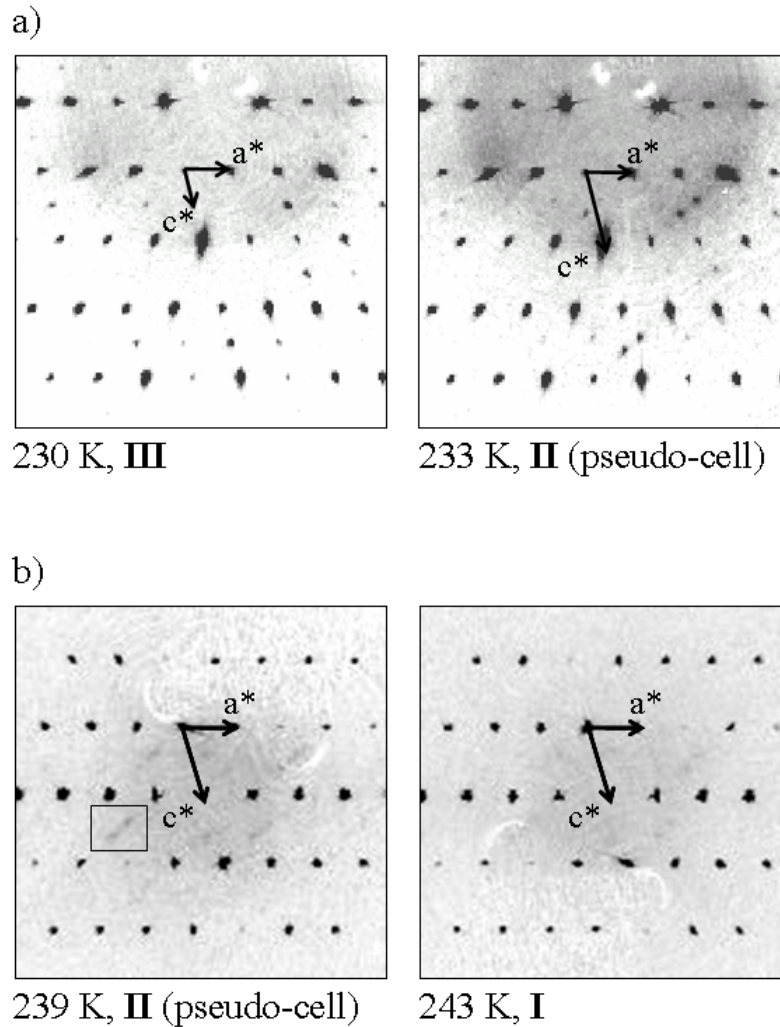


Figure 6.17. (a) Parts of the reciprocal lattice $h1\ell$ digitally reconstructed directly from the measured frames given for 230 (phase III) and 233 K (phase II). At 233 K, the less intense reflections (satellite reflections) appear to be split and are no longer indexable correctly in phase III. The phase transition III \rightarrow II occurs between 230 and 233 K. The indexing in the pseudo-cell (*i.e.*, the indexing for which the most intense reflections are only considered) was chosen so that the two frames are oriented similarly. (b) Parts of the reciprocal lattice $h3\ell$ digitally reconstructed directly from the measured frames given for 239 (phase II) and 243 K (phase I). At 239 K, only very few satellite reflections are observable (see box) and the indexing in phase II is nearly correct. At 243 K, the intensities of all satellite reflections are zero. The phase transition II \rightarrow I occurs between 239 and 243 K.

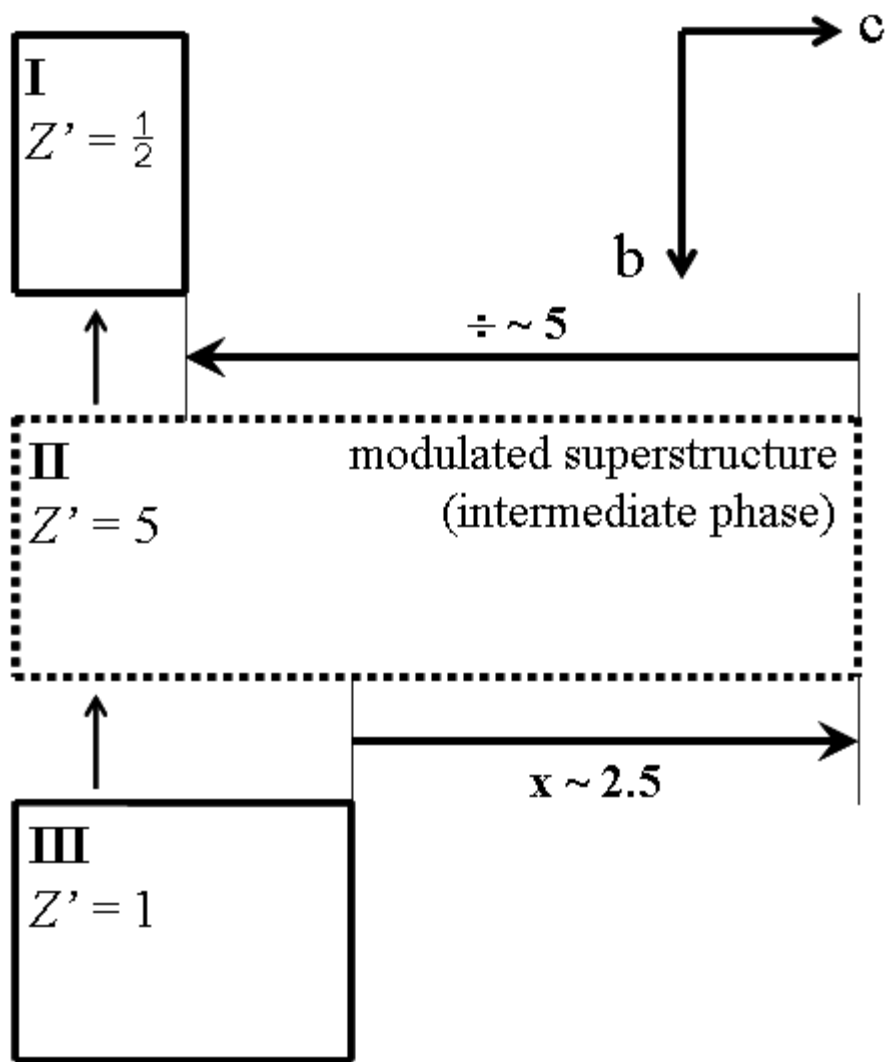


Figure 6.18. Projections of the units cells down the \mathbf{a} direction for phases III and I and down the normal to the plane $(1\ 0\ 0)$ for phase II. The drawing shows that the c direction corresponds to the direction of greatest change in the phase sequence $\text{III} \rightarrow \text{II} \rightarrow \text{I}$. At the phase transition $\text{III} \rightarrow \text{II}$, the c axis increases by a factor of approximately 2.5; at the phase transition $\text{II} \rightarrow \text{I}$, the c axis shrinks by a factor of about 5.

Similarities and Differences Between the Two Polymorphic Systems

$[\text{Ni}(\text{H}_2\text{O})_6](\text{NO}_3)_2 \cdot (15\text{-crown-5}) \cdot 2\text{H}_2\text{O}$ and $[\text{Ni}(\text{MeCN})(\text{H}_2\text{O})_2(\text{NO}_3)_2] \cdot (15\text{-crown-5}) \cdot \text{MeCN}$

In the previous and present chapters, two unusual polymorphic systems with similar phase sequences have been investigated: $[\text{Ni}(\text{H}_2\text{O})_6](\text{NO}_3)_2 \cdot (15\text{-crown-5}) \cdot 2\text{H}_2\text{O}$ (see Chapter 5 for details) and $[\text{Ni}(\text{MeCN})(\text{H}_2\text{O})_2(\text{NO}_3)_2] \cdot (15\text{-crown-5}) \cdot \text{MeCN}$. The following section emphasizes the similarities and the differences observed between the two polymorphic systems.

Similarities

- (i) Three solid-solid phase transitions and four phases were found for each compound. Part of the phase sequence [*i.e.*, $P2_1/c$ ($Z' = 1$) \rightarrow $B2_1$ ($Z' > 2$)^{89,90} \rightarrow $P2_1/m$ ($Z' = \frac{1}{2}$)] was found to be very similar in the two systems.
- (ii) The $Z' > 2$ phase is a commensurate modulated superstructure. The phase is better described as an intermediate phase of the $Z' = \frac{1}{2}$ and $Z' = 1$ structures. This phase is similar to the $Z' = \frac{1}{2}$ structure in some regions and similar to the $Z' = 1$ structure in other regions.
- (iii) The intermediate high- Z' phase was found to be metastable at 90 K after crystals had been flash-cooled from room temperature.

⁸⁹ $Z' = 5$ in $[\text{Ni}(\text{MeCN})(\text{H}_2\text{O})_2(\text{NO}_3)_2] \cdot (15\text{-crown-5}) \cdot \text{MeCN}$.

⁹⁰ $Z' = 7$ in $[\text{Ni}(\text{H}_2\text{O})_6](\text{NO}_3)_2 \cdot (15\text{-crown-5}) \cdot 2\text{H}_2\text{O}$.

(iv) The four phases of the compounds $[\text{Ni}(\text{H}_2\text{O})_6](\text{NO}_3)_2 \cdot (15\text{-crown-5}) \cdot 2\text{H}_2\text{O}$ and $[\text{Ni}(\text{MeCN})(\text{H}_2\text{O})_2(\text{NO}_3)_2] \cdot (15\text{-crown-5}) \cdot \text{MeCN}$ are built of 1-D chains of H-bonds along the *c* direction. The 15-crown-5 molecules and the axial water ligand of the $[\text{Ni}(\text{H}_2\text{O})_6]^{2+}$ ions and of the $[\text{Ni}(\text{MeCN})(\text{H}_2\text{O})_2(\text{NO}_3)_2]$ metal complexes participate in hydrogen bond interactions along the *c* direction. In the phase sequence $P2_1/c$ ($Z' = 1$) \rightarrow $B2_1$ ($Z' > 2$) \rightarrow $P2_1/m$ ($Z' = \frac{1}{2}$) (given for heating), the *c* direction is the direction along which the most important structural changes occur.

(v) The crystal packing is surprisingly similar in the compounds $[\text{Ni}(\text{H}_2\text{O})_6](\text{NO}_3)_2 \cdot (15\text{-crown-5}) \cdot 2\text{H}_2\text{O}$ and $[\text{Ni}(\text{MeCN})(\text{H}_2\text{O})_2(\text{NO}_3)_2] \cdot (15\text{-crown-5}) \cdot \text{MeCN}$ (see Figure 6.19). The cell dimensions *a*, *b*, *c* and the volume *V* for some phases of the two compounds are comparable (see Table 6.4). At 90 K, the difference in the β angles between the phases IV of the two compounds is about 4°.

(vi) In the phase sequence of $[\text{Ni}(\text{H}_2\text{O})_6](\text{NO}_3)_2 \cdot (15\text{-crown-5}) \cdot 2\text{H}_2\text{O}$, the *c* dimension increases by a factor of approximately 3.5 at the phase transition $P2_1/c$ ($Z' = 1$) \rightarrow $B2_1$ ($Z' = 7$) and shrinks by a factor of about 7 at the phase transition $B2_1$ ($Z' = 7$) \rightarrow $P2_1/m$ ($Z' = \frac{1}{2}$). In the phase sequence of $[\text{Ni}(\text{MeCN})(\text{H}_2\text{O})_2(\text{NO}_3)_2] \cdot (15\text{-crown-5}) \cdot \text{MeCN}$, the *c* dimension increases by a factor of approximately 2.5 at the phase transition $P2_1/c$ ($Z' = 1$) \rightarrow $B2_1$ ($Z' = 5$) and shrinks by a factor of about 5 at the phase transition $B2_1$ ($Z' = 5$) \rightarrow $P2_1/m$ ($Z' = \frac{1}{2}$).

Differences

(i) The intermediate phase of $[\text{Ni}(\text{H}_2\text{O})_6](\text{NO}_3)_2 \cdot (15\text{-crown-5}) \cdot 2\text{H}_2\text{O}$ is stable over a surprisingly wide temperature range of about 40 K. The intermediate phase of $[\text{Ni}(\text{MeCN})(\text{H}_2\text{O})_2(\text{NO}_3)_2] \cdot (15\text{-crown-5}) \cdot \text{MeCN}$ is stable over a relatively short temperature range of about 10 K.

(ii) In the compound $[\text{Ni}(\text{H}_2\text{O})_6](\text{NO}_3)_2 \cdot (15\text{-crown-5}) \cdot 2\text{H}_2\text{O}$, the H-bond pattern is built of 1-D chains and 2-D planes. In the compound $[\text{Ni}(\text{MeCN})(\text{H}_2\text{O})_2(\text{NO}_3)_2] \cdot (15\text{-crown-5}) \cdot \text{MeCN}$, the H-bond pattern is built only of 1-D chains. The five O_{ether} atoms of the crown ether are H-bond acceptors along the 1-D chains of the former compound, whereas only four O_{ether} atoms of the crown ether are H-bond acceptors along the 1-D chains of the latter compound.

(iii) The intermediate phases of the two compounds are locally disordered. The amount of disorder found in the $Z' = 7$ structure is less than that found in the $Z' = 5$ structure. The additional diffuse scattering observed for the $Z' = 5$ structure may indicate some short range order within the structure.

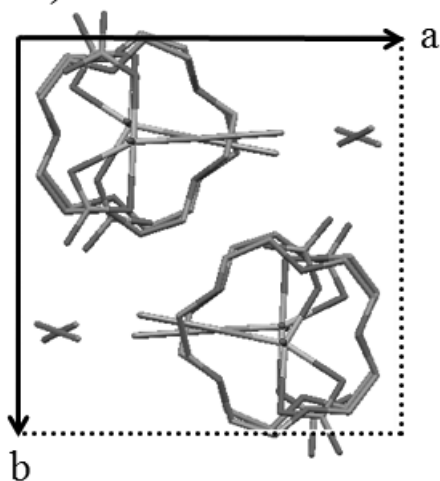
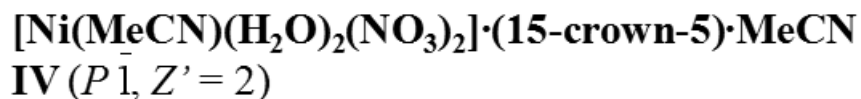
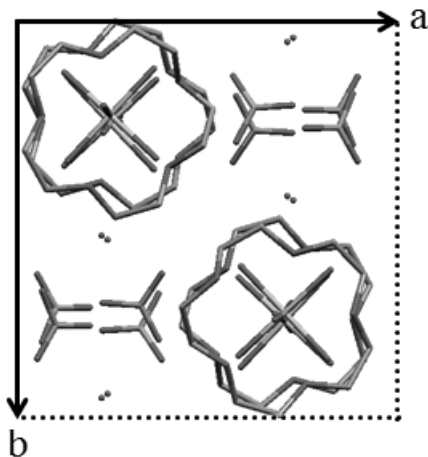
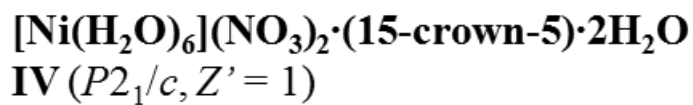


Figure 6.19. Projections down the *c* direction of phases IV of [Ni(H₂O)₆](NO₃)₂·(15-crown-5)·2H₂O and [Ni(MeCN)(H₂O)₂(NO₃)₂]·(15-crown-5)·MeCN. The packing is quite similar for the two chemically different compounds. The *a* axis of the *P*2₁/*c* structure is not in the plane of the drawing. The *a* and *b* axes of the *P*1̄ structure are not in the plane of the drawing.

Table 6.4. Comparisons of the cell dimensions of phases II, III, IV of $[\text{Ni}(\text{H}_2\text{O})_6](\text{NO}_3)_2 \cdot (15\text{-crown-5}) \cdot 2\text{H}_2\text{O}$ (1) with the cell dimensions of phases I, II, III and IV of $[\text{Ni}(\text{MeCN})(\text{H}_2\text{O})_2(\text{NO}_3)_2] \cdot (15\text{-crown-5}) \cdot \text{MeCN}$ (2) at 90, 150 and 250 K (243 K).

	1	2	ratio (1/2)
250 (1), 243 (2) K	II ($P2_1/m$, $Z' = \frac{1}{2}$)	I ($P2_1/m$, $Z' = \frac{1}{2}$)	
a (Å)	12.303 (2)	12.131 (2)	~ 1.01
b (Å)	12.543 (2)	12.339 (2)	~ 1.02
c (Å)	8.049 (1)	8.143 (1)	~ 0.99
V (Å ³)	1220.7 (3)	1174.5 (3)	~ 1.04
150 K	IV ($P2_1/c$, $Z' = 1$)	III ($P2_1/c$, $Z' = 1$)	
a (Å)	12.024 (1)	12.164 (1)	~ 0.99
b (Å)	12.678 (1)	12.183 (1)	~ 1.04
c (Å)	16.016 (2)	16.089 (2)	~ 1.00
V (Å ³)	2392.6 (3)	2298.0 (4)	~ 1.04
90 K	III ($B2_1$, $Z' = 7$)	II ($B2_1$, $Z' = 5$)	
a (Å)	30.632 (3)	27.463 (3)	~ 1.12
b (Å)	12.594 (1)	12.184 (1)	~ 1.03
c (Å)	55.955 (5)	40.229 (4)	~ 1.39
V (Å ³)	16666 (3)	11411.8 (15)	~ 1.46
90 K	IV ($P2_1/c$, $Z' = 1$)	IV ($P\bar{1}$, $Z' = 2$)	
a (Å)	11.950 (1)	12.144 (1)	~ 0.98
b (Å)	12.686 (1)	12.137 (1)	~ 1.05
c (Å)	15.988 (2)	16.039 (2)	~ 1.00
V (Å ³)	2375.0 (3)	2278.4 (4)	~ 1.04

Conclusions

The system $[\text{Ni}(\text{MeCN})(\text{H}_2\text{O})_2(\text{NO}_3)_2] \cdot (15\text{-crown-5}) \cdot \text{MeCN}$ is remarkable for having three solid-solid phase transitions and four phases, which have similar crystal packing. The single-crystal X-ray investigations of this system can be achieved because there is no major loss of crystallinity as single crystals pass through the phase transitions. The phase sequence IV \rightarrow I was investigated *via* a large series of single-crystal X-ray experiments. Only one of the three phase transitions in the phase sequence IV \rightarrow I were located by DSC analyses. The phase sequence is described as a set of four phases (numbered as phases I, II, III and IV). The structure of phase IV ($P\bar{1}$, $Z' = 2$) is completely ordered. The structures of the phases I, II and III have different amounts of disorder that increase as the temperature is raised. Phase III ($P2_1/c$, $Z' = 1$) is slightly disordered and phase I ($P2_1/m$, $Z' = \frac{1}{2}$) is very disordered. The amount of disorder in phase II ($B2_1$, $Z' = 5$) is intermediate to the amounts of disorder found in the phases I and III. Phase II is a commensurately modulated superstructure, which is best described as an intermediate structure because it contains some separate regions of the two phases I and III.

The phase transitions in the phase sequence IV \rightarrow I are characterized by structural changes along the direction of the 1-D H-bonded chains (*i.e.*, along the **c** direction). The transition IV \rightarrow III is characterized by the addition of elements of symmetry (*i.e.*, the *c* glide planes in phase III) with translational component along the **c** direction. The transitions III \rightarrow II and II \rightarrow I are more difficult to understand because the true symmetry along the **c** direction is lost in phase II. Though, the structure of phase II is found to be highly pseudosymmetric. The specific operations that define the pseudosymmetry correspond to pseudoglide planes in some regions and pseudomirror planes and pseudoinversion centers in other regions. The *c* glide planes in phase III are replaced by mirror planes *m* in phase I and the translational component *c*/2 generated by symmetry in phase III is lost in phase I. The crystal structures of $[\text{Ni}(\text{MeCN})(\text{H}_2\text{O})_2(\text{NO}_3)_2] \cdot (15\text{-crown-5}) \cdot \text{MeCN}$ become more symmetrical as the temperature raises except at temperatures for which phase II is stable.

Some parts of the phase sequences of the two chemically different compounds $[\text{Ni}(\text{MeCN})(\text{H}_2\text{O})_2(\text{NO}_3)_2] \cdot (15\text{-crown-5}) \cdot \text{MeCN}$ and $[\text{Ni}(\text{H}_2\text{O})_6](\text{NO}_3)_2 \cdot (15\text{-crown-5}) \cdot 2\text{H}_2\text{O}$ are found to be very similar (*i.e.*, Z' : $1 \rightarrow 5$ or $7 \rightarrow \frac{1}{2}$).

Chapter Seven

-

General Conclusions

Extension of $[M(\text{H}_2\text{O})_2(15\text{-crown-5})](\text{NO}_3)_2$

The system $[M(\text{H}_2\text{O})_2(15\text{-crown-5})](\text{NO}_3)_2$, $M = \text{Mg, Mn, Co, Cu and Zn}$ has been carefully examined and previously discussed⁹¹. This system was found to be polymorphic and all phases have unusual Z' values ($Z' = 2, 3, 5$ and 8). In more recent investigations, the system was extended⁹² to include two new phases with $M = \text{Fe}$ ($Z' = 3, 8$; the former phase was not discussed in the dissertation) and two new phases with $M = \text{Ni}$ ($Z' = 2, 3$).

Attempts to Synthesize $[\text{Ni}(\text{H}_2\text{O})_2(15\text{-crown-5})](\text{NO}_3)_2$

Six Ni(II) complexes⁹³ were discovered during attempts to synthesize the target compound $[\text{Ni}(\text{H}_2\text{O})_2(15\text{-crown-5})](\text{NO}_3)_2$. The Ni^{2+} ions were not found to be coordinated by the crown ether in any of these Ni(II) complexes. Co-crystallization occurs between the 15-crown-5 molecules and $[\text{Ni}(\text{H}_2\text{O})_2L_4]^{2+}$ ions ($L = \text{H}_2\text{O, MeOH, NO}_3^-$)⁹⁴ or $[\text{Ni}(\text{H}_2\text{O})_2LL']$ metal complexes ($L = \text{MeCN; } L' = \text{NO}_3^-$).

The synthesis of the compound $[M(\text{H}_2\text{O})_2(15\text{-crown-5})](\text{NO}_3)_2$ is more complicated for $M = \text{Ni}$ than for $M = \text{Mg, Mn, Fe, Co, Cu and Zn}$. It is believed that the amount of water available may have an important impact on the synthesis of $[\text{Ni}(\text{H}_2\text{O})_2(15\text{-crown-5})](\text{NO}_3)_2$.

⁹¹ Xiang Hao's dissertation includes an exhaustive discussion of the system $[M(\text{H}_2\text{O})_2(15\text{-crown-5})](\text{NO}_3)_2$, $M = \text{Mg, Mn, Co, Cu and Zn}$. Some parts of his work were reported in Hao, Parkin & Brock (2005).

⁹² In the section entitled 'Unanswered Questions' of his dissertation, Hao wrote 'Other metal ions, such as Fe^{2+} , Ni^{2+} and Cd^{2+} are also possible to produce similar compounds, but the structures are unknown'.

⁹³ The six Ni(II) complexes are: (1) $\text{Ni}(\text{H}_2\text{O})_6(\text{NO}_3)_2 \cdot (15\text{-crown-5}) \cdot 2\text{H}_2\text{O}$, (2) the first polymorph of $[\text{Ni}(\text{H}_2\text{O})_6](\text{NO}_3)_2 \cdot (15\text{-crown-5}) \cdot \text{H}_2\text{O}$, (3) the second polymorph of $[\text{Ni}(\text{H}_2\text{O})_6](\text{NO}_3)_2 \cdot (15\text{-crown-5}) \cdot \text{H}_2\text{O}$, (4) $[\text{Ni}(\text{H}_2\text{O})_6](\text{NO}_3)_2 \cdot \text{trans-}[\text{Ni}(\text{H}_2\text{O})_4(\text{MeOH})_2](\text{NO}_3)_2 \cdot 2(15\text{-crown-5})$, (5) $\text{cis-}[\text{Ni}(\text{H}_2\text{O})_4(\text{NO}_3)_2] \cdot \text{trans-}[\text{Ni}(\text{H}_2\text{O})_4(\text{NO}_3)_2] \cdot 2(15\text{-crown-5})$ and (6) $[\text{Ni}(\text{H}_2\text{O})_2(\text{MeCN})(\text{NO}_3)_2] \cdot (15\text{-crown-5}) \cdot \text{MeCN}$.

⁹⁴ Depending on the compounds, there may be a combination of several types of ligands for the $[\text{Ni}(\text{H}_2\text{O})_2L_4]^{2+}$ ions.

Coordination Number of Ni²⁺ in Seven Ni(II) Complexes

In six of the seven Ni(II) complexes discussed in the dissertation, the Ni²⁺ ions were found to be coordinated by water molecules only⁹⁵ or by water molecules and other solvent molecules⁹⁶ or by water molecules and nitrate ions⁹⁷ or by water molecules, nitrate ions and other solvent molecules⁹⁸. These Ni(II) complexes are similar in that six coordination (octahedral geometry) is found around the Ni²⁺ ions. In all of these compounds, hydrogen-bond interactions are found along one dimension between the 15-crown-5 molecules and the [Ni(H₂O)₂L₄]²⁺ ions ($L = \text{H}_2\text{O}, \text{MeOH}, \text{NO}_3^-$) or [Ni(H₂O)₂LL'₂] metal complexes ($L = \text{MeCN}; L' = \text{NO}_3^-$).

The single-crystal X-ray experiments proved that the Ni²⁺ ions in the two phases of [Ni(H₂O)₂(15-crown-5)](NO₃)₂ are disordered⁹⁹. The occurrence of disorder suggests that the Ni²⁺ ions might not be coordinated by all five O_{ether} atoms of the 15-crown-5 molecules, or at least not to the same extent. In the two phases of [Ni(H₂O)₂(15-crown-5)](NO₃)₂, the six-coordination around the Ni²⁺ ion is found to be distorted from the normal octahedral geometry.

These results suggest that the occurrence of six-coordinate Ni(II) complexes (octahedral geometry) might be more favorable than the occurrence of seven-coordinate Ni(II) complexes (pentagonal-bipyramidal geometry).

⁹⁵ [Ni(H₂O)₆](NO₃)₂·(15-crown-5)·*n*H₂O (*n* = 1, 2).

⁹⁶ [Ni(H₂O)₆](NO₃)₂·*trans*-[Ni(H₂O)₄(MeOH)₂](NO₃)₂·2(15-crown-5).

⁹⁷ *cis*-[Ni(H₂O)₄(NO₃)₂]·*trans*-[Ni(H₂O)₄(NO₃)₂]·2(15-crown-5).

⁹⁸ [Ni(H₂O)₂(MeCN)(NO₃)₂]·(15-crown-5)·MeCN.

⁹⁹ However, the disorder is more obvious in the low-temperature phase than in the high-temperature phase.

New Polymorphic Systems

Among the six Ni(II) complexes for which the Ni²⁺ ions are not coordinated by the crown ether, the compounds [Ni(H₂O)₆](NO₃)₂·(15-crown-5)·H₂O (first polymorph), [Ni(H₂O)₆](NO₃)₂·(15-crown-5)·2H₂O and [Ni(H₂O)₂(MeCN)(NO₃)₂](15-crown-5)·MeCN were found to have reversible solid-solid phase transitions between structurally similar phases. These three polymorphic systems are remarkable for having transitions through which there is no significant crystal damage.

The first polymorph¹⁰⁰ of [Ni(H₂O)₆](NO₃)₂·(15-crown-5)·H₂O is the simplest of the polymorphic systems discussed in the three previous chapters of this dissertation. This compound goes through one transition (Z': 2 → 1) from 90 K to room temperature. Structural changes were observed to take place in the lowest-temperature phase at intermediate temperatures.

The two polymorphic systems [Ni(H₂O)₆](NO₃)₂·(15-crown-5)·2H₂O and [Ni(H₂O)₂(MeCN)(NO₃)₂](15-crown-5)·MeCN are very unusual; the two systems go through three transitions (respectively Z': 1 → 7 → $\frac{1}{2}$ → $\frac{1}{4}$ and Z': 2 → 1 → 5 → $\frac{1}{2}$) from 90 K to room temperature and have phase sequences that include high-Z' intermediate phases (*i.e.*, the phases with Z' > 2).

Because the three systems are easy and inexpensive to make, and because there is no significant loss of crystallinity during the phase transitions, these systems are good candidates for potential studies in the field of polymorphism and phase transitions. Investigations of such systems may encourage developing efficient methods of characterization for new polymorphic systems.

¹⁰⁰ A second polymorph of [Ni(H₂O)₆](NO₃)₂·(15-crown-5)·H₂O was discussed in Chapter 3 but no further research was done to know if more phases of this polymorph exist.

Systematic Approach to Study Phase Transitions

The systematic approach that was used to investigate the three polymorphic systems $[\text{Ni}(\text{H}_2\text{O})_6](\text{NO}_3)_2 \cdot (15\text{-crown-5}) \cdot \text{H}_2\text{O}$ (first polymorph), $[\text{Ni}(\text{H}_2\text{O})_6](\text{NO}_3)_2 \cdot (15\text{-crown-5}) \cdot 2\text{H}_2\text{O}$ and $[\text{Ni}(\text{H}_2\text{O})_2(\text{MeCN})(\text{NO}_3)_2] \cdot (15\text{-crown-5}) \cdot \text{MeCN}$ is based on collecting data at different levels.

Thermal analyses (*e.g.*, DSC) were more often performed during the preliminary steps of investigations because these analyses were less time consuming¹⁰¹ than other techniques. DSC may not be a good technique, however, for investigations of phase transitions that involve relatively low latent heat. Second-order or higher-order phase transitions cannot be located reliably *via* DSC experiments.

Other techniques such as optical microscopy¹⁰² or NMR spectroscopy may be considered as additional techniques for characterization of polymorphic systems.

Choosing a strategy for collecting data *via* single-crystal X-ray experiments was important. The approach, which was chosen in the course of this research, includes a collection of full data sets at various temperatures¹⁰³. Doing so is undeniably time consuming¹⁰⁴ but the amount of information obtained is very valuable for characterization of polymorphic systems. This large amount of information allows multiple analyses¹⁰⁵ on a given polymorphic system at various temperatures. Solving and refining structures at various temperatures is also another benefit of this approach in order to examine structural changes that may occur near a transition (see Chapter 4).

¹⁰¹ Depending on the heating rate (or cooling rate), several hours (sometimes less, sometimes more) is generally enough to get enough conclusive data in the DSC experiments.

¹⁰² The three polymorphic systems discussed in Chapters 4, 5 and 6 could have been studied by cold-stage optical microscopy (because all transitions occur below 295 K), but such apparatus was not available at the University of Kentucky.

¹⁰³ In most experiments, data were collected between 90 and 294 K. The upper temperature for data collection was sometimes less than 294 K and sometimes more than 294 K.

¹⁰⁴ Collecting full data sets at various temperatures can take between two to three weeks, but can take more time depending on the strategy of data collection.

¹⁰⁵ Plots of refined cell dimensions against T can be made, the diffraction pattern can be fully reconstructed, plots of integrated intensities of specific classes of reflections against T can be made.

The Ambiguous Nature of Intermediate Phase

The nature of intermediate phase is not well understood because there are not many systems for which an intermediate phase has been observed. In his review paper about the mechanism of some first-order enantiotropic phase transitions (Herbstein, 2006), Herbstein mentioned the term ‘intermediate phase’ to make references to Ubbelohde’s approach of ‘hybrid crystals’.

In Ubbelohde’s approach, a single crystal is said to be hybrid when it contains on average a set of domains of a low- and high-temperature phases (hereafter, *L* and *H*), which are at equilibrium within a *T*-range of stability. The separate domains are large enough (*i.e.*, the level of order in the ‘hybrid crystal’ is large) to produce their own diffraction patterns. One phase¹⁰⁶ of the compound 4,4’-dichlorobenzophenone (Zuniga & Criado, 1995) seems to be in agreement with Ubbelohde’s approach of ‘hybrid crystals’. Ubbelohde suggested that a ‘hybrid crystal’¹⁰⁷ might occur when the structures of the *L* and *H* phases are similar.

When the difference between the unit cells becomes sufficiently small, well oriented domains of either phase can co-exist in the hybrid crystal... Conditions are now present for a transition that in appearance is thermodynamically continuous. However, X-ray methods leave no doubt about discontinuous jumps in structure between the domains of the two phases, provided sufficiently refined methods are used (Ubbelohde, 1962).

Mnyukh rejected Ubbelohde’s approach and argued in favor of a two-phase mixture¹⁰⁸ that is not at equilibrium near the transition.

The diffuseness is not the manifestation of a specific transition mechanism. It is a consequence of the non-simultaneous nucleation in different particles, or parts of the specimen... At intermediate temperatures *T*’ the sample is two-phase (Mnyukh, 2001).

¹⁰⁶ This phase is cited as an intermediate phase in Herbstein’s paper.

¹⁰⁷ Herbstein (2006) pointed out that the term ‘hybrid’ may be ambiguous and wrote “A mule is neither a horse nor a donkey; perhaps it would be best to avoid ‘hybrid’ entirely”.

¹⁰⁸ In contrast to Ubbelohde’s approach, the level of order in the crystal is low near the transition.

In this dissertation, phases for which some regions of a low- and high-temperature phases can co-exist in a single unit cell were defined as being intermediate. This statement suggests that regions of the low- and high-temperature phases are strained within a single unit cell (different from the cells of the low- and high-temperature phases) rather than being strained within a single crystal (*i.e.*, Ubbelohde's approach). As a result, the diffraction pattern of an intermediate phase is different from the diffraction patterns of a low- and high-temperature phases and is not the result of their superposition. One intermediate phase in $\text{Fe}(\text{2-picolylamine})_3\text{Cl}_2 \cdot \text{C}_2\text{H}_5\text{OH}$ (Chernyshov *et al.*, 2003; Chernyshov *et al.*, 2004) seems to be in accordance with this approach.

The existence of an intermediate phase in $\text{Fe}(\text{2-picolylamine})_3\text{Cl}_2 \cdot \text{C}_2\text{H}_5\text{OH}$ is also established, but its nature differs from that found in 4,4'-dichlorobenzophenone. Rather than being a mélange of the low- and high-temperature phases, here an ordered phase is found, based on these phases but different from them (Herbstein, 2006).

Two intermediate phases with high- Z' values^{109,110,111} have been found in $[\text{Ni}(\text{H}_2\text{O})_6](\text{NO}_3)_2 \cdot (15\text{-crown-5}) \cdot 2\text{H}_2\text{O}$ and $[\text{Ni}(\text{H}_2\text{O})_2(\text{MeCN})(\text{NO}_3)_2] \cdot (15\text{-crown-5}) \cdot \text{MeCN}$. The X-ray diffraction experiments have shown significant evidence that these intermediate phases are different (but related) from their respective low- and high-temperature phases. None of these phases show structural similarities with Ubbelohde's 'hybrid crystal'. The two-phase mixture depicted by Mnyukh could not be established either.

¹⁰⁹ $Z' = 7$ for $[\text{Ni}(\text{H}_2\text{O})_6](\text{NO}_3)_2 \cdot (15\text{-crown-5}) \cdot 2\text{H}_2\text{O}$.

¹¹⁰ $Z' = 5$ for $[\text{Ni}(\text{H}_2\text{O})_2(\text{MeCN})(\text{NO}_3)_2] \cdot (15\text{-crown-5}) \cdot \text{MeCN}$

¹¹¹ These two phases were discussed in Chapters 5 and 6.

Phase Predictions

The dissertation is not concerned with polymorphic systems for which phases cannot be related by obvious relationships, that is for which the two crystal packings are quite different. Predictions of new phases in such systems are known to be unreliable. The following discussion is only concerned with the three polymorphic systems $[\text{Ni}(\text{H}_2\text{O})_6](\text{NO}_3)_2 \cdot (15\text{-crown-5}) \cdot \text{H}_2\text{O}$ (first polymorph), $[\text{Ni}(\text{H}_2\text{O})_6](\text{NO}_3)_2 \cdot (15\text{-crown-5}) \cdot 2\text{H}_2\text{O}$ and $[\text{Ni}(\text{H}_2\text{O})_2(\text{MeCN})(\text{NO}_3)_2] \cdot (15\text{-crown-5}) \cdot \text{MeCN}$.

A noteworthy characteristic of these three polymorphic systems is that all phases for each of these systems are structurally similar¹¹² and are easily related by geometrical relationships. Can phase transitions be predicted for such systems? The question is complicated to answer because a positive response would imply that temperatures of phase transitions can be predicted. Nevertheless, phase relationships in the three systems are obvious. This may open new discussions for phase predictions in similar systems, although some factors must be taken into careful consideration.

¹¹² The $Z' = 1, 2$ phases of the compound $[\text{Ni}(\text{H}_2\text{O})_6](\text{NO}_3)_2 \cdot (15\text{-crown-5}) \cdot \text{H}_2\text{O}$ (first polymorph) have similar packing. The $Z' = \frac{1}{4}, \frac{1}{2}, 1, 7$ phases of the compound $[\text{Ni}(\text{H}_2\text{O})_6](\text{NO}_3)_2 \cdot (15\text{-crown-5}) \cdot 2\text{H}_2\text{O}$ have similar packing. The $Z' = \frac{1}{2}, 1, 2, 5$ phases of the compound $[\text{Ni}(\text{H}_2\text{O})_2(\text{MeCN})(\text{NO}_3)_2] \cdot (15\text{-crown-5}) \cdot \text{MeCN}$ have similar packing.

(i) The crystal structure of at least one phase of the phase sequence must be known in order to predict the structures of possible new structurally similar phases. As a starting point, the structure of the lowest-temperature phase seems to be a good candidate. As the temperature decreases, thermal motion (*i.e.*, dynamic disorder and librational effects) decreases. Another benefit is that the hydrogen atoms are more accurately located in the structure of the lowest-temperature phase than in the structures of higher-temperature phases. Care must be taken when crystals are cooled from room temperature to a temperature at which the lowest-temperature phase is stable. Experience shows that some higher-temperature phases can be metastable at temperatures lower than their equilibrium transition temperatures. Using slow cooling rates (*e.g.*, -2 K/min) helps avoid this problem.

(ii) Characterization of a phase sequence should be done from low to high temperatures and from high to low temperatures. However, it may be easier to investigate a given system using the former approach because there are several advantages to examining the structure of the lowest-temperature phase prior to the structures of the higher-temperature phases [see (i)].

(iii) As the temperature is changed¹¹³, the change in thermal motion should be considered as the driving force for the occurrence of phase transitions in such systems.

(iv) The order (or disorder) of phases of the phase sequence should be examined carefully as the temperature of the system is changed. As the temperature is raised, order → disorder transitions (*i.e.*, the system becomes less ordered) are likely to take place because of the increase in thermal motion of the system. In the three systems studied here, the phases become less ordered as the temperature is raised; the lowest-temperature phase was found to be ordered and the highest-temperature phase was found to be less ordered (see Chapter 4) or very disordered (see Chapters 5 and 6).

¹¹³ The pressure of the system remains constant as the temperature is changed.

(v) In the noncentrosymmetric crystal system $[\text{Ni}(\text{H}_2\text{O})_6](\text{NO}_3)_2 \cdot (15\text{-crown-5}) \cdot \text{H}_2\text{O}$ (first polymorph), the symmetry of the two phases ($Z' = 1, 2$) remains the same¹¹⁴ as the temperature increases (or decreases). In the two other crystal systems $[\text{Ni}(\text{H}_2\text{O})_6](\text{NO}_3)_2 \cdot (15\text{-crown-5}) \cdot 2\text{H}_2\text{O}$ and $[\text{Ni}(\text{H}_2\text{O})_2(\text{MeCN})(\text{NO}_3)_2] \cdot (15\text{-crown-5}) \cdot \text{MeCN}$, the symmetry of the systems varies as the temperature is changed. In the phase sequences $Z': 1 \rightarrow 7 \rightarrow \frac{1}{2} \rightarrow \frac{1}{4}$ ($P2_1/c \rightarrow P2_1$ or $B2_1 \rightarrow P2_1/m \rightarrow C2/m$ or $I2/m$) and $Z': 2 \rightarrow 1 \rightarrow 5 \rightarrow \frac{1}{2}$ ($P\bar{1} \rightarrow P2_1/c \rightarrow P2_1$ or $B2_1 \rightarrow P2_1/m$), the systems are generally¹¹⁵ more symmetrical as the temperature is raised. Phases with higher Z' values have less symmetry and phases with lower Z' values have more symmetry. These two systems tend to be more symmetrical as they become less ordered¹¹⁶ (*i.e.*, as the temperature is raised).

(vi) Systems for which the lowest-temperature phases have $Z' > 1$ should be regarded as potential polymorphic systems if the crystallographically independent formula units are related by small fluctuations in position, occupation and/or thermal motion. These units may become crystallographically undistinguishable as thermal motion of the system increases by raising the temperature. Following this logic, the transition $Z': 2 \rightarrow 1$ and the $Z' = 1$ phase for the system $[\text{Ni}(\text{H}_2\text{O})_6](\text{NO}_3)_2 \cdot (15\text{-crown-5}) \cdot \text{H}_2\text{O}$ (first polymorph) may have been expected by assuming that the structure of the $Z' = 2$ phase was known.

(vii) In the system $[\text{Ni}(\text{H}_2\text{O})_6](\text{NO}_3)_2 \cdot (15\text{-crown-5}) \cdot 2\text{H}_2\text{O}$, the $Z' = \frac{1}{4}$ and $\frac{1}{2}$ phases might have been predicted by symmetry consideration and by assuming that the structure of the $Z' = 1$ phase was known (see Figure 7.1 for further details).

(viii) In the system $[\text{Ni}(\text{H}_2\text{O})_2(\text{MeCN})(\text{NO}_3)_2] \cdot (15\text{-crown-5}) \cdot \text{MeCN}$, the $Z' = 1$ and $\frac{1}{2}$ phases might have been predicted by symmetry consideration and by assuming that the structure of the $Z' = 2$ phase was known (see Figure 7.2 for further details).

¹¹⁴ The $Z' = 1, 2$ phases were solved and refined in the same space groups.

¹¹⁵ This is not true for the $Z': 1 \rightarrow 7$ and $Z': 1 \rightarrow 5$ transitions because the systems lose the crystallographic inversion centers in the $Z' = 7$ and $Z' = 5$ phases.

¹¹⁶ This is not true for the $Z' = 7$ and $Z' = 5$ phases, but the nature of these phases is more complicated than the nature of the other phases found in the two phase sequences.

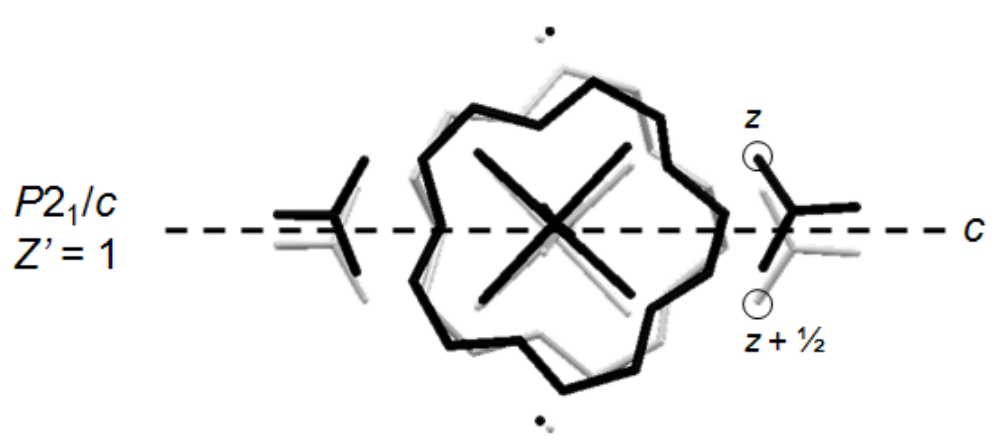
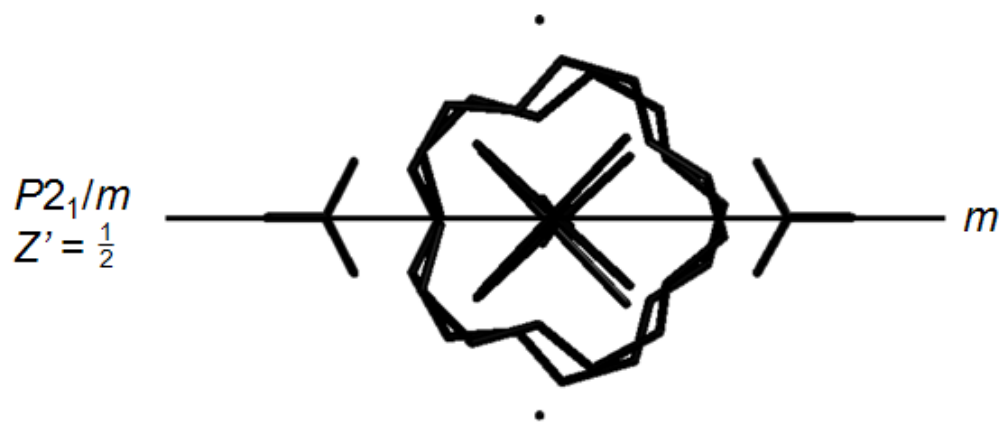
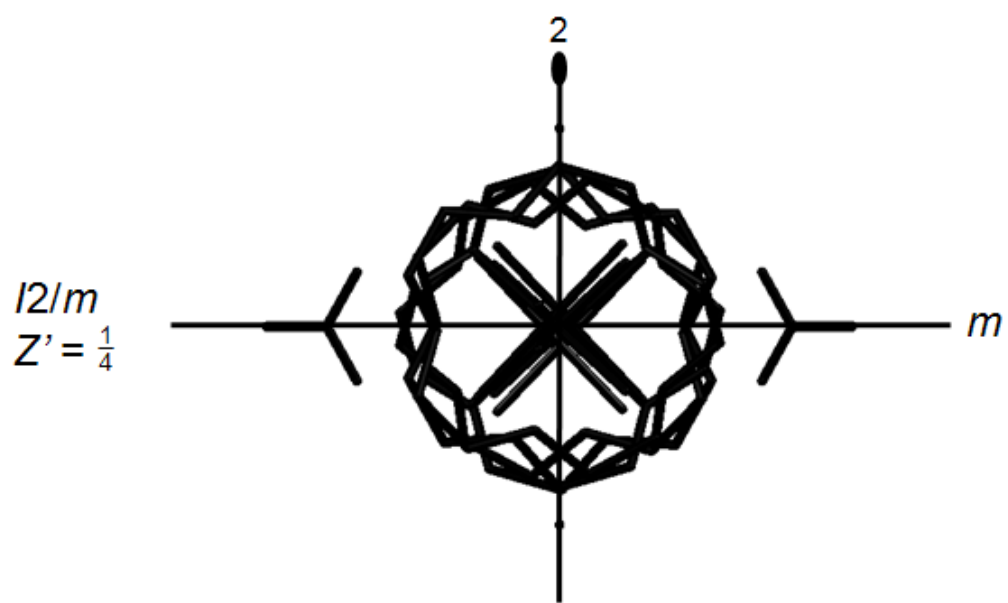


Figure 7.1. Projections of the asymmetric units of the $Z' = \frac{1}{4}$, $\frac{1}{2}$ and 1 phases of the system $[\text{Ni}(\text{H}_2\text{O})_6](\text{NO}_3)_2 \cdot (15\text{-crown-5}) \cdot 2\text{H}_2\text{O}$ down the direction of the 1-D H-bonded chains (*i.e.*, the *c* direction). Two formula units are shown for the $Z' = 1$ phase (the lowest-temperature phase); the black and light gray formula units are related by a *c* glide plane (*i.e.*, a mirror of plane with a translational component of $c/2$). Symmetry considerations suggest that the formula unit of the lowest-temperature phase may become more symmetrical if the thermal motion of the system increases. In the ordered lowest-temperature phase, the conformational enantiomers of the 15-crown-5 molecules, the $[\text{Ni}(\text{H}_2\text{O})_6]^{2+}$ ions and the nitrate ions nearly occupy sites of a *c* glide plane. As a result, the black formula unit and the symmetry generated light gray formula unit (*via* the *c* glide plane) are relatively similar in orientation but statistically distinguishable at low temperatures (since the thermal motion is small). As the temperature of the system increases, the formula units become less distinguishable; when the system passes through the transition $Z': 1 \rightarrow \frac{1}{2}$, the translation component $c/2$ is lost¹¹⁷ and the new phase has a statistical mirror plane¹¹⁸: the nitrate ions lie statistically at sites of the mirror symmetry, the 15-crown-5 molecules are disordered (because the conformational enantiomers cannot be superimposed), the $[\text{Ni}(\text{H}_2\text{O})_6]^{2+}$ ions are also disordered. As the temperature increases, the system becomes even more disordered (because the thermal motion is large); when the system passes through the transition $Z': \frac{1}{2} \rightarrow \frac{1}{4}$, the $Z' = \frac{1}{4}$ phase has a twofold¹¹⁹ and mirror symmetries. Theoretically, the 15-crown-5 molecules and the $[\text{Ni}(\text{H}_2\text{O})_6]^{2+}$ ions should be very disordered, but because the thermal motion in the system is very large, the disorder of the $[\text{Ni}(\text{H}_2\text{O})_6]^{2+}$ ions and of the 15-crown-5 molecules are more difficult to resolve (see experimental section of Chapter 5 for further details).

¹¹⁷ As a result, the *c* axis of the $Z' = \frac{1}{2}$ is approximately shortened by a factor of two compared to the *c* axis of the $Z' = 1$ phase.

¹¹⁸ In the paper entitled ‘Toward a Grammar of Crystal Packing’, Brock and Dunitz wrote ‘Molecules with apparent crystallographic mirror symmetry often show some atomic displacement ellipsoids that are elongated perpendicular to the mirror plane. These displacement parameters may indicate that the apparent mirror symmetry is only statistical in nature (a space or time average over slightly different molecular orientations)...’.

¹¹⁹ The lattice water molecules lie on sites of the twofold symmetry.

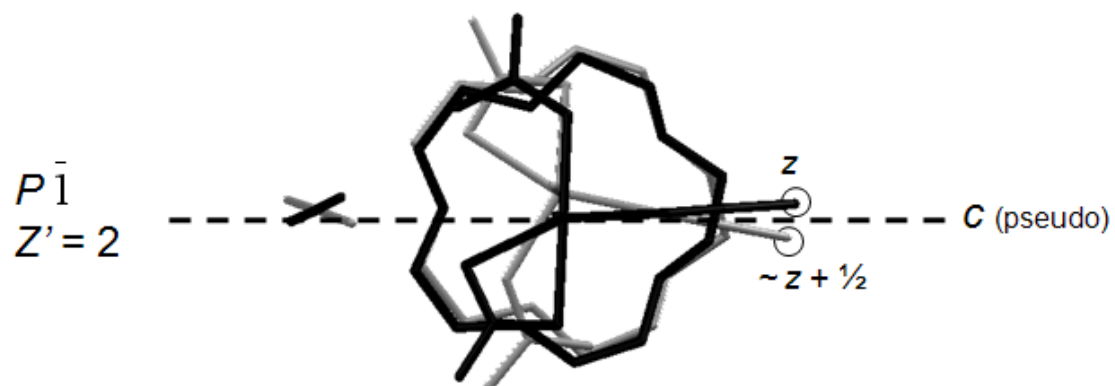
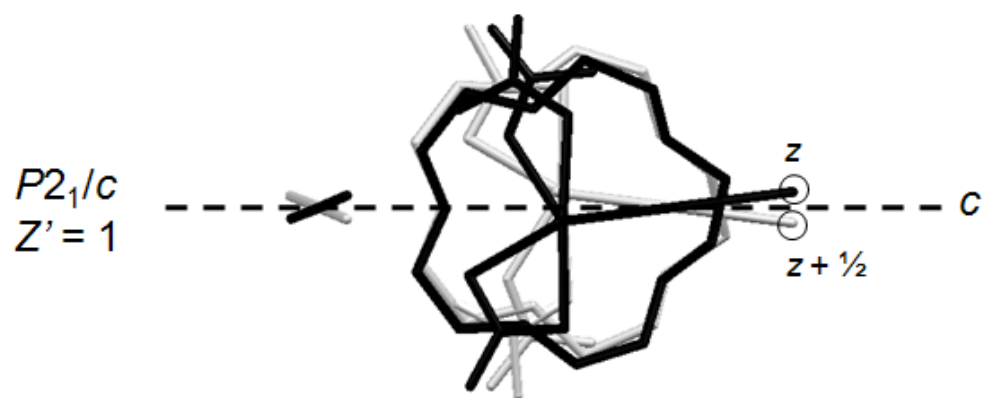
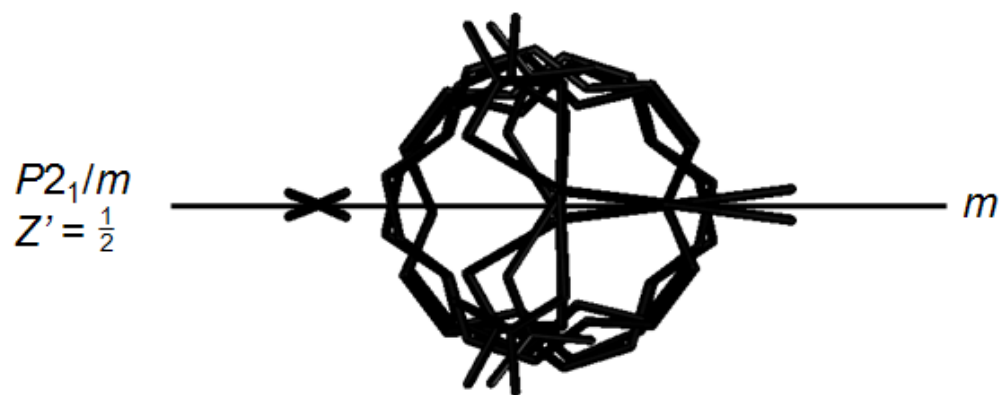


Figure 7.2. Projections of the asymmetric units of the $Z' = \frac{1}{2}$, 1 and 2 phases of the system $[\text{Ni}(\text{H}_2\text{O})_2(\text{MeCN})(\text{NO}_3)_2] \cdot (15\text{-crown-5}) \cdot \text{MeCN}$ down the direction of the 1-D H-bonded chains (*i.e.*, the c direction). The two independent formula units (black and gray) are shown for the $Z' = 2$ phase (the lowest-temperature phase). Two formula units are shown for the $Z' = 1$ phase; the black and light gray formula units are related by a c glide plane (*i.e.*, a mirror of plane with a translational component of $c/2$). Symmetry considerations suggest that the formula units of the lowest-temperature phase may become more symmetrical if the thermal motion of the system increases. In the ordered lowest-temperature phase, which is nearly monoclinic, the conformational enantiomers of the 15-crown-5 molecules, the $[\text{Ni}(\text{H}_2\text{O})_2(\text{MeCN})(\text{NO}_3)_2]$ metal complexes and the lattice acetonitrile molecules nearly occupy sites of a pseudo c glide plane¹²⁰ (the $c/2$ translation is nearly true). As the temperature of the system increases, the thermal motion becomes larger. When the system passes through the transition $Z': 2 \rightarrow 1$, the structure is monoclinic with a true translation component of $c/2$. The two formula units (black and light gray) are crystallographically related by a c glide plane. The black formula unit and the symmetry generated light gray formula unit (*via* the c glide plane) are relatively similar in orientation but distinguishable. As the temperature of the system increases, the formula units eventually become less distinguishable; when the system passes through the transition $Z': 1 \rightarrow \frac{1}{2}$, the translation component $c/2$ is lost and the new phase has a statistical mirror plane. The 15-crown-5 molecules are disordered (because the conformational enantiomers cannot be superimposed and because of the occurrence of pseudoinversion symmetry), the $[\text{Ni}(\text{H}_2\text{O})_2(\text{MeCN})(\text{NO}_3)_2]$ metals complexes are very disordered, the lattice acetonitrile molecules are also disordered. Single-crystal X-ray experiments show that the thermal motion in the system is large in the $Z' = \frac{1}{2}$ phase, the disorder of the acetonitrile ligands and lattice acetonitrile molecules are more difficult to resolve (see experimental section of Chapter 5 for further details).

¹²⁰ It is important to notice that the monodentate nitrate ligands of the two formula units cannot be related by a pseudo c glide plane because the two crystallographically independent Ni^{2+} ion are not coordinated by the same pseudosymmetrically related O atoms.

(ix) The two polymorphic systems $[\text{Ni}(\text{H}_2\text{O})_6](\text{NO}_3)_2 \cdot (15\text{-crown-5}) \cdot 2\text{H}_2\text{O}$ and $[\text{Ni}(\text{H}_2\text{O})_2(\text{MeCN})(\text{NO}_3)_2] \cdot (15\text{-crown-5}) \cdot \text{MeCN}$ are more complicated to understand because of the occurrence of high- Z' phases, which were found to be intermediate to the $Z' = \frac{1}{2}$ and 1 phases. The high- Z' phases were found to have high pseudosymmetry. The high- Z' phases are unpredictable partly because the loss of true inversion centers in the crystal structures were not expected as the temperature of the two systems was raised.

New Polymorphic Systems in the Future

New systems for which hydrogen bond interactions between A and B constituents are found along one dimension and for which at least one of the constituents (A or B) has relatively high internal symmetry should be regarded as good candidates for possible polymorphic systems. The geometry of the 15-crown-5 molecule seems to favor such hydrogen bond interactions because the crown ether can act as a bifacial H-bonded acceptor. Some octahedral metal ions or some octahedral metal complexes that act as H-bond donors¹²¹ to the 15-crown-5 molecules are good candidates.

The likelihood of finding new polymorphic systems that have similar characteristics to the three systems discussed in Chapters 4, 5 and 6 is relatively high¹²². Such systems are convenient to study polymorphism because no significant loss of crystallinity is detectable while single crystals go through a phase transition. As a result, such systems are likely to be good references as polymorphic systems in the literature.

Copyright © Maxime A. Siegler 2007

¹²¹ There are at least two potential ligands along one axis of the octahedron.

¹²² In the six Ni(II) complexes for which 1-D H-bonded chains are found between the 15-crown-5 molecules and the Ni^{2+} ions or Ni(II) metal complexes, three crystal systems were found to be polymorphic.

Appendix A: Crystallographic Tables

In Appendix A, each file (named Tab##.pdf) is a linking file (pdf format) that corresponds to the crystallographic tables of all structures discussed in the dissertation. Each file contains seven tables. Table 1 includes the information of crystal data and structure refinement. Table 2 lists the atomic coordinates and equivalent isotropic displacement parameters for non-hydrogen atoms. Table 3 lists the bond lengths and angles. Table 4 lists the anisotropic displacement parameters for non-hydrogen atoms. Table 5 lists the coordinates and isotropic displacement parameters for hydrogen atoms. Table 6 lists the torsion angles. Table 7 lists the hydrogen bond distances.

Tab01.pdf (x04082, $Z' = 8$, $B2_1$)

A1. Crystallographic tables for diaqua(15-crown-5)magnesium(II) nitrate at 311 K.

Tab02.pdf (x05032, $Z' = 8$, $B2_1$)

A2. Crystallographic tables for diaqua(15-crown-5)iron(II) nitrate at 90 K.

Tab03.pdf (k05062, $Z' = 8$, $B2_1$)

A3. Crystallographic tables for diaqua(15-crown-5)iron(II) nitrate at 90 K.

Tab04.pdf (x05028, $Z' = 8$, $B2_1$)

A4. Crystallographic tables for diaqua(15-crown-5)zinc(II) nitrate at 313 K.

Tab05.pdf (k05253, $Z' = 3$, $P\bar{1}$)

A5. Crystallographic tables for hexaaquanickel(II) nitrate (15-crown-5) monohydrate (2nd polymorph) at 90 K.

Tab06.pdf (k06063, $Z' = \frac{1}{2}$, $P2_1/n$)

A6. Crystallographic tables for hexaaquanickel(II) nitrate (15-crown-5) *trans*-tetraaquadimethanolnickel(II) nitrate (15-crown-5) at 90 K.

Tab07.pdf (k05086, $Z' = 1$, $Pbca$)

A7. Crystallographic tables for *cis*-tetraaquadinitratonickel(II) (15-crown-5) *trans*-tetraaquadinitratonickel(II) (15-crown-5) at 90 K.

Tab08.pdf (k05322, $Z' = 2$, $C\bar{1}$)

A8. Crystallographic tables for diaqua(15-crown-5)nickel(II) nitrate (phase I) at 308 K.

Tab09.pdf (k05256, $Z' = 3$, $P2_1/c$)

A9. Crystallographic tables for diaqua(15-crown-5)nickel(II) nitrate (phase II) at 90 K.

Tab10.pdf (k06368, $Z' = 1$, $P2_1$)

A10. Crystallographic tables for hexaaquanickel(II) nitrate (15-crown-5) monohydrate (1st polymorph, phase I) at 295 K.

Tab11.pdf (k06367, $Z' = 2$, $B2_1$)

A11. Crystallographic tables for hexaaquanickel(II) nitrate (15-crown-5) monohydrate (1st polymorph, phase II) at 90 K.

Tab12.pdf (k02180, $Z' = \frac{1}{4}$, $I2/m$)

A12. Crystallographic tables for hexaaquanickel(II) nitrate (15-crown-5) dihydrate (phase I) at 294 K.

Tab13.pdf (k05178, $Z' = \frac{1}{2}$, $P2_1/m$)

A13. Crystallographic tables for hexaaquanickel(II) nitrate (15-crown-5) dihydrate (phase II) at 250 K.

Tab14.pdf (k06335, $Z' = 7$, $B2_1$)

A14. Crystallographic tables for hexaaquanickel(II) nitrate (15-crown-5) dihydrate (phase III) at 90 K.

Tab15.pdf (k05153, $Z' = 1$, $P2_1/c$)

A15. Crystallographic tables for hexaaquanickel(II) nitrate (15-crown-5) dihydrate (phase IV) at 90 K.

Tab16.pdf (k06117, $Z' = \frac{1}{2}$, $P2_1/m$)

A16. Crystallographic tables for acetonitrilediaquadinitratonickel(II) (15-crown-5) acetonitrile solvate (phase I) at 243 K.

Tab17.pdf (k06077, $Z' = 5$, $B2_1$)

A17. Crystallographic tables for acetonitrilediaquadinitratonickel(II) (15-crown-5) acetonitrile solvate (phase II) at 90 K.

Tab18.pdf (k06073, $Z' = 1$, $P2_1/c$)

















A18. Crystallographic tables for acetonitrilediaquadinitratonickel(II) (15-crown-5) acetonitrile solvate (phase III) at 150 K.

Tab19.pdf (k06078, $Z' = 2$, $P\bar{1}$)

A19. Crystallographic tables for acetonitrilediaquadinitratonickel(II) (15-crown-5) acetonitrile solvate (phase IV) at 90 K.

Appendix B: Symbols

a, b, c	Lengths of the unit cell edges of the direct space.
a^*, b^*, c^*	Lengths of the reciprocal unit cell edges.
$\mathbf{a}, \mathbf{b}, \mathbf{c}$	Unit cell vectors in direct space.
$\mathbf{a}^*, \mathbf{b}^*, \mathbf{c}^*$	Reciprocal unit cell vectors.
a, b, c, n, d	Glide planes. ‘Axial’ glide planes are designated by a, b or c . ‘Diagonal’ glide plane is designated by n . ‘Diamond’ glide plane is designated by d .
D_x	Crystal density.
$e \text{ \AA}^{-3}$	Electron density unit (electrons per cubic angstroms).
F	Structure factor.
h, k, ℓ	Miller Indices (integers).
$\bar{h}, \bar{k}, \bar{\ell}$	Negative Miller Indices (negative integers).
(h, k, ℓ)	Set of lattice planes.
$\{h, k, \ell\}$	Crystal form (<i>i.e.</i> , set of lattice planes equivalent by the symmetry of the crystal).
$I(hk\ell)$	Intensities of the reflection $hk\ell$.
x, y, z	Coordinates in the crystal lattice.
$[x, y, z]$	Direction in the crystal lattice.
P, A, B, C, I, F, R	Lattice centerings. Primitive (P), centered on one set of faces (A, B, C), body-centered (I), face-centered (F) or rhombohedral (R).
N_{obs}	Number of reflections observed for a given structure.
N_v	Number of variables (or number of parameters).
m	Mirror planes.
R	Residual index (R factor). $R = \frac{\sum (F_o - F_c)}{ F_o }$.
Z	Number of formula units in the unit cell.
Z'	Number of formula units in the asymmetric unit.
α, β, γ	Angles between \mathbf{b} and \mathbf{c} (α), between \mathbf{a} and \mathbf{c} (β), between \mathbf{a} and \mathbf{b} (γ).

$\alpha^*, \beta^*, \gamma^*$	Angles between \mathbf{b}^* and \mathbf{c}^* (α^*), between \mathbf{a}^* and \mathbf{c}^* (β^*), between \mathbf{a}^* and \mathbf{b}^* (γ^*).
$\Delta\rho$	Difference electron density.
θ	Angle of the X-ray beam to the “reflection plane”.
λ	Wavelength of the radiation used in the X-ray diffraction experiment.
μ	Linear absorption coefficient.
1	Identity.
$\bar{1}$ 	Inversion center.
2 	Twofold axis.
2 ₁ 	Twofold screw axis: ‘2 sub 1’
3 	Threefold axis.
3 ₁ 	Threefold screw axis: ‘3 sub 1’.
3 ₂ 	Threefold screw axis: ‘3 sub 2’.
4 	Fourfold axis.
4 ₁ 	Fourfold screw axis: ‘4 sub 1’.
4 ₂ 	Fourfold screw axis: ‘4 sub 2’.
4 ₃ 	Fourfold screw axis: ‘4 sub 3’.
6 	Sixfold axis.
6 ₁ 	Sixfold screw axis: ‘6 sub 1’.
6 ₂ 	Sixfold screw axis: ‘6 sub 2’.
6 ₃ 	Sixfold screw axis: ‘6 sub 3’.
6 ₄ 	Sixfold screw axis: ‘6 sub 4’.
6 ₅ 	Sixfold screw axis: ‘6 sub 5’.

Appendix C: Glossary

Absorption effect: the attenuation of the intensity of the X-ray beam by a crystal. The intensity of the incident beam I_0 is related with the intensity I of the beam that passes through the thickness τ of the crystal. The relationship is given by: $I = I_0 e^{-\mu\tau}$ (μ is defined as the linear absorption coefficient).

Anisotropy: a property is said to be anisotropic when it is directionally dependent.

Body-centered lattice: a lattice having lattice points at the corners and at the body center (*i.e.*, $x = y = z = \frac{1}{2}$) of the unit cell. Such lattices are symbolized by the letter I .

Cell dimensions (or cell constants): the cell dimensions are defined by the axes a , b and c and the angles α (*i.e.*, between b and c), β (*i.e.*, between a and c) and γ (*i.e.*, between a and b).

Centrosymmetric structure: a structure that crystallizes in a space group with inversion centers.

Correlation of matrix elements: the interdependence among parameters (*e.g.*, the atomic coordinates and the displacement parameters) of the coefficient matrix used in the least-squares refinement.

Crystal habit: the analysis aimed at determining the crystal shape and the Miller indices of the faces bounding the crystal. Crystal habit may point out some characteristics of the crystal packing.

Cubic unit cell: a unit cell with four threefold axes along the four body diagonals of the unit cell and three fourfold axes parallel to the three cell axes a , b and c . There is one independent parameter for the cell dimensions (*i.e.*, $a = b = c$; $\alpha = \beta = \gamma = 90^\circ$).

DELU: a *SHELXL* instruction that applies a ‘rigid bond’ restraint to the named atoms.

DFIX and DANG: the *SHELXL* instructions that restraints bond distances between pairs of atoms within an effective standard deviation (default: 0.02 for *DFIX* and 0.04 for *DANG*). The *DANG* instruction is usually used for 1,3-distances (or ‘angle distances’).

Difference Fourier map (or Difference Fourier synthesis): a map for which the Fourier coefficients are the differences between the observed and calculated amplitudes of the structure factors, $\Delta F = |F_o| - |F_c|$. Difference Fourier map is generally very useful to locate hydrogen atoms and residual electron densities.

Diffuse scattering: a non-Bragg scattering appearing near reflections with relatively high intensities. The presence of diffuse scattering may indicate short range order in a given structure (*e.g.*, highly disordered structure).

Displacement Parameters: the measures of the mean-square amplitudes of the atomic oscillations. The isotropic displacement parameter corresponds to the temperature factor U_{iso} (or U_{11}) with the amplitude of vibration equal in all directions. The anisotropic displacement parameters are defined by the six parameters U_{11} , U_{22} , U_{33} , U_{23} , U_{13} and U_{12} which describe the magnitudes and the orientations of the vibration ellipsoids.

EADP: a *SHELXL* instruction that aims at assigning the same isotropic or anisotropic displacement parameters for the named atoms. The *EADP* instruction is a constraint.

EXTI: a *SHELXL* instruction (and also a parameter) that estimates extinction in the crystal.

Face-centered lattice: a lattice having lattice points at the corners and at the centers of all faces of the unit cell. Such lattices are symbolized by the letter *F*.

FLAT: a *SHELXL* instruction that restraints the named atoms to lie a common plane.

Hexagonal unit cell: unit cell with a sixfold axis parallel to one cell axis (the c axis by convention) and with a twofold axis perpendicular to the c axis. There are two independent parameters for the cell dimensions (*i.e.*, $a = b \neq c$; $\alpha = \beta = 90^\circ$, $\gamma = 120^\circ$).

Isotropy: a property is said to be isotropic when it is directionally independent.

Least-squares refinement: an analytical method of refinement aimed at minimizing the sum of the squares of the deviations of the experimentally observed values from the corresponding calculated values. In X-ray structure determination, the values of interest are the three positional parameters (x, y, z) and one displacement parameter (U_{11} in the case of an isotropic refinement) or six displacement parameters ($U_{11}, U_{22}, U_{33}, U_{23}, U_{13}$ and U_{12} in the case of an anisotropic refinement) for each atom.

Libration: a vibrational motion along an arc.

Monoclinic unit cell: a unit cell with a twofold axis parallel to one cell axis (the b axis by convention). There are four independent parameters for the cell dimensions (*i.e.*, $a \neq b \neq c$; $\alpha = \gamma = 90^\circ$; $\beta \neq 90^\circ$).

Noncentrosymmetric structure: a structure that crystallizes in a space group with no inversion center.

Occupancy factor: factor that defines the site occupancy of a given atom. In the case of a non-disordered structure, the occupancy factor of a given atom is 1. In the case of a disordered structure, the occupancy of a given atom is partial and the occupancy factor is less than 1. The sum of the occupancy factors for the minor and major components of a disordered atom is 1.

Orthorhombic unit cell: a unit cell with three perpendicular twofold axes parallel to the cell axes a , b and c . There are three independent parameters for the cell dimensions (*i.e.*, $a \neq b \neq c$; $\alpha = \beta = \gamma = 90^\circ$).

Primitive lattice: a lattice having lattice points at the corners of the unit cell. Such lattices are symbolized by the letter P .

Reciprocal lattice slices: the 2-D slices of the diffraction pattern viewed down the \mathbf{a}^* (*i.e.*, $0k\ell$, $1k\ell$, $2k\ell$, *etc.*), \mathbf{b}^* (*i.e.*, $h0\ell$, $h1\ell$, $h2\ell$, *etc.*) or \mathbf{c}^* (*i.e.*, $hk0$, $hk1$, $hk2$, *etc.*) directions.

Residual index (R factor): an index that takes into account the differences between the observed and calculated amplitudes of the structure factors. The residual index gives a basic measure of the correctness of the model. If the R factor is low (< 0.06), the structure is probably correct. Higher R factors may indicate that some significant changes in the model might be needed.

RESI: a *SHELXL* instruction that groups the selected atoms in a specified 'residue'. The *RESI* instruction allows using the same atoms names in different residues, which is particularly useful for high- Z' structures.

Rhombohedral unit cell: a unit cell with a threefold axis along one body diagonal of the unit cell. There are two independent parameters for the cell dimensions (*i.e.*, $a = b = c$; $\alpha = \beta = \gamma \neq 90^\circ$). The rhombohedral lattice is symbolized by the letter R .

SAME: a *SHELXL* instruction that restraints the geometries (the 1,2- and 1,3-distances) of chemically identical but crystallographically independent molecules (or ions) to be the same within an effective standard deviation (0.02 by default).

Separate Wilson plot: a plot of averaged intensities of some classes of reflections in function of $(\sin\theta/\lambda)^2$. Quantitative analyses about the intensity distribution between different classes of reflections may be derived from such plots.

SHELXL: a program that computes the least-squares structure refinement of crystal structures.

Side-centered lattice: a lattice having lattice points at the corners and at the centers of two opposite faces of the unit cell. Such lattices are symbolized by the letters *A* (*i.e.*, the *bc* faces are centered), *B* (*i.e.*, the *ac* faces are centered) or *C* (*i.e.*, the *ab* faces are centered).

Space group: a group of symmetry operations intrinsic to a given crystal structure. There are 230 space groups (see *Volume A of International Tables for Crystallography*).

SUMP: a *SHELXL* instruction that restraints the sum of site occupancy factors to be a constant (generally 1). The *SUMP* instruction is particularly useful to deal with threefold or higher-fold disorder (*i.e.*, when a given atom can have more than two orientations at a site).

Systematically absent reflections: some reflections are systematically absent when there is, at least, one translational symmetry element (*i.e.*, translation, glide planes and screw axes) inherent in the crystal structure.

Tetragonal unit cell: a unit cell with a fourfold axis parallel to one cell axis (the *c* axis by convention). There are two independent parameters for the cell dimensions (*i.e.*, $a = b \neq c$; $\alpha = \beta = \gamma = 90^\circ$).

Triclinic unit cell: a unit cell with no rotational symmetry. There are six independent parameters for the cell dimensions (*i.e.*, $a \neq b \neq c$; $\alpha \neq \beta \neq \gamma$).

Bibliography

Allen, F. H.; Kennard, O.; Taylor, R. *Acc. Chem. Res.* **1983**, *16*, 146-153.

Allen, F. H.; Kennard, O.; Watson, D. G.; Brammer, L.; Orpen, A. G.; Taylor, R. *J. Chem. Soc. Perkin Trans.* **1987**, *2*, S1-S19.

Allen, F. H. *Acta Cryst.* **2002**, *B58*, 380-388.

Allen, F. H.; Motherwell, W. D. S. *Acta Cryst.* **2002**, *B58*, 407-422.

Arakcheeva, A.; Chapuis, G. *Acta Cryst.* **2006**, *B61*, 601-607.

Arakcheeva, A.; Chapuis, G. *Acta Cryst.* **2006**, *B62*, 52-59.

Barnett, S. A.; Broder, C. K.; Shankland, K.; David, W. I. F.; Ibberson R. M.; Tocker, D. A. *Acta Cryst.* **2006**, *B62*, 287-295.

Bendeif, E.-E.; Dahaoui, S.; François, M.; Benali-Cherif, N.; Lecomte, C. *Acta Cryst.* **2005**, *B61*, 700-709.

Bernstein, J. *Polymorphism in Molecular Crystals*; Oxford University Press: Oxford, 2002.

Bernstein, J. *Cryst. Growth Des.* **2005**, *5*, 1661-1662.

Brock, C. P.; Dunitz, J. D. *Chem. Mater.* **1994**, *6*, 1118-1127

Bruno, I. J.; Cole, J. C.; Kessler, M.; Luo, J.; Motherwell, W. D. S.; Purkis, L. H.; Smith, B. R.; Taylor, R.; Cooper, R. I.; Harris, S. E.; Orpen, A. G. *J. Chem. Inf. Comput. Sci.*, **2004**, *44(6)*, 2133-2144.

Bruker *SHELXTL v5.1*; Bruker AXS, Madison, WI, 1997.

Chernyshov, D.; Hostettler, M.; Törnroos, K. W.; Bürgi, H.-B. *Angew. Chem. Int.* **2003**, *42*, 3825-3830.

Chernyshov, D.; Bürgi, H.-B.; Hostettler, M.; Törnroos, K. W. *Phys. Rev. B.* **2004**, *70*, 094116–1-8.

David, W. I. F.; Ibberson, R. M.; Cox, S. F. J., Wood, P. T. *Acta Cryst.* **2006**, *B62*, 953-959.

Desiraju, G. R. *Cryst. Growth Des.* **2004**, *4*, 1089-1090.

Dunitz, J. D. *X-Ray Analysis and the Structure of Organic Molecules*; Cornell University Press: Ithaca, NY, 1979.

Dunitz, J. D. *Chem. Commun.* **2003**, 545-548.

Ehrenfest, P. *Leiden Comm. Suppl.* **1933**, 75b.

Flack, H. D. *Acta Cryst.* **1983**, *A39*, 876-881.

Flack, H. D.; Bernardinelli G. *Acta Cryst.* **1999**, *A55*, 908-915.

Gavezzotti, A. *Acc. Chem. Res.* **1994**, *27*, 309.

Giacovazzo, C.; Monaco, H. L.; Viterbo, D.; Scordari, F.; Gilli, G.; Zanotti, G.; Catti, M
In *Fundamentals of Crystallography*; Giacovazzo, C. Ed.; IUCr Texts on
Crystallography, No. 2; Oxford University Press: New York, NY, 1992.

Giordano, T. J.; Palenik, G. J.; Palenik, R. C.; Sullivan, D. A. *Inorg. Chem.* **1979**, *18*, 9, 2445-2450.

Glusker, J. P.; Trueblood, K. N. *Crystal Structure Analysis* 2nd edition, Oxford University Press, 1985.

Goetha, A. E.; Howard, J. A. K. *Chem. Soc. Rev.* **2004**, *33*, 490-500.

Hao, X. *Studies of Unusual Packing and of Polymorphism in Two Crystal Systems*, 2005.

Hao, X.; Parkin, S.; Brock, C. P. *Acta Cryst.* **2005**, *B61*, 675-688.

Hao, X.; Siegler, M. A.; Parkin, S.; Brock, C. P. *Cryst. Growth Des.* **2005**, *5*, 2225-2232.

Hao, X.; Siegler, M. A.; Parkin, S.; Brock, C. P. Unpublished results.

Herbstein, F. H., Kapon, M., Reisner, G. M., Lehman, M. S., Kress, R. B., Wilson, R. B., Shiau, W. I., Duesler, E. N., Paul, I. C. & Curtin, D. Y. *Proc. R. Soc. London A.* **1985**, *399*, 295-310.

Herbstein, F. *Acta Cryst.* **2002**, *B56*, 547-557.

Herbstein, F. *Acta Cryst.* **2006**, *B62*, 341-383.

Kitagawa, S.; Kitaura, R.; Noro, S. *Angew. Chem. Int. Ed.* **2004**, *43*, 2334-2375.

Larson, S. B.; Simonsen, S. H.; Ramsdsen, J. N. *Acta Cryst.* **1989**, *C45*, 161-163.

Lommerse, J. P. M.; Motherwell, W. D. S.; Ammon, H. L.; Dunitz, J. D.; Gavezzotti, A.; Hofmann, D. W. M.; Leusen, F. J. J.; Mooij, W. M. T.; Price, S. L.; Schweizer, B.;

McCrone, W. C. In *Physics and Chemistry of the Organic Solid State*; Fox, D.; Labes, M. M.; Weissberger, A. Eds.; Interscience: New York, NY, 1965; Vol. II, pp 725-767.

Motherwell, W. D. S.; Ammon, H. L.; Dunitz, J. D.; Dzyabchenko, A.; Gavezzotti, A.; Hofmann, D. W. M.; Leusen, F. J. J.; Lommerse, J. P. M.; Mooij, W. M. T.; Price, S. L.; Scheraga, H. ; Schweizer, B.; Schmidt, M. U.; Eijck, B. P.; Verwer, P.; Williams, D. E. *Acta Cryst.* **2002**, *B58*, 647-661.

Mnyukh, Yu. V.; Petropavlov, N. N. *J. Phys. Chem. Solids.* **1972**, *33*, 2079-2087.

Mnyukh, Yu. V.; Panfilova, N. A. *J. Phys. Chem. Solids.* **1973**, *34*, 159-170.

Mnyukh, Yu. V.; Panfilova, N. A.; Petropavlov, N. N.; Uchvatova, N. S. *J. Phys. Chem. Solids.* **1975**, *36*, 127-144.

Mnyukh, Yu. *Speculations Sci. Tech.* **1983**, *6*, 275-285.

Mnyukh, Yu. *Fundamentals of Solid State Phase Transitions, Ferromagnetism and Ferroelectricity*. 1st Books, 2001.

Orpen, A. G.; Brammer, L.; Allen, F. H.; Kennard, O.; Watson, D. G.; Taylor, R. *J. Chem. Soc. Dalton Trans.* **1989**, S1-S83.

Niangia, A. *Cryst. Growth Des.* **2006**, *1*, 2-4.

Parsons, S. *Acta Cryst.* **2007**, *E63*, 3130.

Pelizzi, C.; Pelizzi G.; Porretta, S.; Vitali, F. *Acta Cryst.* **1986**, *C42*, 1131-1133.

Petricek, V.; Dusek, M. *JANA2000, The Crystallographic Computing System*; Institute of Physics, Praha, Czech Republic, 2000.

Platas-Iglesias, C.; Vaiana, L.; Esteban-Gómez, D.; Avecilla, F.; Real, J. A.; de Blas, A.; Rodríguez-Blas, T. *Inorg. Chem.* **2005**, *44*, 9704-9713.

Rodriguez, S. M. B.; Palatinus, L.; Petricek, V.; Chapuis, G. *Acta Cryst.* **2006**, *B62*, 1043-1050.

Sato, S.; Iida, J.; Suzuki, K.; Kawano, M.; Ozeki, T.; Fujita, M. *Science.* **2006**, *313*, 1273.

Schmid, S.; Wagner, T. *Acta Cryst.* **2005**, *B61*, 361-366.

Schmidt, M. U.; Eijck, B. P.; Verwer, P.; Williams, D. E. *Acta Cryst.* **2000**, *B56*, 697-714.

Schranz, W.; Tröster, A.; Gardon, M.; Krexner, G.; Prem, M.; Carpenter, M. A.; Sondergeld, P.; Armbruster, T. *Z. Kristallogr.* **2005**, *220*, 704-711.

Seddon, K. R. *Cryst. Growth Des.* **2004**, *4*, 1087.

Shannon, R. D. *Acta Cryst.* **1976**, *A32*, 751-767.

Sheldrick, G. M. *SHELXTL PC*; Siemens Analytical Instruments, Inc., Germany, 1994.

Sheldrick, G. M. *SHELXS97, Program for the Solution of Crystal Structures*; University of Göttingen, Germany, 1997a.

Sheldrick, G. M. *SHELXL97, Program for Crystal Structure Refinement*; University of Göttingen, Germany, 1997b.

Sheldrick, G. M. *XPREP6.12, SHELXTL*; Bruker-AXS, Madison, WI, 2001.

Shmueli, U.; Goldberg, I. *Acta Cryst.* **1973**, B29, 2466-2471.

Simonsen, S. H.; Larson, S. B.; Ramsden, A. C. *ACA, Ser.2.* **1982**, 37, 10.

Sparks, R. A. *GEMINI*; Bruker-AXS, Madison, WI, 1999.

Spek, A. L. *PLATON, A Multipurpose Crystallographic Tool*; Utrecht University, Utrecht, The Netherlands, 2005.

Steed, J. W.; Sakellariou, E.; Junk, P. C.; Smith, M. K. *Chem. Eur.* **2001**, J. 7, No. 6, 1240-1247.

Stout, G. H.; Jensen, L. H. *X-ray Structure Determination A Practical Guide*, The Macmillan Company, New York, 1968.

Threlfall, T. *Org. Proc. Res. & Dev.* **2003**, 7, 1017-1027.

Toledano, J.-C.; Glazer, A. M.; Hahn, Th.; Parthé, E.; Roth, R. S.; Berry, R. S.; Metselaar, R.; Abrahams, S. C. *Acta Cryst.* **1998**, A54, 1028-1033.

Ubbelohde, A. R. *Q. Rev.* **1957**, 11, 246-272.

Ubbelohde, A. R. *K. Ned. Akad. Wet. Proc. B.* **1962**, 65, 459-471.

Ubbelohde, A. R. *J. Chim. Phys.* 1966, 62, 33-42.

Van Smaalen, S. *Cryt. Rev.* **1995**, 4, 79-202.

Westrum, E. F. Jr; McCullough, J. P. *Physics and Chemistry of the Organic Solid State*, edited by D. Fox, M. M. Labes & A. Weissberger, Vol. I, pp. 1-178 (see also pp. 75, 151). New York: Interscience, 1963.

Xia, A.; Selegue, J. P.; Carrillo, A.; Patrick, B. O.; Parkin, S.; Brock, C. P. *Acta Cryst.* **2001**, *B57*, 507-516.

Xia, A.; Selegue, J. P.; Carrillo, A.; Patrick, B. O.; Parkin, S.; Brock, C. P. *Acta Cryst.* **2002**, *B58*, 565.

Zuniga, F. J.; Criado, A. *Acta Cryst.* **1995**, *B51*, 880-888.

Vita

Maxime Siegler

Personal

French citizen (born April 10th, 1978, Lille, France)

Education

Sciences of Engineering

Hautes Etudes Industrielles, Lille, France, 2002

Research Area

Small Molecule X-Ray Crystallography, Polymorphism, Solid-State Phase Transitions, Commensurately Modulated Superstructures

Languages

Fluent in French and English

Awards and Fellowship

Kentucky Opportunity Fellowship

University of Kentucky, Lexington, July 2006 – June 2007

Outstanding Research Award

Department of Chemistry

University of Kentucky, Lexington, April 2006

Fast Start Award

Department of Chemistry

University of Kentucky, Lexington, April 2004

Publications (research)

- [7] Siegler, M. A.; Parkin, S.; Brock, C. P.
[Ni(MeCN)(H₂O)₂(NO₃)₂](15-crown-5)·MeCN: a Polymorphic System Analogous to [Ni(H₂O)₆](NO₃)₂·(15-crown-5)·2H₂O. (2007), in preparation.
- [6] Siegler, M. A.; Parkin, S.; Hao, X.; Brock, C. P.
The Unusual Phase Sequence of [Ni(H₂O)₆](NO₃)₂·(15-crown-5)·2H₂O with an Intermediate High-Z' Phase. (2007), in preparation.
- [5] Siegler, M. A.; Parkin, S.; Brock, C. P.
The First Polymorph of [Ni(H₂O)₆](NO₃)₂·(15-crown-5)·H₂O: a Two-Phase System. (2007), in preparation.
- [4] Siegler, M. A.; Parkin, S.; Selegue, J. P.; Brock, C. P.
Toward the Insertion of the Ni²⁺ Ion Inside the 15-crown-5 Molecule. *Cryst. Growth & Des.* (2007), in preparation.
- [3] Hao, X.; Siegler, M. A.; Parkin, S.; Brock, C. P.
The High-*T* Phases of [M(H₂O)₂(15-crown-5)](NO₃)₂ with *Z'* = 8 (*M* = Mg, Fe, Zn), with *Z'* = 2 (*M* = Ni, Cu) and with *Z'* = ½ (*M* = Co). *Acta Cryst. B.* (2007), in preparation.
- [2] Siegler, M. A.; Fu, Y.; Simpson, G. H.; King, D. P.; Parkin, S.; Brock, C. P.
An Unexpected Co-Crystal with a Variable Degree of Order: 1:1 *trans*-1,2-Cyclohexanediol/Triphenylphosphine Oxide *Acta Cryst. B.* (2007), submitted.
- [1] Hao, X.; Siegler, M. A.; Parkin, S.; Brock, C. P.
[M(H₂O)₂(15-crown-5)](NO₃)₂: A System Rich in Polymorphic and Modulated Phases. *Cryst. Growth & Des.* (2005), **5**, 6, 2225-2232.

Publications (collaboration)

- [10] Xu, Y.-H.; Siegler, M.; Long, S.
(3*R*,7*R*)-Bis(4-nitrophenyl) 2-oxoperhydrobenzo[*d*]imidazole-1,3-dicarboxylate
Acta Cryst. E (2007), **63**, 3835.
- [9] Zhong, M.; Siegler, M.; Long, S.
tert-Butyl N-[(1*R*,2*R*)-2-(isothiocyanato)-cyclohexyl]carbamate
Acta Cryst. E (2007), **63**, 3589.
- [8] Long, S.; Siegler, M.; Li T.
2,4,6-Trimethylbenzenaminium chloride
Acta Cryst. E (2007), **63**, 3080.
- [7] Sonar, V. N.; Ring, J. R.; Siegler, M.; Crooks, P. A.
(*E*)-1-[(2-Chlorophenyl)methyleneamino]guanidinium chloride
Acta Cryst. E (2007), **63**, 974-975.
- [6] Sonar, V. N.; Neelakantan, S.; Siegler, M.; Crooks, P. A.
(*E*)-1-[(2-Methoxyphenyl)methyleneamino]guanidinium chloride
Acta Cryst. E (2007), **63**, 535-536.
- [5] Long, S.; Siegler, M.; Li T.
6-Chloronicotinic acid
Acta Cryst. E (2007), **63**, 279-281.
- [4] Long, S.; Siegler, M.; Li T.
2-Oxo-1,2-dihydropyridine-3-carboxylic acid
Acta Cryst. E (2006), **62**, 5644-5665.
- [3] Siegler, M.; Long, S.
(4*R*,5*R*)-4,5-Diphenylimidazolidin-2-one
Acta Cryst. E (2006), **62**, 5310-5311.
- [2] Long, S.; Siegler, M.; Li T.
N-(3-Chloro-2-methylphenyl)-2-oxo-1,2-dihydropyridine-3-carboxamide
Acta Cryst. E (2006), **62**, 4278-4279.
- [1] Long, S.; Siegler, M.; Li T.
2-(2-Isopropylanilino)pyridine-3-carboxylic acid
Acta Cryst. E (2006), **62**, 4211-4213.

Abstracts and Presentations

- [5] M. A. Siegler, S. Parkin, C. P. Brock.
[Ni(MeCN)(H₂O)₂(NO₃)₂](15-crown-5)·MeCN: Another Polymorphic System With An Intermediate, High-Z' Phase.
Lecture by M. A. Siegler. American Crystallography Association Meeting, July 21-26, 2007, Salt Lake City, UT.
- [4] M. A. Siegler, X. Hao, S. Parkin, C. P. Brock.
The Unpredictable Intermediate High-Z' Phases in the Polymorphic Systems [Ni(H₂O)₆](NO₃)₂·(15-crown-5)·2H₂O (PS 1) and [Ni(MeCN)(H₂O)₂(NO₃)₂](15-crown-5)·MeCN (PS 2).
Lecture by M. A. Siegler. Midwest Organic Solid State Chemistry Symposium XVII, June 8-9, 2007, Lexington, KY.
- [3] C. P. Brock, M. A. Siegler, X. Hao, S. Parkin.
Phases Sequences in Some Crystals Containing M(NO₃)₂, Water and 15-Crown-5.
Lecture by C. P. Brock. British Crystallography Association Meeting, April 17-20, 2007, Cambridge, UK.
- [2] M. A. Siegler, X. Hao, S. Parkin, C. P. Brock.
[Ni(H₂O)₆](NO₃)₂·(15-crown-5)·2H₂O: An Uncommon Polymorphic System.
Lecture by M. A. Siegler. American Crystallography Association Meeting, July 22-27, 2006, Honolulu, HI.
- [1] C. P. Brock, X. Hao, M. A. Siegler, S. Parkin.
The many crystal forms of [M(15-crown-5)(H₂O)₂](NO₃)₂.
Acta Cryst. (2005). **A61**, C336.

Society Membership

American Crystallographic Association (ACA): 2005 – present